National Society of Black Physicists
XXV Annual Day of Scientific Lectures
and
21st Annual Meeting

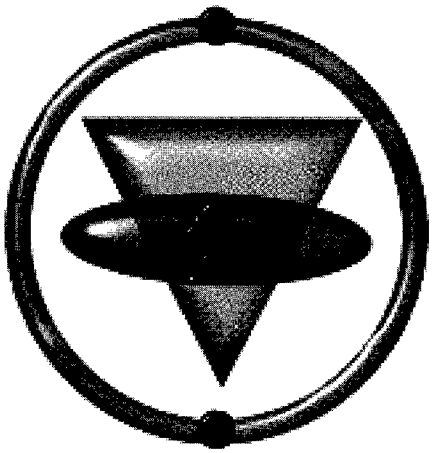

March 4-7, 1998
University of Kentucky
Kentucky State University

12th Annual National Conference of Black Physics Students

March 5-8, 1998
University of Kentucky

JOINT CONFERENCE

REPORT DOCUMENTATION PAGE

Form Approved
OMB No. 0704-0188

1. AGENCY USE ONLY (*Leave Blank*)	2. REPORT DATE	3. REPORT TYPE AND DATES COVERED
	Mar 99	Final 10/01/1997--03/31/1999

4. TITLE AND SUBTITLE
Proceedings of the National Society of Black Physicists 1998 Annual Meeting

5. FUNDING NUMBERS
G: N00014-98-1-0034
PR: 98PR00683-00

6. AUTHORS
Alan D. MacKellar, Editor

7. PERFORMING ORGANIZATION NAME(S) AND ADDRESS(ES)
University of Kentucky, Dept. of Physics and Astronomy, Lexington, KY 40506-0055
Kentucky State University , Department of Mathematics and Physical Sciences, Frankfort, KY

8. PERFORMING ORGANIZATION REPORT NUMBER
4-61444

9. SPONSORING / MONITORING AGENCY NAME(S) AND ADDRESS(ES)
Office of Naval Research Regional Office, Chicago, 536 S. Clark Street, Room 208, Chicago, IL 60605-1588

10. SPONSORING / MONITORING AGENCY REPORT NUMBER
N00014-98-1-0034

11. SUPPLEMENTARY NOTES

12a. DISTRIBUTION / AVAILABILITY STATEMENT
Copies available from Alan MacKellar, Dept. of Physics and Astronomy , University of Kentucky

12b. DISTRIBUTION CODE

13. ABSTRACT *(Maximum 200 words)*

The 1998 National Society of Black Physicists (NSBP) Annual Meeting was held jointly with the National Conference of Black Physics Students (NCBPS). The two groups and approximately 75 high school students interested in science (from several regions in Kentucky) were in attendance for one joint session. Members of the NSBP and invited distinguished minority physicists presented scientific papers of current research, sharing cutting edge research with their colleagues in the minority community. Several NSBP members also led sessions for the NCBPS in such topics as "Frontiers in Physics", "How to get into Graduate School", "Surviving Graduate School". All meals were shared by the two organizations, with speakers and discussion sessions. This NSBP meeting provided unique opportunities for mentoring and encouragement of minorities of all levels in physics. According to the American Institute of Physics survey (page 233, Table 3, Proceedings) of the student evaluation of performance of the 1998 joint conference in meeting goals, 92% rated "Networking with Black Professionals" as excellent or good.

DISTRIBUTION STATEMENT
Approved for Public Release
Distribution Unlimited

14. SUBJECT TERMS
Physics Conference
Minority Physicists

15. NUMBER OF PAGES
234

16. PRICE CODE

17. SECURITY CLASSIFICATION OF REPORT	18. SECURITY CLASSIFICATION OF THIS PAGE	19. SECURITY CLASSIFICATION OF ABSTRACT	20. LIMITATION OF ABSTRACT
Unclassified	Unclassified	Unclassified	UL

NSN 7540-01-280-5500

Standard Form 298 (Rev. 2-89)
Prescribed by ANSI Std. Z39-1

National Society of Black Physicists XXV Annual Day of Scientific Lectures

and

21st Annual Meeting

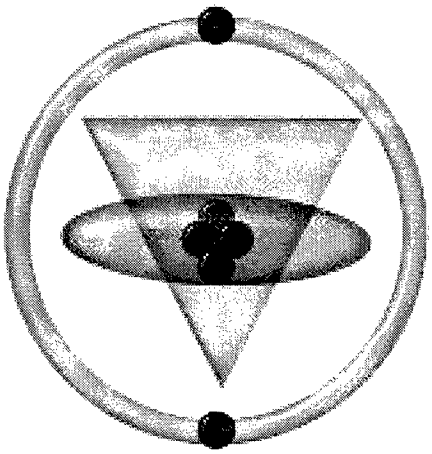

NSBP '98:
"The Next Generation"

March 4-7, 1998
University of Kentucky
Kentucky State University

12th Annual National Conference of Black Physics Students

NCPBS '98:
"Physics/Life in Motion"

March 5-8, 1998
University of Kentucky

JOINT CONFERENCE

Message to NCBPS and NSBP

We, the National Conference of Black Physics Students (NCBPS), are very pleased to co-convene with the National Society of Black Physicists (NSBP) during our respective annual meetings. This is the 12th consecutive annual meeting of NCBPS. We wish to thank our host institution, the University of Kentucky, Lexington, for giving us the opportunity to join the professional society, NSBP, in celebrating their 25th year.

The goal of NCBPS is to increase the number of Black students obtaining advanced degrees in physics. To this end, our special joint meeting provides us a unique opportunity to establish closer contact with Black Physicists, to broaden mentoring, to provide greater exposure to scientific research, to explore career options with physics degrees and to learn the history of Black contributions to physics. The opportunity to meet with the professiona society does not occur often, full advantage should be taken of this educational meeting.

Dr. Cynthia R. McIntyre, Co-Founder, NCBPS

March 1998

Message from the President

Welcome to the 25th Annual Day of Scientific Lectures and the 21st Annual Meeting of the National Society of Black Physicists. We are extremely proud and happy to be at this point in our existence. NSBP has a rich history. One that is inspirational, that must be told over and over again to a much wider audience. There are young people out there that will find our history "awesome, tight and cool." It is our responsibility to make sure that this rich history is available to inspire all youths: those bright-eyed and questioning, those bold and daring, and those unconcerned and unmotivated.

The Society had its beginnings in the need and desire to recognize, honor and celebrate the work of outstanding Black scientists. As we embark upon this 25th Day of Scientific Lectures, we should view this as a time to celebrate. Many organizations have come and gone in this 25-year period. NSBP has grown and flourished. So let us have a grand celebration during these next two and one-half days.

To help us celebrate, we are very pleased to have the National Conference of Black Physics Students concurrently meeting with us. This is historic, for it marks only the second time that the two conferences have met simultaneously with overlapping events. We extend a hearty welcome to all associated with NCBPS and extend a sincere invitation to join NSBP so that this relationship can continue into the future!

The Society has undergone tremendous change and made significant strides in the 90's. We will recognize and celebrate those accomplishments. We will also begin the process of recognizing and celebrating those individuals who have made significant contributions to NSBP's survival and prosperity. In the midst of the celebrations, we will do what got us where we are today; i.e., good science and good outreach. We will be treated to a full program of interesting talks both theoretical and applied, addressing both old and new problems, by both professionals and students. Again, welcome to NSBP-98. Enjoy the celebration!

Lonzy J. Lewis, President and Chair, NSBP

March 1998

Acknowledgements

The National Society of Black Physicists 1998 Meeting is sponsored by:

The Office of Naval Research
The University of Kentucky:
- Research and Graduate Studies
- Office of Minority Affairs
- College of Arts and Sciences
- Department of Physics and Astronomy

Western Kentucky University

The 1998 National Conference of Black Physics Students is Sponsored by:

National Aeronautics & Space Administration/Kentucky Space Grant Consortium
The National Science Foundation
The US Department of Energy
Oak Ridge National Laboratory
The Southeastern Universities
Research Association
Oak Ridge Associated Universities
The Tennessee Valley Authority
The University of Kentucky:
- Research and Graduate Studies
- Office of Minority Affairs
- College of Arts and Sciences
- Department of Physics and Astronomy

National Student Planning Committe

Alphonse L. Loper, University of Kentucky, Chair
Jamie Valentine, Brown University
Jeremy J. Jackson, Southern University
Clemente Adu, University of Kentucky
G. Y. Ndefru, University of Kentucky
Taravia Taylor, Fisk University

Local Planning Committee/Joint Conference

Alan MacKellar, Chair, University of Kentucky Department of Physics & Astronomy
Lauretta Byars, University of Kentucky Vice Chancellor for Minority Affairs
Dana Cox, University of Kentucky College of Arts and Sciences
Keh-fei Liu, University of Kentucky Department of Physics & Astronomy
Suketu Bhavsar, University of Kentucky Department of Physics & Astronomy
Al Shapere, University of Kentucky Department of Physics & Astronomy
Emmett "Buzz" Burnam, University of Kentucky African American Recruitment Office
Donald Byars II, University of Kentucky Admissions Office
Charles McGruder, Western Kentucky University
Richard Hackney, Western Kentucky University
Karen Hackney, Western Kentucky University

The Local Planning Committee would like to thank the following people for their support:
Carolyn Elery, Pat Tremble, Tony Thomas, Joyce Beatty, Mildred Bailey, Danyel Bell, Charmaine Neal, and Rene Hales

Joint Conference Coordination

Connie S. Blakemore, University of Kentucky International Business & Management Center
Ana Miranda, University of Kentucky International Business & Management Center
Jessika Berry, University of Kentucky
Rene M. Hales, University of Kentucky Media Design & Production

Table of Contents

Conference Papers

The Pointwise Dimension Applied to Astronomical Clustering Studies

Dr. Jason S. Best

Shepherd College

Abstract

It can be said that one of the fundamental goals of cosmology is to describe the Universe as accurately as possible. In order to do this, the multiple aspects of the Universe, both past and present-day, must be completely modeled. Some of these characteristics include the age, density, temperature, and extent of the Universe and its components. The modern motivation for fractal geometry may best be summed up by this quote of Benoit Mandelbrot: "Mountains are not cones, clouds are not spheres, coastlines are not circles, and bark is not smooth, nor does lightning travel in a straight line.". Fractals are, in simplest terms, "objects which are (approximately) self-similar on all scales". The renewed modern interest in fractals found as one of its applications the study of the large-scale structure of the Universe, giving a quantitative descriptive scheme to ideas that had been expressed qualitatively as early as C.V.L. Charlier's map of extragalactic nebulae in the 1920s. The focus of this paper will be on results of studies of galaxy catalogs and galaxy cluster catalogs using the pointwise dimension, or PD. The PD is an easy-to-use fractal statistic which has numerous advantages over the more traditional methods used to study the clustering of astronomical objects. It is believed that much new information can be gleaned with this statistic about the environments of the galaxies and of the clusters in these catalogs.

1. Introduction to the Astronomical Issues

Two components of the modern-day Universe that can be analyzed in order to understand its evolution are the clustering of objects in the Universe and the relationship between a galaxy's morphology and its environment.

On the largest scales, the Universe is believed to be everywhere homogeneous and isotropic: this is evidentially verified by such observations as the isotropy of the cosmic microwave background. However, on smaller scales, the universe is certainly not observed to be homogeneous. For instance, the average density of a galaxy is $\sim 10^5$ times that of the Universe, while a cluster's average density is $\sim 10^2$ times that of the Universe (Peebles 1993). Furthermore, galaxies are observed to be distributed not at random, but clustered with respect to each other; the "soap bubbles" of de Lapparent, Geller, and Huchra 1986 are one of the more famous demonstrations of this. Any theory of structure formation must also be able to account for this observed clustering of objects.

Hubble and Humason 1931 demonstrated that the morphological fractions of ellipticals, lenticulars, and spirals are related to the density of the environment. The fraction of ellipticals ranges from less than 10% in the lowest density environments to more than 50% in the centers of galaxy clusters (Dressler 1980a). It is still not apparent whether this is a result of conditions conducive to formation

of a particular morphological type (nature) or to an evolutionary process (nurture). There are multiple scenarios that can account for this "morphological segregation", including scenarios based on star formation rate dependence on the level of the density fluctuation that forms a galaxy (Zurek, Quinn, and Salmon 1988), the stripping of a spiral or lenticular galaxy's disk by tidal or pressure forces in the center of a galaxy cluster (Gunn and Gott 1972), or merger scenarios (Toornre 1977, Hernquist 1980).

It is very difficult to determine which of the various nature and nurture mechanisms dominate. It would appear that the clustering properties of different morphological types should be diagnostic of the formation mechanism, but in practice the distinctions are very subtle. If nature is the motivating factor, then whatever local properties are needed to make ellipticals could tend to exist over a large region. If a nurture mechanism involving mergers is the dominant mechanism, then initial correlations in the positions of spirals could lead to numerous mergers in one region. Thus, in both mechanisms, a correlation between morphology and environment will arise. Whitmore, Gilmore, and Jones 1993 argue for a hybrid model of origin of morphology in which the same fractions of spirals, lenticulars, and ellipticals are set by nature to form everywhere in the Universe.

2. Methods of Analyzing Clustering

The two-point correlation function is the most common way of describing the distribution of galaxies. As defined by Peebles 1980, the two-point spatial correlation function $\xi(r_{12})$ can be written as

$$\delta P = n^2 \delta V_1 \delta V_2 [1+\xi(r_{12})] \qquad (1)$$

where n is the galaxy number density, and δP is the joint probability of finding an object in both volumes δV_1 and δV_2 at separation r_{12}. It is convenient to compute ξ as

$$\xi(r_{12}) = (N_{real} / N_{rand}) - 1 \qquad (2)$$

where N_{real} is the number of galaxy pairs in the observed sample with separations between r and $r + \Delta r$, and N_{rand} is the number of pairs in the same interval for the same number of galaxies distributed randomly over an identical volume.

The two-point correlation function, however, shows some limitations when providing a complete description of galaxy distribution. A major problem is that the technique assumes that the galaxy distribution becomes spatially homogeneous on a length scale that is smaller than that of the catalog being analyzed. If this assumption is invalid, the amplitude of the correlation function and the length scale where the function becomes small are sample dependent (Pietronero 1987). The two-point correlation function is also limited in that it averages together amplitudes on a given scale that come from galaxy pairs in many different environments. This can yield a large amplitude for $\omega(\theta)$ because there are a large number of close neighbors for a small fraction of the galaxies in the sample or because of a smaller number of neighbors for nearly all galaxies in the sample. In other words, while the two-point correlation function indicates that the galaxies are correlated, it does not reveal the number of galaxies that contribute to give the value. Finally, this statistic is most often applied either to all galaxies in a sample or to galaxies of the same morphology (e.g. elliptical-elliptical pairs) . Some environmental influences on morphology might have more to do with the total number of galaxies in the environment of a particular type.

Observational determinations of the correlation function $\xi(r)$ yield a relationship of a power law form

$$\xi(r)=Br^{\gamma} \qquad (3)$$

which has been determined to have a nearly constant slope over more than two orders of magnitude in distance (from galactic scales to galactic cluster scales). This behavior for object clustering suggests that the concept of fractal geometry may apply (Mandelbrot 1983, Peebles 1993). The modern motivation for fractal geometry may best be summed up by this quote: "Mountains are not cones, clouds are not spheres, coastlines are not circles, and bark is not smooth, nor does lightning travel in a straight line." (Mandelbrot 1983). Fractals are, in simplest terms, "objects which are (approximately) self-similar on all scales". Imagine a cauliflower having a piece broken off: that piece resembles a miniature cauliflower. This is an example of self-similarity.

The pointwise dimension, or PD, is particularly useful for analyses of correlations between morphology and environment. It also has the distinction of being conceptually simple and easy to apply to two- and three-dimensional object catalogs.

I can consider a function $N_{\vec{x}_m}(r)$ which is the count of the number of data points within a distance r from a reference point $\vec{x}_m$. In a log-log representation, there is a scaling region over which a slope can be defined; within that scaling region, which is bounded by $r_{\min}$ and $r_{\max}$, this slope $d_{\vec{x}_m}$ is interpreted as the pointwise dimension, and is defined as (Mayer-Kress 1994)

$$d_{\vec{x}_m} = \frac{log(N_{x_m}(r_{max})) - log(N_{x_m}(r_{min}))}{log(r_{max}) - log(r_{min})} \qquad (4)$$

In other words: one can characterize the environment of an object (known as the primary: it can be a galaxy, galaxy cluster or indeed any object the environment of which we wish to describe) by calculating how the number of objects surrounding the primary (the surrounding objects are known as secondaries) changes as a function of distance from the object. The maximum distance from the primary out to which we choose to calculate the slope is known as the "fitting range".

This research has two ends. First, I am attempting to quantify clustering of astronomical objects via the pointwise dimension. Second, I am trying to, when possible, study the possible relation between a galaxy's morphology and its complete environment.

3. Description of Data

The pointwise dimension has been used by this author to study a variety of catalogs. Three such catalogs are the RC3, the Dressler catalog, and the ACO.

The Third Reference Catalog of Bright Galaxies, or RC3 (de Vaucouleurs 1991), has been studied in a previous paper by this author (Best, Charlton, and Mayer-Kress 1996). The total number of galaxies in the catalog is 23,024, and it is complete for galaxies of apparent diameters greater than 1 aremin, B-band magnitudes brighter than 15.5, and radial velocities less than 15,000 km/s. For these analyses, we considered only a subsample of the catalog, where each galaxy needed to have either an apparent diameter of greater than 1 arcmin, or a B magnitude brighter than 15.5. This reduced the number to just under 22,000. In order to apply the analyses to the largest continuous areas possible (to avoid boundary effects), we analyzed the northern and southern hemispheres as separate populations. Boundaries of ±20 degrees galactic latitude were also used in order to avoid the galactic dust lane and an area of undersampling in the catalog. There remained 10493 galaxies in the northern sample and 8560 in the southern sample. Among the conclusions of that work were: 1) The PD elucidates the tendency for early-type galaxies to cluster more than late-type galaxies; however, there is considerable overlap between these populations. 2) The pointwise dimension, or PD statistic, does not find a significant relationship between luminosity and clustering in RC3, but it could be an effective diagnostic in larger 2D catalogs. 3) The majority of galaxies in RC3 (excluding clusters) are spread out in space much like a random distribution.

PD analyses have also been conducted on Dressler's 1980 catalog of morphological types in 55 rich clusters of galaxies (Dressler 1980b). Dressler's main selection criteria were cluster richness (a measure of the number of galaxies within the cluster), low redshift (a measure of the distance of the cluster from the observer), and containment and definition within a few square degree area of the sky. In this catalog, the smallest number of galaxies in a cluster is 44 and the largest cluster redshift is ~0.064. Dressler took from the Abell Catalog (Abell 1958) 38 clusters, and completed the catalog with 17 previously unstudied clusters, which were obtained "...from a rather complete inspection of a plate copy of the ESO Quick Blue Survey". Dressler considers the overall quality of the data "good to excellent".

The catalog contains, for each cluster galaxy (~6000 galaxies in all), information on its position, morphology, apparent visual magnitude, estimated bulge size, and ellipticity. Dressler also lists a redshift for each cluster. The characteristics most

immediately relevant to my PD analyses of this catalog are redshift and morphology. Redshifts had been previously obtained for 26 of the clusters between 1973-1979 by other observers. Dressler used the du Pont telescope to obtain redshifts for at least two galaxies per cluster for each of the other clusters.

Morphological classifications for galaxies are determined by Dressler via the following criteria. Ellipticals have smooth radial profiles, and no intensity discontinuities. Lenticulars contain a non-spheroidal component, or an intensity discontinuity between the bulge and disk. Spirals show either disks with clear spirals or outer rings, or dust lanes extending through the disk length. Irregulars are amorphous dusty objects, while the Unclassified category contains anything not contained in the first four categories. Dressler also allows for transition cases. Transitions between ellipticals and lenticulars are discriminated by intensity discontinuities, while transitional spiral/lenticular cases are assigned due to uncertain detection of spiral structures.

The ACO Catalog (Abell, Corwin, and Olowin 1989) is the largest all-sky cluster catalog currently available to the public, and thus makes a good candidate for a PD study. The ACO catalog contains 4073 rich clusters of galaxies, each having at least 30 members within a magnitude range m_3 to m_3+2 (where m_3 is the magnitude of the third brightest member of the cluster). As well, the 1989 sample had nominal redshifts less than 0.2. The authors claimed completeness to this level; however, a detailed analysis by Scaramella 1991 proved that the catalog is truly complete only to a redshift of 0.1. Consequently, that value will be used as the completeness threshold in PD analyses of this dataset. The catalog also contains information on position, richness class (the number of clusters not more than two magnitudes fainter than the third brightest cluster), distance class, V magnitude, and apparent cluster center. The catalog is separated into a northern and a southern catalog by the ACO authors, with northern being Abell's original catalog and southern being the 1989 completion. The combined catalogs have been divided by this author with respect to the galactic equator. From this point onward, unless specifically noted, the northern catalog contains those galaxies north of the galactic equator, while the southern catalog refers to those galaxies south of the galactic equator.

Since I wished to do a three-dimensional analysis, redshift information was desirable. In some cases, a redshift had been determined previously. In some cases, information on redshifts was obtained from the ESO Nearby Abell Cluster Survey, or ENACS (Katgert 1996), which studied 5634 galaxies in the direction of 107 clusters from the ACO catalog. The authors of that paper conclude that "...we do not find systematic velocity offsets [between ENACS data and previously published work] at a level which would prevent a useful combination between our data and those from the literature" (Katgert 1996). This being the case, the ENACS redshift information has been incorporated into these PD analyses when no other redshift data was available.

4. Three-dimensional ACO Analysis

This paper will focus on a single result of this research: the large-scale clustering extent of the ACO catalog. A 3D analysis of the ACO has subsequently been undertaken. A Hubble flow with no deviations is used to get a distance to each cluster. This distance, along with the galactic latitude and galactic longitude, can be used to convert into a 3D distribution using standard spherical coordinate transformations.

Aside from the dust lane boundary in effect, a 3D analysis must take another boundary into account. In spherical polar coordinates, a distribution of points (galaxies, clusters, etc.,) with a galactic latitude cutoff has a boundary defined by a trigonometric function of that cutoff (the function is unimportant; it is enough to know that it exists) I as well as an outer edge due to the lack of galaxies past the limiting redshift. Both boundaries are taken into consideration before a cluster is considered as a primary for a particular fitting range. The outer edge of the data has been set to a distance corresponding to a redshift of 0.1. The fitting ranges chosen were 0-10, 0-25, 0-50, 0-100, and 0-200 Megaparsecs (Mpc).

What I actually want to know, if possible, is the following: is the true distribution of clusters in the Universe random on large scales, or does it differ significantly from that of a random distribution? The best case scenario would be to have an all-sky catalog to answer this; this would give you a maximum extent. This is nearly the situation present here (only the galactic plane boundary imposed prevents this). For each hemisphere, one can compare the real data to a 3D random catalog, since on the scales of interest there should be little effect from velocity dispersions.

5. Discussion and Conclusion

Incorporating a minimum galactic latitude boundary of ±20 degrees (to avoid the galactic dust lane) and a redshift maximum of 0.1, the ACO cluster and random catalog distributions are compared directly using a KS (or Komolgorov-Smirnov) two-distribution test for both the northern and southern galactic hemispheres. This test is designed to determine to what significance we can say that the two distributions are or are not drawn from the same parent distribution. For both hemispheres, in all but one case the distribution of PDs for the random catalog and the ACO catalog are not similar to the 99th percent level using a KS test. That one case is the largest fitting range: that of 200 Mpc. This means that on scales below 200 Mpc, the ACO and random catalogs are not statistically similar to the 99th percent level.

Unfortunately, there were not enough data in the 25 Mpc fitting range of either the northern or southern random catalog to get a comparison to the "cluster correlation length" of 25 Mpc (Bahcall and Soneira 1983). However, in the range 0-50 Mpc, which is the first range for which there are enough data to compare ACO and Random results, the northern and southern distribution of the PDs from the ACO significantly differ from the randomly distributed PDs to the 99% level, and their median PDs and error bars do not overlap significantly.

I note that clustering on scales greater than the cluster correlation length has been found by other authors (Bahcall 1993, Borgani, Plionis, and Valdarnini 1993, Pietronero, Montuori, and Sylos Labini 1997, Sylos Labini, Pietronero, and Montuori 1997). Bahcall goes as far as to say that "The universal dimensionless cluster correlation function is consistent with a fractal structure in the distribution of clusters". She also notes that the ACO catalog is consistent with this picture. This does not rule out homogeneity on the largest scales; this does, however, push the cluster correlation length scale up quite a bit. In fact, it is found that the random catalogs' 3D PD values are not always 3.0, the value expected for a homogeneous distribution. This is to be expected, since a random catalog is not necessarily a homogeneous catalog on all scales. In fact, we should expect some small-scale clustering in a random catalog. The argument is, or should be, as to whether or not the Universe is homogeneous not on all scales but on the largest scales. Even proponents of the cosmological principle (CP) will admit that the structure seen in the Universe eliminates the possibility of a universe homogeneous on all scales (Davis 1997). What this research results in is not a denial of the CP. It is argued only that on the scales of the ACO catalog, we still see a structure that would be significantly different than that of a homogeneous catalog on the majority of scales probed. It is also noted that Kerscher 1997 finds that "the scale of homogeneity is considerably larger than $200h^{-1}$Mpc". These authors used an alternative method on the IRAS 1.2 Jy catalog. Sylos Labini, Pietronero, and Montuori 1997 claim structure on scales even larger than this from pencil-beam studies. Of course, these studies take into account only luminous matter. Dark matter, distributed homogeneously on large scales would of course gravitationally dominate on those scales. It is also quite possible that we may have not yet probed deep enough to see homogeneity. Evidence for a fractal distribution in COBE data (de Gouveia Dal Pino, Hetem, and A. de Araujo 1995) further adds to the possibility that while homogeneity may be the actuality, it may not occur until scales much greater than previously thought.

References

Abell, G. 0. 1958, *ApJS*, **3**, 11.

Abell, G. O., Corwin, H. G., and Olowin, R. P. 1989, *ApJS*, **70**, 1.

Bahcall, N. 1993, *Proc. Natl. Acad. Sci. USA*, **90**, 4848.

Bahcall, N. and Soneira, R. M. 1983, *ApJ*, **270**, 20.

Best, J., Charlton, J., and Mayer-Kress G 1996, *ApJ*, **456**, 55.

Borgani, S., Plionis, M., and Valdarnini, R. 1993, *ApJ*, **404**, 21.

Davis, M. 1997, in *Critical Dialogues in Cos-mology*, (Princeton: Princeton University Press).

de Gouveia Dal Pino, Hetem, E. M., and A. de Araujo, J. 1995, *ApJ*, **442**, 2.

de Lapparent, V., Geller, M., and Huchra, J. 1986, *ApJL*, **302**, L1.

de Vaucouleurs, G. e. a. 1991. *Third Reference Catalog of Bright Galaxies*, 1. (New York: Springer-Verlag).

Dressler, A. 1980a, *ApJ*, **236**, 351.

Dressler, A. 1980b, *ApJS*, **42**, 565.

Gunn, J. and Gott, J. 1972, *ApJ*, **176**, 1.

Hernquist, L. 1980. *The Environment and Evolution of Galaxies*, 327. eds. J.M. Shull, H.A. Thronson Jr. (Dordrecht: Kluwer Academic Publishers).

Katgert, P. e. a. 1996, *A&A*, **310**, 8.

Kerscher, M. e. a. 1997, in *Proceedings of the Workshop "Astro-particle physics"*, (held in Ringberg Castle Oct 10-15 1996), in preparation.

Mandelbrot, B. 1983. *The Fractal Geometry of Nature*, Chapter 1. (New York: W.H. Freeman and Company).

Mayer-Kress, G. 1994, *Integrative physiologi-cal and behavioral science*, **29**, 203.

Peebles, P. J. E. 1980. *The Large-Scale Struc-ture of the Universe*, 143. (Princeton: Princeton University Press).

Peebles, P. J. E. 1993. *Principles of Physical Cosmology*, Section 1. (Princeton: Princeton University Press).

Pietronero, L. 1987, *Physica*, **114a**, 257.

Pietronero, L., Montuori, M., and Sylos Labini, F. 1997, in *Critical Dialogues in Cosmology*, (Princeton: Princeton Uni-versity Press).

Scaramella, R. e. a. 1991, *AJ*, **101**, 342.

Sylos Labini, F., Pietronero, L., and Montuori, M. 1997. *Proceedings of the Workshop "Astro-particle physics"*, chapter in preparation. (held in Ringberg Castle Oct 10-15 1996).

Toomre, A. 1977. *The Evolution of Galax-ies and Stellar Populations*, 401. eds. B. Tinsley, R. Larson (New Haven: Yale Univ. Obs.).

Whitmore, B., Gilmore, D., and Jones, C. 1993, *ApJ*, **407**, 487.

Zurek, W., Quinn, P., and Salmon, J. 1988, *ApJ*, **330**, 519.

The Kinetics of Graphitization Revisited: A First Principles Derivation

Robert H. Bragg

T. E. Glover

University of California, Berkeley

Abstract

Graphitization has been modeled as a solid state chemical reaction involving four metastable graphite self-interstitial compounds wherein phase i transforms to phase i-1 with rate constants $k_i = \overline{K}_i \exp(-E_i/kT)$. The solution of the corresponding set of coupled linear first order ordinary differential equations, combined with the corresponding interlayer spacings, 0.355 nm, 0.344 nm, 0.340 nm, and 0.3375 nm provides an expression that describes the time-temperature history of the annealing process. Results of E_i obtained using literature data are E_1 = 7.46 eV, E_2 = 5.81 eV, E_3 = 4.55 eV, and E_4 = 3.36 eV. Within experimental error E_1 matches the heat of sublimation of graphite, and E_4 is equal to the activation energy for a-direction vacancy migration in graphite.

I. Introduction

Many studies of the conversion of carbon materials to graphite by high temperature isothermal annealing of soft carbon have employed X-ray data of the apparent interlayer spacing d_{002} in the equation[1,2]

$$d_{002}=d=d_0+(d_1-d_0)\exp(-k_1t)+(d_2-d_1)\exp(-k_2t) \quad (1)$$

where d_0 = 0.3354 nm, d_1 = 0.338 nm and d_2 = 0.344 nm, and $k_i = \overline{K}_i \exp(-E_i/kT)$. The form of this equation seems to be appropriate for describing the annealing process for a variety of structure sensitive properties, e.g., diamagnetic susceptibility and the Hall coefficient. However, the calculated value of E_i often exceeds the heat of vaporization of graphite, and it is usually necessary to resort to a distribution of rate constants to obtain a reasonable fit of the data. Typical annealing data are shown in Fig. 1.

Equation (1) has not heretofore been obtained from a first principles derivation. There is no reason, *a priori,* to assume only one or two E_i's, especially since the rate of annealing at a given temperature decreases as the *extent* of annealing increases, i.e., the closer d approaches d_0. The model of Maire and Mering of turbostratic graphite provides a promising alternative to the intuitive approach just described.[3] In this model there are four metastable graphite self-interstitial compounds, and a given carbon may contain a mixture of all, and in addition of course, graphite. Bragg and co-workers have presented strong evidence in support of this model,[4] and in fact assign the values d_4 = 0.355 nm, d_3 = 0.344 nm, d_2 = 0.340 nm, and d_1 = 0.3375 nm to the interlayer spacings of these phases. With this refinement the process of graphitization is simply the sequential transformation from phase i to phase i-1 with rate constant $k_i = \overline{K}_i \exp(-E_i/kT)$. In this work the appropriate set of differential equations is set up, solved and tested with available literature data.

II. Derivation

A. The reaction kinetics

We assume that a general starting carbon material prior to annealing is a mixture of phases whose volume fractions are $x_i = x_i(t)$, where $\Sigma x_i=1$. During annealing the set of

simultaneous equations that describes the process is

$$\left.\begin{aligned}
\frac{dx_1}{dt} &= -k_4 x_4 \\
\frac{dx_3}{dt} &= -k_3 x_3 + k_4 x_4 \\
\frac{dx_2}{dt} &= -k_2 x_2 + k_3 x_3 \\
\frac{dx_1}{dt} &= -k_1 x_2 + k_2 x_2 \\
\frac{dx_0}{dt} &= k_1 x_1
\end{aligned}\right\} \qquad (2)$$

where $k_i = \bar{K}_i \exp(-E_i/kT)$, and at t = 0, $x_i = \bar{X}_i(0)$. Since $x_i(t) = 1$, it follows that $\sum x_1(t)=1$, $\sum \bar{X}_1(0)=1$. The solution of Eqs. (2) can be obtained by standard techniques of ordinary differential equations. The expressions for the $x_i(t)$ are a big lengthy and are not shown here. However, if $x_4 >> x_3 >> x_2 >> x_1$, then the results are simpler and are used later in this paper.

B. The significance of d_{002}

If the d_{002} X-ray lines of the constituent phases were resolved the amounts of these phases could be determined using the fact that the integrated intensity I_i of a characteristic peak of the i_{th} phase is given by

$$I_1 = I_0 Q_i V_i \qquad (3)$$

Where I_0 is the incident beam intensity, Q_i is the reflecting power per unit volume and V_i is the volume of phase i. However, the peaks of the component phases partially overlap because the nominal peak separations, about 0.1 to 0.5 degrees 2θ, are comparable to the line breadths (due to small crystallite size) of these peaks, as shown in Fig. 2. Thus the appropriate parameter to characterize the distribution of peaks is the centroid <2θ>. Now for each component i, whose line profile is $P_i(2\theta)$,

$$\int_{-\infty}^{\infty} P_i(2\theta)d2\theta = I_i; \quad \int_{-\infty}^{\infty} 2\theta P_i(2\theta)d2\theta = <2\theta>_i I_i \qquad (4)$$

here $<2\theta>_i$ is the centroid of peak i. The line profile of the mixture is the sum of the components,

$$P(2\theta)=\sum P_i(2\theta) \qquad (5)$$

With Eq. (3), Eq. (4) and Eq. (5) one finds that the centroid <2θ> of the mixture is

$$<2\theta>=\sum <2\theta>_i I_i / \sum I_i \qquad (6)$$

And with the assumption that $Q_i = Q_j = Q$, Eq. (6) can be rewritten

$$<2\theta>=\sum <2\theta>_i x_i \qquad (7)$$

where $x_i = V_i/\sum V_i$ is the volume fraction of the i^{th} phase.

C. The connection to annealing kinetics

By combining Eq. (7) with the solutions of Eqs. (2) one obtains a very lengthy expression. If we make the assumption, justified *a posteriori,* that $k_i >> k_i\text{-}1$, then a much simpler expression is obtained. If we further note that over the narrow range of 2θ spanned by a composite peak the *differences* in 2θ are a linear function of the *differences* in the corresponding d's, then the annealing kinetics are represented by

$$\begin{aligned}
<d> = d_0 &+ \{d_1 - d_0\}\{\bar{X}_1(0) + \bar{X}_2(0) + \bar{X}_3(0) + \bar{X}_4(0)\}\exp(-k_1 t) \\
&+ \{d_2 - d_1\}\{\bar{X}_2(0) + \bar{X}_3(0) + \bar{X}_4(0)\}\exp(-k_2 t) \\
&+ \{d_3 - d_2\}\{\bar{X}_3(0) + \bar{X}_4(0)\}\exp(-k_3 t) \\
&+ \{d_4 - d_3\}\{\bar{X}_4(0)\}\exp(-k_4 t)
\end{aligned} \qquad (8)$$

III. Test of Eq. (8)

A proper test of Eq. (8) requires annealing data wherein <d> or <2θ> was measured, but heretofore data have been reported only for the peak position $\hat{d}$. Figure 2 shows a (004) line profile obtained from a thin plate of pyrolytic carbon which has been decomposed into its component peaks. Note that the peak at 0.355 nm makes a significant contribution

to the centroid, but only a small contribution to $\hat{d}$. Thus by setting $d_4 = 0$ in Eq. (8) one can use the literature data taking $\langle d \rangle \approx \hat{d}$ to a good approximation. Data of Figs. 4, 16 and 19 of Reference (1) were fitted using Eq. (8) with d_4 set equal to zero. The best fit using all of these data gave

i	E_i,eV	$\bar{K}_i$,min^{-1}
1	7.46	1.1×10^{8}
2	5.81	2.8×10^{7}
3	4.55	6.0×10^{6}
4	3.36	0.7×10^{4}

IV. Discussion

Equation (8) evidently contains Eq. (1) as a very special case, and it also explains why different investigators obtain annealing data that differ at the lowest annealing temperatures, but they are all very similar for large T and long t. It is also clear that one cannot bring a carbon to a standard state by preliminary anneals. The results are very preliminary but very encouraging, especially the results obtained for E_1 and E_4. For purposes of comparison, the heat of vaporization of graphite is 7.41 eV and the activation energy for vacancy migration, a-direction in graphite, is 3.10 ± 0.20 eV. The authors have no proposal for the mechanism corresponding to E_2 and E_3.

One implication for future research is that investigators should measure line profiles instead of peak positions. With such data one obtains the x_i directly from peak decomposition analysis, and in addition from $\langle d \rangle$ the validity of Eq. (8) can be tested. To the extent that Eq. (8) is corroborated, it will be possible to predict the entire course of the annealing process from one X-ray measurement.

References

[1]D. B. Fischbach, Chemistry and Physics of Carbon **7**, 71 (1971).

[2]A. Pacault, Chemistry and Physics of Carbon **7**, 107 (1971).

[3]J. Maire and J. Mering, Chemistry and Physics of Carbon **6**, 125 (1970).

[4]J. Lachter and R. H. Bragg, Phys. Rev. B **33**, 893 (1987).

FIG. 1. The unit-cell height c = 2d as a function of the logarithm of isothermal HTt at various temperatures for a pyrolytic carbon.

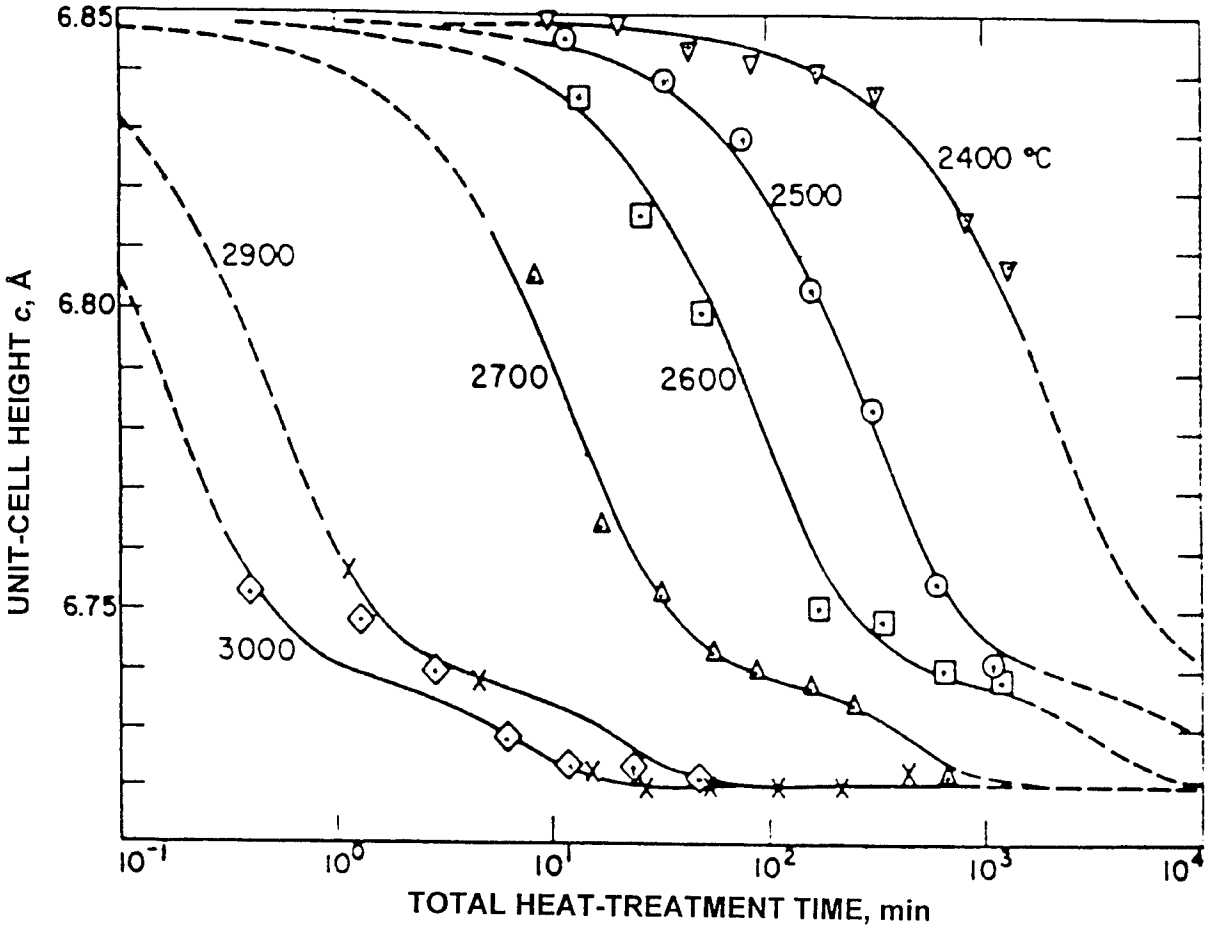

Figure 1. The unit-cell height c=2d as a function of the logarithm of isothermal HTt at various temperatures for a pyrolytic carbon.

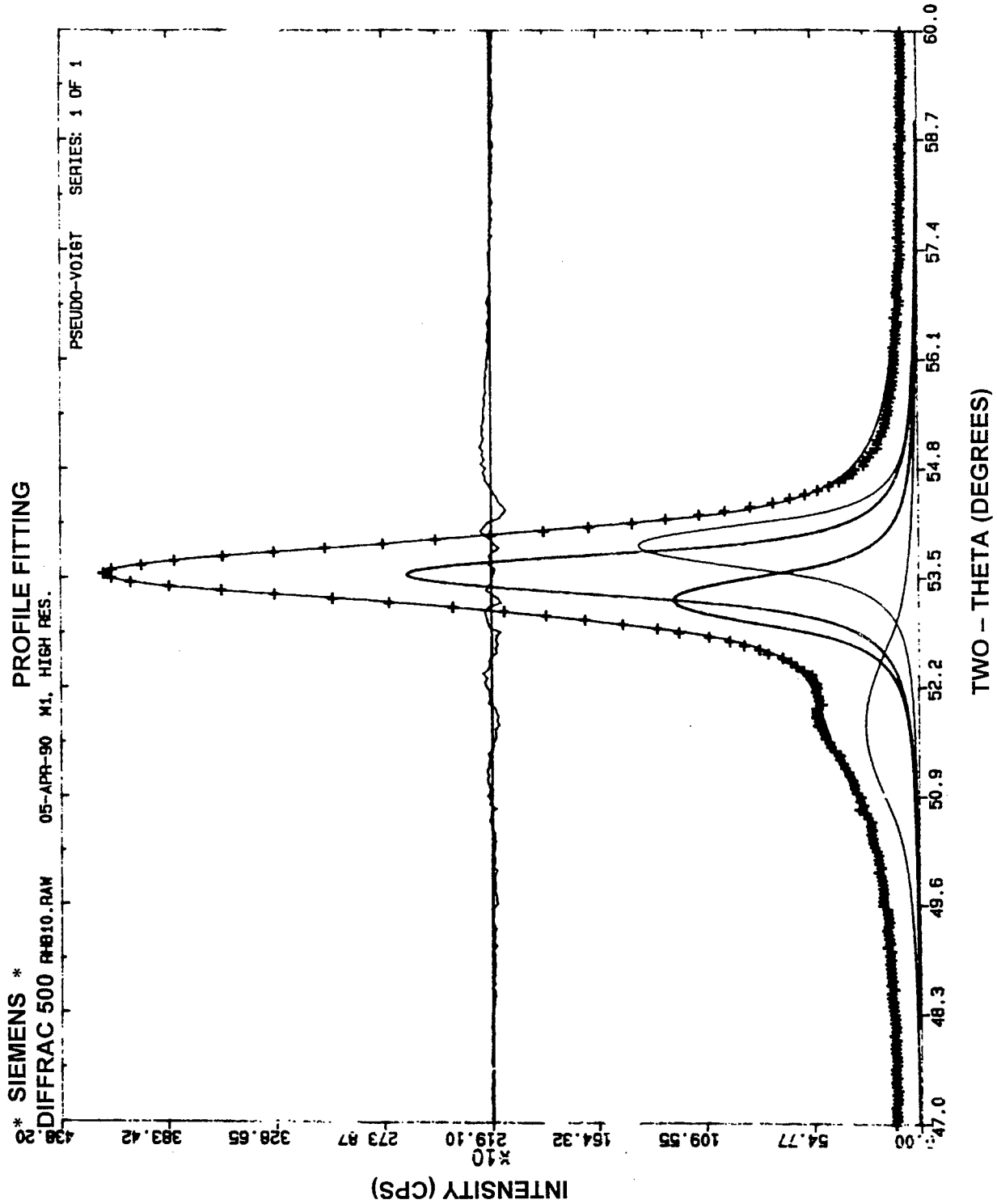

Figure 2. (064) line profile of as-received pyrolytic carbon showing profiles of component phases.

A New View of the X-Ray Emission from Elliptical Galaxies

Beth A. Brown

University of Michigan

Abstract

We have obtained an optically flux-limited sample of 34 elliptical and SO galaxies, observed with high and low angular resolution detectors on the X-ray Röntgen Satellite (ROSAT). The survey is large enough to test the present picture of cooling flow models developed to explain the origin, behavior, and evolution of hot gas found to be present in elliptical galaxies. For this sample of galaxies, we have established well-defined X-ray luminosities, and have determined X-ray gas temperatures for a subset of the survey. A steep relationship is found between the X-ray and optical luminosities with a slope of 2.72±0.27, with a large dispersion about the correlation. We confirm a correlation between the X-ray temperature (T_X) and stellar velocity dispersion temperature (T_σ), with $T_X \propto T_\sigma^n$ where n = 1.43±0.21. We also find X-ray gas temperatures 2 - 3 times hotter than expected for some galaxies. The results are inconsistent with predictions of the standard cooling flow model for elliptical galaxies, and we suggest a modification of the model that places environment in a central role in determining the X-ray emission properties. In our model, early-type galaxies attempt to drive partial or total galactic winds, which can be stifled by the pressure of their environment. Stifled winds should lead to hotter and higher luminosity systems, which would occur most commonly in the richest environments, as observed.

1. Introduction

The *Einstein Observatory* discovered that some early-type galaxies are powerful emitters of X-rays, and that their X-ray luminosity is correlated with their optical luminosity (Forman, Jones, & Tucker 1985; Canizares, Fabbiano, & Trinchieri 1987). It also showed that the temperature of the hot gas is approximately that expected for gas that is gravitationally bound to the system. For the more luminous X-ray-emitting ellipticals, where we are confident that the X-ray emission is dominated by the hot gas, the current model posits that gas is lost by stars through normal stellar evolution and is subsequently thermalized in the potential well of the galaxy, or heated by supernovae (e.g., Sarazin 1990). The gas then radiatively cools (producing the X-ray emission), and slowly flows into the center of the galaxy.

The existing picture makes certain predictions, such as that the X-ray luminosity should be proportional to the mass loss rate of stars and the depth of the potential well (approximately L_x *oc* $L_B^{1.7}$), with modest dispersion, and that the temperature of the hot gas (T_x) should be proportional to the stellar velocity dispersion (σ) squared. Studies with the *Einstein Observatory* led to luminosity relationships that were either consistent with or steeper than the expected L_X - L_B slope, but with considerable dispersion about the best-fit line (Canizares, Fabbiano, Trinchieri 1987; Donnelly, Faber & O'Connell 1990; White & Sarazin 1991; Bregman et al. 1992; Kim et al. 1992). The *Einstein Observatory* did not provide accurate temperature information for comparison with the velocity dispersion. The Röntgen Satellite (*ROSAT*), with a factor of two improvement in spectral resolution, does permit accurate

determinations of gas temperature. The first published *ROSAT* sample is that of Davis and White (1996), who found a correlation between X-ray temperature and stellar velocity dispersion, with temperatures greater than anticipated. Here we present X-ray luminosities from our complete survey of optically selected elliptical galaxies, and temperatures for a subset of the sample. An extensive discussion of the sample, data processing techniques, and additional statistical analysis of the sample appear elsewhere (Brown 1998).

2. Sample Selection and Flux Determinations

The primary goal was to define an unbiased sample of early type galaxies for which a complete set of X-ray data could be obtained. We chose an optically-selected flux-limited sample of galaxies based upon the work of Faber et al. (1989), who obtained a consistent set of distances for these galaxies. This is essential for accurately establishing the L_X - L_B relationship and defining the scatter about the relationship.

The number of galaxies in the sample is a compromise between the desire to have many targets while avoiding many upper limits in the sample. Based upon the L_X - L_B relationship from the *Einstein Observatory,* we estimated that the percentage of detectable galaxies decreases significantly beyond the 30 - 40 optically brightest galaxies, for sensible exposure times with the PSPC or HRI on *ROSAT.* With 30 - 40 objects, calculations showed that we should be able to define the L_X - L_B relationship with sufficient accuracy to discriminate between competing models. Our final sample (Table 1) is comprised of the 34 optically brightest early-type galaxies in Faber et al. (1989) with $|b| > 20°$, while avoiding dwarf galaxies (e.g., NGC 185, NGC 205, NGC 221) and X-ray bright quasars (e.g., M87). X-ray data for about two-thirds of the sample were obtained from archival sources, with the remainder specifically observed for this project.

It is unclear how to best choose the region within which to define the X-ray emission from ellipticals because the flux increases logarithmically with radius for a typical X-ray surface brightness distribution. We have chosen to define the flux within an optically-defined radius since we are trying to test models related to the galaxy (e.g., mass loss from the stars). We extract our signal within a radius of $4r_e$, (r_e is de Vaucouleurs half-light radius), within which 85% of the optical light is contained. The background is taken between 4-6.3r_e for all galaxies, which removes the X-ray emission surrounding the galaxy, while maximizing the signal-to-noise. This method creates a very well defined L_X for this sample, although we recognize there may be an underestimation of the flux in some galaxies. For a few galaxies, such as the weakest sources observed with the HRI, the signal is defined within $1r_e$ and extrapolated to $4r_e$ to maintain consistency within the sample.

Raymond-Smith thermal plasma models were fit to X-ray spectra, under the assumption of a fixed metallicity of 50% solar and adopting the Galactic neutral hydrogen density column (N_H, fixed for each galaxy), which is accurate to about 5% (Hartmann & Burton 1997) in the northern hemisphere and to about 10% in the southern hemisphere (Dickey & Lockman 1990). For the 19 PSPC galaxies with enough photon counts to constrain the temperature (generally, >300 counts), a single-temperature model was fit. If the resulting x^2 was unacceptable, a two-temperature model was subsequently fit, with a "hard" component whose temperature was fixed at 2 keV (presumably, reflecting a stellar binary contribution); the softer component is assumed to be from the hot gas.

For the extraction of the flux, we used either the fitted temperatures or, for objects with few counts, we usually assumed $T_X = 1.5T_\sigma$ For a few objects with very low values of $1.5T_\sigma$, a minimum temperature of 0.3 keV was assumed, since lower temperatures were clearly a poor fit, even for objects with only 100 counts. We note that the luminosities are nearly independent of the metallicity assumed, and the temperatures have a modest dependence on the metallicity (for a metallicity that differs by a factor of two from our adopted value, the temperature changes by 10% or less).

3. Analysis and Interpretations

There can be a large correction to the flux from 0.1 - 0.5 keV due to Galactic absorption, so we will focus our discussion on the luminosities determined for the 0.5 - 2.0 keV band which is fairly insensitive to Galactic absorption corrections. A logarithmic plot of L_B (derived from Faber et al. 1989 magnitudes) against L_X is shown in Figure 1. Also included on the plot are stellar lines calculated from Cen A (Turner et al. 1997, van den Bergh 1976) and from M31 (Irwin & Sarazin 1998), an energy line contributed to thermalization and gravitational heating, and a line from supernovae heating.

The X-ray luminosity of the brightest galaxies can be compared to the maximum amount of energy expected from gravitational energy release (L_{grav}) or supernovae (L_{SN}). We find $\log L_{grav} = 23.57 + (5/3)\log L_B$ assuming that gas falls nearly to the center of the galaxy before cooling (Canizares, Fabbiano, & Trinchieri 1987; Dressler 1984), and $\log L_{SN} = \log L_B + 30.22$ using a supernova rate given by Turatto et al. 1994. Both L_{grav} and L_{SN} may contain uncertainties of a factor of around two (see Brown 1998).

The slope of the relationship between L_X and L_B is potentially quite important and has been the subject of much previous discussion. If we exclude NGC 5102 (where the X-ray emission is consistent with a stellar origin), the $\log L_X$-$\log L_B$ relationship has a slope of 2.72±0.27, using an orthogonal linear regression bisector method (OLS bisector; Feigelson & Babu 1992); there is considerable scatter, approximately 1.5 dex in L_X for a fixed L_B. When the hard X-ray component from Cen A is subtracted, so that L_X is only from the hot gas, the relationship becomes steeper, with a slope of 3.03±0.32. This is much steeper than the slope of approximately 5/3 that is expected from the model where gas is thermalized, remains bound to the galaxy, and falls inward.

The wide range of L_X for a given L_B and the steepness of the L_X - L_B relationship for the gaseous emission are inconsistent with the standard cooling flow model. We suggest a modification of the model that may help to resolve these problems. In this revised picture, environment plays a central role in determining the luminosity - galaxies are trying to drive galaxtic winds, but the visibility of the X-ray emission depends on whether the wind is stifled (pressure confined) by the ambient cluster or group medium. Observations support this in that the most X-ray luminous galaxies are generally associated with the richest environments, such as the Virgo cluster (NGC 4406, NGC 4472, NGC 4636, NGC 4649), the Fornax cluster (NGC 1399, NGC 1404), or in the centers of moderate richness groups (e.g., NGC 5846).

We find that many of these luminous galaxies are significantly hotter than T_σ, another inconsistency with the basic model (Figure 2). The slope of the $\log T_X$ - $\log T_\sigma$ relationship is 1.43±0.21, which is steeper than the nominal theoretical expectation ($T_X = T_\sigma$). Eight galaxies that are "too hot" relative to T_σ are NGC 1399, NGC 1404, NGC 1407, NGC 3923, NGC 4406, NGC 4472, NGC 4636, and NGC 5846. This list is nearly identical, with an overlap of 7/8 galaxies, to a list of the eight most X-ray luminous galaxies: NGC 1399, NGC 1404, NGC 1407, NGC 4406, NGC 4472, NGC 4636, NGC 4649, and NGC 5846 (in increasing NGC number). These overly hot temperatures would occur in a supernova-heated atmosphere confined by cluster or group medium.

There is a positive correlation between the L_X/L_B ratio and richness of environment (see Figure 3). Only X-ray faint galaxies are found in relatively isolated regions of space, whereas galaxies with the highest L_X/L_B ratios have many bright neighboring galaxies. Environment may have several effects on the hot gas content of a galaxy. In a very dilute surrounding medium, a supernova-driven galactic wind would occur (lowering the observed X-ray luminosity), but in a poor cluster (i.e., Virgo), the ambient medium may be adequate to pressure confine a wind, enhancing the X-ray luminosity of a galaxy. A competing process in richer environments is ram-pressure stripping, which would remove hot galactic gas, ultimately reducing its X-ray luminosity (Takeda, Nulsen, & Fabian 1984; Gaetz, Salpeter, & Shaviv 1987; Sarazin & White 1988). In very rich clusters, ram-pressure stripping should be the dominant

process, so X-ray emission from hot galactic gas may be unimportant.

The primary weakness of our suggestion lies with the metallicity, which is expected to be above the solar value given the observed supernova rates. The X-ray metallicities would suggest that the true supernova rate is 3 - 10 times lower than the published rates. An alternative explanation is that the observed supernova rates are accurate but that the metals are not mixed effectively into the hot galactic gas (see also Ciotti et al. 1991). Ineffective mixing of the metals would be necessary for our picture to remain viable. We look forward to the results of the ongoing supernova searches with CCD detectors, which should determine the observed rate to much higher accuracy.

We would like to thank a variety of people for valuable discussion: J. Irwin, J. Mohr, P. Hanlan, R. White, M. Loewenstein, G. Worthey, J. Parriott, M. Roberts, D. Hogg, and R. Mushotzky. Special thanks is due to the members of the *ROSAT* team and to the archiving efforts associated with the mission. Also, we wish to acknowledge the use of HEASARC and the NASA Extragalactic Database (NED), operated by IPAC under contract with NASA. Support for this work has been provided by NASA through grants NAGW-2135, NAG5-1955, and NAG5-3247; BAB would like to acknowledge support through a NASA Graduate Student Researchers Program grant NGT-51408.

References

Bregman, J. N., Roberts, M. S., & Hogg, D. E. 1992, ApJ, 387, 484

Brown, B. A. 1998, Ph.D. Thesis, University of Michigan.

Canizares, C. R., Fabbiano, G., & Trinchieri, G. 1987, ApJ, 312, 503

Ciotti, L., D'Ercole, A., Pellegrini, S., & Renzini, A. 1991, ApJ, 376, 380

Davis, D. S., & White, R. E. 1996, ApJ, 470, L35

Dickey, J. M., & Lockman, F. J. 1990, ARA&A, 28, 215

Donnelly, R. H., Faber, S. M. & O'Connell, R. M. 1990, ApJ, 354, 52

Dressler, A., 1984, ApJ, 281, 512

Faber, S. M., Wegner, G., Burstein, D., Davies, R. L., Dressler, A., Lynden-Bell, D., & Terlevich, R. J. 1989, ApJS, 69, 763

Feigelson, E. D., & Babu, G. J. 1992, ApJ, 397, 55

Forman, W., Jones, C., & Tucker, W. 1985, ApJ, 293, 102

Gaetz, T. J., Salpeter, E. E., & Shaviv, G. 1987, ApJ, 316, 530

Hartmann, D., & Burton, W. B. 1997, "Atlas of Galactic Neutral Hydrogen", Cambridge University Press

Irwin, J. A., & Sarazin, C. L. 1998, ApJ, **499**, 650.

Kim, D. W., Fabbiano, G., & Trinchieri, G. 1992, ApJ, 393, 134

Sarazin, C. L. 1990, in The Interstellar Medium in Galaxies, ed. H. A. Thronson, Jr. & J. M. Shull (Dordrecht: Kluwer), p. 201

Sarazin, C. L. & White, R. E. 1988, ApJ, 331, 102

Takeda, H., Nulsen, P. E. J., & Fabian, A. C. 1984, MNRAS, 208, 261

Tully, R. B. 1988, Nearby Galaxies Catalog (Cambridge University: Cambridge)

Turner, T. J., George, I. M., Mushotzky, R. F., & Nandra, K. 1997, ApJ, 475, 118

van den Bergh, S. 1976, ApJ, 208, 673

White, R. E., & Sarazin, C. L. 1991, ApJ, 367, 476

Table 1. Galaxy Properties

Name	D (Mpc)	logL_B ($L_\odot$)	logL_x erg/s	T_σ (keV)	T_X	Name	D (Mpc)	logL_B ($L_\odot$)	logL_x erg/s	T_σ (keV)	T_X
N 0720	41.00	10.95	41.10	0.387	0.436*	N 4278	29.40	10.72	40-55	0.450	...
N 1316	28.44	11.34	41.08	0.403	0.351*	N 4365	26.66	10.79	40.48	0.390	0.200
N 1344	28.44	10.66	39.47	0.163	...	N 4374	26.66	10.99	41.09	0.524	...
N 1395	39.80	11.02	41.04	0.424	0.437*	N 4406	26.66	11.10	41.80	0.397	0.823
N 1399	28.44	10.88	41.44	0.610	0.944	N 4472	26.66	11.32	41.77	0.524	0.936
N 1404	28.44	10.74	41.27	0.323	0.557*	N 4494	13.90	10.20	39.28	0.300[a]	...
N 1407	39.80	11.16	41.34	0.517	0.913	N 4552	26.66	10.71	40.92	0.434	0.405*
N 1549	24.26	10.73	40.04	0.267	0.186	N 4621	26.66	10.78	39.79	0.367	...
N 2768	30.64	10.79	40.41	0.248	...	N 4636	26.66	10.96	41.81	0.232	0.717
N 3115	20.42	10.83	39.74	0.450	...	N 4649	26.66	11.14	41.48	0.740	0.823
N 3377	17.14	10.21	39.42	0.108	...	N 4697	15.88	10.58	40.13	0.173	0.206*
N 3379	17.14	10.49	39.78	0.257	...	N 5061	23.92	10.53	39.54	0.233	...
N 3557	47.98	11.10	40.61	0.541	...	N 5102	3.10	8.95	37.70	0.500[a]	...
N 3585	23.54	10.72	39.84	0.308	...	N 5322	33.22	10.80	40.11	0.319	0.205
N 3607	39.82	11.18	40.82	0.390	0.372	N 5846	46.72	11.26	42.01	0.491	0.733
N 3923	31.66	10.99	40.90	0.297	0.549	I 1459	44.50	11.14	41.19	0.601	0.414*
N 4125	39.72	11.16	41.01	0.332	0.283	N 7507	35-00	10.82	40.13	0.361	...

Distance, L_B, and T_σ derived from Faber et al. (1989) values. H_0 = 50 km/s/Mpc used throughout.
Starred values in the T_X column denote a two temperature fit value where the 2nd component is fixed at 2.0 keV.

[a]Adopted value for T_σ

Figure 1

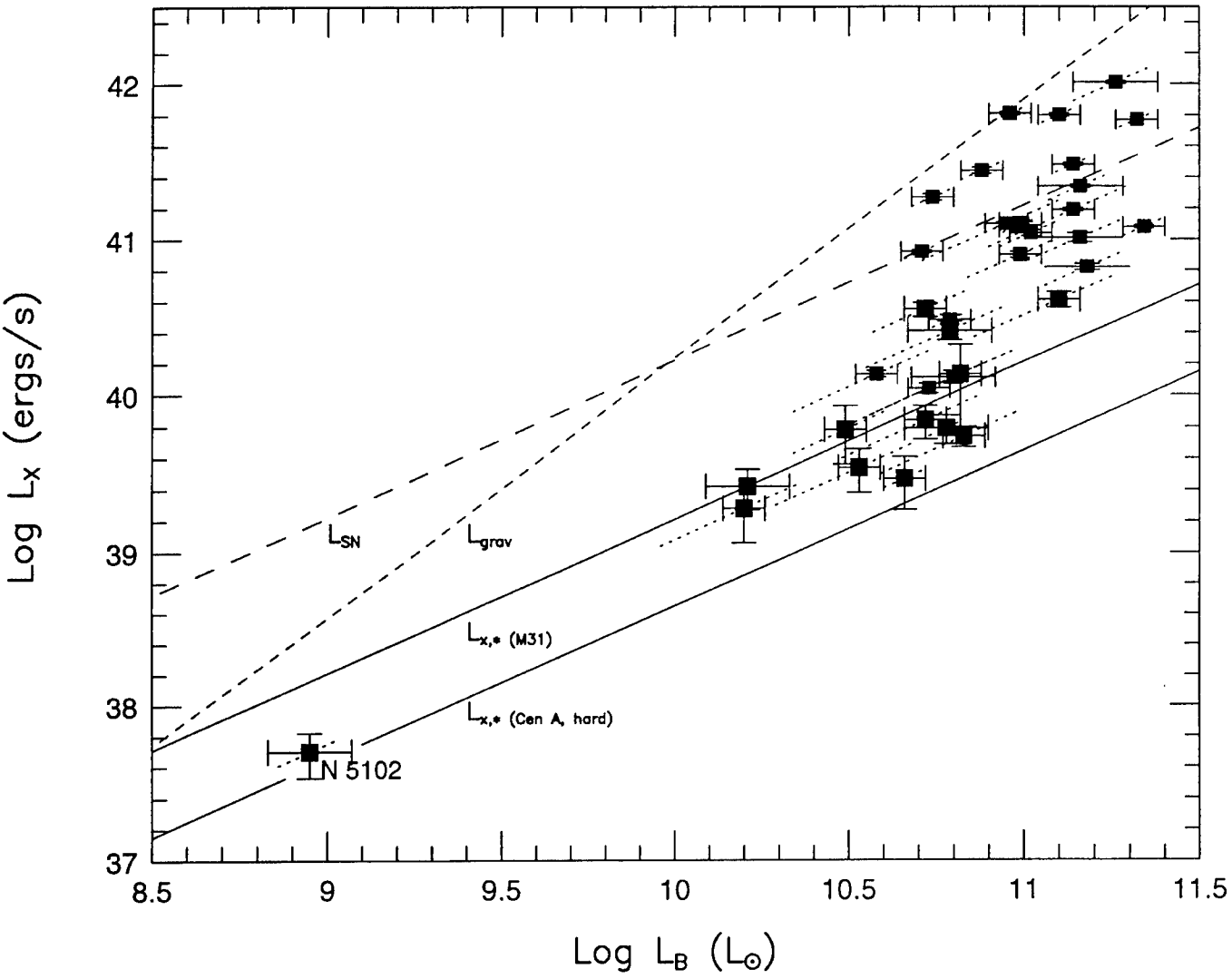

Figure 1. The 0.5-2.0 keV luminosities (in ergs s^{-1}) from the *ROSAT* PSPC and HRI instruments are given against their optical blue luminosities (in solar luminosities). The uncertainties due to distances are shown as dashed lines of slope unity while errors due to distance-independent effects (e.g., photon statistics) are shown as the usual horizontal and vertical lines. The solid lines, $L_{x,*}$, are the stellar X-ray contributions as determined from M31 and the hard component of Cen A, while the dashed lines labeled L_{SN} and L_{grav} represent the energy released from supernovae or available from thermalization and gravitational infall.

Figure 2

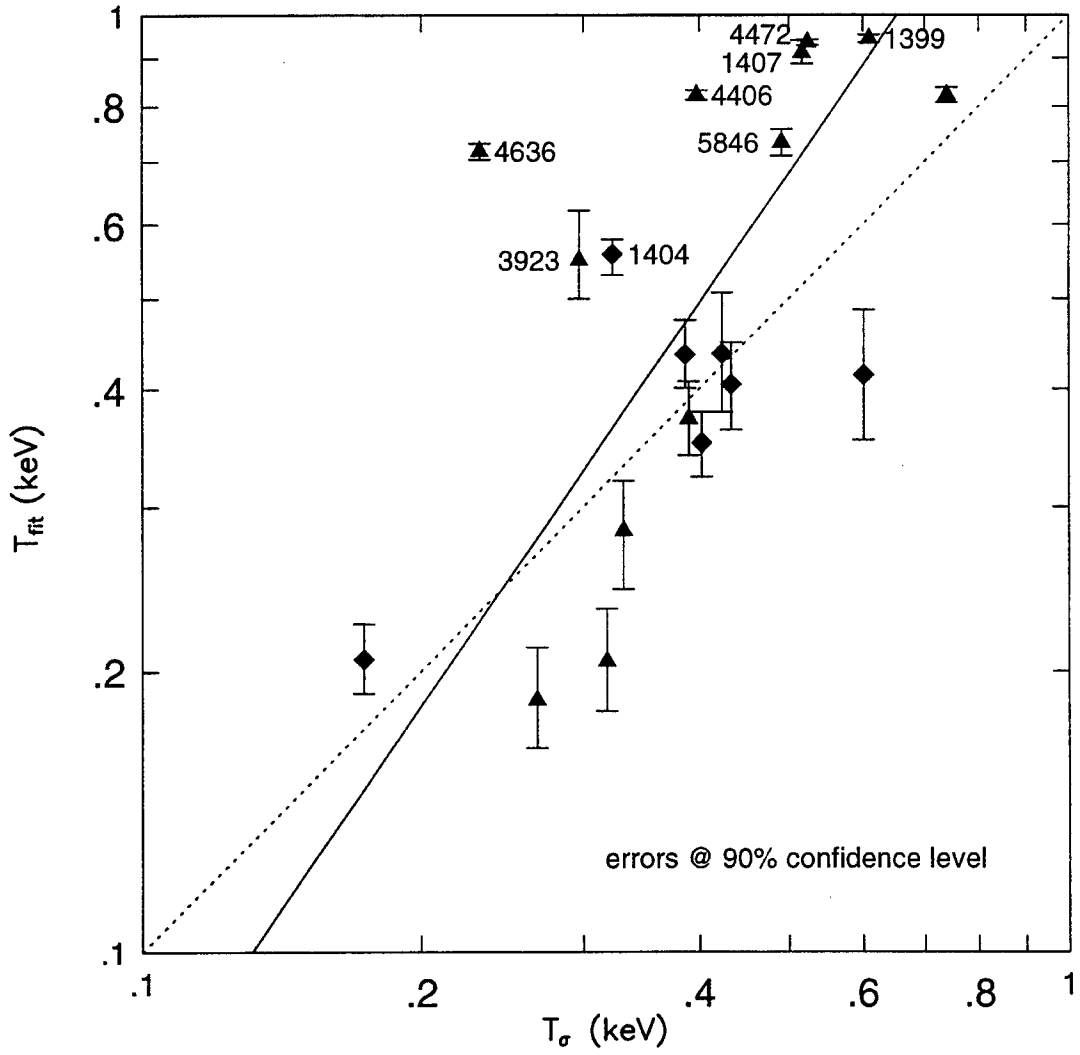

Figure 2. The gas temperature, as determined from fitting the X-ray spectral distribution vs the temperature corresponding to the velocity dispersion of the stars for high-count galaxies. The triangles denote single-temperature fits while the diamonds denote two-temperature fits. The uncertainties shown are 90% confidence errors. The dashed line denotes the $T_1 = T_\sigma$ relation. The solid line is the orthogonal linear regression bisector fit line.

Figure 3

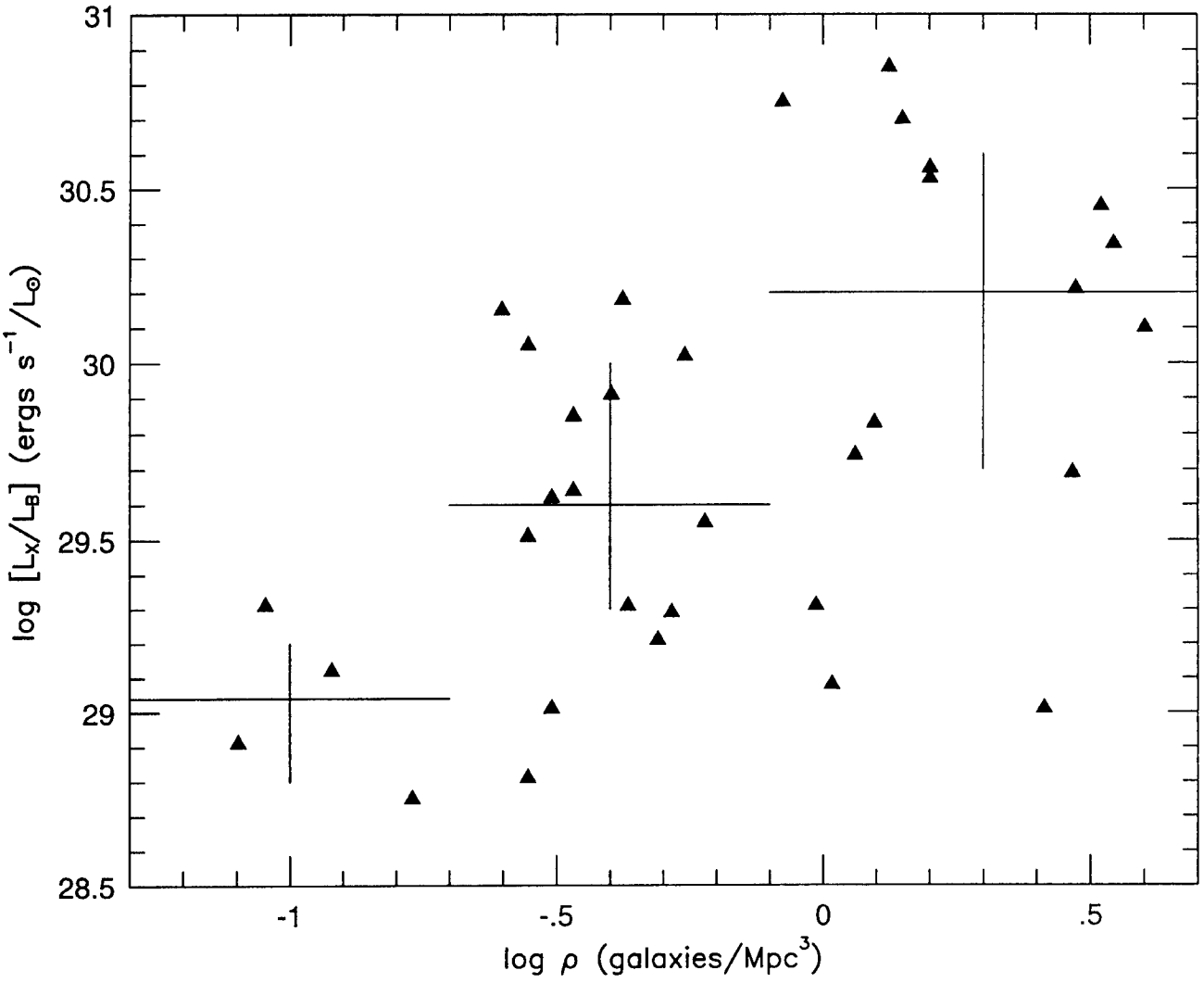

Figure 3. The ratio of the X-ray to optical luminosity vs. the local density of galaxies (per Mpc^3) brighter than -16mag in the vicinity of each galaxy (Tully 1988 values). The horizontal lines delineate the width of each bin and mark the median ration within each bin. The vertical lines are the magnitude of the upper and lower quartile values within each bin.

VIGILANTE: An Overview of a GPS Based ATR System

Kenneth A. Brown
Carl Christian Liebe
Suraphol Udonikesmaleel
Curtis Padgett
Michael Brenner
Ayanna Howard
Terry Wysocky
David Brown
California Institute of Technology

Steven Suddarth
Ballistic Missile Defense Organization

Abstract

The VIGILANTE project is a planned vision system capable of tracking and recognizing targets in real time, on a small airborne platform. The project consists of two parts, 1) the Viewing Imager/Gimballed Instrumentation Laboratory (VIGIL), which is an infrared and visible sensor platform with appropriate optics and 2) the Analog Neural Three-dimensional processing Experiment (ANTE), a massive parallel, neural based, high-speed processor.

The VIGIL platform is mounted on a helicopter equipped with Global Position System (GPS), Inertia Measurement Unit (IMU), gimbal, radio-link and anti-vibration platform. Also, a jet powered, radio controlled VIGILANTE Target Vehicle (VTV) has been manufactured and equipped with GPS. In the first stages of the project, the VIGIL system is used to acquire image sequences of the VTV for training and testing of the ANTE image recognition processor. Based on GPS and IMU input, the gimbal is pointed toward the VTV and acquires images.

This paper describes the VIGIL system in detail. It discusses position-based pointing, tracking algorithms and the alignment procedure. Test imagery and an evaluation of the system will be presented.

1. Introduction

Small air and space borne systems capable of autonomous acquisition and identification of hostile targets (e.g., cruise missiles, missile launchers etc.) will become an essential component of the Ballistic Missile Defense Organization's (BMDO) planned defensive mechanisms. Such Automatic Target Recognition (ATR) capability could greatly increase the capabilities of interceptors (for cruise and ballistic missiles), surveillance platforms (for missile launchers), and ground-based fire control.

The VIGILANTE project at Jet Propulsion Laboratory (JPL) [1] provides a low-cost

airborne platform that combines new sensors with advanced neural network processing algorithms for detection, recognition and tracking of missile threats. The project consists of two parts, the airborne VIGIL platform and the ANTE ATR processor.

VIGIL (Viewing Imager/Gimballed Instrumentation Laboratory) is a helicopter-based gimballed camera platform providing data acquisition for target training/ recognition experiments as well as testing of novel active and passive focal plane imagers. VIGIL provides realistic image conditions for airborne targets seen from above. To point the sensors toward the target (before the ANTE ATR becomes operational), both the helicopter and the VTV are equipped with GPS receivers, to provide the pointing information. ANTE (Analog Neural Three-dimensional processing Experiment) is a prototype image-processing/target-recognition computer architecture based upon technology developed under the ongoing 3 dimensional artificial neural network (3DANN) program. 3DANN is a sugar-cube-sized, low-power neural processor. It is capable of performing 64 simultaneous image convolutions with a 64x64-kernel size in real time [2] - [6]. This system will not be described further in this paper.

This paper describes VIGIL in detail. The algorithms for pointing the cameras towards the VTV are described. Also, the alignment procedures and noise sources are discussed.

2. Description of the VIGIL system

The VIGIL system consists of an airborne helicopter equipped with the gimbal sensor platform and a jet-powered target called the VTV.

The VTV: A reusable, remote controlled target vehicle supports testing of VIGILANTE. Field testing of actual target signatures and backgrounds provides realistic scenarios needed to train and evaluate the ANTE system and its associated ATR algorithms. The VTV resembles a cruise missile, but is flown as a remote-controlled aircraft. An infrared signature is obtained from a Turbomin turbine engine producing 22 pounds of thrust for a flight time of about 15 minutes. The VTV is depicted in figure 1. It is 2.42 meters long, has a 1. 18 meter wingspan and a mass of ≈ 20 kilos.

The airborne platform: The system is currently mounted on a Hughes 500 helicopter.[1] The helicopter and the system are depicted in figure 2.

As shown in figure 2, the VIGILANTE system consists of many sub-systems. In figure 3, a sketch of the system is shown. The rest of this section will describe the subsystems in details.

Quantom Well Infrared Photo Detector (QWIP) is a 256x256 pixel, real-time (30 to 120 Hz) IR sensor array. QWIP is a major advancement compared to state-of-the-art HgCdTe sensors. The sensor has an 8 to 9 pm central wavelength detection capability with a 1 pm full width at half maximum, and the design uses a random reflector on each pixel to maximize light trapping. The QWIP sensors are based on GaAs.

Visible Camera: A color Cohu CCD 768 x 494 pixel camera is used. The camera is mounted with a Fujinon 300 mm zoom lens. In near future, the CCD camera will be replaced with an active pixel sensor camera.

Vibration Isolation System: The Mechanical Engineering Department, University of Maryland has built an active/passive two stage vibration isolation control system for the project. The system operates on passive air mounts arranged in series with another stage of active electromagnetic actuators. The active stage is used to isolate the base excitation from the intermediate platform whose vibration is isolated from the primary system by the passive stage. The vibration isolation control system is broken into two parts. The first part is the two stage vibration isolation control box and the other is the control computer. The vibration isolation box is made of a composite material and contains the actuators, passive isolation, accelerometers and rate triad. The control computer contains the executable code, which logs the data and controls the I/0. There are two modes of operation for the system. The first mode is a continuous operation mode that isolates the optical bench with S/W controlled gain parameters, which have been optimized for a specific camera configuration.

The other mode of operation is the data acquisition mode where the computer logs the output of the accelerometer and rate triads- Under most conditions, the vibration bench reduces vibration-related acceleration by a factor of ten.

TWO AXES GYRO-STABILIZED GIMBALED MIRROR: The VIGILANTE gimbal is a two-axis gyro stabilized gimbal mirror constructed by Fraser-Volpe. The gimbal system consists of the gimbal electromechanical device and support electronics. The gimbal has an inner (horizontal) and outer (vertical) axis. The inner axis moves from -20 to +52 degrees and the outer axis moves +/- 45 degrees. The gimbal has two modes of operation: in position mode the mirror moves to the commanded position, in rate mode the mirror slews at the command rate. The gimbal has RS 232 interface to the telemetry system for commands and data. The gimbal position is read out automatically and transmitted to the ground station at ≈ 20 Hz.

TELEMETRY SYSTEM: The VIGILANTE Telemetry system consists of three subsystems, as shown in figure 3. The first subsystem is the Ground Station, which receives all the data from the helicopter and the VTV. The second subsystem is the helicopter telemetry system consisting of two video down link channels (only one is shown in figure 3), command and data system, an attitude GPS system, gimbal and an IMU. The third subsystem is the GPS system on the VTV.

- The airborne telemetry subsystem for the VIGILANTE helicopter is comprised of. Two video transmitters (one is depicted in figure 3) that sends the images from the camera platform at 2.35-2.45 GHz down for ground-based recording and processing. A Communication Router (CR) distributes the commands from the ground to the airborne instrumentation and returns the GPS, Inertial Measurement Unit (IMU) and gimbal data to the ground station. The CR is a Motorola-based processor that receives commands from the ground and sends the data back at 57.6 K baud. The CR contains a 900MHz Freewave modem that sends and receives the data. The Attitude GPS system consists of a Pentium computer and 4 GPS receivers. The Attitude GPS system collects the GPS data from the 4 antennas, applies the received differential correction from the ground station and calculates a 4-antenna attitude solution (note the GPS antennas on figure 2). It then transforms the attitude solution from the GPS antenna reference frame to the aircraft reference frame. The attitude system then sends the attitude (pitch, yaw and roll), position of the aircraft (north, east, and altitude), velocities (north, east and down) and the GPS time to the ground control station. The Inertial Measurement Unit (IMU) is located on the optical bench so it is vibration isolated. The IMU transmits the accelerations and the roll rates in three axes through the CR at 50Hz.
- The ground station receives GPS data from a GPS antenna. It calculates the differential corrections and sends that information to the VTV and the helicopter. The ground station receives all the data from the aircraft and the VTV and sends it to VIGIL computer. The ground station contains two 57.6 K baud freewave modems and antennas (only one is show at figure 3), one for the VTV and the other for the helicopter command and data.
- The VTV hardware consists of a GPS antenna/receiver and a freewave modem/ antenna to receive the differential corrections and to send the position and velocity data to the ground station. The VTV calculates the latitude, longitude and altitude as well as the velocities east, north and down and transmits them to the ground station at 10Hz. The ground station calculates the relative VTV position with respect to the ground station.

3. Algorithms

The algorithms will evolve through two phases: In the early phases of the project, they will point the gimbal mirror toward the target, exclusively based on GPS information. The resulting acquired images will be used for training and evaluation of the ANTE recognition processor. Later in the project, the ANTE recognition processor will be included in a closed loop. Based solely on imagery, ANTE commands the gimbal mirror without

GPS information to demonstrate real time image processing capabilities. This paper will exclusively deal with pointing based on GPS information.

VIGIL's algorithms are based on four different coordinate systems (CS):

- The Ground Station Coordinate System (Ground-CS). The origin of the GROUND-CS is defined in the WGS-84[2] system. The geographical position of the GROUND-CS origin is irrelevant to VIGILANTE, as only the relative position of the helicopter and the VTV are important. The GROUND-CS is a Cartesian (flat earth) right hand coordinate system. The axes are defined as follows: The X-axis is pointing toward North. The Y-axis is pointing toward East and the Z-axis is pointing downwards. The units are in meters. Both the VTV and the helicopter positions are given in this coordinate system.
- The Helicopter body based CS (Helicopter-CS) is a right hand coordinate system. The origin is defined as being the right of the 4 GPS antennas on the helicopter. The X-axis is pointing forward on the helicopter. The Y-axis is pointing to the right (seen from above), and Z-axis is pointing downwards. The units are in meters. The IMU is aligned with the helicopter CS.
- The camera coordinate system (Camera-CS) is a right hand coordinate system. The origin is at the intersection of the optical axis and the CCD chip. The Z-axis is pointing backwards on the helicopter towards the gimbal mirror. The X-axis is pointing to the left (seen from above) and Y-axis is pointing down. The units are in meters.
- The gimbal-based coordinate system (Gimbal-CS) is a right hand coordinate system referring to the optical axis caused by the Gimbal mirror. The origin of the Gimbal-CS is at the center of the Gimbal mirror. The Gimbal-CS is defined as the CAMERA-CS translated to the Gimbal mirror center, and rotated ϕ degrees (right hand positive) around the Camera-CS z-axis. Successively the CS is rotated φ degrees (right hand positive) around the new y-axis. The units are in meters.

In figure 4 a sketch of the helicopter and the CS's is shown.

The attitude of the helicopter is a combination of IMU and GPS attitude data that is updated continuously. This is because the GPS attitude data has proven to be unreliable, and hence the attitude system was made redundant by utilizing an IMU. The algorithm for calculating the attitude is shown in figure 6.

4. Alignment

There are position and angular uncertainties in the mechanical mountings. The position uncertainty on the helicopter due to inaccurate measurements or mountings is estimated to be on the order of centimeters. Assuming that the target is several hundred meters away from the helicopter, these uncertainties can be neglected. However, there are 3 rotational uncertainties that can not be neglected:

- Rotation from Ground-CS to the GPS antenna plane is very accurate. However, the successive rotation to the Helicopter-CS (described in 2. DESCRIPTION OF THE VIGIL SYSTEM) is based on a rotation provided by the user. This rotation is initially found using a compass and leveler etc. It is estimated that the user, trying to measure this rotation could introduce an error of several degrees in each axis.
- The camera mounts are not precision mounts. It is estimated that there may be several degrees of error in each axis.
- The commanded gimbal angles may have an offset; i.e. 0 degrees may not be pointing orthogonal to the helicopter. It is estimated that this angle may have several degrees of error in each axis.

A realistic model of the rotations (translations not included in this model) that the VTV coordinates undergoes is sketched in figure 7.

There are at least 8 unknown angles in this model. It would be a very cumbersome procedure to determine and correct all these angles. Besides, the configuration of the helicopter changes often, so a calibration procedure that only takes minutes is absolutely necessary. The following

approximation has been made for making an easy calibration procedure: All misalignment rotations are collected in one single calibration rotation, which is supposed to counter rotate all the misalignments. This is depicted in figure 8.

The procedure for calibration is as follows: The tracking algorithm as displayed in figure 5-6 is initiated. The VTV is placed approximately orthogonal to the helicopter (by eyeballing). Most likely the gimbal is not pointed toward the VTV. Buttons can be used to adjust the calibration angles interactively until the VTV is in the center of the field of view. This procedure takes only a few minutes. It is estimated that the error introduced by this procedure is a fraction of a degree, which is acceptable for this experiment.

5. Experimental results

The VIGIL system has been debugged and tested at the Flight Research Inc., Mojave airport, CA. Initially the noise of a static scene is considered. This is the noise equivalent angle (NEA) of the system.

Position error on the VTV and the helicopter: The VTV and the helicopter positions are differential GPS positions at 10 Hz. In figure 9, the north/altitude of the VTV position is displayed for a static VTV. It is estimated that north/east noise (RMS) is less than a meter for the VTV and the helicopter, and that the altitude noise (RMS) is a couple of meters for both. It is expected that the noise would be larger in altitude due to the satellite geometry.

Attitude noise from the GPS system. The attitude of the helicopter is calculated at 10 Hz and based on updates from the 4 GPS antennas (shown in figure 2). Figure 10 shows the raw yaw and roll output of the GPS attitude. The noise (RMS) is significant lower than a degree. The roll angle is noisier than the pitch/heading angle because of a shorter baseline.

Unfortunately, the GPS attitude is not very stable. Hence, it is backed up by an IMU that is being integrated with 50 Hz. The algorithm was shown in figure 6. To illustrate the superiority of this approach, the raw yaw GPS attitude is shown together with the combined yaw attitude for a helicopter flight in figure 11.

All small individual noise contributions are added together in the noise on the gimbal angles. The two gimbal angles are shown in figure 12.

The NEA is only one element of the total pointing error budget. When things are moving, additional errors are introduced. At this early stage of the project it is impossible to make a complete error budget. However, a qualitative description of the source of additional error terms are given below:

- Nonlinearity due to collecting all alignment rotations in one alignment rotation: It is not mathematical correct to merge different rotations with different origins in the same rotation. This will introduce an error. It is estimated that this error is less than one degree.
- Flexin in the fuselage of the helicopter: During calibration, the helicopter is on the ground and the skids are carrying the weight of the helicopter. In flight, the rotor pulls the weight of the helicopter. This generates some flexing in the fuselage of the helicopter. This could amount to one degree.
- Propagation delay : There is a propagation delay in the radio modem at approximately 30 milliseconds. This means that GPS positions are old when they are received and, once the new gimbal angles are calculated it will take another 30 milliseconds before they reach the gimbal. This effect is somewhat mitigated by extrapolating the gimbal angles to the future. This effect is only significant when the VTV is making turns.
- Limited sampling frequencies: All signals are sampled. IMU is 50 Hz, GPS is IOHz, VTV position is 10 Hz and Gimbal position is 20 Hz. This limited sampling frequency will introduce an error when things are moving.

It has not yet been possible to make a thorough assessment of the equipment. However, during the first flights the equipment worked fine. The best way to illustrate the system capabilities is to show a series of selected pictures that was acquired of

a prototype VTV, with the VIGIL helicopter on the ground. The images are shown in figure 13.

6. Summary

This paper has been describing the VIGILANTE system. The flying target is equipped with GPS and radio modem. The helicopter is equipped with an active vibration isolated bench and a radio modem. On the bench, an IMU, gimbal, IR and visible camera are mounted. Outside the helicopter fuselage 4 GPS antennas are mounted. These provide a 4-antenna GPS attitude solution.

There are defined four coordinate systems, a ground based CS, a helicopter based CS, a camera based CS and a gimbal mirror based CS. The algorithms consist of successive coordinate translations and rotations of the target coordinates though the coordinate systems until the gimbal angles are calculated. The gimbal is finally commanded to a rate proportionally to the difference between the present mirror position and the calculated gimbal mirror position. The attitude GPS has proven to be unreliable, and is therefore backed up by the IMU.

There are multiple sources of mechanical misalignment on the helicopter. Positional errors are small compared to the target distance and are ignored. All rotational uncertainties are collected in one alignment rotation. It is possible to adjust the Euler angles of this alignment rotation iterative, until the target is boresighted. This procedure only takes a few minutes and introduces an insignificant error.

The system has been tested in the Mojave dessert. The random noise of the system is a fraction of a degree. The noise is larger when both the helicopter and the VTV are airborne simultaneous. With a target distance of $\approx$ 1 km and a field of view of 2.5 degrees, the VTV is in the field of view most of the time.

7. Acknowledgement

The research described in this paper was carried out by the Jet Propulsion Laboratory, California Institute of Technology, and was sponsored by the Ballistic Missile Defense Organization through an agreement with the National Aeronautics and Space Administration. Additional funding provided by the National Physical Science Consortium.

References herein to any specific commercial product, process, or service by tradename, trademark, manufacturer, or otherwise, does not constitute or imply its endorsement by the United States Government or the Jet Propulsion Laboratory, California Institute of Technology.

8. Notes

1 A dedicated VIGILANTE helicopter has been constructed, and will be used in later stages of the project. The algorithms are constructed for this helicopter, assuming that the mirror is pointing to the right. However, on the Hughes 500 helicopter it was necessary to mount the system pointing to the left. Therefore there are small inconsistencies between the images and the figures.

2 World Geodetic System 1984

9. References

1) S. Udomkesmalee et al: VIGILANTE: An Advanced Sensing/Processing Testbed for ATR Applications, SPIE Vol. 3069, p. 82-93.

2) S. Udomkesmalee, S. C. Suddarth: VIGILANTE: Ultrafast smart sensor for target recognition and precision tracking in a simulated CMD scenario. AIAA/BMDO Technology Readiness Conference, San Diego, August 18-22, 1997.

3) N. Alhambra, S. C. Suddarth, S. Udomkesmalee: VIGILANTE Data Handling System: ASIM for Automatic Target Recognition. GOMAC'98 Micro-Systems and Their Applications, Arlington, Virginia, March 16-19, 1998.

4) A. Howard, C. Padgett, and C. C. Liebe: A multi-stage Neural Network for Automatic Target Detection, to appear in international Joint Conference on Neural Networks (IJCNN), May 1998.

5) C. Padgett and G. Woodward: A Hierarchical, Automated Target Recognition for a Parallel Analog Processor. The 1997 IEEE International Symposium on Computational Intelligence in Robotics and Automation, p. 374-379, Monterey, July 1997,

6) C. Padgett, M. Zhu, and S. Suddarth: Detection and orientation classifier for the VIGILANTE image processing system, Proceedings of SPIE Vol. 3077 pp. 191-201. Editors Rogers, S. April 1997.

7) J. Werts. Spacecraft Attitude Determination and Control. D. Reidel Publishing Co., MA, 1978.

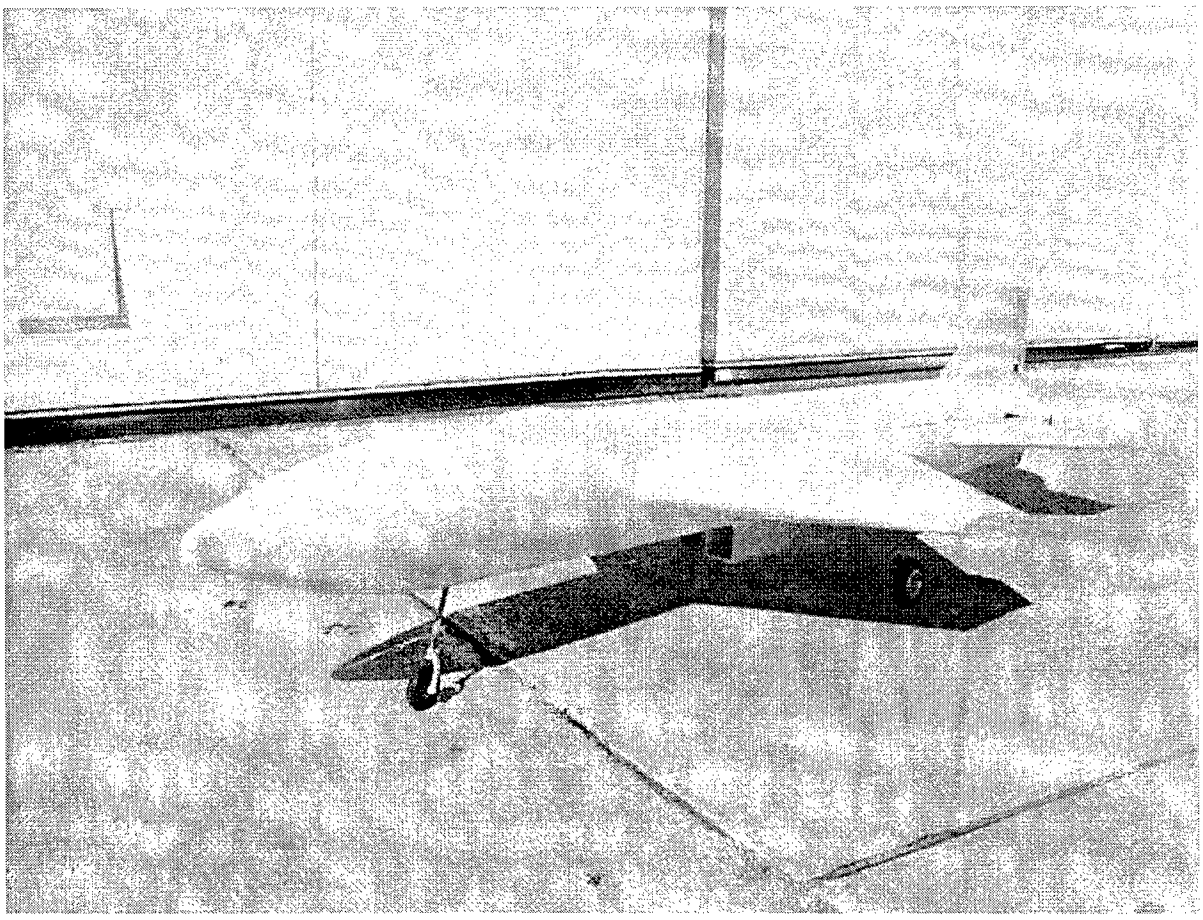

Figure 1. The VTV.

Figure 2a. The VIGIL helicopter.

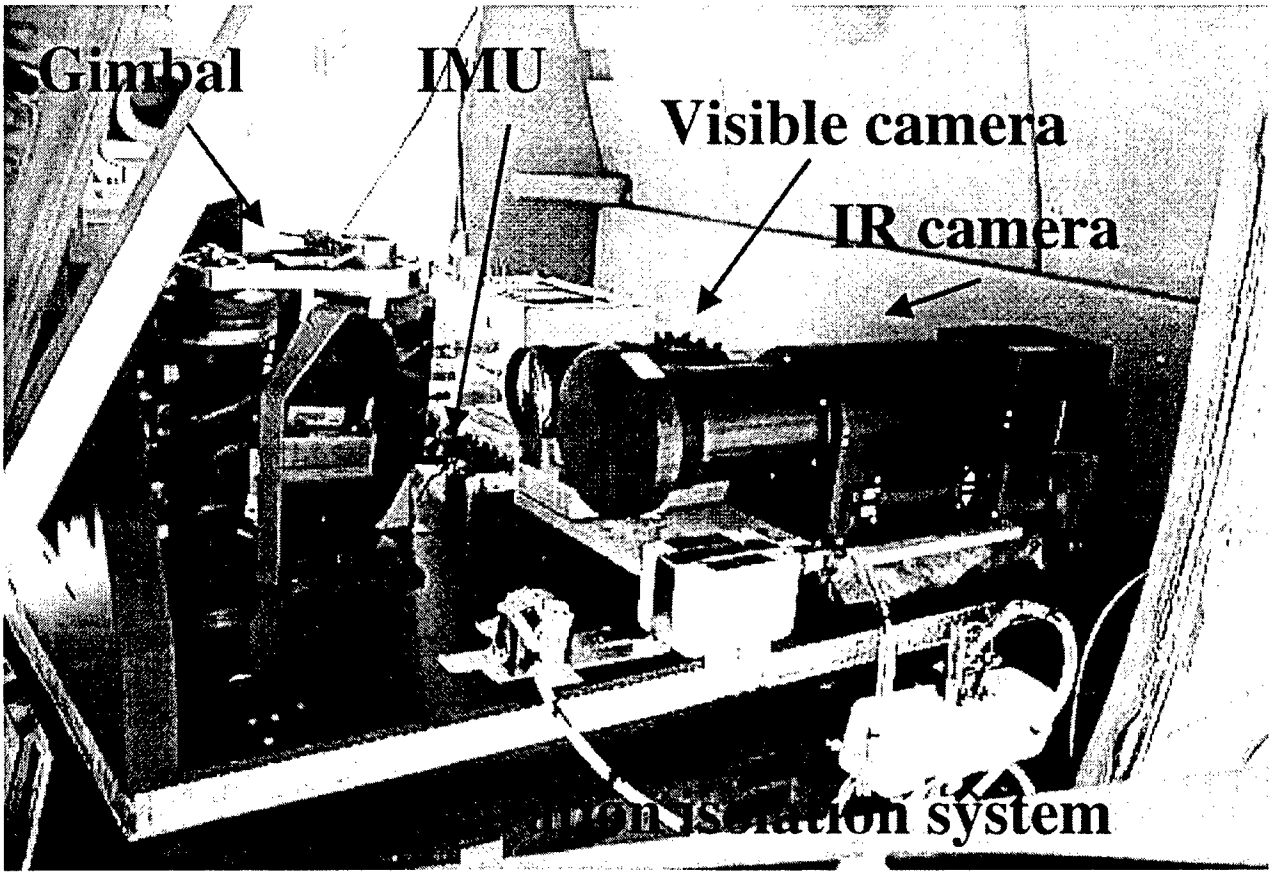

Figure 2b. Close up of the cargo bay in the helicopter with the camera platform.

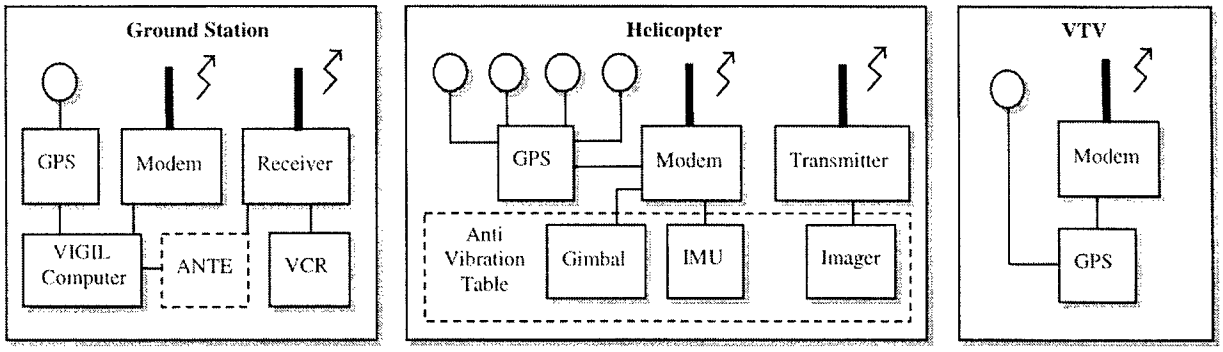

Figure 3. Block diagram of teh VIGILANTE system.

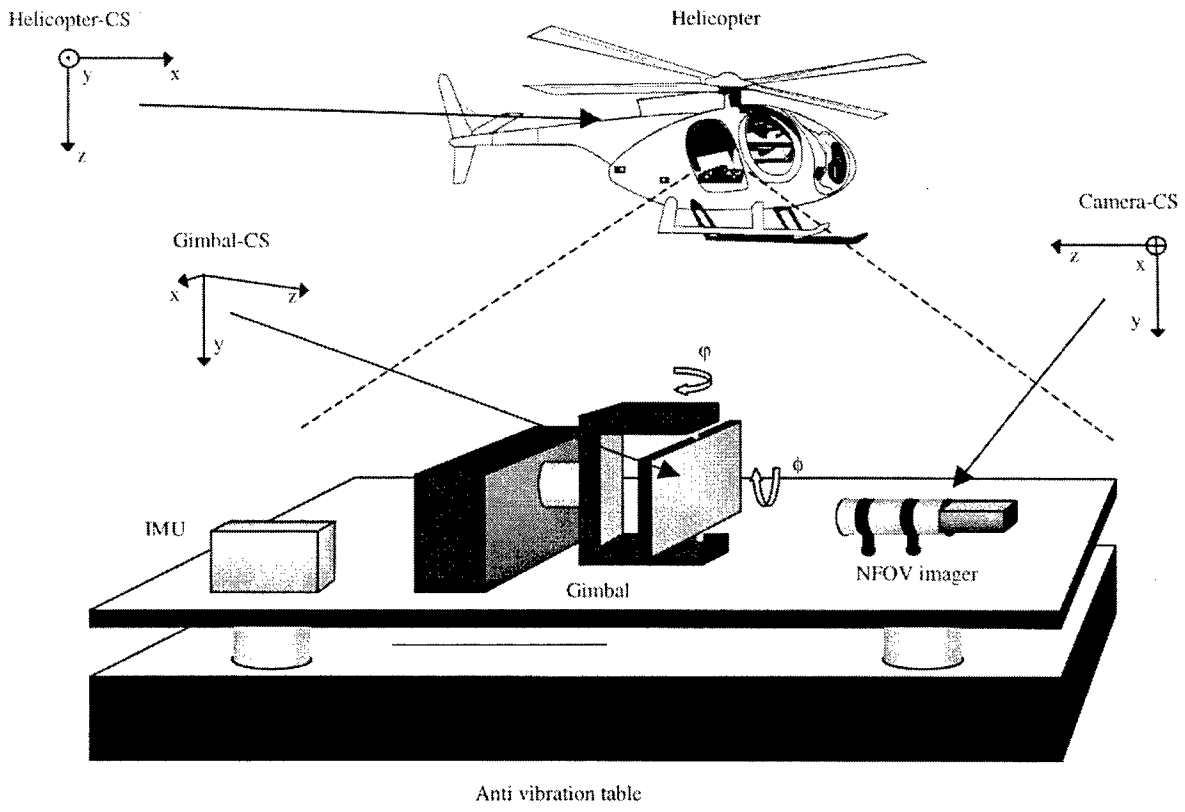

Figure 4. Sketch of the VIGIL helicopter, with its different coordinate systems (NFOV = Narrow Field of View).

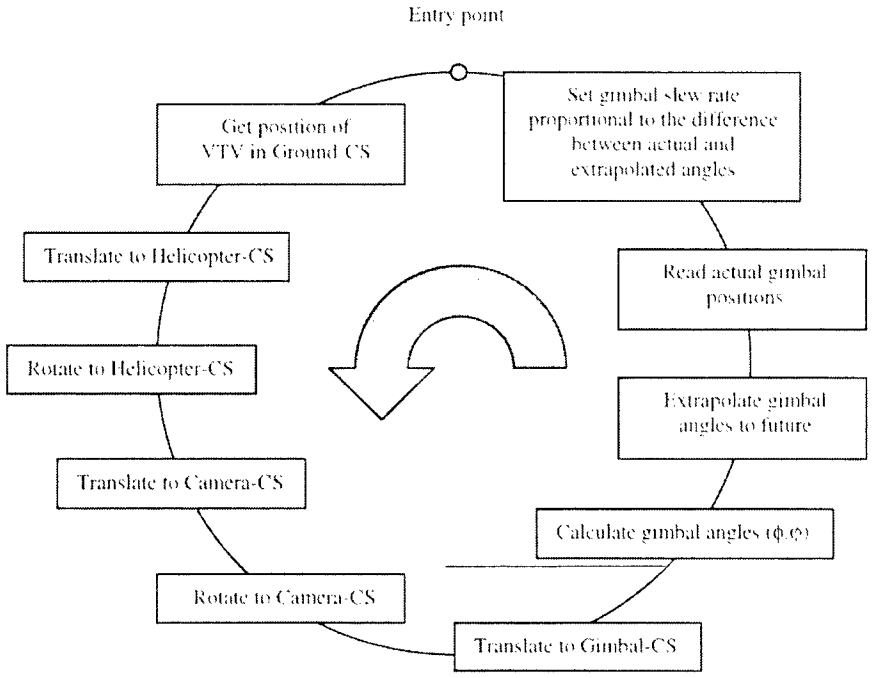

Figure 5. The gimbal pointing algorithm. The algorithm calculates gimbal rates. The commanded gimbal rate is proportional to the error, in the control-loop.

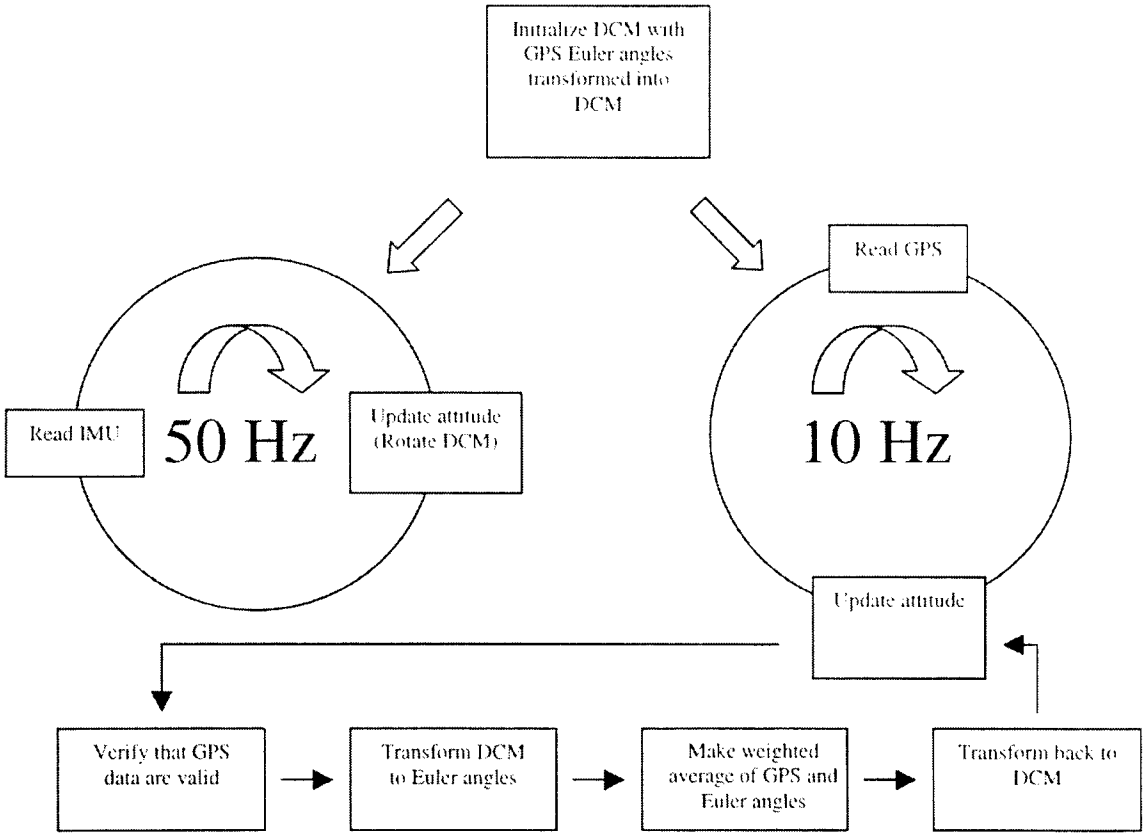

Figure 6. Algorithm for updating the attitude (DCM = Directional cosine matrix).

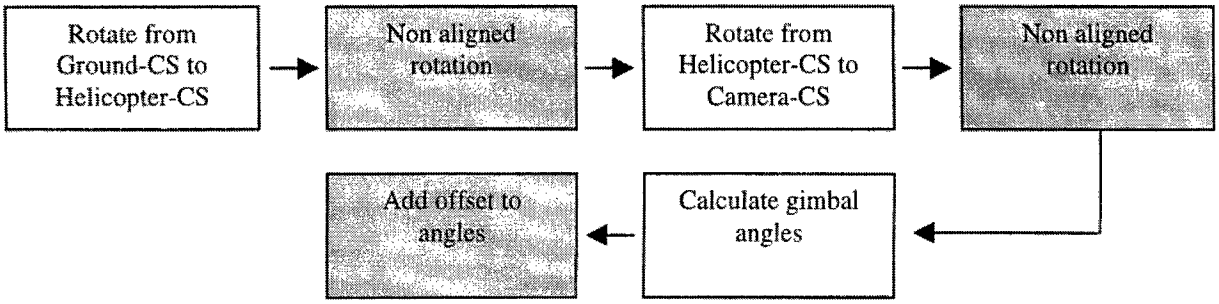

Figure 7. A realistic model of coordinate rotations, 8 degrees of freedom.

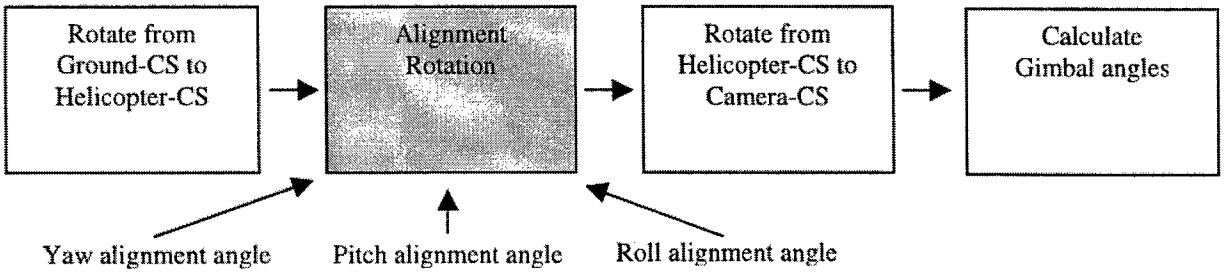

Figure 8. An approximation of the coordinate rotations, 3 degrees of freedom.

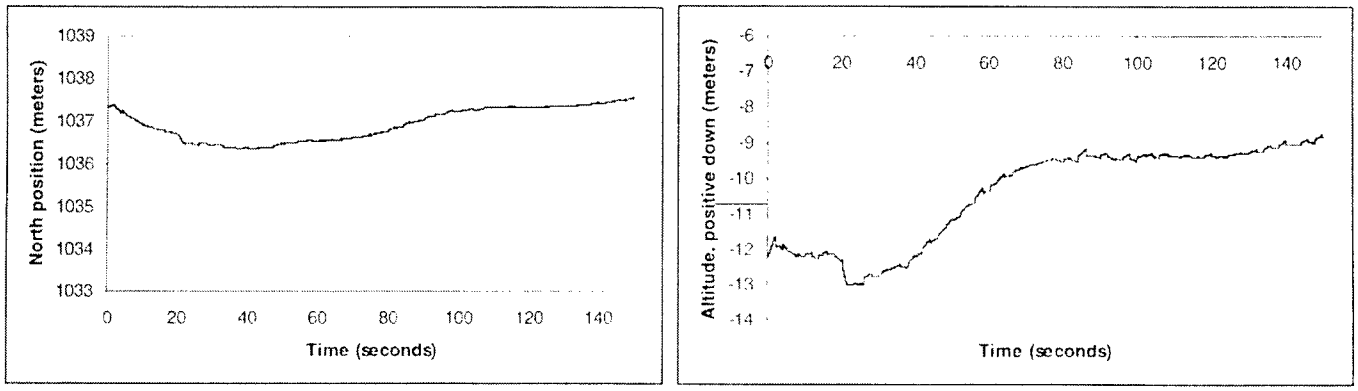

Figure 9. The VTV position of North and Altitude. The RMS noise is 0.4 and 1.4 meters.

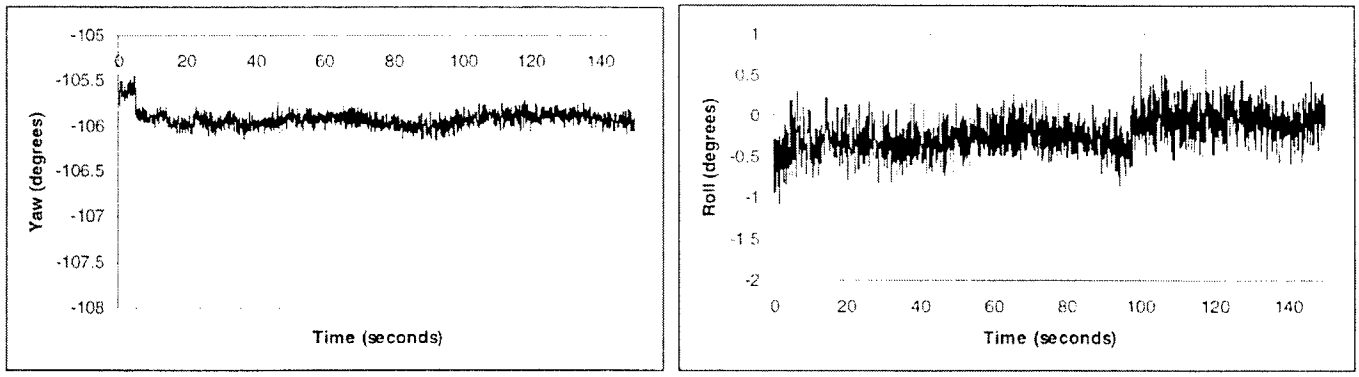

Figure 10. The raw yaw and roll attitude from the GPS. The RMS for yaw is 0.09 degrees and for roll is 0.24 degrees.

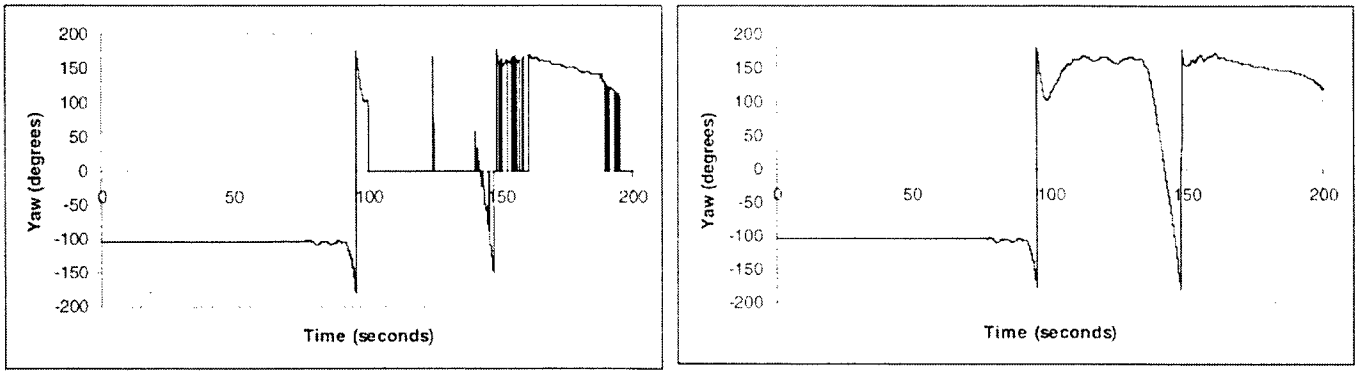

Figure 11. The raw yaw GPS attitude and the combines attitude. The jump from -180 to 180 degrees occurs crossing south. GPS attitude is 0 degrees when no valid attitude exists.

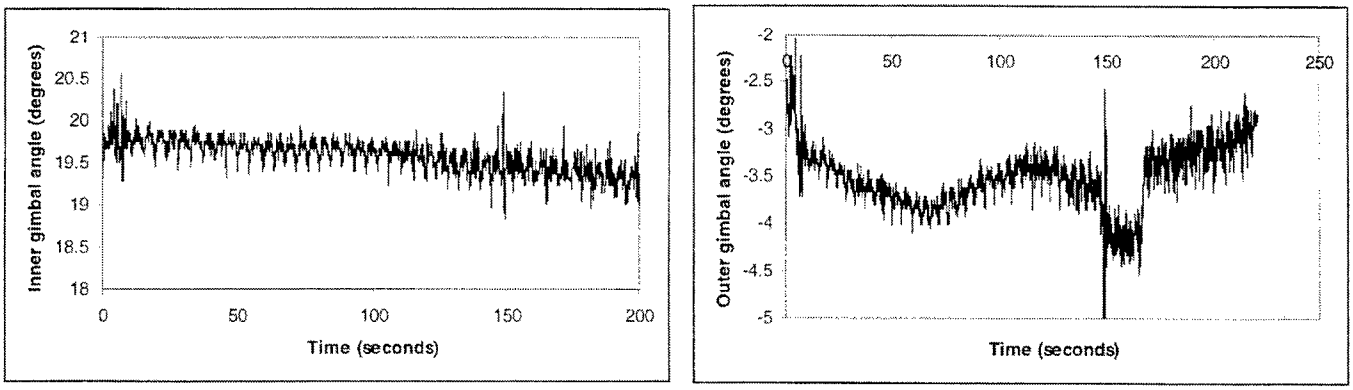

Figure 12. The gimbal angles. The target distance is approximately 830 meters. The RMS noise is 0.20 degrees for inner axis (horizontal) and 0.43 degrees for outer axis (verticle). There is a noise spike on the outer angle, due to a jump in the GPS position. It is observed that there is a periodic noise component. This will be analyzed further in the near future.

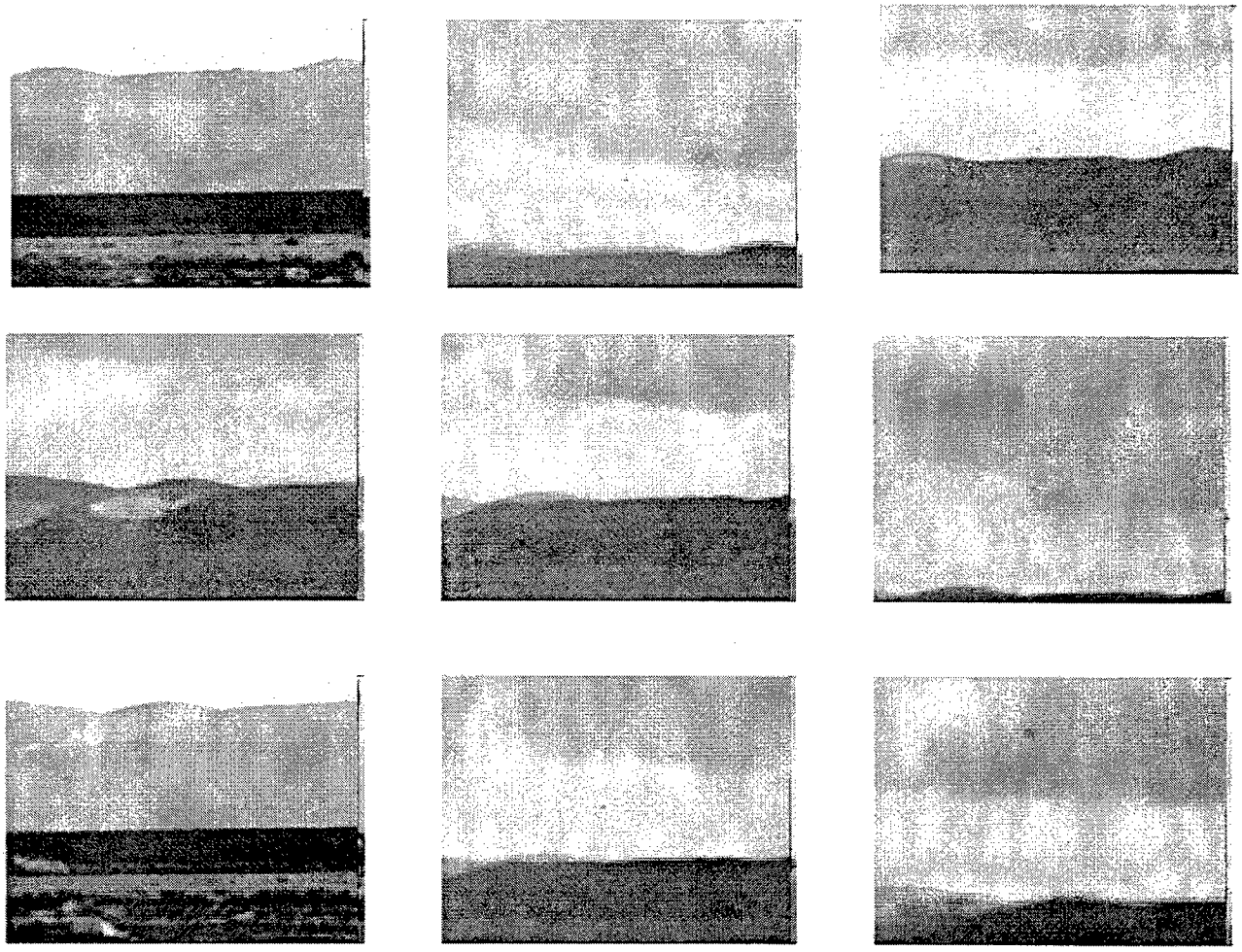

Figure 13. Selected images from a tracking video of the VTV. The images shown are preliminary, and a small radio controlled helicopter was used as VTV. The distance was approximately 830 m. The helicopter is the black spot in the cener of the images. The field of view of the camera is approximately 3 degrees.

Molecular and isotopic analysis of organic compounds from carbonaceous meteorites

George Cooper

NASA Ames Research Center

Introduction

Meteorites and interplanetary dust particles are the oldest items available for laboratory study of early solar system chemical and physical processes. Most carbonaceous meteorites, a class of meteorite relatively enriched in carbon and organic compounds, are as old or older than the solar system planets, approximately four and a half-billion years. As a group they are also the most unaltered early solar system objects as illustrated by their near solar (Sun) abundances in all but the most volatile elements. For this reason their content of organic compounds is a record of the earliest known abiotic organic synthesis. Meteorites, along with comets and interplanetary dust particles, may have delivered much organic matter to the early Earth.

The best characterized carbonaceous meteorite with respect to organic chemistry, Murchison, has been found to contain a large number of water-soluble organic compounds [1]. These include amino acids, carboxylic acids, dicarboxylic acids, hydroxycarboxylic acids, amides, purines, pyrimidines, phosphonates and sulfonates. The presence of most of these compounds along with clay minerals indicate the action of liquid water on their precursors. Other carbonaceous meteorites, such as Murray, are similar to Murchison in their content of organic matter.

Previous stable isotope analyses of some classes of meteorite organic compounds (amino acids, carboxylic acids, etc.) indicate that they may have formed in the meteorite parent body from smaller interstellar molecules [1], i.e., molecules that were present before the solar system and meteorites formed [2]. In both meteoritic and interstellar compounds, the ratios of heavy to light isotopes of hydrogen (D/H), carbon ($^{13}C/^{12}C$), and nitrogen ($^{15}N/^{14}N$) are anomalous (high) relative to bulk terrestrial (Earth) and even relative to bulk meteoritic values. In most cases, the isotope ratios of the interstellar molecules are much larger than the meteoritic.

An example of a likely synthesis of meteoritic compounds from interstellar precursors is the Strecker synthesis of amino acids. In this synthesis, aldehydes, ketones, cyanide, ammonia, and water (all observed in meteorites [1] and interstellar space [2]) combine to produce amino acids and other products - many of which are also seen in carbonaceous meteorites [1]. The precursors were most likely trapped as part of frozen ices into the growing meteorite parent body and reacted in an aqueous phase as the water-ice melted due to heating of the parent body.

The sulfonates and phosphonates, found recently in Murchison [3], are the first well characterized series of sulfur and phosphorus containing organic compounds found in meteorites. These compounds are of interest because of the importance of organic phosphorus and sulfur compounds in contemporary biology. The recent isotopic analysis of these compounds [5] illustrate the information that can be gained about the synthetic mechanisms and environments present in the early solar system.

Experimental

The primary techniques used in the analysis of the sulfonates and phosphonates were gas chromatography-mass spectrometry (GC-MS), ion exchange chromatography, and isotope ratio mass spectrometry. Complete descriptions of reagents, sample preparation, and GC-MS can be found in references 3 and 4. Details of isotope measurements are given in reference 5.

Results

Carbon, hydrogen, and sulfur isotope measurements of the sulfonates and phosphonates are shown in Table 1. Definitions and formulae are given in the legend and references 4]. In general, carbon and hydrogen isotope ratios, $\delta^{13}C$ and δD, of meteoritic compounds are well above terrestrial values [1]. On Earth, the ranges for organic matter are $\delta^{13}C \sim -50$ to -10 and δD -200 to - 50 [7]. Sulfur isotope anomalies, as observed in the meteoritic sulfonates (Table 1), have not been reported for terrestrial organic compounds.

The $^{13}C/^{12}C$ ratios of the sulfonates decrease with carbon number suggesting that the hydrocarbon side chains were synthesized in a stepwise fashion. The deuterium enrichments of the sulfonates and phosphonates indicate formation of the hydrocarbon portion of these compounds in a very low temperature environment (~ 10 to 50 K) consistent with that of interstellar clouds. The ^{33}S enrichment observed in methanesulfonic acid could have resulted from gas-phase ultraviolet irradiation of a precursor, such as CS_2. Irradiation of symmetrical molecules such as CS_2 has been shown to produce isotopic anomalies (enrichments or deficits) [8], and ultraviolet radiation is common in interstellar space [2].

The source of the sulfonic acid precursors, CS_2 and larger unsaturated carbon-sulfur compounds (C_xS_x), may have been the reactive interstellar molecule, CS. CS is reactive and relatively abundant in interstellar space[2]. Molecule formation from CS in the solid phase has been reported at temperatures as low as 33K [9]. In addition, a high resolution mass-spectrometry study of organic matter in the Murray carbonaceous meteorite identified sulfur species of elemental compositions CS_2, C_2S, C_3S, C_3S_2, and C_3SO, in addition to others [10] (carbon disulfide, CS_2, is common in carbonaceous meteorites). These compounds may have been transformed into the observed meteoritic sulfonic acids of the same carbon number after hydrogenation and reactions with water on the meteorite parent body.

In the near future, isotopic and molecular analysis of meteorites (and comets) will greatly increase our understanding of pre-Earth organic chemistry.

References

1 Cronin, J. R. and Chang, S. "The Chemistry of Life's Origin", J. M. Greenberg et al., Eds. (Kluwer Academic Publishers, The Netherlands, 1993) p. 209-258.

2 E. F. Van Dishoeck, G. A. Blake, B. T. Draine, J. I. Lunine, "Protostars and Planets III", E. H. Levy and J. I. Lunine, Eds. (Univ. of Arizona, Tucson, 1993), pp.163-241.

3 Cooper, G. W., Onwo, W. M. and Cronin, J. R. **Geochim. Cosmochim. Acta** 56, 4109 (1992).

4 Cooper, G.W. Cronin, J.R. **Geochim. et Cosmochim. Acta** 59, 1003-1015 (1995).

5 Cooper, G.W., Thiemens, M.H., Jackson, T.L. and Chang, S. **Science** 277, 1072-1074 (1997).

6 Gao, X. and Thiemens, M. H. **Geochim. Cosmochim. Acta 55**, 2671 (1991).

7 Hoefs, J. "Stable Isotope Geochemistry", P. J. Wyllie, A. E. Goresy, W. Von Englehardt, and T. Hahn, Eds. (Springer-Verlag, New York, 1987).

8 Colman, J. J., XU, X., Thiemens, M. H. and Trogler, W. C. **Science 273**,774 (1996).

9 Bohn, R. B., Hannachi, Y., and Andrews, L. **J. Am. Chem. Soc.** 114, 6452 (1992).

10 Hayes J. M. and Biemann, K. **Geochim. Cosmochim. Acta** 32, 239 (1968).

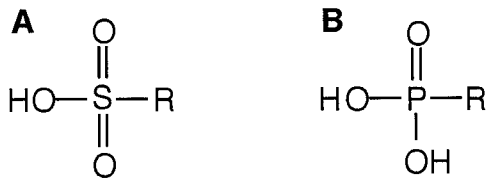

Figure 1. Organic sulfates (A) and phosphonates (B) found in the Murchison meteorite. The identified side chains R were methyl through butyl isomers.

Table 1. Results of intramolecular measurements of stable isotopes of sulfur, carbon, and hydrogen, from Murchison sulfonic acids. MSA = methanesulfonic acid, ESA = ethanesulfonic acid , nPSA = n-propanesulfonic acid, iPSA = isopropanesulfonic acid. See below for explanation of symbols.

R (in R-SO_3)	compound	mmoles	$\delta^{13}C$ (‰)	δD† (‰)	$\delta^{33}S$ (‰)	$\delta^{34}S$ (‰)	$\delta^{36}S$ (‰)	$^{33}\Delta$ (‰)
CH_3	MSA	3.8	+29.8	+483	+7.63	+11.27	+22.5	+2.00
CH_3CH_2	ESA	1.7	+9.1	+787	+0.33	+1.13	+0.8	-0.24
$CH_3CH_2CH_2$	nPSA	0.9	-0.4	+536‡	+0.20	+1.20	+2.1	-0.40
$(CH_3)_2CH$	iPSA	0.7	-0.9	+852	+0.32	+0.68	+2.9	-0.02
Bulk R-SO_3			+6	+600				
Phosphonics (uncorrected due to small amounts)			-20	+219				

Also see [6]. The stable isotopes of sulfur have masses of 32 (95.02%), 33 (0.75%), 34 (4.21%), and 36 (0.02%) atomic mass units (amu). The deviation of the ratio of sulfur isotopes in a sample from the standard (sulfur in the Canyon Diablo iron meteorite) is given in parts per thousand or per mil (‰), defined as $\delta^xS = \{[(^xS/^{32}S)sample/(^xS/^{32}S)standard]-1\} \times 1000$ where x = 33, 34, or 36. If plotted on a three-isotope graph, normal mass-dependent fractionations should lie on the line $\delta^{33}S = 0.5\ \delta^{34}S$, because the difference between ^{33}S and ^{32}S is one amu and between ^{34}S and ^{32}S is two amu, giving 0.5 as the slope. Similarly $\delta^{36}S = 1.97\ \delta^{34}S$. Therefore any mass-independent isotopic anomaly in ^{33}S and ^{36}S is given by (in ‰): $^{33}\Delta = \delta^{33}S - 0.5\ \delta^{34}S$ and $^{36}\Delta = \delta^{36}S - 1.97\ \delta^{34}S$, respectively. All known terrestrial sulfur lie on normal mass-dependent fractionation lines, i.e., their $^{33}\Delta$ values are zero. The calculation of δ values for carbon and hydrogen is similar to that of sulfur, i.e., $\delta H = [\{(H/L)_{sample}/(H/L)_{standard}\}-1]\ 1000$. Where H and L are the heavy and light isotopes, respectively, of each element.

†The δD values are corrected for blank and exchangeable hydrogen.

‡+536 is obtained after correcting for exchangeable hydrogen only.

Ultra-Highspeed Communications and Data Links Using a Hybrid WDM-TDM Physical Layer

Peter J. Delfyett

H. Shi

B. Mathason

University of Central Florida

Abstract

This paper describes the development of an ultra-highspeed data and communication link, suitable for transmitting and processing data at rates exceeding 100 Gbit/s, with the potential to be upgraded to transmission rates of 840 Gbit/s. The key technology is the WDM-TDM transmitter, which is a single modelocked semiconductor laser diode that produces > 20 wavelengths simultaneously, with each wavelength transmitting at 5 Gbit/s.

Introduction

Ultra-highspeed data links will become wide spread with the deployment of broadband switched digital networks and services, e.g., teleconferencing, video telephony, and computer services. The key hurdle in the commercial development of these networks is the availability of cost effective photonic technologies that will enable the generation, transmission and processing of these vast amounts of data. Present state of the art optical communications and signal processing typically rely on a wavelength division multiplexed (WDM) or a time division multiplexed hardware platform. In either case, in order to achieve the maximum data transmission and processing rates, the user is required to operate at the limits of either technology. An alternate approach to achieving ultrahigh-speed signal processing and transmission rates is to combine the advantages of both technologies, i.e., to develop a hybrid technology that relies on both WDM and TDM technologies. In this case, this hybridized data format is allowed to exploit the advantages of both technologies to provide the user with the required state of the art processing and transmission rates without pushing an individual technology to its limits.

Recently, we have developed a novel modelocked semiconductor laser that can generate over twenty independent wavelengths from a single device. Data is transmitted by modulating each wavelength at a data rate of 5 Gbit/s. Owing to the modelocked nature of the semiconductor laser, the optical data is transmitted in the R-Z data format. At the receiver, the data is demultiplexed by employing an all-optical clock recovery oscillator in conjunction with an ultrafast nonlinear optical loop, which uses a semiconductor optical amplifier as the nonlinear element. Owing to the temporal duration of the data bits (~10 psec.), aggressive temporal interleaving of the data should allow for single wavelength channel data rates of 40 Gbit/s, implying a total aggregate data transmission of 840 Gbit/s from a single semiconductor laser diode (see link diagram below).

Multiwavelength Semiconductor Laser Transmitter

The multiwavelength laser can produce a multiplicity of wavelengths that can be accurately controlled, i.e., the exact frequency and channel spacing can be designed in accordance with network standards. In

addition, owing to the design, the wavelength and channel spacing is unaffected by temperature variations, which normally plague devices which incorporate monolithic wavelength selective components. The laser can generate over twenty wavelengths with a long-term temporal jitter of < 100 fsec, with the added benefit of having correlated jitter between each wavelength channel.

In Figure 1 is a schematic of the multiwavelength modelocked diode laser system[1]. The laser is comprised of a semiconductor optical amplifier, which is used as the gain element and is enclosed in an external cavity. Within the external cavity, a spectral filter is employed to define individual spectral channels. This is accomplished by forming an intracavity spectrometer a using a spatial mask in the spectrometer plane. Modelocking is formed by applying a d.c. and r.f. current through a bias tee. The output spectrum is monitored using a spectrometer in conjunction with a diode array, while the temporal characteristics are measured using a fast photodetector with a sampling oscilloscope and nonlinear optical autocorrelation techniques. The output of the modelocked diode laser is directed into a temporal interleaver to achieve high pulse repetition rates between 5 and 15 GHz.

In Figure 3 are the spectral and temporal output of the multiwavelength modelocked diode laser. The output spectrum of the laser can be controlled by employing different spatial masks in the spectrometer plane. Optical spectra ranging from 4 individual modelocked channels to over 20 individual channels are obtained using this technique (Fig. 3a). In addition the spectral separation between each channel can also be varied from 0.8 nm. to over 2.4 nm[2]. The temporal output of the laser are modelocked optical pulse of ~10 picoseconds in duration. It should be noted that each wavelength channel is modelocked and produces its own train of modelocked pulses. In addition, the output pulses in each wavelength channel are produced simultaneously, i.e., the pulses at each wavelength channel are produced synchronously within the gain medium. Figure 3b shows an oscilloscope trace of the laser with the output pulses temporally interleaved to a pulse repetition rate of 5 GHz. It should be noted that each pulse in this oscilloscope trace contains 20 individual wavelengths.

All Optical Clock Recovery and Demultiplexing

For demonstrating an all optical, hybrid WDM-TDM optical link, an ultrafast optical demultiplexer is required. For this purpose, an optical clock recovery oscillator, based on a passively modelocked semiconductor diode laser is employed. For this application, a small amount of optical power from the WDM-TDM laser transmitter is used to injection lock the passively modelocked diode laser. Typical operating modes of the optical clock recovery oscillator are minimum injection powers of 3 microwatts for robust clock recovery, a fractional locking bandwidth of ~ $3x10^{-3}$, immunity to bit patterns of 2^{50}-1, and > 8:1 data to clock rate conversion[3]. To demonstrate the robustness of the clock recovery oscillator, Figure 4 shows an oscilloscope trace of clock recovery with repetitive data packets containing a single login "one" data bit followed by 49 clock cycles of logic zero. The generation of stable clock recovery suggests that the clock recovery process is immune to pseudo random bit patterns of greater than 2^{50}-1. It should be noted that the sinusoidal modulation on the recovered optical clock pulse train is owing to unavoidable undersampling and alaising necessary in order to display both the entire clock stream and two consecutive logical ones within the data packet.

The capability of rate conversion is shown in Figure 5(a). In this oscilloscope trace, the data transmitter is displayed operating at a rate equal to eight times the free running clock rate, along with the recovered, synchronized optical clock pulse train. This case shows the ability of the clock recovery process to lock onto a signal with a data rate equal to a multiple of the fundamental clock rate, thus enabling the clock to be employed in demultiplexing applications.

Upon achieving robust clock recovery, the subsequently generated optical modelocked optical pulses are amplified in a semiconductor optical amplifier and used as control pulses in a nonlinear optical loop

mirror for ultrafast optical demultiplexing. The configuration employed for the demultiplexing is based on utilizing a semiconductor optical amplifier asymmetrically displaced from the center of the optical loop. Typical launch pulse energies into the optical switch are ~10 pJ, not including coupling losses into the SOA.

In Figure 5(b) is an oscilloscope trace showing the performance of the all optical switch. The figure shows the temporal output of the optical switch when an optical logic pulse of state "one" is present at the input of the switch. The two traces represent the output of the switch when the control or switching pulse is either present or absent. The relative ratio of the peak detected signal represents the switching contrast, which in this case is greater than 10dB.

Summary

In summary, we have shown experimental results of a hybrid WDM-TDM optical link, which employs a novel hybrid modelocked multiwavelength semiconductor, capable of simultaneously generating over 20 independent wavelength channels at rates of greater than 5 Gbit/s. In addition, ultrafast optical demultiplexing, which relies on all optical clock recovery techniques and nonlinear optical loop mirrors, is used to demultiplex multiwavelength data down to rates suitable for conventional electronic photoreceivers. The temporal duration of the optical pulses suggest that aggressive temporal interleaving may lead to optical data and transmission systems operating at rates in excess of 800 Gbit/s, based solely on semiconductor optical amplifier technology.

References

1 H. Shi, G. Alphonse, J. Connolly, P. J Delfyett, Electronics Letters, vol. 34, no. 2, 179-181, (1998)

2 H. Shi, G. Alphonse, J. Connolly, P.J. Delfyett, IEEE Photon. Tech. Lett., vol. 9, no. 11, 1439-1441, (1997).

3 B. Mathason, G. Alphonse, J. Connolly, P. J. Delfyett, Optical Fiber Conference, WM12, San Jose, CA, (1998).

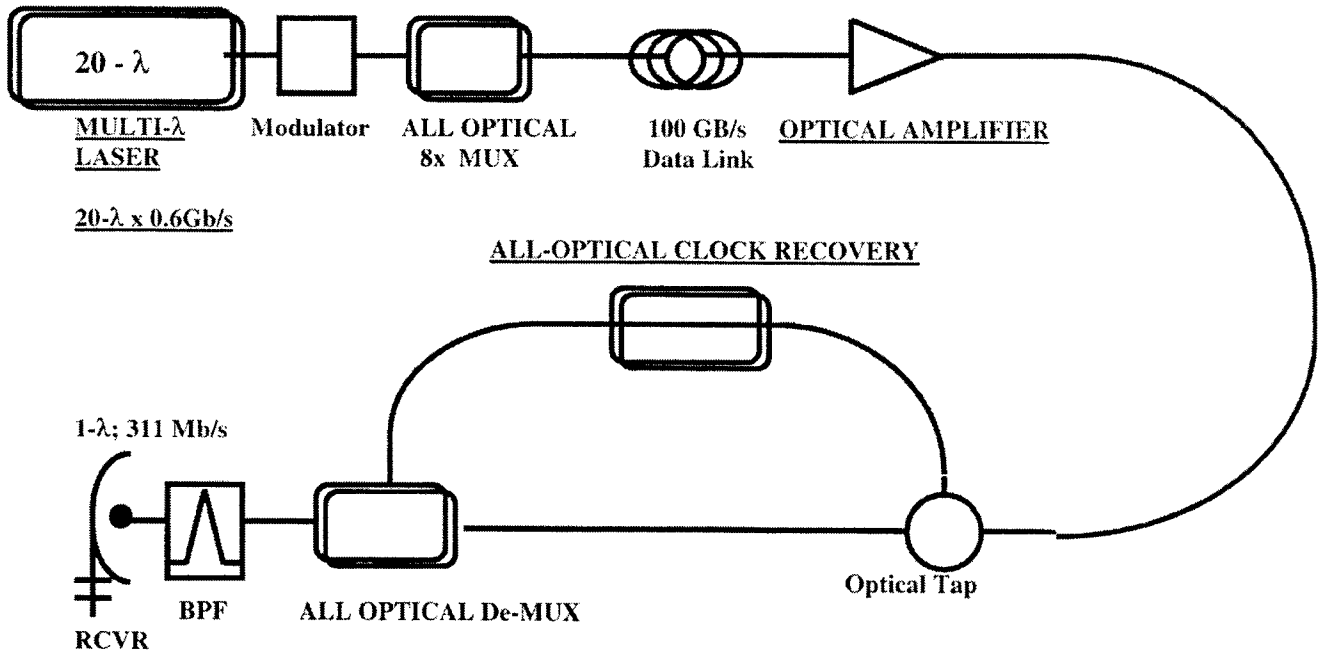

Figure 1. Schematic representation of the high-speed hybrid WDM-TDM optical link, showing the multiwavelength transmitter, optical clock recovery oscillator and the all optical switch.

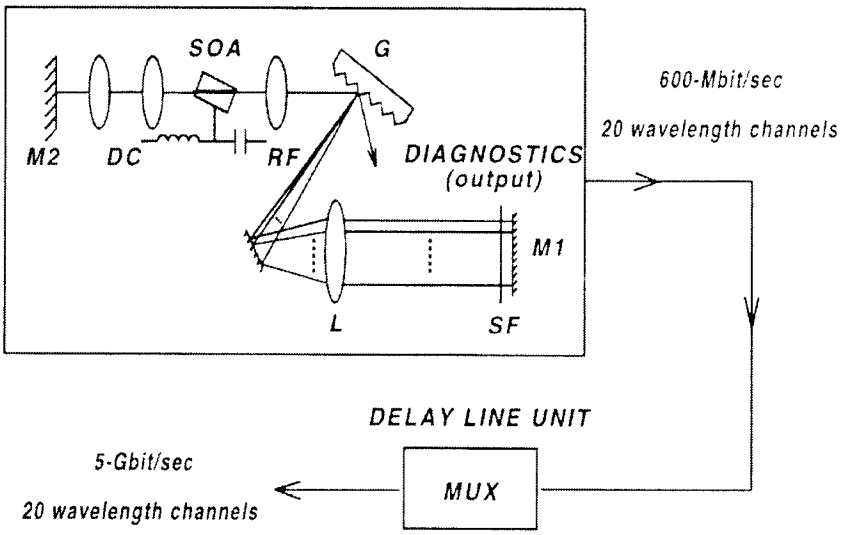

Figure 2. Schematic diagram of the multiwavelength modelocked diode laser system.

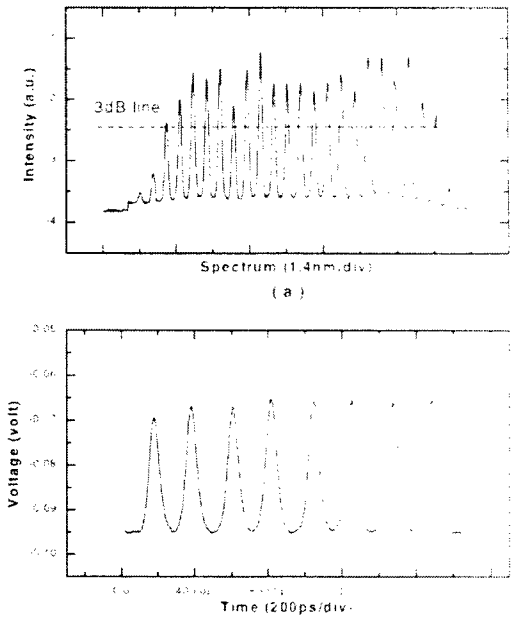

Figure 3. Spectral (top) and temporal (bottom) output of the multiwavelength modelocked diode laser.

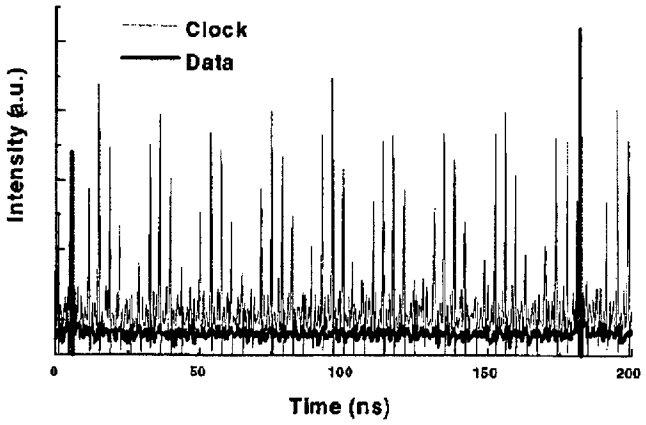

Figure 4. Oscilloscope trace of the recovered clock superimposed on the input data train.

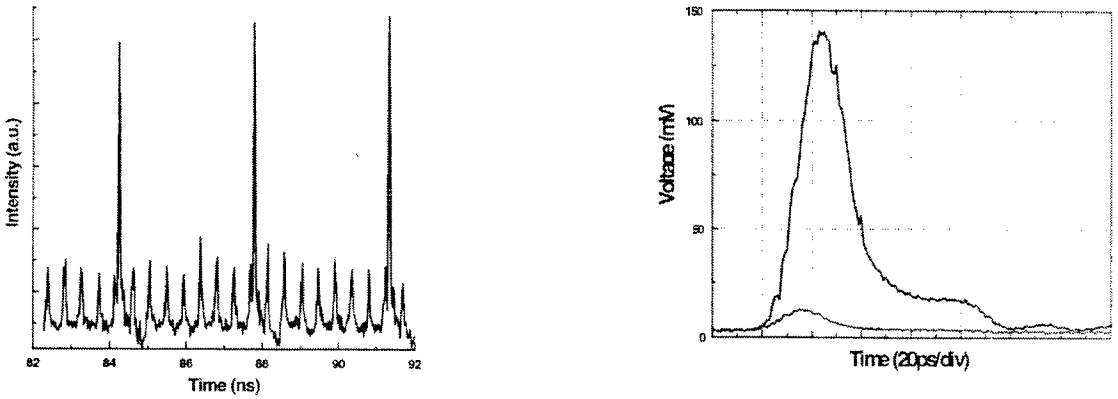

Figure 5 (a,b). Oscilloscope traces of the input data at 2.25 GHz overlaid with the recovered clock at 1/8 of the data rate (left). The demultiplexed output port of the optical switch showing both the switched state and the unswitched state, demonstrating a contrast of >10 dB.

The Role of Magnetic Reconnection in the Terrestrial Magnetosphere

F. Hall, IV
A. Otto
University of Alaska

H. E. Petschek
Boston University

Abstract

Earth's magnetosphere and the associated plasma processes are of fundamental importance for our understanding of space plasma physics and plasma processes in astrophysical systems. The magnetosphere plays a unique role in this understanding because it provides an opportunity to develop a theoretical understanding of time-dependent nonlinear plasma physics and to test these models by in situ observations with satellites. A central problem of space physics is the interaction of plasmas of different origins. The frozen-in flux condition, found to hold in the collisionless plasmas of magnetospheric and astrophysical systems, inhibits the mixing of plasmas on different magnetic flux tubes. It would seem to prevent the entry of solar wind plasma into the magnetosphere. Yet plasma of solar origin is found in the terrestrial magnetosphere. Magnetic reconnection provides a means by which to reconcile these observations with the frozen-in flux condition. This process is important in the transport of mass, momentum, and energy in the magnetosphere. The large scale convection of magnetospheric plasma is an example of a magnetospheric process in which magnetic reconnection plays an important role. Magnetic x-lines formed during reconnection serve as markers of the conversion of magnetic energy into plasma energy. The motion of these x-lines can be understood through consideration of the momentum densities of the adjacent plasma regions. Visualization of the output of computer simulations is discussed, providing further insight into this motion.

I. Introduction

Space plasma physics concerns the study of the electromagnetic environment of planets and other celestial bodies. A plasma is an ionized gas, composed of charged particles (as opposed to neutral atoms). In a plasma, the kinetic energy of a typical particle is much larger than the potential energy due to its nearest neighbor [1]. Because of their composition, plasmas respond much more strongly to electromagnetic fields than do neutral gases. Much of the Universe is in the form of plasma (on the order of 99% of the visible Universe), so it is advantageous to study their behavior. Because of their great distance, we can study most astrophysical plasma systems (for example, the plasma environments of stars and galaxies) only remotely, by analyzing the radiation that they generate. Fortunately, there are analogous, but closer, plasma systems which we can study in situ through the use of satellites and probes.

Let's consider the prototypical space plasma system: the planetary magnetosphere. Many

of the planets in the solar system, including Earth, possess intrinsic magnetic fields. These planetary magnetic fields interact with the solar wind, a plasma flowing out from the Sun. One can describe the solar wind plasma using magnetohydrodynamics (MHD). MHD is a single-fluid model of plasma behavior. It averages over the behavior of the charged particles constituting the plasma, allowing one to treat the plasma as a single continuous fluid. Like other fluid theories, MHD holds only on those time and length scales which are larger than those associated with the motion of the particles comprising the fluid. Hence MHD is valid on the time and length scales larger than those associated with the gyromotion of the charged particles in the magnetic field. Accordingly, it holds especially well over the large length scales found in space plasmas. Embedded in the solar wind is the interplanetary magnetic field (IMF) - the solar magnetic field drawn out into interplanetary space. The IMF interacts with the planetary magnetic fields it encounters as the solar wind flows out from the Sun. And just as a rock in a stream carves out a region in the water around it, so too does a planetary magnetic field carve out a region of space - the magnetosphere - in which it is dominant.

The interaction between the Earth's roughly dipolar magnetic field and the flowing solar wind generates the terrestrial magnetosphere, the structure of which is shown in Figure 1. The magnetosphere is shaped somewhat like a comet: the solar wind compresses Earth's magnetic field to roughly a distance of 10 R_E (where 1 $R_E \approx 6375$ km is Earth's radius) on the side facing the Sun, and draws it out into a long magnetotail more than 220 R_E long on the side facing away from the Sun. The supersonic solar wind is slowed to subsonic speeds upon encountering the bow shock, a standing shock in the solar wind in front of the magnetosphere. The magnetosphere itself is bounded by the magnetopause, a roughly cylindrical current layer with an "average" diameter of 20 to 30 R_E. The shocked solar wind is diverted around the magnetopause, forming the magnetosheath. Moving inward, we find a boundary layer marking the transition between the magnetosheath and the magnetotail. Close to the center of the magnetotail lies the plasmasheet, a region of moderately energetic plasma. The tail current sheet lies roughly in the middle of the plasmasheet, separating the oppositely directed magnetic fields in the northern and southern halves, or lobes, of the magnetotail. Closer to Earth we find largely dipolar magnetic field lines and the plasmasphere, a region of dense, low-energy plasma corotating with Earth.

As indicated above, Earth is not the only planet with a magnetosphere. Mercury, Jupiter, Saturn, Uranus, and Neptune are also magnetized planets with magnetospheres of their own. Planets are not the only celestial bodies which possess magnetospheres. Stars and even galaxies are also surrounded by regions which are analogous to planetary magnetospheres. Figure 2 depicts the magnetospheres of various celestial bodies. Despite the differences in their detailed configurations and (even more notably) spatial scales, one can see that these magnetospheres share the same basic structure. Although the magnetospheres of other planets can be directly probed by spacecraft, it is still most convenient to make *in situ* measurements of the terrestrial magnetosphere and use the knowledge gained from analysis of these measurements to obtain additional insights about the magnetospheres of other celestial bodies. It should also be mentioned that the investigation of these plasma environments allows the study of plasmas under conditions (of low plasma densities, for example) which cannot be achieved in human-made plasma laboratories.

II. Magnetic Reconnection

Let's return to our consideration of the terrestrial magnetosphere, as a prototypical magnetosphere. Matter, energy, and momentum are transferred from the solar wind to the magnetosphere in the course of their interaction. The actual processes through which these physical quantities are transferred are of considerable interest - especially after one considers the nature of the plasmas in this domain.

To motivate the discussion, let's consider the transfer of matter from the solar wind to the magnetosphere. The initial discussion

indicates that this process is non-trivial: note that the solar wind is diverted around the magnetosphere, rather than simply flowing through it. Why is the former behavior observed, rather than the latter? We can begin by considering what is called the "frozen-in flux condition."

As indicated above, magnetohydrodynamics (MHD) can be used to describe the solar wind and its interaction with Earth's magnetic field. For our purposes, it is even appropriate to describe the solar wind as an ideal MHD fluid, a plasma in which the electrical conductivity is infinite. Recall that resistivity arises from collisions. The mean free path between collisions is often so large in space plasmas that the collisional time scale is much larger than the dynamical time scale. We call these plasmas "collisionless." The conductivities of these plasmas are large enough to be considered nearly infinite. If there is a magnetic field threaded through such a plasma, it is said that the magnetic flux is "frozen into" the fluid. The plasma and the magnetic field then move together. The plasma parcels C and D depicted in Figure 3 are free to flow along field lines, but they cannot flow across them. For the same reason, these plasma parcels are at all times connected by the same magnetic field line as it moves through space. While this tying together of the plasma and the magnetic field is strictly valid only in the limit of infinite conductivity, it does holds quite well for plasmas with very high conductivities - such as the solar wind. Now reconsider the picture of the magnetosphere presented earlier (in Figure 1). The solar wind plasma cannot directly penetrate the magnetosphere, since the interplanetary magnetic field is "frozen" into it. Instead the plasma is diverted around the magnetosphere, flowing along the interplanetary magnetic field lines which are draped over the magnetopause, the boundary of the magnetosphere. So it seems that the transfer of mass from the solar wind to the magnetosphere is not quite as straightforward as one might originally suspect.

In order to further motivate the discussion, let's consider a rather simple plasma system (as depicted in Figure 4). Consider two different plasmas, with anti-parallel magnetic fields $\pm\mathbf{B}_0$ "frozen" into them, adjacent to one another. What happens at their interface? Applying Ampère's law across the interface, we find that there is a surface current $\mathbf{K}$ there, arising from the discontinuity in the tangential magnetic field across the interface. In general, the time evolution of the magnetic field $\mathbf{B}$ is given by

$$\frac{\partial \mathbf{B}}{\partial t} = \frac{1}{\mu_0 \sigma}\nabla^2\mathbf{B} + \nabla \times (\mathbf{u} \times \mathbf{B}). \qquad (1)$$

The first term describes the diffusion of the magnetic field, while the second term describes the convection of the magnetic field with the plasma. If the two plasmas are at rest with respect to one another (so that the velocity $\mathbf{u}$ vanishes), and the conductivity σ, is finite, then Ohmic dissipation will lead to reduction of the magnitude of the current at the interface. The magnitude of the opposing magnetic fields must likewise decrease. One can say that the opposing magnetic fields are "annihilating" one another.

Let's consider what happens if the two plasmas are moving toward one another with velocities $\pm\mathbf{u}$. In the general case of finite conductivity, the reduction of the magnetic field due to Ohmic dissipation will be countered by the convection of the magnetic field (lines) into the interaction region. The eventual fate of the system will depend on the relative strengths of these two mechanisms. Now let's reconsider the case which we have been considering, that of collisionless plasmas with infinite, or at least very large, conductivities. In this limiting case, there is no dissipation of the magnetic field adjacent to the interface. The magnetic field on either side of the interface continues to increase in magnitude without limit, as does the current flowing along the interface. Of course, infinite current densities are not observed between different plasma regions. What explains this discrepency? Recall that MHD only works for very large conductivities and/or very large length scales. The current sheet, by its very nature, is very thin; MHD does not hold on such scales. We find that MHD breaks down over a small region of the current sheet, where "anomalous" resistivity arises. The charged particle dynamics, which are not explicitly treated in a fluid theory such as MHD, play an important role in this "anomalous" resistivity (the nature of which

is still a matter of considerable study). In this so-called diffusion region (darkly shaded in Figure 4), where the magnitude of the magnetic field is very small, the magnetic field lines lose their identity and "reconnect." The resulting magnetic field lines, and the plasma to which they are now reattached, are expelled from the reconnection region. Notice that this process of magnetic reconnection allows the mixing of what were previously separate plasma populations (represented in Figure 4 by the two shaded plasma parcels) tied to different magnetic field lines. Furthermore, magnetic reconnection converts energy stored in the magnetic field into plasma energy, in the form of both directed bulk flow and plasma heating. This mechanism plays a very important role in the transport of mass, momentum, and energy in the magnetosphere.

As Figure 4 indicates, the system no longer has a simple planar geometry. Although the magnetic field lines are more or less straight far from the interface between the plasma regions, they begin to bend once they approach the interface. We find that the magnetic field strength becomes zero, not at a planar interface, but rather along a line (of finite extent) - the x-line. (This x-line appears as a point where the magnetic field lines intersect in the two-dimensional figure.) The opposing magnetic field lines can be considered to actually reconnect at the x-line. Note that the diffusion region, wherein the conversion of magnetic energy into plasma thermal and kinetic energy occurs, surrounds the x-line. Accordingly, the x-line serves as a marker for that energy conversion.

III. Magnetospheric Convection

Now that we have discussed the need for and the nature of magnetic reconnection, let's re-examine its role in the magnetosphere. Magnetic reconnection plays an important role in various magnetospheric processes, including the large-scale convection of plasma in the magnetosphere. Figure 5 depicts the participation of a magnetic field line in magnetospheric convection. Once an IMF field line (1) undergoes magnetic recon-nection at the dayside magnetosphere (2), the new magnetic field line (3) has one end attached to the solar wind and one end attached to Earth. This magnetic field line is convected anti-Sunward (4,5,6), as the magnetosheath plasma to which it is attached flows away from the Sun. This motion of the magnetic field line induces an electric field $\mathbf{E} = -\mathbf{v}\times\mathbf{B}$ across Earth's polar caps. [Alternatively, one may consider the motion of the plasma (a conductor) through the magnetic field as the mechanism by which this electric field is induced.] This induced electric field interacts with the magnetic field to establish a drift of plasma down through the lobes of the magnetotail and into the plasma sheet. Since the magnetic field is frozen to this plasma, it also drifts down toward the plasma sheet (7). This drift, along with the anti-Sunward motion of the plasma, drives reconnection in the magnetotail (8). As a result of this process, plasma is accelerated back toward Earth [as well as away from Earth, further into the magnetotail (9)] at the reconnection site in the magnetotail. This "reconnection" of magnetic field lines in the magnetotail balances, at least in part, their "opening" at the magnetopause.

IV. The Motion of X-Lines

Referring back to Figure 1, we find current sheets separating plasma regions with oppositely directed magnetic fields. When such plasma regions are forced together, magnetic reconnection is initiated at the interface between the two regions; and an x-line forms, marking the site of the reconnection. Section II presented a simple analysis of a simple system. Systems found in Nature can be considerably more complicated. More thorough and/or more general analyses of these systems have been presented elsewhere. (See, for example, [2], [3], and [4].) For now, it will suffice to consider the following argument. In the highly symmetrical system considered in Section II (and depicted in Figure 4), it seems reasonable to argue that the magnetic x-line - the site of magnetic reconnection and plasma energization - does not move. What happens in a system in which that symmmetry is broken? That symmetry would be broken by differences in the plasma densities and/or the magnetic fields in the two plasma regions. Would the magnetic x-line remain in the same location throughout the evolution of the system? It was this

question which motivated our research. Using Otto's two-dimensional, resistive MHD computer model [5], we followed the motion of x-lines in a magnetic geometry similar to that found at the dayside magnetopause. (Refer to Figures 1 and 5.) Magnetic reconnection was triggered by an enhancement in resistivity in a current layer separating two plasma regions. By invoking momentum balance in the center of momentum frame and the constancy of reconnected magnetic flux, one can derive the following expression for the z-component of the velocity of the x-line:

$$v_z = \frac{\rho_1 v_1 b_2 + \rho_2 v_2 b_1}{\rho_1 b_2 + \rho_2 b_1} \qquad (2)$$

One can see that the x-line velocity depends on the mass densities (ρ_1 and ρ_2), plasma velocities (v_1 and v_2), and magnetic fields (b_1 and b_2) on the two sides of the current layer. Note that quantities in the simulation are normalized to values characteristic of the physical system. For example, velocities are normalized to the Alfvèn velocity

$$v_A = \frac{|B|}{(\mu_0 \rho)^{\frac{1}{2}}} \qquad (3)$$

In this system, the typical Alfven velocity is 400 km/s and the characteristic length scale is L_0 = 400 km; the corresponding time scale is τ_A = 1 sec. Once the appropriate initial conditions were established in the simulation, the system was allowed to evolve in time. The velocity of the x-line could be determined using the output of the simulation.

Figure 6 presents a representative visualization of the output of the simulation. It shows the magnetic field configuration of one of the systems which we investigated at times t = 20 τ_A and t = 60 τ_A. In this particular system, a constant plasma flow velocity in the positive z direction was superposed initially. In this case it is relatively easy to identify the single x-line in this system: it lies at z ~ 2.551 L_0 at the time t = 20 τ_A and at z ~ 9.727 L_0 at time t = 60 τ_A.

It is possible for a system to develop multiple x-lines as it evolves. An example of such a system is shown in Figure 7. At time t = 20 τ_A, there is a single x-line at z ≈ 0.028 L_0. At time t = 60 τ_A, there are two x-lines: one at z ≈ 12.622 L_0 and the other at z ≈ 1.411 L_0. In cases with multiple x-lines, Equation (2) gives the average velocity of the x-lines.

In the course of our research, plasma systems featuring asymmetry in the initial velocity v_z plasma density ρ, and magnetic field **B** were simulated. This discussion is intended to give only a flavor of this research. A more detailed discussion of the results is presented elsewhere [6].

V. Conclusion

This discussion has been designed as an introduction to magnetic reconnection and its role in the terrestrial magnetosphere. Once one understands the importance of magnetic reconnection in the transfer of mass, momentum, and energy in plasma systems such as the magnetosphere, one can appreciate the utility of studying the motion of magnetic x-lines; doing so allows one to identify the location at which magnetic energy is converted into plasma energy, accelerating and heating that plasma. This knowledge can be utilized to better understand magnetospheric processes such as the large-scale convection of plasma in the magnetosphere. Numerical simulation of asymmetric plasma systems in which magnetic reconnection is initiated can yield further insight into the motion of these magnetic x-lines.

Acknowledgements

F. Hall would like to thank Laura Peticolas, Veronika Besser, Karen Remick, Matt Heavner, Hua Zhu, and Peter Delamere for helpful comments and suggestions. The research described herein was sustained in part by fellowship support from the National Physical Science Consortium and NASA Marshall Space Flight Center.

References

[1] D. R. Nicolson, *Introduction to Plasma Theory* (Krieger Publishing Company, Malabar, Florida, 1992), p. 1.

[2] G. K. Parks, *Physics of Space Plasmas: An Introduction* (Addison-Wesley Publishing Company, Redwood City, California, 1991).

[3] M. G. Kivelson and C.T. Russell, ed. *Introduction to Space Physics* (Cambridge University Press, Cambridge, England, 1995).

[4] W. Baumjohann and R. A. Treumann. *Basic Space Plasma Physics* (Imperial College Press, London, England, 1997).

[5] A. Otto, K. Schindler, and J. Birn, J.Geophys. Res. **95**, 15023 (1190).

[6] A. Otto, H.E. Petschek, and F. Hall, IV, in *EOS Transactions, AGU 1997 Fall Meeting, 77,* pF625.

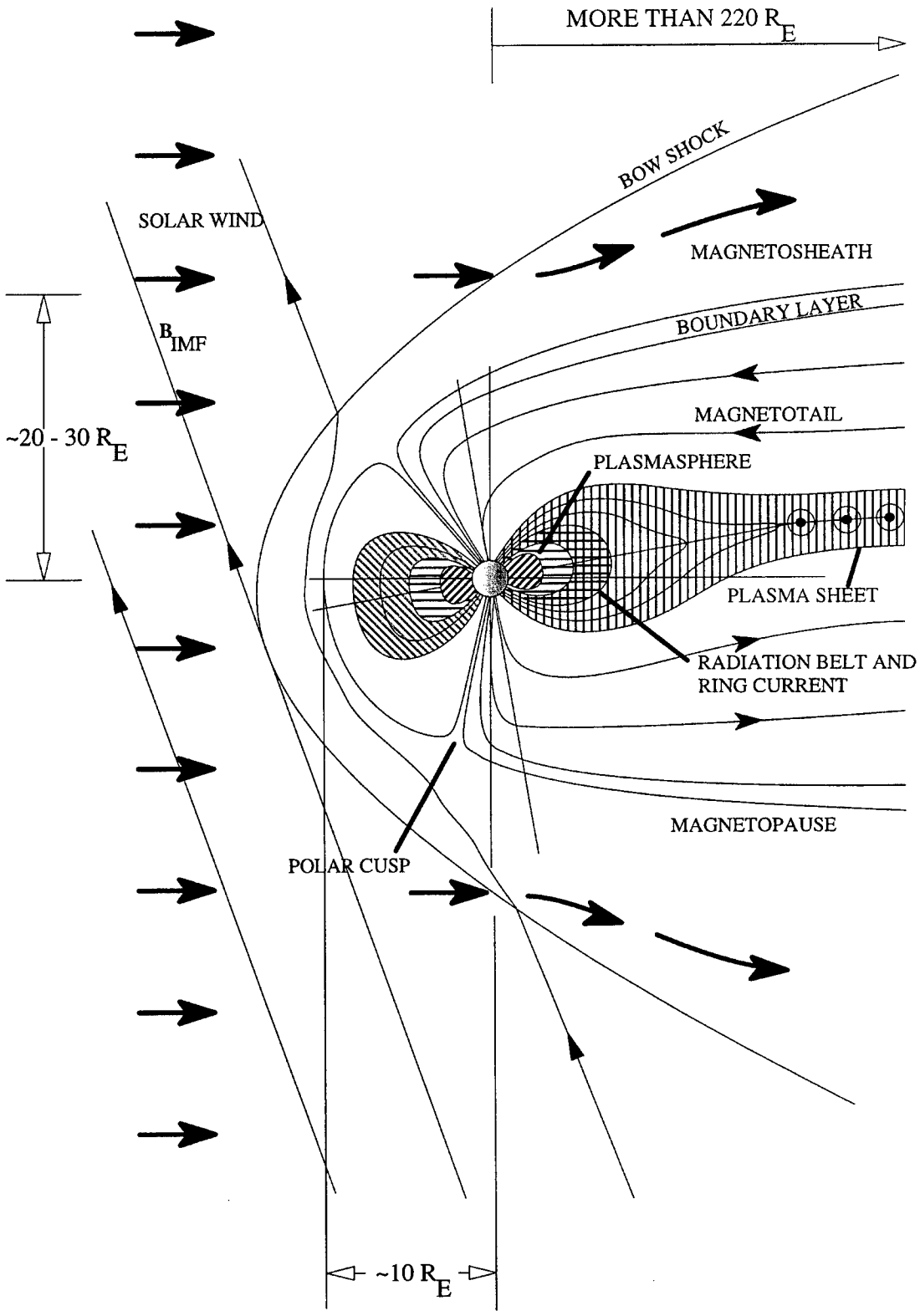

Figure 1. The terrestrial magnetosphere. The magnetotail current sheet is shown as coming out of the page in the latter portion of the plasmasheet. (Adapted from [2].)

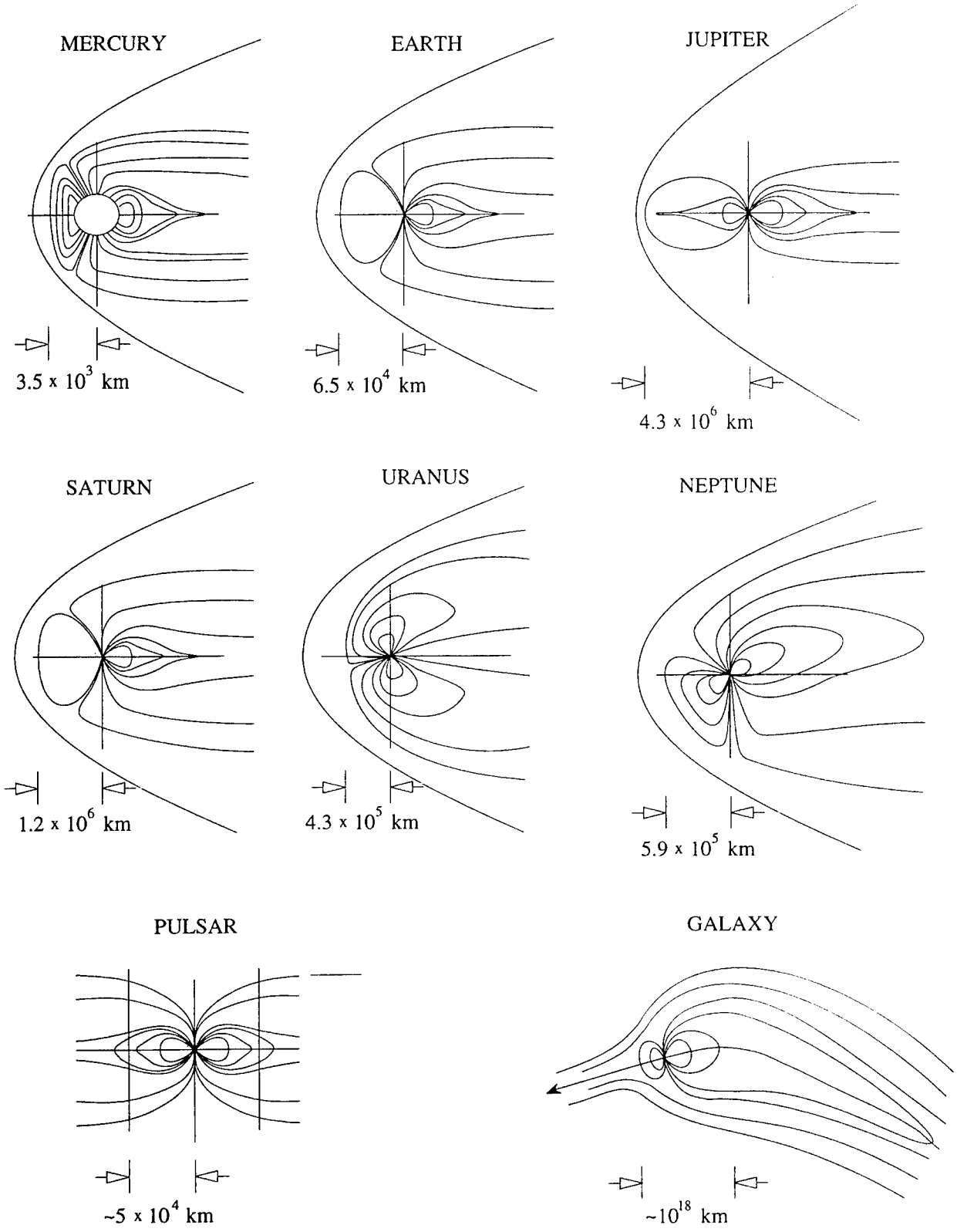

Figure 2. Magnetospheres of various celestial bodies. (Adapted from [2].)

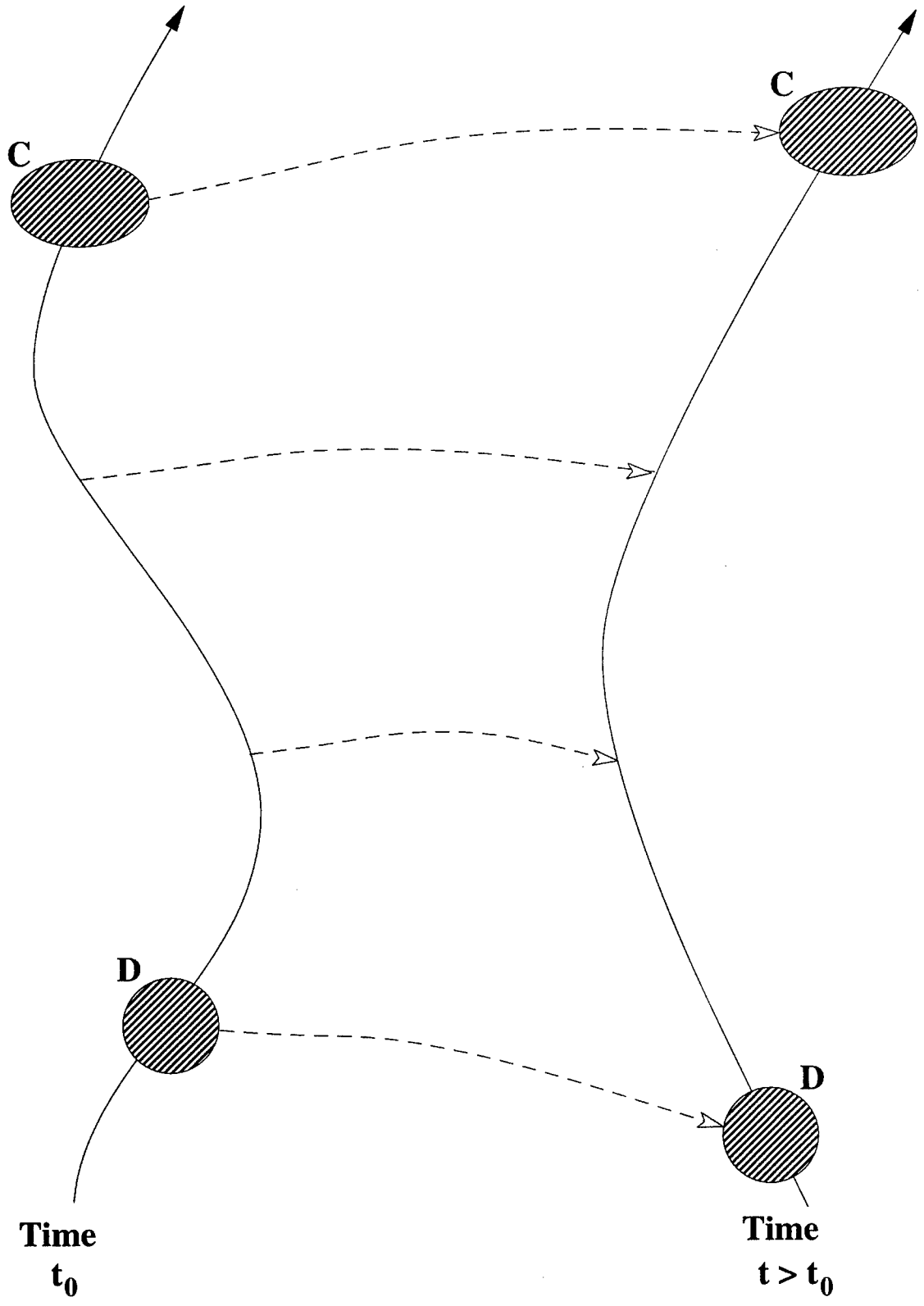

Figure 3. The frozen-in flux condition. The plasma parcels C and D remain fixed to the same field line as it moves from its position at time to to its position at time $t > t_0$.

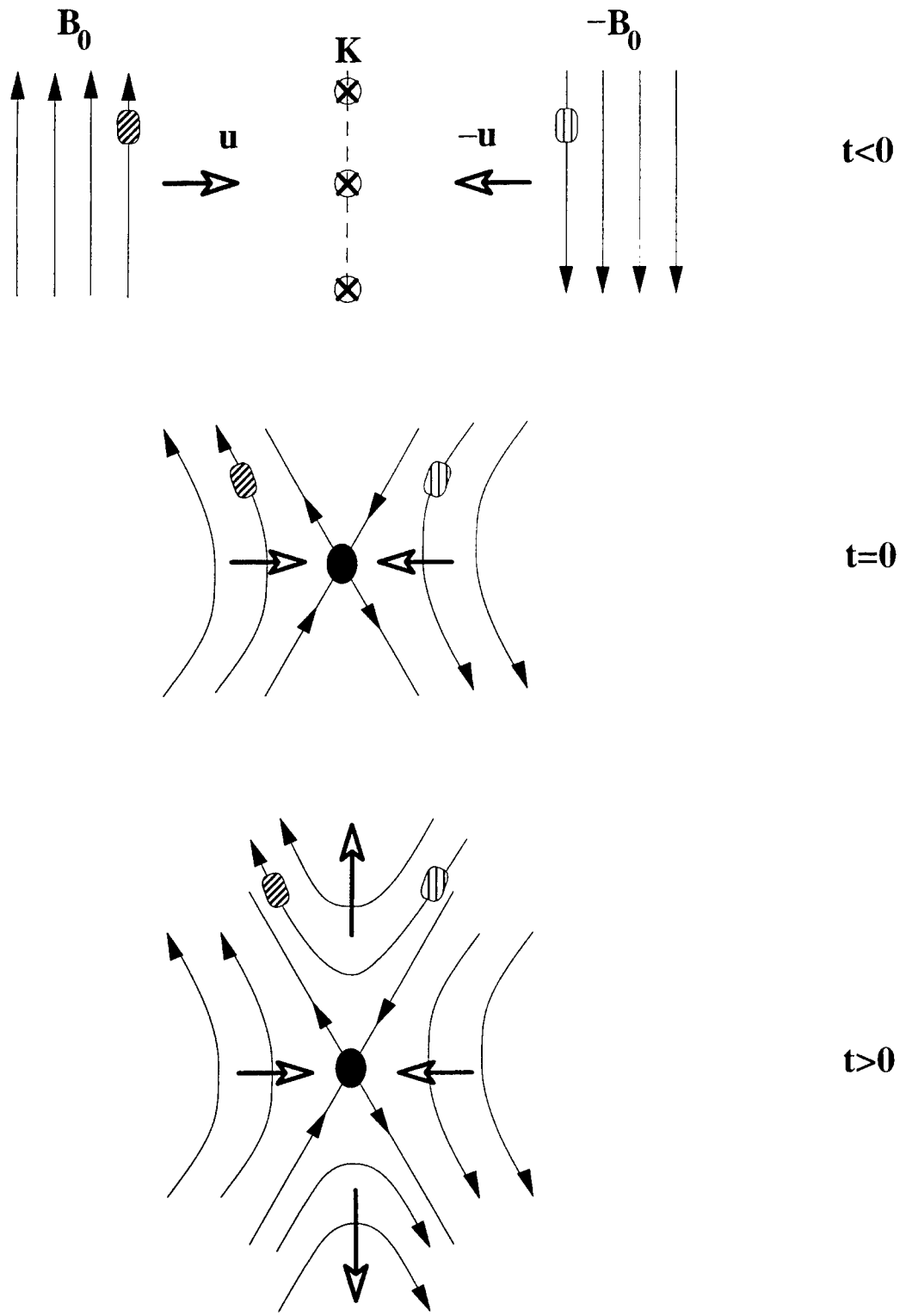

Figure 4. Magnetic reconnection. The magnetic x-line is depicted as a point at the intersection of the magnetic field lines at times $t = 0$ and $t > 0$. The diffusion region is depicted as a shaded region surrounding the x-line. Plasma motion is indicated by the thick arrows with open arrowheads. (Adapted from [4].)

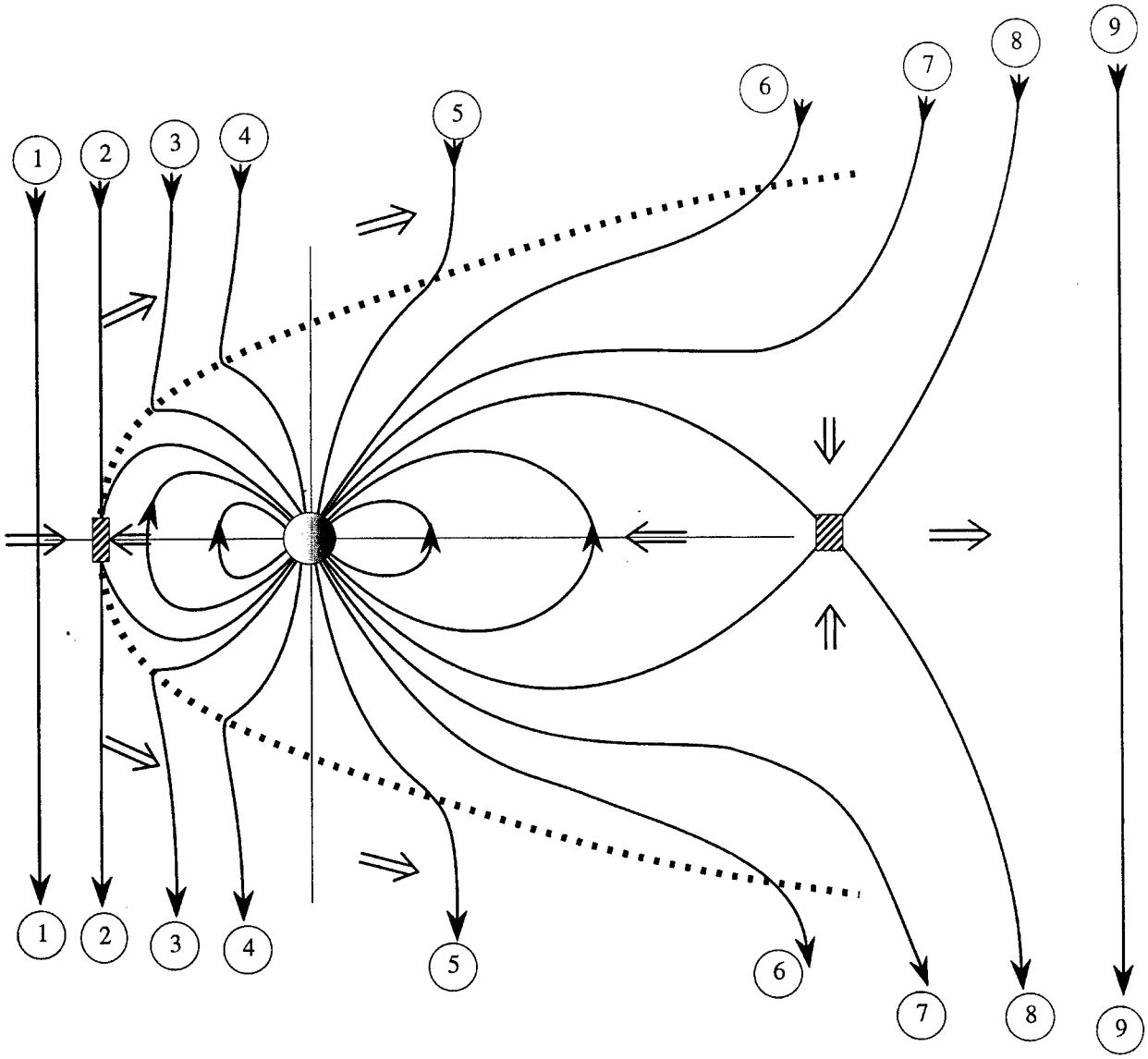

Figure 5. Magnetospheric convection. The shaded regions indicate the sites where magnetic reconnection occurs. The dotted line indicates the position of the magnetopause. Plasma motion is indicated by the open arrows. (Adapted from J.W. Dungey, in *Geophysics, The Earth's Environment,* ed. C. Dewitt, J. Hieblot, and A. Lebeau (Gorden & Breach, New York, New York, 1963).

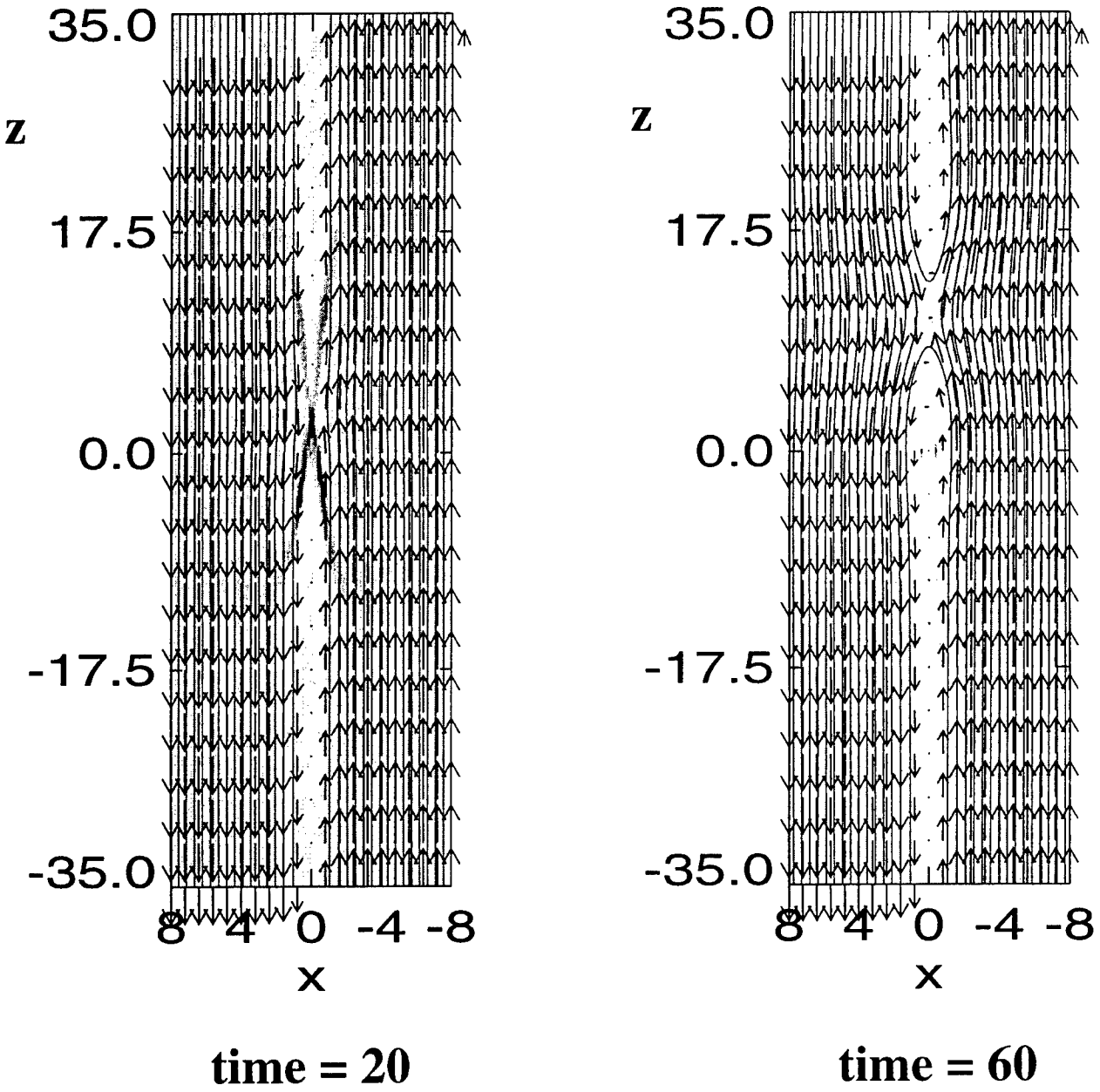

Figure 6. Visualization of simulation output showing the motion of a magnetic x-line.

Magnetic Field

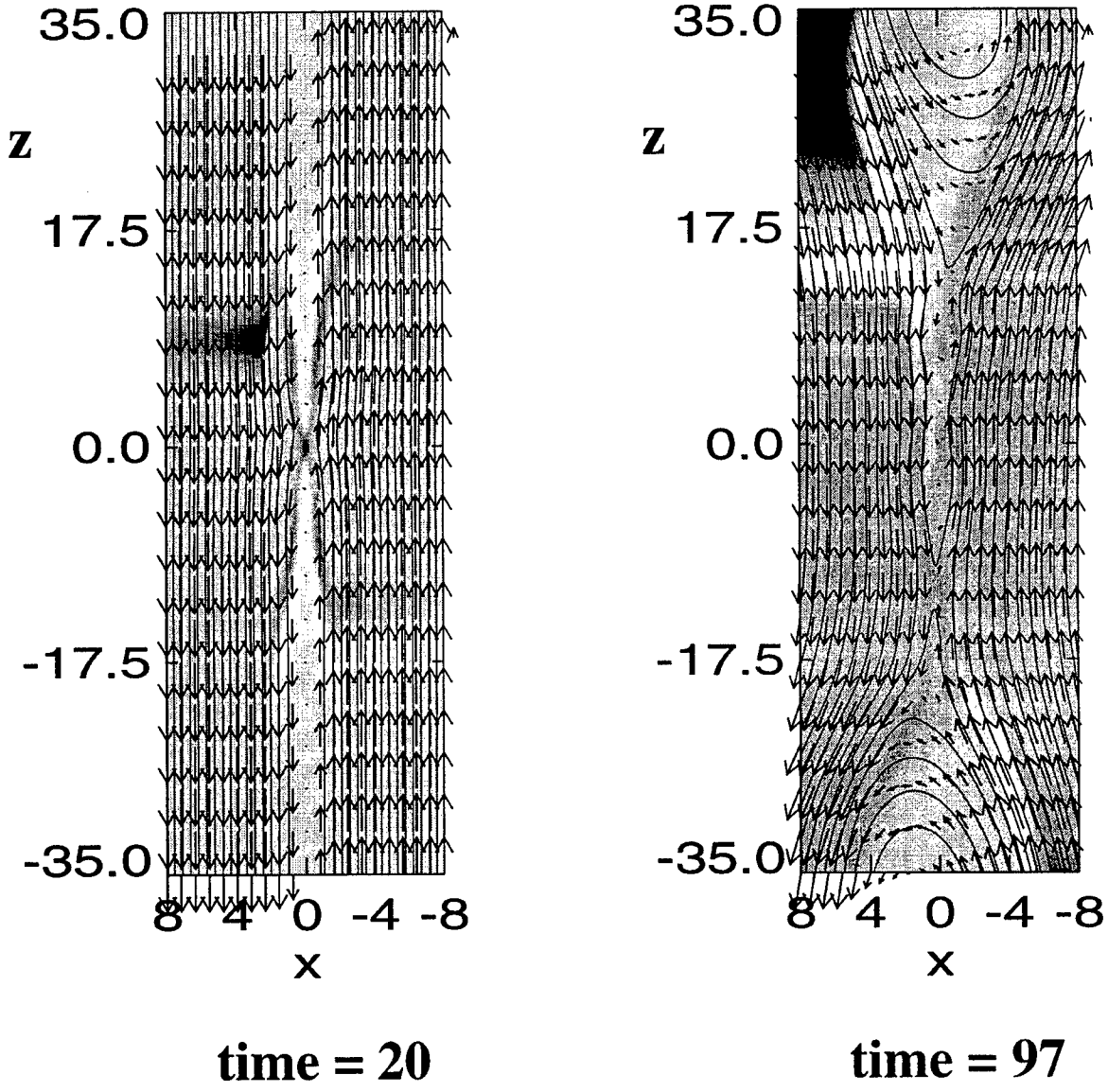

Figure 7. An example of a system with two magnetic x-lines.

Atoms and Molecules in Strong Laser Fields

Wendell T. Hill, III

University of Maryland

Introduction

The study of atoms and molecules in intense laser fields is now more than twenty years old yet it continues to command the attention of atomic theorists and experimentalists. The reasons can be traced to new and peculiar physics associated with "dressing" the quantum states of the system by the radiation field. This new physics is not only interesting in its own right, it has the potential for important technological spin-offs such as new light sources (e.g., high harmonic generation, sub-femtosecond generation), compact accelerators and controlling reaction dynamics at the quantum level. Unlike weak or moderately intense laser fields, strong fields are accompanied by an average electric field that can exceed the atomic field strength, $e/a_o \sim 5$ GV/cm, which corresponds to the electric field produced by a proton at a distance of the Bohr radius. Since the applied electric field is not a small perturbation compared with the internal fields holding the atom together, it modifies the internal structure of the atom or molecule and alters significantly the decay dynamics. In addition, a perturbative description of the physics associated with strong-field radiation-matter interaction is severely strained. As we will show below, an atom placed in a strong field will not survive as a neutral atom but will lose one or more electrons. This turns out to be true of a molecule placed in a strong field as well. At the same time, however, the multiple charge centers characteristic of a molecular system lead to additional degrees of freedom for decay via dissociation. Although the nuclei are considerably more massive than the electrons, dissociation and ionization are interlaced even when the system is excited with short duration pulses; the Born Oppenheimer approximation is invalid in many cases. This coupling between ionization and dissociation makes strong-field dissociative-ionization of molecular systems extremely interesting and will be the subject of this paper.

Strong Field Limits

We begin our discussion by establishing the limits of strong field effects. As mentioned above, when the average electric field associated with the laser reaches about 5 GV/cm (corresponding to an intensity of about 3.5×10^{16} W/cm^2) we might expect strange things to occur. In fact, interesting things start to happen at substantially lower intensities. To appreciate this, we will treat the effective electric field due to the laser as a static field. That is, we will assume we can ignore the fact that the field actually oscillates sinusoidally in time. This is a reasonable approximation for near infrared radiation (e.g., Nd:YAG and Ti:Sapphire lasers). If we combine the Coulomb potential of the nucleus, q/r, with the static field potential of the laser, eEr, the electrons then move in a distorted potential similar to that shown in the top panel of Fig. 1. The central features of this potential are (1) the electrons are only quasi-bound on one side of the atom since they can tunnel through the barrier to freedom and (2) the higher the intensity, the more the ground state energy level (potential barrier) is pushed upward (downward). Clearly at some intensity, the ground level will reach the top of the barrier. This occurs at about 10^{14} W/cm^2 for the ground state of the hydrogen atom. At this intensity a neutral hydrogen atom will not survive in the laser field (it will lose its electron. It turns out that this is also true for many electron systems; they too will not survive as neutral atoms at an intensity of about 10^{14} W/cm^2. Since the distortions to the potential are in the direction of the laser's electric field, the electrons are ejected in the direction of the laser polarization.

This field ionization picture depends on the validity of treating the laser field as a static electric field. This is reasonable if there is enough time for the electron to escape before the direction of field changes sign. Often the Keldysh parameter, γ [1], is used as a measure

of when the static field approach is valid. Specifically, when
$\gamma << 1$, where

$$\gamma \equiv \frac{\omega_{laser}}{\omega_{tunnel}} = \sqrt{\frac{U_{IP}}{1.87\times10^{-13} I\lambda^2}} \quad , \qquad (1)$$

the static field approach is a reasonable assumption. Ionization rates can be estimated by the ADK theory [2]. In Eq. (1) U_{IP} is the ionization potential of the atom, I the intensity in W/cm^2 and λ the wavelength in microns. In the opposite limit, $\gamma >> 1$, it is appropriate to view ionization as a multiphoton process and employ perturbation theory to determine the ionization rate. The ionization rate is obtained from the transition amplitude $T_{i\to f}^{(n)}$ for an n-photon absorption process where

$$T_{i\to f}^{(n)} \propto \delta(\omega_f - \omega_i - n\omega) \sum_{j,k,\ldots} \frac{\langle f|\vec{E}\cdot\vec{d}|l\rangle\langle l|\vec{E}\cdot\vec{d}\ldots\vec{E}\cdot\vec{d}|k\rangle\langle k|\vec{E}\cdot\vec{d}|j\rangle\langle j|\vec{E}\cdot\vec{d}|i\rangle}{(\omega_l - \omega_i - (n-1)\omega)\ldots(\omega_k - \omega_i - 2\omega)(\omega_j - \omega_i - \omega)} \quad . \qquad (2)$$

In Eq. (2) $\vec{E}$ is the effective electric field of the laser, $\vec{d}$ the induced dipole moment, ω the laser frequency and $\eta(\omega_l - \omega_i)$ is the transition energy between states $|i\rangle$ and $|l\rangle$. Perturbation theory is valid as long as $T_{i\to f}^{(n)} > T_{i\to f}^{(n+1)}$ otherwise the series will not converge and the perturbative approach breaks down. It has been shown experimentally that these two terms become comparable in size at an intensity of 10^{14} W/cm^2 as well [3]. As a consequence, we can set an intensity of about 10^{14} W/cm^2 as the demarcation of the onset of strong field effects.

Strong Field Signatures

Since the strong fields will remove electrons from an atom or a molecule, our understanding of the underlying physics has come through studying the continuum spectra (photoelectron and photoion spectra. One of the most conspicuous features of the strong-field photoelectron spectrum is excess photon absorption. As indicated in Fig. 2a, the spectrum is characterized by the absorption of more photons than the minimum number necessary to ionize the atom. This structure has been given the name above threshold ionization (ATI). This was first observed in atoms [4] but is now routinely seen in molecules as shown in Fig. 3 for H_2. The spectrum is characterized by peaks spaced by the photon energy. In molecules, as indicated in Fig. 2b the dissociation spectrum also exhibits excess photon absorption. This effect goes by the name above threshold dissociation (ATD) [5]. This is also shown in Fig. 3 for H_2 as well. Since the photon energy that goes into dissociation must be shared between the two nuclei that separate, the peaks are separated by half the photon energy for homonuclear diatomic systems. The angular distribution of the ejected ions is strongly peaked along the polarization direction.

In addition to ATI and ATD, molecules also under go Coulomb explosion. An example is shown in Fig. 4 for H_2^{2+}. This occurs when two or more electrons are removed from the molecule and the remaining atomic ions are blown apart by their mutual Coulomb repulsion. In the absence of any residual binding between the two ions, which is the case for H_2^{2+}, the nuclei separate with a total energy of 1.44 eV/R_{CE} where R_{CE} is expressed in nanometers.

Diatomic Molecules In Strong Fields

The Coulomb explosion spectra of diatomic systems has fascinated investigators for a number of years because the energies of the atomic fragments gives a direct measure R_{CE}, assumed to be equal to R_{eq}, at which dissociation occurs. It was originally believed that it could be used to take a snap shot of complicated molecular structure in various excited states. It turns out, however, in almost all diatomic cases the energy measured is less than what is expected for dissociation from R_{eq}. This implied that the final ionization prior to Coulomb explosion begins at some critical distance, $R_C > R_{eq}$. Although the origin of why this occurred remained a mystery for sometime, we now have an explanation.

It is perhaps best described using the static field picture where the strong field distorts the molecular potential in much the same fashion as it did for the atomic potential. Since the diatomic molecule is cylindrically symmetric, the electric field of the laser can be aligned either parallel or perpendicular to

the internuclear axis connecting the two nuclei. When the field and the internuclear axis are perpendicular, the distorted potential looks nearly the same as for the atom in Fig. 1. When the field is aligned with the internuclear axis, the distorted potential looks similar to those shown in Fig. 5. Since the molecule is longer than it is wide, it turns out to be easier to ionize it when the field and the internuclear axis is aligned since the potential is depressed further (r larger). Electrons are again ejected along the polarization axis. At the same time, the subsequent dissociation of the molecular ion also occurs along the polarization axis since the molecule is pre-aligned by the field. As we did for hydrogen, we can estimate the intensity required to push the ground state of the molecule over the barrier. In the case of H_2^+ at $R = R_{eq} \sim 0.1$ nm, this occurs about 5×10^{14} W/cm^2 as shown in the lower panel of Fig. 5 [6]. If we allow R to increase, we observe something remarkable. First, the ground state splits into two with part being in the left- and part in the right-hand well. At R = 0.4 nm, for example, we note that the portion of the ground state in the left-hand well reaches the top of the inner barrier at an intensity of about 5×10^{13} W/cm^2, an order of magnitude less than at $R = R_{eq}$ and a factor of 2 less than the intensity needed to ionize H. Evidently, it is easier to ionize the molecule when it is extended than when it is at it equilibrium position. If we allow R to increase to infinity, we would have to ionize the neutral atom that also requires a higher intensity. Thus, the ionization rate should peak at some extended distance larger than R_{eq} but less than ∞. This simple idea qualitatively explains the results of early [7] and contemporary experiments [12, 8, 8, 9, 10]. It can be shown that the rate is expected to peak at approximately $R_C = 4/U_{IP}$ in atomic units (a.u.) [11], where U_{IP} is the ionization potential for the atomic system in atomic units. For H_2^+ $R_c \sim 0.4$ nm compared with R_{eq} of 0.1 nm. Several calculations have confirmed this effect in H_2 as well as other systems [12, 13, 14] and provide specific details about the ionization process that can be used to make quantitative comparisons between theory and experiment and to test the robustness of concept of R_c. This has been done by Gibson et al [9] at two intensities and by Zhang and Hill [15] over a wide range of intensities. A comparison of the theoretical and experimental ionization yields as a function of internuclear separation at several intensities is shown in Fig. 6. In closing we point out that when the static field limit is not valid, one must modify the discussion of the Coulomb explosion. For example, it was shown by Hill et al [16] that in the ultraviolet, the Coulomb explosion photoion spectrum is best explained by multiphoton transitions to specific molecular states. This work was supported by the National Science Foundation under grants PHY 9600203 and PHY-9512313.

References

1 Keldysh, Sov. Phys. *JEPT* **20**, 1307 (1996).

2 M.V. Ammosov, N.B. Delone and V.P. Krainov, Sov. Phys. JETP **64**, 1191 (1986); F.A. Ilkov, J.E. Decker and S.L. Chin, J. Phys. B**25**, 4005 (1992).

3 See, for example, J.H. Eberly, J. Javanainen and K. Rzazewski, Phys. Rep. 240, 331 (1991).

4 Agostini *et al.* Phys. Rev. Lett. **43**, 1127 (1979).

5 A. Zavriyev, P.H. Bucksbaum, H.G. Muller and D.W. Schumacher, Phys. Rev. A**42**, 5500 (1990); A. Guisti-Suzor, X. He, O. Atabak and F.H. Mies, Phys. Rev. Lett **64**, 515 (1990).

6 The fact that the intensity to ionize the molecular ion, H_2^+ in this case, requires a higher intensity than that of the corresponding neutral atom, H (which ionizes at 10^{14} W/cm^2), can be understood because the molecular system is more tightly bound with respect to ionization; the dissociation energy must be supplied as well as the atomic ionization energy.

7 M. Schmidt, D. Normand and C. Cornaggia, Phys. Rev. A**50**, 5037 (1994).

8 J. Ludwig, H. Rottke and W. Sandner, Phys Rev A**56**, 2168 (1997).

9 G.N. Gibson, M. Li, C. Guo and J. Neira, Phys Rev. Lett **79**, 2022 (1997).

10 T.D.G. Walsh, F.A. Ilkov and S.L. Chin, J. Phys B **30**, 2167 (1997).

11 S. Chelkowski and A.D. Bandrauk, J. Phys B **28**, L723 (1995).

12 T. Seideman, M. Yu. Ivanov and P.B. Corkum, Phys. Rev Lett. **75**, 2819 (1995).

13 J.H. Posthumus, L.J. Frasinski, A.J. Giles and K. Codling, J. Phys. B **28**, L349 (1995).

14 T. Zuo and A.D. Bandrauk, Phys Rev. A**52**, R2511 (1995).

15 G. Zhang and W.T. Hill, III, *Submitted to* Phys Rev. A

16 W.T. Hill, III, J. Zhu, D.L. Hatten, Y. Cui, J. Goldhar and S. Yang, Phys. Rev. Lett, **69**, 2646 (1992).

17 J. Zhu and W.T. Hill, III, JOSA B**14**, 2212 (1997).

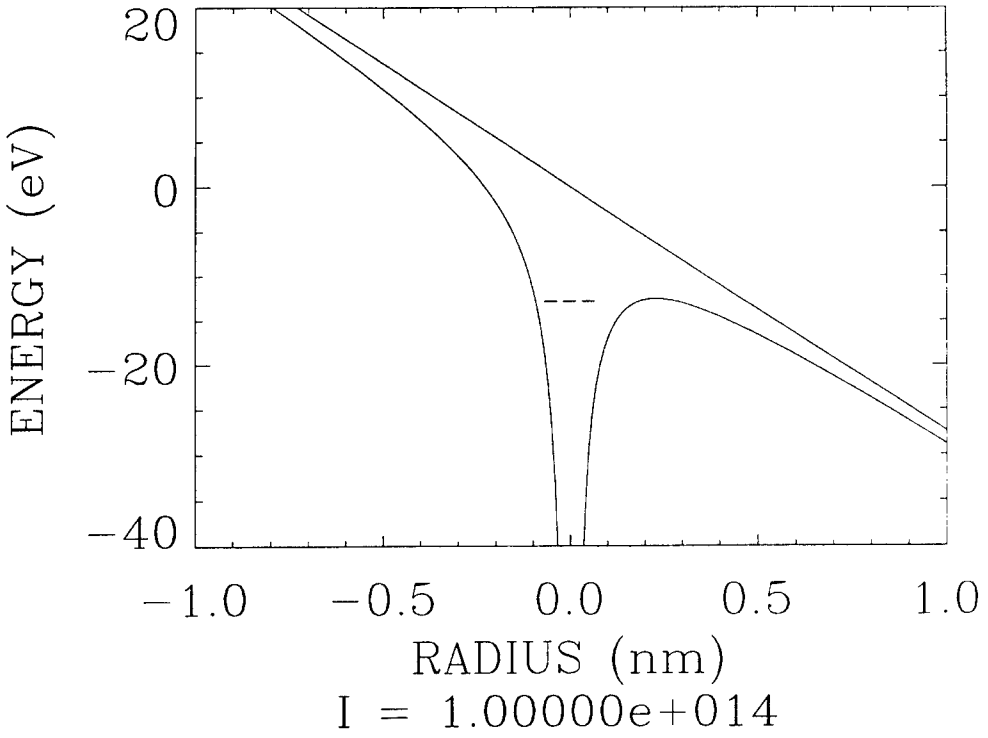

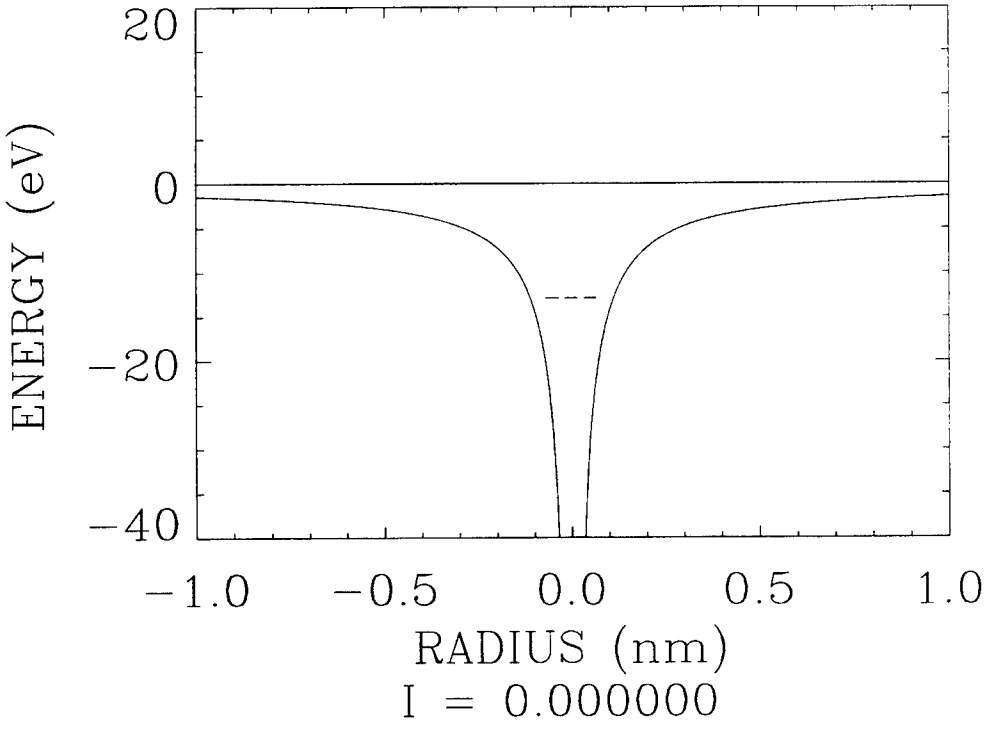

Figure 1. Distorted Coulomb potential in the static field model for hydrogen in the absence of the radiation field (lower) and in a field of intensity 10^{14} W/cm^2. The dashed line marks the location of the ground state of H (-13.6 eV).

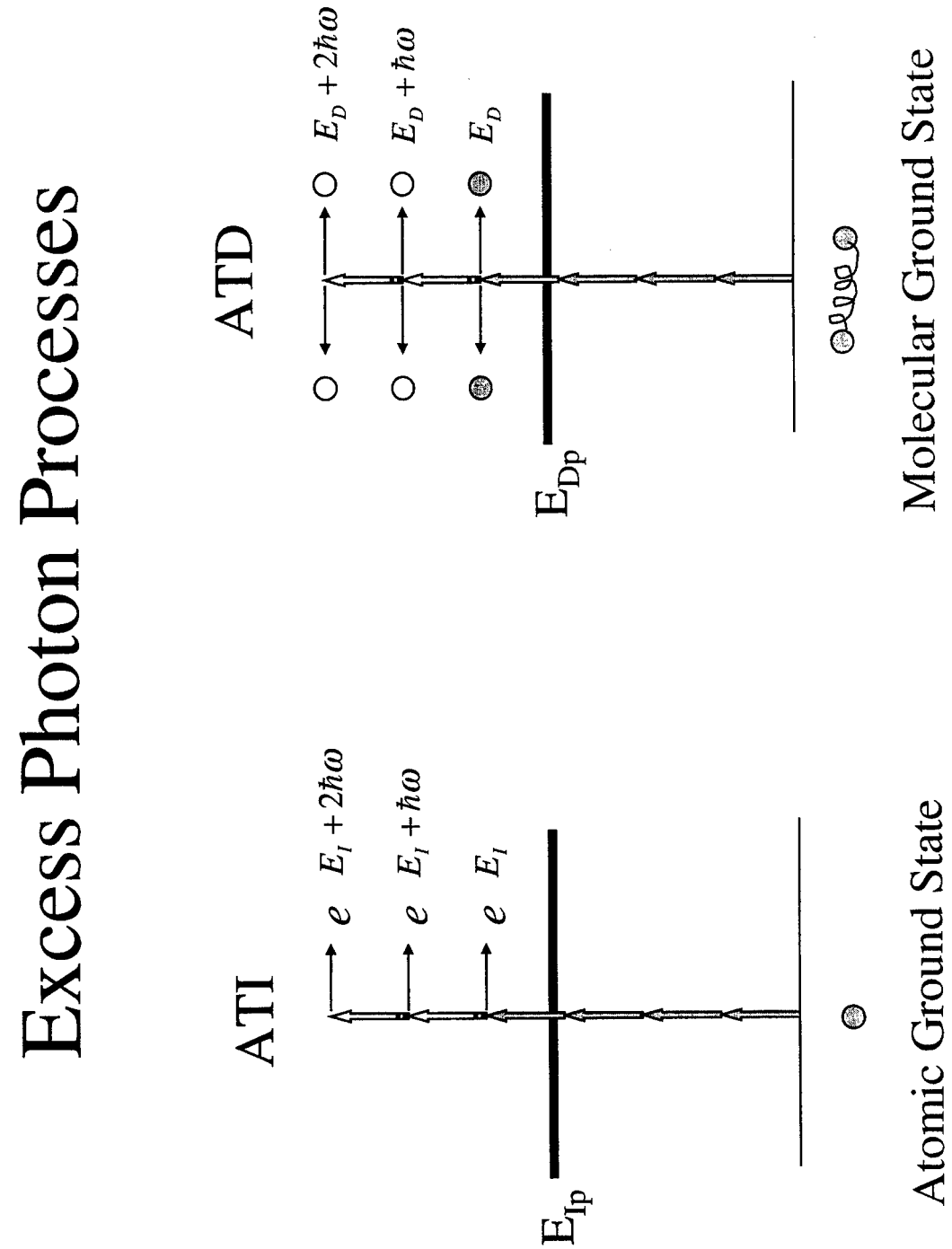

Figure 2. Schematic of above threshold ionization (ATI) and above threshold dissociation (ATD).

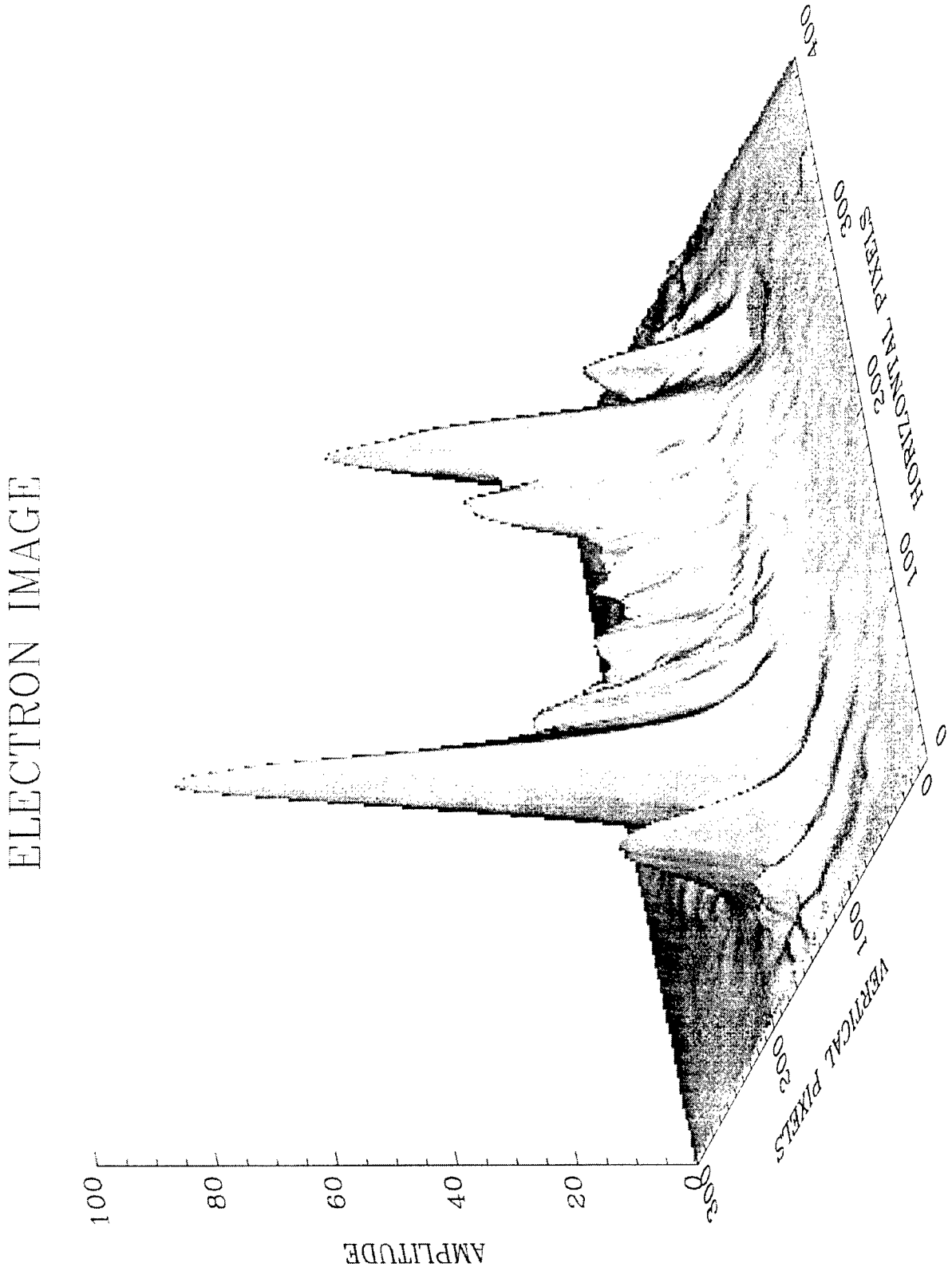

Figure 3. Typical ATI spectrum of H_2 obtained at 10^{14} W/cm^2 with 532 nm 70 ps radiation taken from Ref. 17.

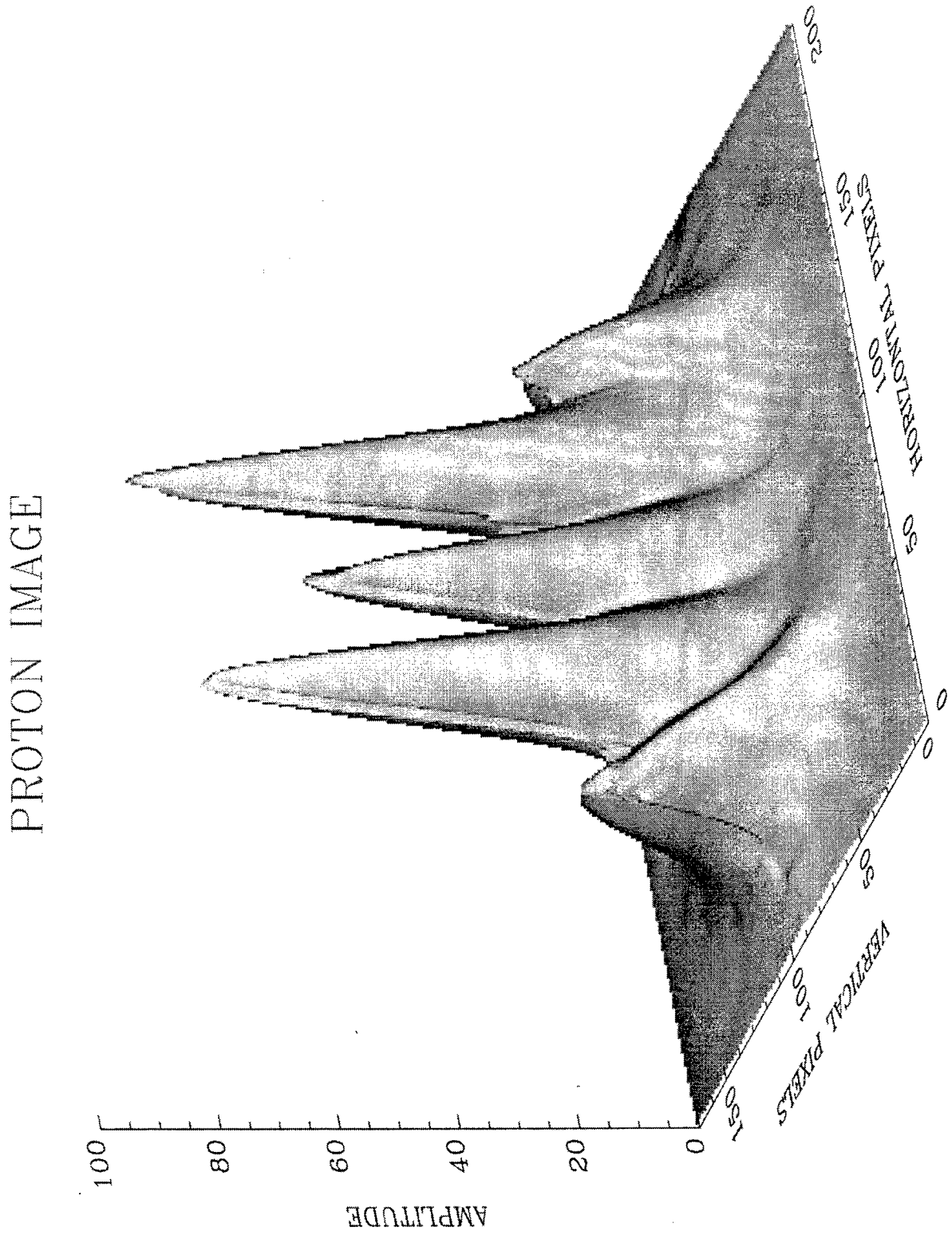

Figure 4. Typical ATD spectrum of H_2 obtained at 10^{14} W/cm^2 with 532 nm 70 ps radiation taken from Ref. 17.

Dissociative Ionization of H_2 @ ~ 10^{15} W/cm^2

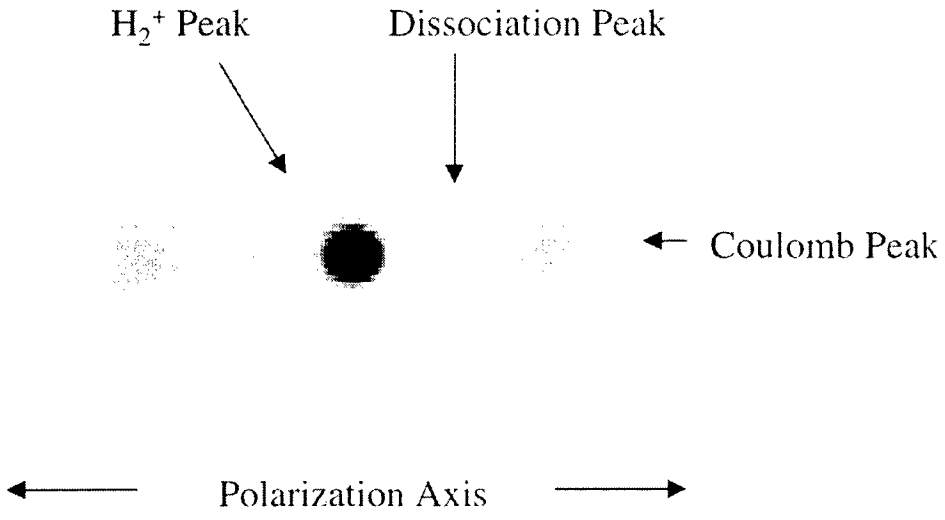

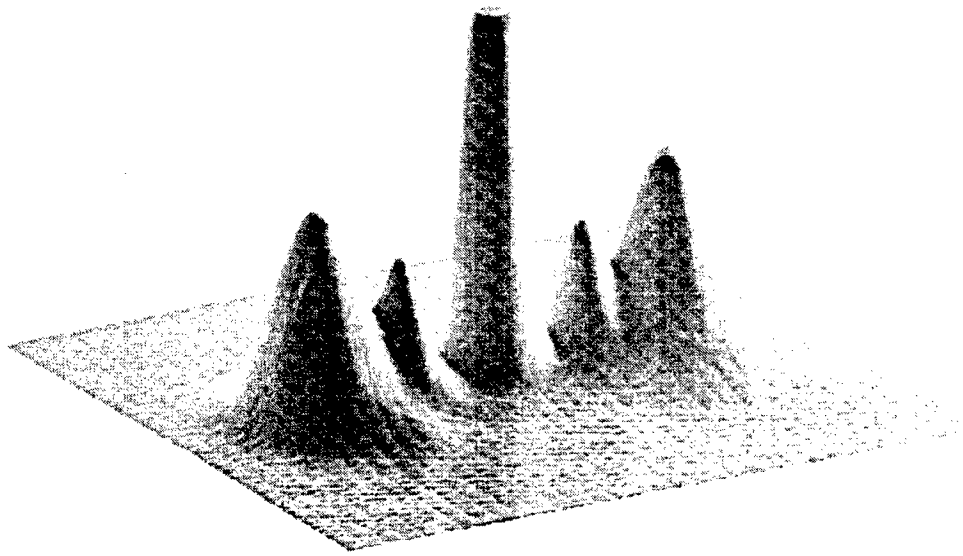

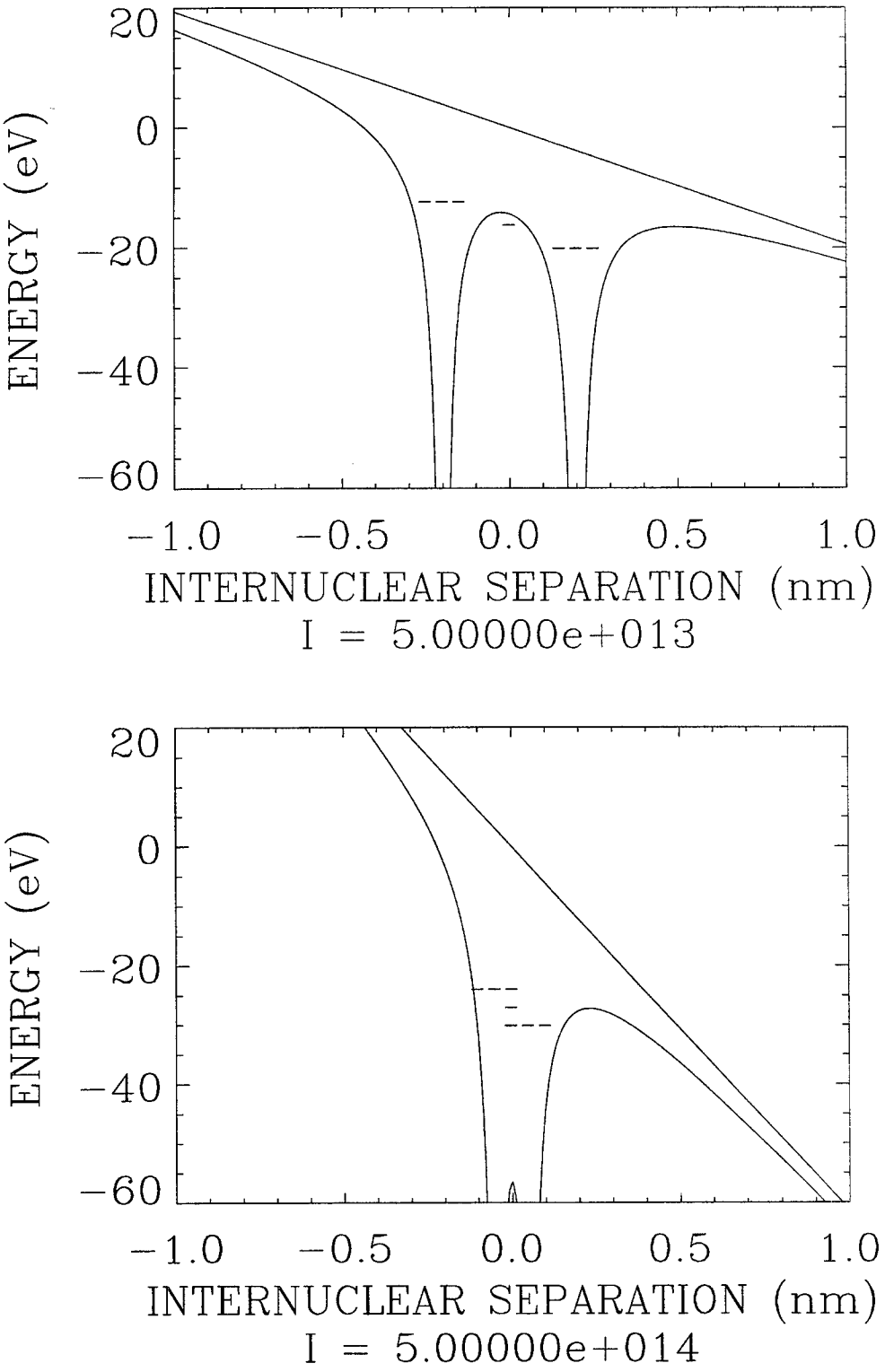

Figure 5. Distorted molecular potential for H_2^+ at $R = R_{eq} \sim 0.1$ nm (lower) and $R = R_C \sim 0.4$ nm. The triple long dashed lines indicate the location of the shifted ground states in the left and right wells. The single dashed line indicates the field-free location of the ground state.

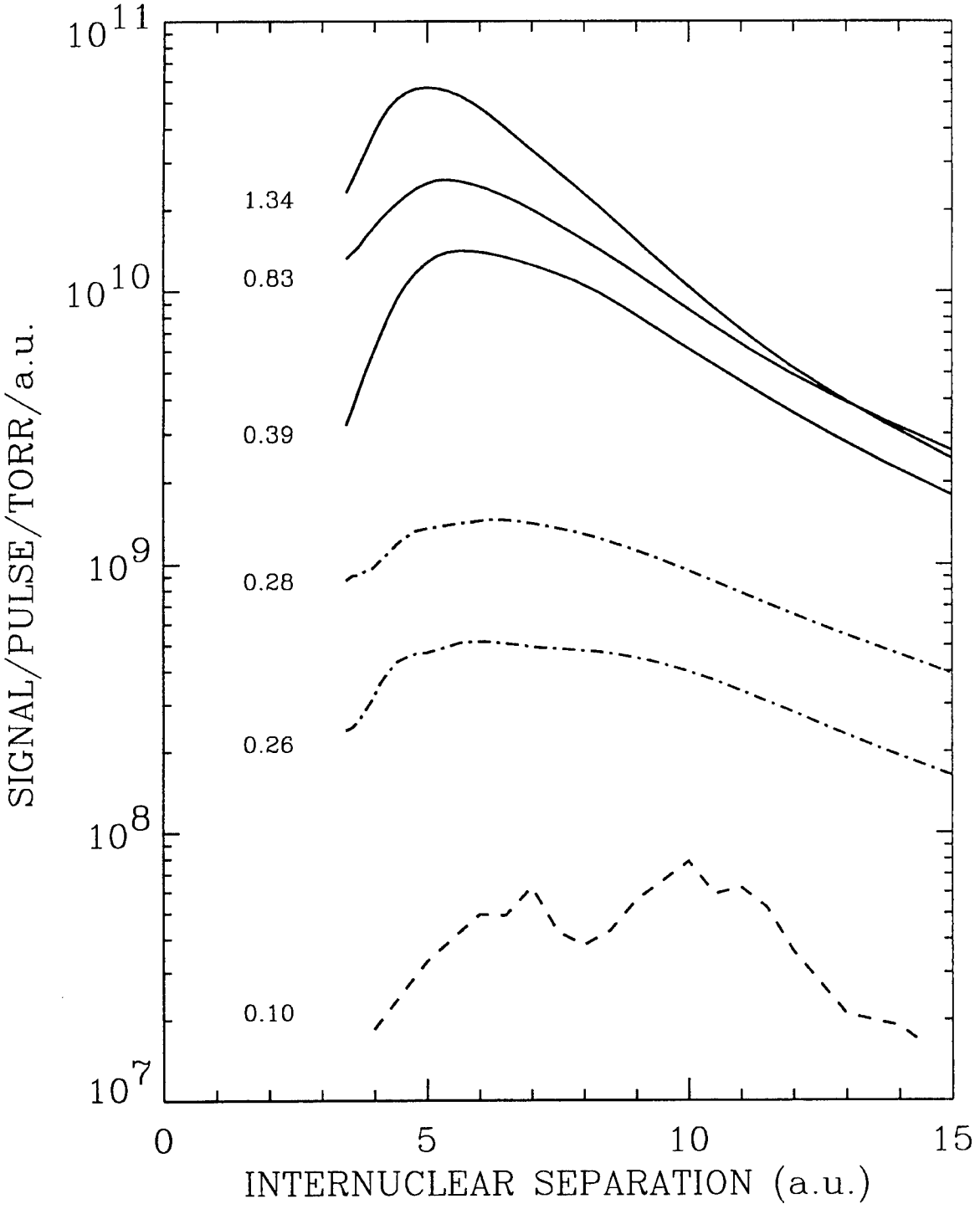

Figure 6. Production yields for Coulomb explosion protons subsequent to excitation with 800 nm 100 fs radiation taken from Ref. 15. The numbers to the left of each trace correspond to the laser intensities (10^{15} W/cm^2 at which the trace was obtained. The solid curves are the experimental yields for intensities near and above the saturation intensity for ionization of H_2 (~ 4 (10^{14} W/cm^2), the dot-dashed curves are the experimental yields below saturation and the dashed curve is the theoretical yield (10^{-4} (s^{-1}) taken from Rev. 14.

African Astronomy

Jarita Holbrook

University of Californis, Los Angeles

The title of this paper "African Astronomy" tends to cause readers to scratch their heads in confusion and ask for more details as to what exactly it means. Does it mean academic or European astronomy conducted on African soil? Not in this case. Instead, "African Astronomy" refers to the astronomical beliefs, artifacts, and practices of indigenous African peoples. Why study African Astronomy? The night sky is the heritage of all peoples and each took countless generations to watch, justify and map the heavens in addition to defining their relationship with it. Indigenous European, Arabic, American, and Polynesian astronomies have been the focus of many scholars over the last century. These works have revealed a intimate knowledge and understanding of the night sky and its phenomena. There is a decided lack of scholarship on African astronomy. However, two African sites of astronomy have been studied in great detail: Egypt and the Dogon region of Mali, West Africa. My research goes beyond these two sites to sites all over Africa where various forms of astronomy have been and in some cases are still being practiced today, thus I leave it to the reader to review the extensive literature on those two sites. A brief overview of the types of astronomy and the locations in Africa where they are practiced are presented. Several sites exist but detailed astronomical analysis has not been conducted. Thus, in addition to describing established sites of astronomy, I present many sites where research still needs to be done. I hope this article serves as a starting point for individual projects on African Astronomy.

Star Lore: Star Lore refers to the myths and legends surrounding celestial bodies. Examples of star lore include the names of the planets, stars, and constellations along with the stories created about them. Star lore often incorporates origin and creation myths of people as well as insightful tales that reflect important aspects of their culture (Krupp 1991). For example, in Greek/Indo-European culture, the constellation Canis Major is the faithful dog of the hunter, the constellation Orion, reflecting an idealized and permanent relationship between man and dog. While in Egyptian star lore Orion becomes Osiris, the Lord of everything, while Sirius, the brightest star in Canis Major, becomes Isis his female companion. Africa extends from 35 degrees north to 35 degrees south covering an area of 11.6 square miles (Europe is 3.8 million square miles). The star lore of Africans spanning the continent focus on the constellations visible in their sky. As one travels from North Africa to South Africa Polaris, the Big Dipper and the Pleiades give way to Orion, Sirius, Canopus, the Magellanic Clouds, and the Southern Cross. Thus the star lore of North Africa differs from the star lore of southern Africa. Instead of telling the star lore of the various African peoples, I summarize a few of the regions/peoples and those celestial bodies that are important to them. The Pleiades and Sirius figure largely in the star lore of the peoples of Mali (Bass 1990) and Ethiopia (Lynch & Robbins 1983, Aveni 1993), and Sirius, and Canopus appear in the star lore of South Africa and Botswana (Snedegar 1997, Cuff 1997). Physically, Sirius, Canopus, the constellation Orion, and the star cluster the Pleiades are bright distinctive objects in the night sky, this is most likely the reason for their distinction in African star lore. The Milky Way which spans the sky and Venus which is bright and remains close to the Sun are focused on all over Africa (Senkintu 1956, Aveni 1993, Doyle 1997). The Southern Cross is important to the Zulu, Sotho, and Tswana of southern Africa and is recognized as a navigation constellation (Cuff 1997, Snedegar 1997). For a treatment of the legends and myth behind the stars and constellations see E.C. Krupp's Beyond the Blue Horizon and the bibliography of this paper.

Equinoxes and Solstices: Due to the 23.5 degree tilt of the polar axis of the earth, the apparent motion of the Sun, in addition to traveling east to west over the course of a day,

travels south, to north, to south over the course of a year (limits 23.5 degrees north and south). The north and south extremes of the Sun's path are called the solstices, and the equinoxes mark the half-way points in between the two. For the northern hemisphere, winter solstice is when the Sun is the furthest south, and the summer solstice is when the Sun reaches its northernmost position. For the southern hemisphere, the seasons are reversed. The equinoxes are when the sun rises due east and sets due west at the Earth's equator. Africans in Zimbabwe, Togo. and Benin built physical structures aligned to the positions of the solstices and equinoxes. In the Great Zimbabwe stone city, a chevron pattern is bisected by the solstice Sun (Doyle 1997). Great Zimbabwe was built around 400 AD and a finished city around 1350 AD. It is credited to the Karanga people. In Togo and Benin, the Batammaliba people have designed their houses such that their crossbeams are aligned to the equinox sunrise and sunset (Aveni 1993). Finally, there are over 1600 stone circles in Senegal, the Gambia, and Togo which have yet to be astronomically analyzed and may have no astronomical significance (Posnansky 1982), however in East Africa, the stone circle, Namorotunga II, has been shown to be an astronomical calendar but this is still under debate (Lynch & Robbins 1983, Doyle 1997).

Calendrical Systems: Agricultural calendars, migration calendars, and rain schedules are all important to African people. Possibly the oldest lunar calendar is the Ishango bone dated at 6500 B.C. (Van Sertirna 1983, Aveni 1993), though it may be two or three times that age (Finch 1998). The Ishango bone was found at the site of a fishing village on the shores of Lake Edward which border the Congo (Zaire) and Uganda. The lunar cycles regulate the tides and marine activity, thus, it's not unexpected to find a lunar calendar along the shores of a lake (Aveni 1993). The problem of following a lunar calendar is that it doesn't accurately measure the solar and seasonal year. Twelve months only adds up to 354 days about I I and a quarter days short of the 365 and one quarter days of the solar year. The Borana of Ethiopia follow a lunar calendar but add an extra month to compensate for this difference (Aveni 1993, Ruggles 1987). But as a result, telling time among the Borana is not a simple matter but debated because of this. In the Congo (Zaire) the Milky Way is called "God's clock" and is orientated east-west during the wet season and oriented north-south during the middle of the dry season (Aveni 1993). In Mali, the Bozo people migrate along the delta of the Niger river when the Pleiades transit overhead and begin their fishing season when the Pleiades leave the night sky (Bass 1993). The equinoxes, solstices, and stars are more closely aligned to the solar cycle, thus observing these phenomena establishes a more exact year than following a lunar calendar.

Stellar Navigation: Stellar navigation is a method of using the stars to determine directions when traveling at night. During my field work in Tunisia, North Africa, I discovered that the fishermen of the Kerkennah Islands still used stellar navigation to reach their fisheries at night (Holbrook 1998). Since then I've unveiled several sites of stellar navigation all over Africa. A second site which I am researching is the Afar people in Eritrea. During the struggle for independence which ended in 1993, the Afar where consulted to navigate troops at night. Other potential stellar navigation sites are in Senegal, Ghana, Nigeria, and Madagascar. Most but not all of the sites as associated with ocean travel.

Summary: My preliminary findings on African Astronomy reveals a continent rich in astronomical traditions. I have presented four of these traditions as separate from each other, but in fact they overlap in interesting and unexpected ways. Such as stars being named for their use in navigation or being named for the season which begins with their appearance. In addition to the four topics mentioned here there are several more focusing on the moon, the sun, the major planets, and the relationship between the stars and man. I continue to search the literature for mention of African astronomical traditions as well as taking trips to Africa to interview people about their astronomy.

Aveni, A., " Africa's Socialized Astronomy", in Ancient Astronomers, Montreal: St. Remy Press, 1993.

Bass, T. A., " Camping with the Prince", in Camping with the Prince , Boston: Houghton Mifflin, 1990.

Krupp, E. C. Beyond The Blue Horizon: Myths & Legends Of The Sun, Moon, Stars, & Planets, New York: Oxford Univ Press, 1991.

Doyle, L., Frank, E. "Astronomy in Africa", Encyclopedia of the HistoKy of Science, Technology, and Medicine in Non-Westem Cultures, Helaine Selin, Dordrecht: Kluwer, 1997.

Holbrook, J. "Stellar Navigators of the Kerkennah Islands, Tunisia", **Archeaoastronorny & Ethnoastronomy Newsletter,** submitted.

Lynch, B. M., Robbins, L. H., " Namoratungu: The first archaeoastronomical evidence in sub-saharan Africa", in Blacks in Science: Ancient and Modern, Van Sertima, I., New Brunswich, N.J.: Transaction Books, New Brunswich, NJ, 1983.

Posnansky, M., "Complex Societies, Megaliths and the Early State in West Africa", **Quarterly Review of Archaeology**, pg 14, June 1982.

Ruggles, C., "The Borana Calendar: Some Observations", **Archeaoastronomy** Supplement 11, pg 35, 1987.

Sekintu, C. M., Wachsmann, K. P., Wall Patterns in Hima Huts, Kampala: the Uganda Museum, 1956.

Van Sertima, Ivan, " The Lost Sciences of Africa: An Overview", in Blacks in Science: Ancient and Modern, Van Sertima, I., New Brunswich, N.J.: Transaction Books, New Brunswich, NJ, 1983.

For readings on Star Lore:

Cuff, K. "African Skies", publication of the Lawrence Hall of Science Holt Planetarium, UC Berkeley, 1997.

Krupp, E. C. Beyond The Blue Horizon: MZhs & Legends Of The Sun, Moon, Stars, & Planets, New York: Oxford Univ Press, 1991.

Snedegar, K., "lkhwezi", **Mercury**, pg 13, Nov 1997.

Essence of M-Theory

Clifford V. Johnson
University of Kentucky

Abstract

A brief review of some recent advances in the search for unified theories of the fundamental interactions is given. The focus is initially on the physics of "String Theories", starting with perturbation theory and then considering non-perturbative issues. A striking family of non-perturbative relationships between the string theories, called "duality", is summarized. These relationships have been reinterpreted as properties of an even more basic theory, called "M-Theory", from which all of the string theories arise in different dynamical limits. The search for a complete understanding of M-theory has begun with a definition of it in the light-cone gauge called "Matrix Theory", which is also described. This work has uncovered many exciting features of the type of theory we need to explain the most basic properties of our universe, the most striking being the cooperation between supersymmetry and quantum mechanics to dynamically produce spacetime.

1. THE PROMISE OF STRING THEORY

All of the physical interactions that we have studied in Nature are attributable to one of four forces; the Electromagnetic interaction, (which are studied with a type of "quantum field theory" known as a "U(1) gauge theory"), the Weak interaction (SU(2) gauge theory), the Strong interaction (SU(3) gauge theory), and the Gravitational interaction, which is not described as a quantum field theory. In addition, there are various families of matter, the quarks and leptons. Together, matter and force are described to some extent by the "Standard Model of Particle Physics" (which does not include gravity).

At various higher and higher energy scales (*i.e.*, smaller and smaller distances), the various forces (with the exception of gravity) are known to merge, combining into one single interaction. Ultimately, the interactions of matter via the first three forces may be described very successfully in a *"unified theory"* in the context of field theory. (In Figure 1, we show this schematically by plotting, as a function of interaction energy, a dimensionless measure of the interaction strength of each interaction: the strong, weak, and electromagnetic forces, from top to bottom, respectively.)

One of the long-standing puzzles is gravity. *It cannot be fully described by any known quantum field theory.* Technically, four (and higher) dimensional field theories of quantum gravity are known to be non-renormalizable, which means (roughly) that they become inconsistent at short distances. Quantum gravity therefore cannot fit into the unified field theory framework. However at high enough energies (the characteristic scale at which this happens is called the "Planck scale", approximately 10^{19} GeV, or a length scale of about 10^{-33} cm) we will not be able to ignore the lack of a quantum field theory description of gravity. It must somehow fit into our framework for describing Nature if we are to understand such things as the very early universe, the evolution of black holes, the origins of the Standard Model, and the nature of spacetime itself.

Over the last 20-25 years, a framework has emerged which holds much promise for understanding all of the forces and matter.

Much of the arbitrariness (like the plethora of particle species) of the standard model, is naturally absent in this framework which is often called *"String Theory"*.

String theory is a theory of extended one-dimensional objects [1]. All particle species (both matter particles like quarks and electrons and force particles like gluons and photons) have their origins in *different modes of vibration* of the single basic string. (Figure 2 denotes an open string and a closed string.) This fits comfortably with our present-day observations that the fundamental constituents of matter are particles if one sets the energy scale at which one sees their stringy extent to be much higher than our currently accessible energy scales. This is usually set to be around the Planck scale.

Why? This is due to one of the remarkable properties of string theory (or at least the types relevant to this discussion*). As a consequence of basic internal consistency, they all describe a massless spin two particle in their spectrum of excitations.* This type of particle -the "graviton"- carries the quantized gravitational force (just like the photon, a spin one massless particle, carries the quantum electromagnetic force), and so it is natural to set the scale at which it appears to be the Planck scale, as discussed above. So all strings naturally describe quantum gravity right at the outset! As we shall see later, they also naturally give rise to other fields which can be identified with the rest of the forces we see in Nature.

Another attractive aspect of strings is the fact that their interactions are described simply by their splitting and joining, which can only be done in a very small number of ways, in contrast to interactions in field theory, where there are very many more ways. It turns out that this way of generating interaction has many properties which are very desirable in a quantum theory.

The interaction vertex is smooth and not fixed at a particular point in space-time, producing a theory with good short-distance properties (See Figure 3). This is in contrast to a field theory vertex, where the vertices there can sometimes produce bad behaviour (like the aforementioned non-renormalizability).

The theory is surprisingly free of adjustable parameters: there is only one free parameter in a string theory, the string tension ($T_s \sim 1/L_s^2$). Everything else is dynamically generated. (In the units we are using, the string tension has dimensions of inverse length squared. This also defines for us what we will call the "string length", L_s, which is the characteristic length scale at which the stringy effects begin to switch on.)

Given those properties above, it is natural to try to understand if we can describe our world in terms of strings. In about 1984, the "1st Superstring Revolution" happened: The means for constructing quantum consistent "Superstring" theories were discovered.

A. Superstring Theories

Following a logical path similar to that taken historically to develop consistent particle theories, a study of the properties of quantum string theories began [1]. The perturbative analysis took place initially in "first quantization", where one introduces quantum mechanical canonical commutation relations at the level of the coordinates of the string to be quantized. The next type of analysis would logically be "second quantization", where the canonical commutation relations are *instead* introduced at the level of fields which create and destroy the strings in the theory.

(These historical terms are of course misnomers. The former method of quantization is merely "quantum mechanics" while the latter is simply "quantum field theory"; there is only one step of quantization in each case, despite the names.)

In contrast for the situation for quantum particle theories, we do not have a full understanding of quantum field theories of strings, which we can call "string field theory", leaving "field theory" as used before for field theories of particles. That second step in the development of strings was never completed. In the light of the discoveries to be outlined below, it is not clear what the role of that development should be.

Call the strength of the interaction between strings λ. For λ small ("weak coupling") it is possible to develop a perturbative analysis of strings which is very powerful indeed, despite

not having a complete string field theoretic description, even at weak coupling. The perturbative quantum mechanical analysis was able to show that there are tight restrictions on the consistent types of strings that can exist.

Actually, for a long time, it seemed that there were technical problems which prevented *all* string theories from being consistent. The result of the 1st Revolution was to show that those technical difficulties (called "anomalies") could be surmounted in certain cases. The cases for which it can be done resulted in five consistent string theories, the "Type IIB & Type IIA" theories, the "Type I" theory, and the "SO(32) & $E_8 \times E_8$ Heterotic" theories [1].

These theories are all *"supersymmetric"*, and propagate most naturally in ten (9+1) space-time dimensions. Supersymmetry is a space-time symmetry which relates *"bosonic"* (integer spin) excitations to *"fermionic"* (half-integer spin) excitations of the same mass-energy.

As force particles (like photons and gluons) are bosonic, and matter particles (like electrons and quarks) are fermionic, it is clearly a remarkable symmetry. It has many attractive properties even in theories of only particles, and is expected by many to be a symmetry of Nature. Indeed, the next phase of interesting standard model physics is intimately related to supersymmetry and there are machines being built to look for signals of this symmetry.

All of the consistent string theories require supersymmetry. Indeed, it was invented in this context. Any symmetry group has a (set of) basic *generators* from which all elements of the group may be constructed. The generator of supersymmetry can be associated with a certain massless particle in the theory: the "super-partner" of the graviton, called the *"gravitino"*, which is a spin 3/2 particle (a fermion).

The superstring theories may be classified (roughly) in terms of their gravitino content: The Type II strings are closed strings with two supersymmetry generators, and hence two gravitini, while the Type I and the heterotic strings (open and closed strings, respectivly) have one supersymmetry.

The resulting strings are very different, as can be seen in their spectrum of excitations. The excitations of a string theory look (at distances large compared to L_s) like spacetime fields of various types, which create and destroy the various particles the string can pretend to be in this low energy limit.

All closed strings have the following massless fields in their spectrum: $G_{\mu\nu}$, $B_{\mu\nu}$ and ϕ. The indices μ and ν are spacetime indices (they run from 0 to 9). The field $G_{\mu\nu}$ is a symmetric tensor field ($G_{\mu\nu} = G_{\nu\mu}$), which is associated to the graviton. ϕ is a scalar field called the dilaton. The field $B_{\mu\nu}$ is an anti-symmetric tensor field ($B_{\mu\nu} = -B_{\nu\mu}$) It shall be denoted as $B^{(2)}$ for short, showing that it is an anti-symmetric tensor field with two indices, *i.e.*, "rank two".

There are other anti-symmetric tensor fields, depending upon the type of string. Type IIB theory also has fields $A^{(0)}$, $A^{(2)}$, $A^{(4)}$, $A^{(6)}$ and $A^{(8)}$, while instead, the type IIA theory also has fields $A^{(1)}$, $A^{(3)}$, $A^{(5)}$, $A^{(7)}$ and $A^{(9)}$. These fields play an important role in the theories, and may have a role to play in phenomenology too, but we will not describe these matters here.

The heterotic strings have a gauge field A_μ ($=A^{(1)}$) which describes a 10 D non-Abelian gauge theory with either gauge group $E_8 \times E_8$ or SO(32). Meanwhile, the type I string has in addition to $G_{\mu\nu}$, and ϕ, a gauge field $A^{(1)}$ with gauge group SO(32), and a family of anti-symmetric tensor fields $A^{(2)}$, $A^{(6)}$ and $A^{(10)}$

So the theories are very different, having a completely different field content at low energy.

B. Compactification

One of the attractive properties of the five string theories is the fact that they live in ten dimensional space-time. Therefore, in order to describe four dimensional space-time physics, it is natural to 'hide' the other six dimensions in such a way that we do not see them too easily.

This process is called "compactification". Figure 4 shows how ten dimensional spacetime can be split into the product of a six dimensional internal manifold Q_6 and the 3+1 dimensional manifold that we live in, M_4 .

The product means that at every point in the 3+1 dimensional spacetime, there is a hidden copy of the manifold Q_6.

A very attractive feature of this geometrical construction is that the internal six-dimensional manifold Q_6 adds new structure (e.g. multiple similar families of leptons) to the spectrum of the string model. Some properties of the manifold contribute new additional particles and symmetries, to the theory. They also can help to break some of the 10 D symmetries.

We will not describe this procedure in full generality here, but will pause to consider a special example of compactification, called *"Kaluza-Klein Theory"*.

Compactification was actually invented *before* string theory. It is probably the earliest modern (*i.e.,* 20th Century) attempt at unification using geometry. The context was gravity and electromagnetism.

Consider a five dimensional gravity theory, making the five dimensions of spacetime have topology $R^4 \times S^1$, where the circle S^1 has radius R. See figure 5.

Imagine that the circle is very small. Four dimensional viewers will not easily detect the circle because it is small. However, there is a choice, at every 3+1 dimensional spacetime point, of where one is on the circle. In other words there is an internal symmetry.

From the point of view of 4+1 dimensions, one can do a transformation called an isometry. This is a symmetry of the metric. From the point of view of 3+1 dimensions, a symmetry which acts on the circle is an internal symmetry, while a symmetry of the rest of 3+1 dimensions is a symmetry of the 3+1 dimensional metric (including all of the properties which define 3+1 dimensional gravity).

This internal symmetry is U(1). It is a "gauge symmetry" because it is a local symmetry: the circle can be rotated differently depending upon where one is in the 3+1 dimensions. As mentioned at the beginning of this article, this is the gauge theory which underlies electromagnetism. We have unified it with gravity, showing that it arises from putting 4+1 dimensional gravity in a special geometrical situation. Meanwhile, the 3+1 dimensional observer sees a 3+1 dimensional theory of gravity coupled to a 3+1 dimensional theory of electromagnetism.

There are some additional features: There are *"Kaluza-Klein particle"* excitations in the 3+1 dimensions, whose masses are quantized in units of m=1/R, they arise as analogues of the discrete spectrum one would obtain by placing a particle in a box. The box this time is the circle, S^1, of radius R.

Given their mass dependence, as R shrinks away they are very massive particles. 3+1 *dimensional observers do not see them at low energy.*

In terms of four dimensional fields, we note that the 4+1 dimensional graviton field (metric tensor) G_{MN} decomposes into the following 3+1 dimensional fields: $G_{\mu\nu}$, $G_{\mu 5}=A_\mu$, and $G_{55}=f$. Here A_μ is the four dimensional gauge field. It is pure geometry from a 4+1 dimensional point of view!

Such Kaluza-Klein mechanisms are common in string theory compactifications, the higher dimensional graviton fields G_{MN} contained in those theories giving rise to lower dimensional graviton fields, gauge fields and scalar fields, as we have seen briefly above. In addition, the other fields in the string theories (the various antisymmetric tensor fields and non-Abelian gauge fields) give rise to 3+1 dimensional fields in similar fashion, producing the candidates for the phenomenology of the standard model at low energy, new physics at higher energy, and so on.

(Historically, Kaluza-Klein theories were abandoned before string theories came along: They don't have good phenomenology, nor do they have good quantum properties on their own, as they were originally based upon field theories of gravity, instead of string theories.) The idea of unification via geometry remained, and survived to be incorporated into string theory. We shall see it come back in a dramatic fashion later on in this article.

C. Phenomenology

Many interesting properties of strings were discovered over the years, strengthening the

resolve of researchers that this was likely to be a great new theory of Nature.

It is quite easy to find compactifications to four dimensions where the physical gauge group is any of the commonly studied grand unified groups, like SO(10) or SU(5), or even directly SU(3) x SU(2) x U(1). For a long time then, the main pursuit in string theory was to play with ways of finding the right compactification of the $E_8 \times E_8$ heterotic string, giving the gauge groups needed, and the particle species and multiplicities required by what we see in Nature. The other strings were regarded as interesting curiosities, but not useful for formulating a final theory of nature for many technical reasons, one of which was their less phenomenologically interesting gauge groups.

Eventually, certain phenomenological questions led us to ask the following questions: What happens to strings when we allow them to interact strongly amongst themselves? How do we describe the theory in such a situation?

Then came the 2nd Revolution.

2. STRONG/WEAK COUPLING DUALITY

Recently (1994-1996), we have understood much about the nature of string theory when the splitting-joining interaction, whose strength is set by 1, *is no longer small* [2,3,4].

A *new symmetry of both point particle theories and string theories* was discovered, which gives clues about their properties. This new, poorly understood phenomenon at the heart of string and field theory is called *"Strong/Weak Coupling Duality"* (or "duality" for short).

This phenomenon relates strongly coupled theories to weakly coupled ones. Duality has *vitally important consequences* for the whole program of particle physics. Its very existence confirms that we presently lack understanding of the basic formulation of both *gauge theories* and *string theories.* Although we do not understand its origins, we have learned a lot about it using a number of powerful techniques.

In particular, the five types of superstring which we described above, which seem manifestly different, are only so at weak coupling (small λ). We get a surprise when we consider them at large λ. *At strong coupling, they are all related to one another!* (Figure 6 attempts to denote these relationships very schematically. The interior of the figure represents the largely unknown region of physics described by a theory called "M-theory". See later).

For example, start with the SO(32) heterotic string, with coupling λ_h. For small λ_h, the physics is described in terms of the string perturbation theory we discussed earlier. The spectrum of excitations is as described. A consistent theory of the weakly coupled interactions may also be developed, and useful calculations performed, etc.

For intermediate values of λ_h, where we no longer have the techniques to formulate a perturbative description, the properties of the theory are unknown to us. We have no techniques to describe this situation. However, for extremely large λ_h, the degrees of freedom of the theory reorganize themselves into something familiar: The spectrum of the SO(32) type I string theory, at weak coupling λ_I! Conversely, start with the type I theory at weak coupling (λ_I small) and move to strong coupling (λ_I large). In this limit the physics is described by the SO(32) heterotic string at weak coupling (λ_h small)!

This phenomenon, exchanging the two theories and simultaneously doing $\lambda_h \leftrightarrow 1/\lambda_I$ is what is called *'Strong/Weak Coupling Duality'*. Notice that it is an extremely dramatic relationship between theories. In this example, recall that the type I string is an open string theory while the heterotic string is a closed string theory. Nevertheless, the duality relates these theories non-perturbatively. Similar relationships hold among the other string theories. This leads to the suspicion that string theories might not be the whole story [5].

A. Is there a Parent Theory?

Dualities relate very different string theories, or relate string theories to theories which are not string theories as we shall see. They therefore drive home the idea that *the non-perturbative definition of strings will likely not be based upon strings at all.*

So string theory is not really a theory of strings. Stringy physics is simply an artifact of some perturbative limit of a 'parent theory', which remains to be understood.

Now that *all of the string theories are relevant*, the prospects for phenomenology are much better, as we do not have to explain why we throw out four of the theories and keep only one. All of the interesting and perhaps useful properties of the 'different' string theories can be used to help study Nature.

Very quickly, we are led to the idea that now that the string theories are all related to one another in such an unlooked-for manner, there is the possibility that there is an underlying theory from which all of the string theories arise dynamically. Then the duality relationships between the string theories become elevated to symmetries of the parent theory.

A general question arises, however. If we cannot yet formulate the complete theory, how do we discover some of its symmetries, like the dualities mentioned above? The success in doing this was due to the discovery of the most powerful tool in the duality game: *"D-Brane Technology"*[6], which we will not have time to describe here.

We will see a little of how they are used in what follows.

B. Type IIA / M-Theory Duality

The type I, IIA and IIB string theories were shown to contain other sorts of very special objects. Using special techniques, they were shown to be "solitons" whose masses go like $M_0 \sim n/(\lambda_{IIA} L_s)$, where λ_{IIA} is the string coupling. These solitons are extended objects of various dimensions and have an important role to play in the duality story due to the fact that they are the basic sources [7] of the various anti-symmetric tensor fields $A^{(n)}$ which were mentioned earlier. These objects are called *"D-branes"* [6].

They are special states called "BPS saturated" states[7]. Such states are of special interest in theories with the amount of supersymmetry that string theories have. They have certain general properties as a result of the supersymmetry of the theory alone. One such property is the fact that a mass formula such as the one above can be proven to be *true at all values of the coupling.* This means that we can extrapolate the formula to all values of the string coupling λ_{IIA}.

Let us concentrate on the type IIA theory, and the set of point-like D-branes called "D0-branes". In the above formula, *n* is any integer, and the mass formula represents a bound state of *n* of these D-particles.

Looking at the formula we can see that at weak string coupling, *they are infinitely heavy.* What happens at strong coupling?

Well as $\lambda_{IIA} \to \infty$, we get a whole family of states going massless. It is difficult to make sense of this new aspect of the spectrum at strong coupling. *Indeed, it is impossible to do so in the context of type IIA string theory, as they do not fit into the massless string spectrum.* One reason is that these new massless states are charged under the $A^{(1)}$ field which the type IIA strings themselves are not charged under, and therefore they cannot appear as an elementary type IIA string excitation.

But we have seen this formula before, *in the context of Kaluza-Klein theory.* There, we had charged particles whose masses went like *n*/R, where R was the radius of a hidden circle. The gauge field $A^{(1)}$ came from the components of a one dimension higher graviton hidden in the circle. So if we identify $\lambda_{IIA}=R/L_s$, we deduce [2,3] that strongly coupled type IIA string theory is *an eleven dimensional theory*!

It turned out that a limit of this eleven dimensional theory has been studied before. It is a field theory of gravity! This "supergravity" theory, here with Planck scale $L_p=(\lambda_{IIA})^{1/3}L_s$, had been studied before as a candidate theory of Nature, but had been abandoned because it *had bad short-distance properties*, like all field theories of gravity in 3+1 dimensions or more. (It is crucial to note that here we arrive at this eleven dimensional theory in the long-distance limit, and so we are firmly in the regime where the supergravity is wel-behaved.)

At long distances eleven dimensional supergravity is known to have two BPS solitons, a membrane and a fivebrane called the *"M2-brane"* and the *"M5-brane"*,

respectively[4].

In the duality relationship, the type IIA string itself arises from wrapping the M2-brane around the shrinking circle! As $\lambda_{IIA} \sim R/L_s \to 0$ it becomes a string. (This is denoted in Figure 6. One should imagine that the cylinder is just a segment of a toroidal membrane, such that a closed string results in the limit. Other dualities can give open strings by having a cylindrical membrane shrink away a dimension like this.)

So although string theory seemed to make the study of eleven dimensional supergravity irrelevant, duality tells us that it is *very relevant.* On the way it does so by introducing us to a new phenomenon: The dimension of spacetime can change dynamically.

Of course, the full eleven dimensional theory cannot be supergravity alone, because of the poor short-distance properties. It is believed that there is a complete theory called "M-theory", which will complete the story. It reduces to eleven dimensional supergravity in the long-distance (low energy) limit, which in turn produces the type IIA string upon compactification on a circle, as we have seen.

It turns out that all of the string dualities are phrased geometrically in terms of M-theory, by compactifying it on different surfaces, with the string coupling arising as some aspect of the geometry.

3. M-THEORY

Ironically, we do not know what M-theory actually is, as a theory, but we do know, on general grounds and from duality that it has eleven dimensional supergravity as a low-energy limit, as we saw above. It also has a number of symmetries (both geometrical and otherwise) which imply duality in the stringy limits. Furthermore, it has degrees of freedom which significantly modify the behaviour of the theory at short distance, surmounting the apparent problem of appearing to be a theory of gravity only.

Another interesting property is that it has no intrinsic adjustable "classical coupling", like string or more common field theories. (This is evident from the eleven dimensional supergravity lagrangian, which has no continuously adjustable parameters. All terms are constrained by the amount of supersymmetry[8].) So it looks naively that we cannot start with a weakly coupled, classical theory and quantize it to find the full theory, which is usually the traditional route to finding a quantum theory of Nature.

So M-theory is a new kind of theory *which must be written down directly as a quantum mechanical theory.* There is a candidate theory which captures much of the above physics, and which might hold the clues to the final definition. It is called *"Matrix Theory"* [9].

A. Matrix Theory

Ironically, matrix theory is a supersymmetric *quantum mechanical* theory of nine N¥N hermitian matrices, X^i, with hamiltonian:

$$H = R\ Tr\left\{\frac{\Pi_i \Pi_i}{2} + \frac{[X^i, X^j]^2}{4} + \theta^T \gamma_i [\theta, X^i]\right\}$$

It has a U(N) gauge symmetry. There is supersymmetry between the bosons X^i and the components of the femion q. The Π^i are the canonical conjugate partners of the X^i.

This Hamiltonian appears to have no reference to any of the physics we discussed previously. Nevertheless, as the size of the matrices becomes infinite, *i.e.,* $N \to \infty$, it is suggested [9] that it captures all of M-theory boosted an infinite amount in a hidden direction called X^{10}. This "Infinite Momentum Frame" is defined by first placing X^{10} on a circle of radius R. Momentum is then discrete: $P_{10} \sim N/R$. It is equivalent to the more standard term "light-cone gauge", where the light-cone directions are $X\pm = t \pm X^{10}$.

Notice that when the X^i are large the commutator term $[X^i,X^j]^2$ is very costly in energy. Therefore, in this case it is energetically preferable to excite the sector where $[X^i,X^j]=0$. We therefore have ground state solutions with nine large, commuting X^i's. *These are the 9 spatial transverse dimensions!* Together with t and X^{10}, we have the full eleven dimensions.

Recall that we were supposed to recover 11D supergravity in the large distance limit. We

have done so, in the infinite momentum frame. (This is further demonstrated by the existence of states in the spectrum corresponding to eleven dimensional gravitons with the correct interactions. Also, it can be shown that in the limit of large N, the Hamiltonian can be re-interpreted as the quantum mechanics of the M2-brane in the light-cone gauge.)

(As an important aside, it should be noted that this Hamiltonian comes from the theory of N coincident D0-branes, which we met in the previous subsection. In some sense, they are the basic degrees of freedom of M-theory in the light-cone gauge. A graviton in this frame, with momentum n in the light-cone direction is simply a bound states of n D0-branes.)

Supersymmetry ensures that those "flat directions", solutions representing the ability to have large spatial separations between the constituent degrees of freedom of the theory, *are not spoiled by the interactions with the fermionic degrees of freedom.* Quantum fluctuations from the fermions are exactly cancelled by fluctuations from the bosons, as a consequence of the (super) symmetry between them. (This is a restatement of the fact that D0-branes are BPS states, as mentioned before, and as such feel no static force amongst themselves.)

So we see that spacetime emerges as a consequence of taking a long distance limit, together with supersymmetry. Notice that at short distances, the usual concepts of space break down. They are replaced by a non-commutative generalization, as configurations in the quantum mechanics involving non-zero $[X^i,X^j]$ are allowed.

This is the anticipated evidence of a revolution in our ideas about the origins of spacetime. A mechanism for the dynamical appearance of conventional spacetime at long distance (low energy) has long been sought, and this is evidence that M-theory has these properties quite naturally and simply. In this "infinite momentum" frame, it is described by a simple model of quantum mechanics! We also see that the correct description of spacetime at short distances is replaced by a well-defined notion of non-commutative geometry.

To summarize, we have seen that M-theory is intrinsically quantum mechanical, i.e. there is no conventional classical limit. We have seen that spacetime emerges dynamically as an approximate phenomenon at low energies. We have also seen that it is crucial that the theory be supersymmetric in order for spacetime (and widely separated gravitons) to emerge. (This is the first time that we have seen in a working model a "reason" for quantum mechanics: without it and supersymmetry, we would have no large spacetime in which to exist!)

It is believed that these properties are likely to survive in any 'final theory'. This is the first time we have seen a *direct reason* for quantum mechanics to exist in Nature. The final theory of spacetime and everything else is necessarily quantum mechanical in nature.

B. Looking to the Future

The matrix theory definition of M-theory has many other remarkable properties which were not mentioned in this article. Physicists have now learned how to reproduce the physics of the string theories, by finding ways of "compactifying" Matrix theory[10].

Many of the dualities between string theories indeed arise as intrinsic properties of the compactified Matrix theory. (Ironically, compactified matrix theory often resembles field theory. Various known properties of field theories translate into non-trivial relations like stringy dualities!)

There are however, many conceptual and technical problems left. We need to understand more about how to compactify on manifolds of dimension greater than five. We also need to understand how to control the theory with less supersymmetry. Also needed is a formulation which leads to a description of the theory beyond the infinite momentum frame, *i.e.*, we need a manifestly 10+1 dimensionally Lorentz invariant formulation.

New advances occur almost every day, and so there is hope that we will make great progress in the next few years.

ACKNOWLEDGEMENTS

I would like to thank the 1998 organizers of the Annual Conference of the National Society

of Black Physicists, especially Alan MacKellar, for inviting me to present this lecture. I also thank Marc Kamionkowski and the other staff and members of the Columbia University Physics department for their hospitality during the preparation of this manuscript.

REFERENCES

1 For background and details, see *"Superstring Theory"*, vols. I and II, M. B. Green, J. H. Schwarz and E. Witten, Cambridge University Press, 1987.

2 *"The Eleven-Dimensional Supermembrane Revisited"*, P. K. Townsend, Phys. Lett. **B350** (1995) 184-187; e-print archive: hep-th/9501068.

3 *"String Theory Dynamics In Various Dimensions"*, E. Witten, Nucl. Phys. **B443** (1995) 85-126; e-print archive: hep-th/9503124.

4 For a review with references, see *"Lectures On Superstring And M Theory Dualities"*, J. H. Schwarz, Nucl. Phys. Proc. Suppl. **55B** (1997) 1-32; e-print archive: hep-th/9607201.

5 For an early paper on this conclusion from duality, see *"Is String Theory A Theory Of Strings?"*, C. V. Johnson, N. Kaloper, R. R. Khuri and R. C. Myers, Phys. Lett. **B368** (1996) 71-77; e-print archive: hep-th/9509070.

6 For notes and references, see *"Notes On D-Branes"*, J. Polchinski, S. Chaudhuri and C. V. Johnson; e-print archive: hep-th/9602052.

7 *"Dirichlet Branes And Ramond-Ramond Charges"*, J. Polchinski, Phys. Rev. Lett. **75** (1995) 4724-4727; e-print archive: hep-th/9510017

8 *"Supergravity Theory In Eleven-Dimensions"*, E. Cremmer, B. Julia and J. Scherk, Phys. Lett. **B76** (1978) 409-412.

9 *"M Theory As A Matrix Model: A Conjecture"*, T. Banks, W. Fischler, S. H. Shenker and L. Susskind, Phys. Rev. **D55** (197) 5112-5128; e-print archive: hep-th/9610043.

10 For a review with references, see *"Matrix Theory"*, T. Banks, Nucl. Phys. Proc. Suppl. **67** (1998) 180-224; e-print archive: hep-th/9710231.

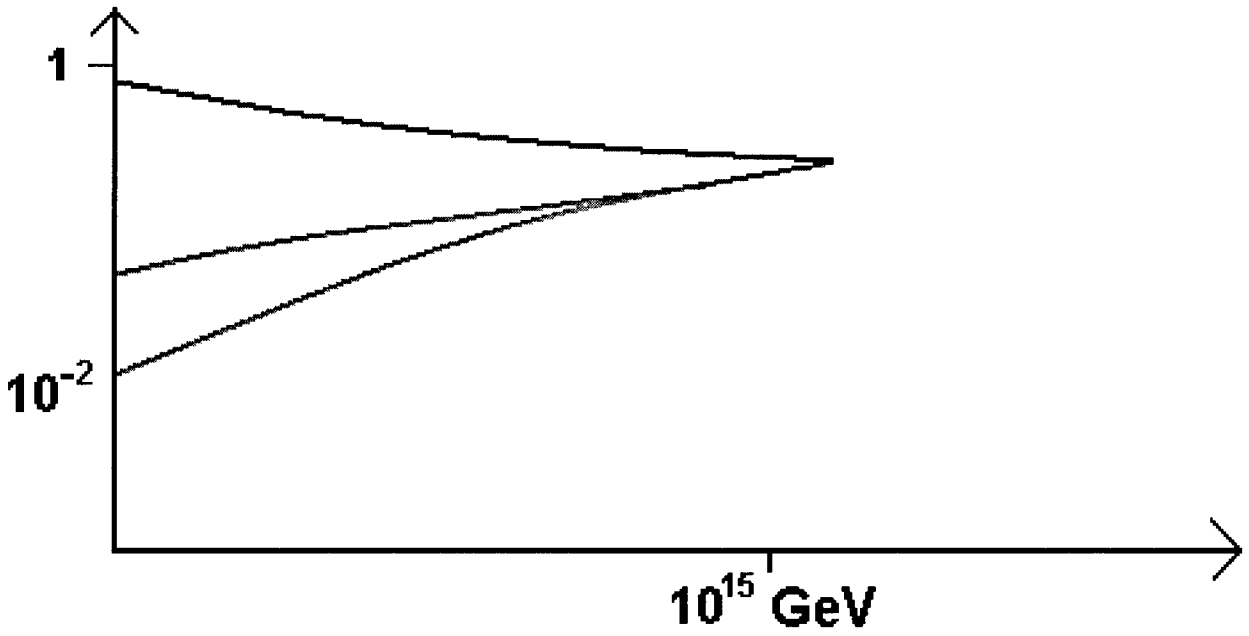

Figure 1

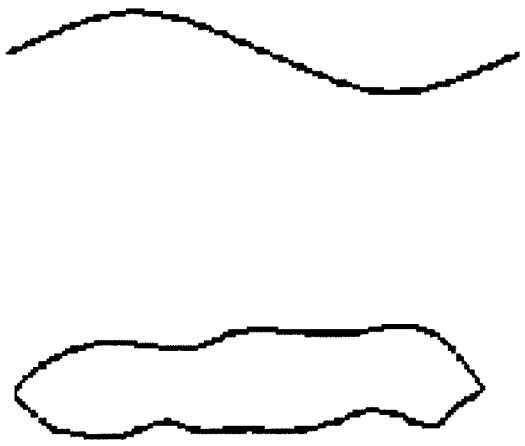

Figure 2

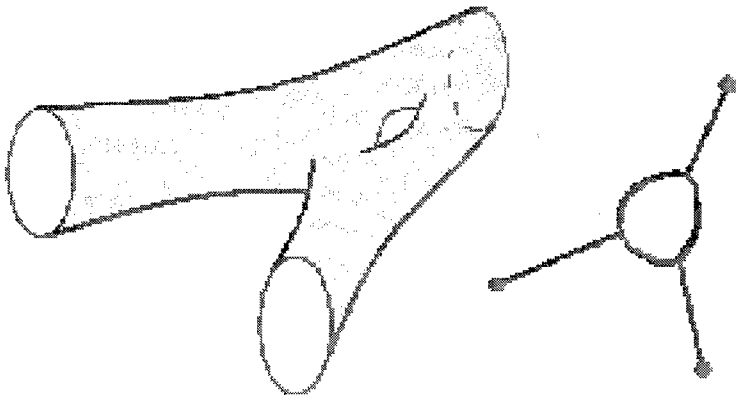

Figure 3

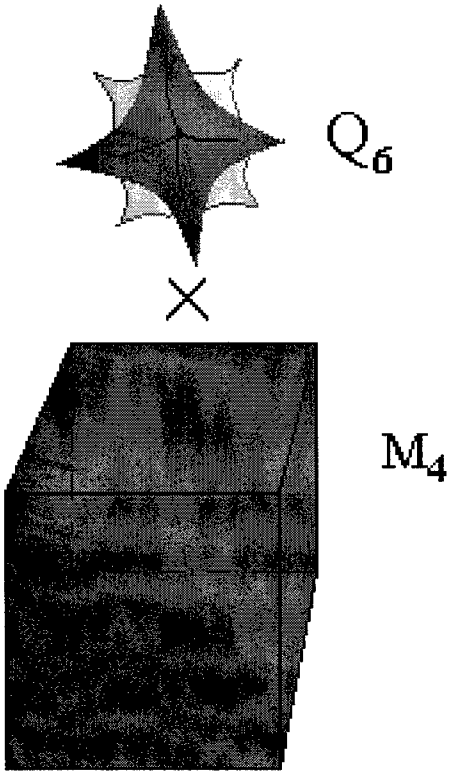

Figure 1

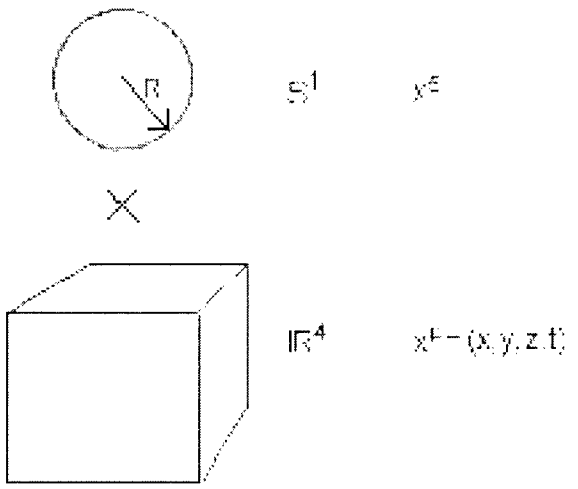

Figure 5

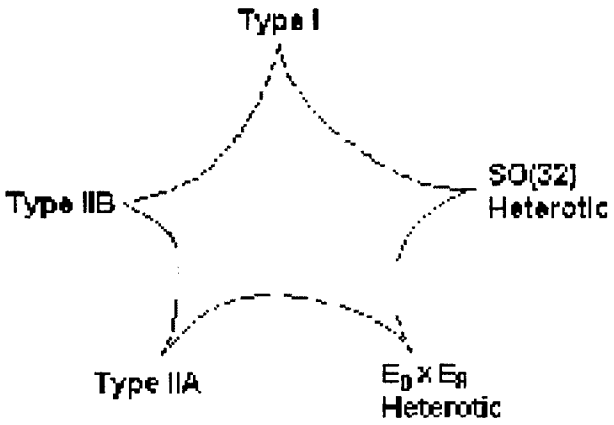

Figure 6

The Electron

Ronald E. Mickens

Clark Atlanta University

This brief essay is a summary of my after dinner comments given at the National Conference of Black Physics Students Banquet on Saturday 7 March 1998 at the University of Kentucky, Lexington, Kentucky.

I have been asked to discuss the history of the electron. In large measure, this request reflects the fact that 1997 was the centennial of the "discovery" of the electron. Since this is not a technical presentation, I will not burden you with references to the original research papers on the topic to be discussed. However, a short listing of certain books and papers of relevance to this history have been given at the end of this paper and provides a beginning point to locating all of the important published work on the electron.

Both the concept and eventual discovery of the electron are closely tied to questions related to the structure of matter. In the earliest times, the central focus was on the ultimate causes for the various properties shown by macroscopic matter. At the beginning of the nineteenth century, experimental evidence strongly suggested that the existence of "atoms" could readily explain a wide range of physical observations. In particular, we had the works of John Dalton (1804) giving the law of multiple proportions and Joseph Louis Gay-Lussac (1808) the law of relative volumes for reacting gases, and the hypothesis based on experiments by Amedeo Avogadro (~1810) that equal volumes of gases at the same temperature and pressure contain equal numbers of molecules. Also, Michael Faraday's experiments (1833) on electrolytes strongly favored the hypothesis that matter is composed of atoms and that electricity appears in discrete units. In 1853, James P. Joule gave arguments to compute the mean speed of molecules, provided they existed. This result was placed on a firm theoretical basis by James Clark Maxwell (1860) when he was able to calculate the most probable distribution of molecular speeds for a gas at equilibrium.

In the period from 1860 to about 1890, both arguments for and experimental evidence in support of a possible internal structure for molecules were given. An important result was the application of the equipartition theorem to the specific heat of hydrogen. The equipartition theorem predicts a contribution of approximately 1 calorie/°K · mole per degree of freedom to the molar specific heat, C_v. At 15°C, the measured value for hydrogen is ≈5. Taken at face value, this implies that the hydrogen molecule has 5 internal degrees of freedom and, hence, an internal structure. Again, assuming the existence of "molecules," it was possible to estimate values for molecular diameters from mean-free-paths/viscosity measurements in gases: the calculated values were always (in order of magnitude) close to 10^{-8} cm.

Thus, by the seventh decade of the 19th century, strong experimental evidence, backed by the kinetic theory of gases, suggested that atoms exist, atoms can combine in larger units to form molecules, atoms and molecules have definite sizes, and that a basic unit of electricity exists. To proceed, several questions had to be answered: If there is a smallest unit of electric charge, what is its magnitude? Assuming that this charge is carried by a particle, what is the mass of the particle? Finally, what is the relationship of this particle to atoms/molecules and their structure and properties?

The eventual resolution of these issues actually began with work done much earlier by a number of researchers investigating electric and magnetic phenomena. It was well known for many centuries that amber, when rubbed with fur, acquires the property to attract bits of other materials. William Gilbert

(~1580) showed that other substances, such as glass, gems, wax, and sulfur also had similar properties. He was one of the first persons to systematically study magnetic and static electric effects. It was Gilbert who coined the word electric after the Greek word "electron" for amber. In 1733, Charles-Francois de Cisternay Dufay discovered that two kinds of electricities existed, which he called "vitreous" and "resinous." In experiments, he showed that unlike kinds of electricity attract each other, while like types repel. The behavior of the forces between the two electricities was clarified by Coulomb (1785) with the use of a torsion balance. He proved the inverse square law for electrical interactions. However, somewhat earlier (~1743) Benjamin Franklin began his experiments on electricity and from these results proposed a theory that electricity was a single fluid composed of "extremely subtle particles," thus hinting at a possible atomic theory of electrical charge.

As mentioned earlier, electrolysis played an important role in the euclidation of the nature of electricity. Electrolysis was accidentally discovered by William Nicholson and Anthony Carlisle in 1800 when they found that water could be decomposed into hydrogen and oxygen by the action of an electric current. Later Humphrey Davy (~1812) carried out an extensive set of experiments and found that various salts could also be decomposed by passing an electric current either through the molten salt or solutions of the salt in water. This program of experiments led him to discover two elements: sodium and potassium. Michael Faraday, who started as Davy's assistant in 1812, continued this line of inquiry and had by the 1830's constructed an essentially correct theory of electrolysis. This work was based on the idea that the electrolytic unit of electricity has a definite, finite value, and that in reactions caused by electrolysis definite numbers of molecules are produced when a given quantity of electric current flows through the wires. However, the magnitude of the electrolytic unit of electric charge, just as the magnitude of the unit of atomic weight, was unknown. But their ratio could be determined. This value was determined by Faraday to be $(1.044)10^{-8}$ Kg/Coulomb for a hydrogen atom. The next step was to make either a direct determination of m_H or the charge.

Note that two important ideas have been introduced: the discrete structure of matter (atoms) and the discrete unit of electrical charge as carried by the ions in electrolysis. In 1874, G. Johnstone Stoney proposed that the unit of electricity gained or lost when atoms become charged ions should be called the "electron." He also did a very rough estimate of the magnitude of this "atom of electricity."

A major experimental activity in the latter part of the nineteenth century was the study of the discharge of electricity through rarefied gases. Under proper conditions so-called *cathode rays* would form. There was initially intense speculation about the exact nature of these rays. Two major camps existed concerning this issue. The first thought that they were of the same essence as light. The second thought that they were charged particles. A resolution was achieved in 1895 when Jean Perrin devised an experiment in which cathode rays were caught in an insulated container and the charge of the container was found to be negative. Thus, cathode rays were particles having negative charge. The critical problem was now to see if the charge and mass of these particles could be separately determined.

The years 1896 and 1897 provided three critical experiments for understanding cathode rays. First, Peter Zeeman showed that a magnetic field increased slightly the width of the *D* lines of sodium. Hendrik Antoon Lorentz had an immediate explanation of this result based on an atomistic interpretation of Maxwell's electromagnetic equations. According to Lorentz (1892) the light was emitted by "ions" orbiting within the sodium atom. From the measured broadening he deduced a value for the ratio *e/m* of the bound ions:

$$\left(\frac{e}{m}\right)_{"ions"} \approx 2000\left(\frac{e}{m}\right)_{hydrogen\ atom} \quad !!$$

Second, in an interesting experiment J. S. E. Townsend at the Cavendish Laboratory used the fact that ions can serve to start the growth of droplets of water in humid air to estimate an average value for the ionic charge. He

found charges of $(0.9)10^{-19}$ Coulombs for positive ions and $(1.0)10^{-19}$ Coulombs for negative ions.

Third, the classic experiment of Joseph John Thomson (1897) gave rise to the now popular view that the electron was discovered in 1897. In this experiment, Thomson used a combination of crossed electric and magnetic fields to determine the mass to charge ratio of cathode rays:

$$\frac{m}{e} \cong (1.3)10^{-10}\, Kg / Coulomb.$$

He concluded: "From these determinations we see that the value of m/e is independent of the nature of the gas, and that its value 10^{-10} is very small compared with the value 10^{-7}, which is the smallest value of this quantity previously known, and is the value for the hydrogen ion in electrolysis. ... Thus for the carriers of the electricity in the cathode rays m/e is very small compared to the value in electrolysis. The smallness of m/e may be due to the smallness of m or to the largeness of e, or to a combination of these two..." Thus, it became essential that either the charge or the mass be measured separately. The charge of gaseous ions had been previously measured in Thomson's laboratory. If this charge is assumed to be the same as that on the cathode ray particles, then the mass of the cathode particles was very small compared with the mass of the hydrogen atoms, i.e.,

$$\frac{m}{m_H} \approx 10^{-3}.$$

It should be noted that Thomson, in his 1897 paper, called the cathode particles "corpuscles." The word "electron" was used only to denote the amount of charge carried by a corpuscle. This usage was consistent with Stoney's suggestion given in 1874. Later it became standard practice to call the cathode particle itself an electron.

The later detailed experiments of Robert Millikan (1906-1916) allowed an accurate determination of the electron's charge. He did this by measuring the charges on oil droplets and assumed that the smallest unit of charge was the same as that of the electron.

The discovery of the electron by Thomson led to the natural identification of the electrolytic unit of electric charge to be equal to that of the electron (in magnitude). Based on his knowledge of m/e and m_H/e, Thomas concluded that atoms must be thousands of times heavier than the electrons which they contain. He also concluded from a variety of other experiments, including those involving the passage of electrons through matter, that the number of electrons per atoms should be approximately equal to the atomic weight. Also, since the normal atom is electrically neutral, then the quantity of positive electricity per atom must be exactly the same as the quantity of negative electricity. A derived fact from these results is that if masses are associated with the charges, then it can be concluded that essentially the total mass of the atoms is associated with its positive charge. Thomson would later construct a model of the atom based on these ideas which extended the earlier work of Lord Kelvin (1902).

The electron, after its "discovery" by J. J. Thomson in 1897, played a significant role in almost every area of "modern" physics. The following is a partial listing of a number of important phenomena studied during the first half of the 20th century which involved the electron:

- photoelectric effect — Hertz (1887), Einstein (1905)
- models of the atom — Thomason/ Rutherford/Bohr (~1900-1913)
- discrete energy levels in atoms/molecules — Frank and Hertz (1914)
- Compton effect (1922)
- matter waves — de Broglie (1924)
- electron spin — Uhlenbeck and Goudsmit (1925)
- exclusion principle — Pauli (1925)
- electron diffraction by crystal lattices — Davisson and Germer (1927)
- properties of a conductor following from the assumption of a degenerate electron gas — Sommerfeld (1927-28)
- relativistic invariant formulation of the theory of the electron — Dirac (1928)

- "hole" theory — Dirac (1930)
- electron-positron pair formation and annihilation — Blackett and Occhialini (1933)
- decay of neutron — Chadwick (1932) and Fermi (1934)
- birth of quantum electrodynamics — Feynman, Schwinger, and Tomonaga (1948).

I will end with a brief comment and a question. When one looks at the modern physics periodic table of fundamental particles, the electron is the only elementary particle which was "known" in the 19th century. (One could also, with little effort, include the photon as the other ancient fundamental particle.) The 20th century, from the standpoint of science and technology, has been the century of the electron. The knowledge of its existence and its physical properties has played a central role in the study of the fundamental interactions and also in applications giving rise to the creation of new technologies for the now ubiquitous electronic age.

My question should be of interest to those who have an interest in the history of physics. In the construction of the Thomson model of the atom, it was taken for granted that the electrons were discrete particles, each having exactly the same electric charge. Question: Why was such a "quantization" of charge not extended to the positive charges of the atom?

References

Books

1. Oliver Lodge, *Electrons or the Nature and Properties of Negative Electricity* (George Bell and Sons, London, 1906).
2. Robert A. Millikan, *The Electron: Its Isolation and Measurements and Determination of Some of Its Properties* (University of Chicago Press, Chicago, 1917).
3. Oswald H. Blackwood, et al., *An Outline of Atomic Physics* (Wiley, New York, 1937, 2nd edition).
4. F. L. Friedman and L. Sartori, *The Classical Atom* (Addison-Wesley; Reading, MA; 1965).
5. Gerald Holton and Stephan G. Brush, *Introduction to Concepts and Theories in Physical Science* (Addison-Wesley; Reading, MA; 1973, 2nd edition).
6. Steven Weinberg, *The Discovery of Subatomic Particles* (Freeman, New York, 1983).
7. *Physics Today* (October 1997), Special Issue: "The Ubiquitous Electron."

Articles

8. C. E. Behrens, "Atomic theory from 1904 to 1913," American Journal of Physics 11 (1943), 60.
9. N. Bohr, "On the constitution of atoms and molecules," Philosophical Magazine (Series 6) 26 (1913), 1, 476, 852.
10. J. Chadwick, "The existence of a neutron," Proceedings of the Royal Society A 136 (1932), 692.
11. E. Fermi, "Versuch einer Theorie der b-Strahlen," Zeitschrift fur Physik 88 (1934), 161.
12. E. W. Garber, "Clausius and Maxwell's kinetic theory of gases," Historical Studies in the Physical Sciences 2 (1970), 299.
13. R. A. Millikan, "On the elementary electrical charge and the Avogadro constant," Physical Review 32 (1911), 349.
14. E. Rutherford, "The scattering of a and b particles by matter and the structure of the atom," Philosophical Magazine (Series 6) 21 (1911), 669.
15. G. J. Stoney, "Of the 'electron' or atom of electricity," Philosophical Magazine 38 (1894), 418.
16. J. J. Thomson, "Cathode rays," Philosophical Magazine 44, 295.
17. W. C. Walker, "The detection and estimation of electric charges in the eighteenth century," Annals of Science 1 (1936), 66.

Teaching Density Functional Theory to Undergraduates

H. L. Neal

Clark Atlanta University

Abstract

We consider the Density Functional Theory from the point of view of one-dimensional two particle model systems, where the particles are either spin-1/2 fermions or spin-0 bosons. The basic equations are derived and applied to the system of two coupled harmonic oscillators. An exact density functional solution is constructed from the exactly known single-particle density for this system. We demonstrate how this solution may be applied to other two-particle systems to calculate the exact single-particle density and energy. We assert that our presentation is suitable for incorporation into undergraduate quantum physics and computational physics courses.

1. Introduction

Most quantum mechanics textbooks present some discussion of the variational and perturbational theories for solving problems in quantum mechanics. With the exception of the closely related Thomas-Fermi theory,[1] we have found no presentation of the very elegant density functional theory[2] (DFT) in the standard textbooks. The reasons for this are perhaps largely due to two factors: (1) the extremely small number of model systems to which the method may be simply and easily applied and (2) the fact that, generally, DFT solutions must be obtained numerically. In this paper we address the first factor by giving a general discussion of DFT for one-dimensional two-particle systems with an application to two coupled harmonic oscillators. We believe that the second factor is addressed by the increasing importance of computational physics and the easy access to computers in undergraduate physics programs. Widely used in quantum chemistry and physics,[3,4] the advantages of DFT are that it allows a many-particle problem to be transformed into an equivalent single-particle problem, and that it is in principle exact. Thus the single-particle density ρ may be directly determined without the need of the many-particle wavefunction. Our aim in this paper is to give a discussion of DFT that is (at least) appropriate at the advanced undergraduate level. We hope that students and teachers of quantum mechanics will find our presentation of pedagogical value.

In Sec. II we give a general discussion of the density functional theory of two-particle systems in one dimension. The particles may be either spin-1/2 fermions or spin-0 bosons. For further simplicity we consider only the ground state. In Sec. III we apply the results of Sec. 11 to the system of two coupled harmonic oscillators. An exact DFT solution is presented for this system. In Sec. IV we use DFT to calculate the exact single-particle density and energy for three different systems. In Sec. V a summary and some final remarks are given.

II. Density Functional Theory of Two-Particle Systems

The Hamiltonian we consider is

$$\boldsymbol{H} = \sum_{i=1}^{2} \left(\frac{\boldsymbol{p}_i^2}{2\boldsymbol{m}} + \boldsymbol{v}(\boldsymbol{x}_i) \right) + \boldsymbol{u}(\boldsymbol{x}_1, \boldsymbol{x}_2), \quad (1)$$

where p_i is the particle momentum, m is the particle mass, $v(x)$ is the external potential, and $u(x_1, x_2)$ is the interaction potential. The ground state wave function[5] $\Psi(x_1, x_2,)$ and energy E must satisfy the equation

$$H\Psi = E\Psi. \quad (2)$$

For subsequent discussions it is convenient to write

$$E = T + V + U, \tag{3}$$

where T, V, and U are, respectively, the kinetic, external potential, and interaction energies of the ground state. Equation (2) follows from the variational principle being applied to the functional

$$E'[\Psi'] = \frac{\langle \Psi' | H | \Psi' \rangle}{\langle \Psi' | \Psi' \rangle}. \tag{4}$$

if $\Psi' = \Psi$, $E'[\Psi] = E$, otherwise $E'[\Psi'] \geq E$. In other words, Ψ minimizes E'[Ψ']. Our goal in this section is to derive the functional $E[\rho']$ which is minimized by the single-particle density ρ given by

$$\rho(\boldsymbol{x}) \equiv 2 \int d\boldsymbol{x}' \, |\Psi(\boldsymbol{x}, \boldsymbol{x}')|^2 \tag{5}$$

such that $E'[\rho] = E$. This functional will allow us to transform from the two-particle problem of Eq. (2) to an equivalent single-particle problem. The approach we adopt was first proposed by Kohn and Sham,[2] who assumed the existence of a *noninteracting reference system* with a Hamiltonian of the form

$$H_r = \sum_{i=1}^{2} \left(\frac{p_i^2}{2m} + v_{\text{eff}}(\boldsymbol{x}_i) \right), \tag{6}$$

where the effective potential $v_{eff}(x)$ is chosen so that this system has a single-particle density identical to that given by Eq. (5). This assumption will be referred to as the KS assumption. The ground state wave function $\Psi_r(x_1, x_2)$ of the reference system is written as

$$\Psi_r(\boldsymbol{x}_1, \boldsymbol{x}_2) = \phi(\boldsymbol{x}_1)\phi(\boldsymbol{x}_2), \tag{7}$$

where $\phi(x)$ is the normalized ground state solution of the single-particle Hamiltonian

$$h_r = \frac{p^2}{2m} + v_{\text{eff}}(\boldsymbol{x}); \tag{8}$$

it is related to the density by

$$\rho(\boldsymbol{x}) = 2|\phi(\boldsymbol{x})|^2. \tag{9}$$

The ground state kinetic energy of the reference system is

$$\begin{aligned} T_r &= -\frac{\hbar^2}{2m} \sum_{i=1}^{2} \int \phi^*(\boldsymbol{x}_i) \frac{d^2}{d\boldsymbol{x}_i^2} \phi(\boldsymbol{x}_i) d\boldsymbol{x}_i \\ &= -\frac{\hbar^2}{m} \int \phi^*(\boldsymbol{x}) \frac{d^2}{d\boldsymbol{x}^2} \phi(\boldsymbol{x}) \, d\boldsymbol{x} \end{aligned} \tag{10}$$

We may express E as

$$E = T_r + V + F_r, \tag{11}$$

$$F_r = F - T_r, \tag{12}$$

$$F = T + U \tag{13}$$

From Eqs. (5), (9) and (10), and assuming that ϕ is real, we may express T_r and V as explicit functionals of

$$T_r[\rho] = -\frac{\hbar^2}{2m} \int \sqrt{\rho(\boldsymbol{x})} \frac{d^2}{d\boldsymbol{x}^2} \sqrt{\rho(\boldsymbol{x})} \, d\boldsymbol{x}, \tag{14}$$

$$V[\rho] = \int v(\boldsymbol{x}) \rho(\boldsymbol{x}) \, d\boldsymbol{x}. \tag{15}$$

The functional $F[\rho]$ is generally not known. It does, however, have a very useful property[3] in that it is universal: its functional form as a functional of ρ is independent of the external potential $v(x)$. In principle, if it is known for one particular external potential and interaction potential, it may be applied to systems with different external potentials with the same interaction potential. We will say more about $F[\rho]$ in the next section. For now we use it in defining the functional

$$E'[\rho'] = T_r[\rho'] + V[\rho'] + F_r[\rho']. \tag{16}$$

This functional is a minimum at $\rho' = \rho$ where $E'[\rho] = E$. For all other values of ρ' it satisfies the condition $E'[\rho] \geq E$. The density ρ may be determined by varying $E'[\rho']$ with the constraint

$$\int \rho'(\boldsymbol{x}) \, d\boldsymbol{x} = 2. \tag{17}$$

The condition that $E'[\rho]$ is a minimum is therefore

$$\delta \left(E'[\rho'] - \mu \int \rho'(\boldsymbol{x}) \, d\boldsymbol{x} \right) = 0, \tag{18}$$

where μ is the Lagrange multiplier. This variation may be equivalently carried out

with respect to ϕ'. The direct result of this minimization is the Schrödinger-like equation

$$\left(-\frac{\hbar^2}{2m}\frac{d^2}{dx^2} + v(x) + \frac{\delta F_r[\rho]}{\delta\rho(x)}\right)\phi(x) = \mu\phi(x) \tag{19}$$

A derivation of this equation is given in Appendix A, where we also show how to compute the variational (or functional) derivative of $F_r[\rho]$ with respect to $\rho(x)$, $\delta F_r[\rho]/\delta\rho(x)$. Comparing Eq. (19) with Eq. (8) gives

$$v_{\text{eff}}(x) = v(x) + \frac{\delta F_r[\rho]}{\delta\rho(x)}. \tag{20}$$

Since v_{eff} is a functional of ρ, the nonlinear single-particle Schrödinger-like Eq. (19) must in general be solved iteratively. We emphasize that no approximations have been made in arriving at Eq. (19). If $F_r[\rho]$ (or more precisely $F[\rho]$) is known exactly, then ρ and E may be exactly determined with ρ given by Eq. (9) and E given by

$$E = 2\mu + F_r[\rho] - \int \frac{\delta F_r[\rho]}{\delta\rho(x)}\rho(x)\,dx. \tag{21}$$

III. An Exact DFT Solution for Two Coupled Harmonic Oscillators

In this section we consider the system of two coupled harmonic oscillators described by the Hamiltonian

$$H = \sum_{i=1}^{2}\left(\frac{p_i^2}{2m} + \frac{m\omega_o^2}{2}x_i^2\right) + \frac{k}{2}(x_1 - x_2)^2, \tag{22}$$

where k is a positive constant. The exact ground state energy E and wave function Ψ are[6]

$$E = \hbar(\omega_o + \omega)/2 \tag{23}$$

$$\Psi(x_1, x_2) = \left(\frac{m^2\omega\omega_o}{\hbar^2\pi^2}\right)^{1/4}\exp\left(\frac{-m\omega_o(x_1 + x_2)^2 - m\omega(x_1 - x_2)^2}{4\hbar}\right), \tag{24}$$

$$\omega = \sqrt{\omega_o^2 + 2k/m}. \tag{25}$$

According to DFT, Ψ and all physical quantities are functionals of the single particle density $\rho(x)$ which is given by

$$\rho(x) = \left(\frac{8m\omega_o\omega}{\pi\hbar(\omega_o + \omega)}\right)^{1/2}\exp\left(-\frac{2m\omega_o\omega}{\hbar(\omega_o + \omega)}x^2\right). \tag{26}$$

Since $\rho(x)$ is known, we will use it to obtain the unknown functional $F[\rho]$. Note that from Eqs. (3), (13), (15) and (23), $F[\rho]$ may be expressed as

$$\begin{aligned} F[\rho] &= E - V[\rho] \\ &= \frac{\hbar}{2}(\omega_o + \omega) - \frac{m\omega_o^2}{2}\int x^2\rho(x)\,dx, \end{aligned} \tag{27}$$

where the integration limits are from $x = -\infty$ to $x = +\infty$. From Eq. (26) we have

$$-\frac{m\omega_o^2}{2}x^2 = \frac{\hbar(\omega_o + \omega)\omega_o}{4\omega}\ln\left(\rho(x)/\rho_o\right), \tag{28}$$

$$\rho_o \equiv \rho(0) = \left(\frac{8m\omega_o\omega}{\pi\hbar(\omega_o + \omega)}\right)^{1/2}. \tag{29}$$

Substituting this result into Eq. (27) allows us to write

$$F[\rho] = \frac{\hbar(\omega_o + \omega)}{4}\int\left(1 + \frac{\omega_o}{\omega}\ln\left(\rho(x)/\rho_o\right)\right)\rho(x)\,dx \tag{30}$$

With ω_0 expressed in terms of ρ_0 (see Appendix B), $F[\rho]$ is an explicit functional of ρ. We assert that $F[\rho]$ is *exact*. It may be used in Eqs. (19) and (21) to calculate $\rho(x)$ and E for all *two-particle systems with the harmonic interaction* $u(x_1, x_2) = k(x_1 - x_2)^2/2$.

To calculate v_{eff} from Eq. (20) we need the functional derivatives $\delta F[\rho]/\delta\rho(x)$, and $\delta T_r[\rho]/\delta\rho(x)$. Applying the definition given by Eq. (A3) in Appendix A,

$$\frac{\delta F[\rho]}{\delta \rho(x)} = \frac{\hbar(\omega_0+\omega)}{4}\left\{1+\frac{\omega_0}{\omega}\left[1+\ln\left(\rho(x)/\rho_0\right)\right]\right\}, \tag{31}$$

$$\frac{\delta T_r[\rho]}{\delta \rho(x)} = -\frac{\hbar^2}{8m}\left\{\frac{d^2}{dx^2}\ln\rho(x)^2+\left(\frac{d}{dx}\ln\rho(x)\right)^2\right\}. \tag{32}$$

Inserting the exact density of Eq. (26) into these equations gives

$$\frac{\delta F_r[\rho]}{\delta \rho(x)} = m\left[2\left(\frac{\omega_0\omega}{\omega_0+\omega}\right)^2-\frac{1}{2}\omega_0^2\right]x^2+\hbar\frac{(\omega_0+\omega)^2}{4\omega}-\hbar\frac{\omega_0\omega}{(\omega_0+\omega)}. \tag{33}$$

From Eq. (20) the effective potential for the coupled oscillators is

$$v_{\text{eff}}(x) = 2m\left(\frac{\omega_0\omega}{\omega_0+\omega}\right)^2 x^2+\hbar\frac{(\omega_0+\omega)^2}{4\omega}-\hbar\frac{\omega_0\omega}{(\omega_0+\omega)}. \tag{34}$$

Solving Eq. (19) with this effective potential gives

$$\mu = \frac{\hbar(\omega_0+\omega)^2}{4\omega}, \tag{35}$$

$$\phi(x) = \left(\frac{2m\omega_0\omega}{\pi\hbar(\omega_0+\omega)}\right)^{1/4}\exp\left(-\frac{m\omega_0\omega}{\hbar(\omega_0+\omega)}x^2\right), \tag{36}$$

Inserting the expression above for $\phi(x)$ into Eq. (10) we get

$$T_r[\rho] = \frac{\hbar\omega_0\omega}{(\omega_0+\omega)}\int dx\left\{1-\left(\frac{2m\omega_0\omega}{\hbar(\omega_0+\omega)}\right)x^2\right\}\rho(x) \tag{37}$$

$$= \int\frac{\delta T_r[\rho]}{\delta\rho(x)}\rho(x)\,dx.$$

From Eqs. (30) and (31) we also have

$$F[\rho] = \int\frac{\delta F[\rho]}{\delta\rho(x)}\rho(x)\,dx-\frac{\hbar}{2}(\omega_0+\omega)\frac{\omega_0}{\omega}. \tag{38}$$

From Eq. (21) the ground state energy becomes

$$E = 2\mu - h(\omega_0+\omega)\omega_0/2\omega \tag{39}$$

The results of Eqs. (35) -(39) prove our assertion that the functional given by Eq. (30) is exact since $2|\phi(x)|^2$ gives the exact density and Eq. (39) gives the exact energy with the μ of Eq. (35) for the system of two coupled harmonic oscillators. Equation (39), however, is quite general for the harmonic interaction with ω_0 written in terms of ρ_0.

IV. Application of DFT

In this section we consider the two-particle systems described by the Hamiltonian

$$H = \sum_{i=1}^{2}\left(\frac{p_i^2}{2m}+v(x_i)\right)+\frac{k}{2}(x_1-x_2)^2. \tag{40}$$

From Eqs. (20) and (33), the effective potential is

$$v_{\text{eff}}(x) = v(x)+m\left\{2\left(\frac{\omega_0\omega}{\omega_0+\omega}\right)^2-\frac{\omega_0^2}{2}\right\}x^2 \tag{41}$$

$$+\hbar\frac{(\omega_0+\omega)^2}{4\omega}-\hbar\frac{\omega_0\omega}{(\omega_0+\omega)}.$$

We will use this effective potential to calculate the exact $\rho(x)$ and E for three cases: (1) $v(x) = \alpha+\beta x^2$, (2) $v(x) = \alpha|x|$, and (3) $v(x) = \alpha\exp(\beta x^2)$, where α and β are constants. For convenience we measure x in units of the convenient length

$$L = \left(\frac{\hbar^2/m}{1\text{ Joule}}\right)^{1/2} \tag{42}$$

and energies in units of $h^2/mL^2 = 1$ Joule.

A. CASE 1: $v(x) = \alpha + \beta x^2$

The external potential in this case is just a

different version of the harmonic oscillator potential of the previous section. It yields an effective potential that is also a version of the harmonic oscillator potential. The exact ground state density is obtained by setting
$\omega_0 = (2\beta)^{1/2}$ in Eq. (26), and the exact ground state energy is

$$E_{\text{exact}} = \hbar \left(\sqrt{2\beta} + \sqrt{2\beta + 2k/m} \right) /2 + 2\alpha. \tag{43}$$

The DFT solution from Eq. (19) gives

$$\rho(x) = 2 \left(2m\gamma/\hbar^2\pi^2\right)^{1/4} \exp\left(-\sqrt{2m\gamma/\hbar^2}x^2\right), \tag{44}$$

$$\gamma = \beta + 2m \left[\omega_o\omega/\left(\omega_o + \omega\right)\right]^2 - m\omega_o^2/2, \tag{45}$$

$$\mu = \hbar \left\{ \sqrt{\gamma/2m} + \alpha/\hbar + (\omega_o + \omega)^2/4\omega - \omega_o\omega/(\omega_o + \omega) \right\}. \tag{46}$$

The ground state energy is given by Eq. (39). The quantities ω_0 and ω (see Appendix B) are functions of ρ_0, which is determined from

$$\rho_o = 2 \left(2m\gamma/\hbar^2\pi^2\right)^{1/4}. \tag{47}$$

Inserting the exact ω_0 (= $(2\beta)^{1/2}$) into the DFT solution gives the exact density and energy.

B. CASE 2: $v(x) = \alpha|x|$

For this case the Schrodinger-like Eq. (19) is solved numerically with v_{eff} given by Eq. (41). The iterative procedure for obtaining the complete DFT solution is as follows:

Step 1. Solve Eq. (19) using an initial guess density $\rho^{(0)}$ to compute the density $\rho^{(1)}$.

Step 2. Solve Eq. (19) using the density $\rho^{(1)}$ to compute the density $\rho^{(2)}$.

Step 3. Continue iterating until $\rho^{(i+1)} = \rho^{(i)}$ or, more conveniently, $\mu^{(i+1)} = \mu^{(i)}$.

Step 4. Use Eq. (9) to compute ρ and Eq. (39) to calculate E.

Koonin[7] gives a very good discussion of the numerical techniques for solving Eq. (19). In Fig. 1 we compare the DFT solution with the variational solution obtained with the wave function

$$\Psi_{var} = 2 \left(c_1c_2/\pi^2\right)^{1/4} \exp\left\{-c_1(x_1 + x_2)^2 - c_2(x_1 - x_2)^2\right\}. \tag{48}$$

The corresponding density and energy are

$$\rho_{var}(x) = 4\sqrt{2\frac{c_1c_2}{\pi(c_1 + c_2)}} \exp\left(-8\frac{c_1c_2}{(c_1 + c_2)}x^2\right) \tag{49}$$

$$E_{var} = \sqrt{\frac{(c_1 + c_2)}{2\pi c_1c_2}}\alpha + k/8c_2 + \hbar(c_1 + c_2)/m. \tag{50}$$

The variational parameters c_1 and c_2 are given by the solution to the equations

$$\left(\hbar^2/m + k/8c_1^2\right)\left\{\alpha^2m^2/\left(8\hbar^4\pi c_1^3\right) - 1\right\}^2 - \hbar^2/m = 0, \tag{51}$$

$$c_2 = c_1/\left\{\alpha^2m^2/\left(8\hbar^4\pi c_1^3\right) - 1\right\}. \tag{52}$$

The DFT results are in close agreement with the variational results except near $x = 0$.

C. CASE 3: $v(x) = \alpha \exp\{\beta x^2\}$

The iterative procedure is employed to obtain the complete DFT solution for $\alpha = 1$ J and $\beta = 0.1\ L^{-2}$. Shown in Fig. 2 are the DFT and, for comparison, the results of the variational calculation with the wave function of Eq. (48). The variational energy is

$$E_{\text{var}} = \hbar^2(c_1 + c_2)/m + \sqrt{\frac{2c_1c_2}{8c_1c_2 - \beta(c_1 + c_2)}} + k/8c_2, \tag{53}$$

The variational parameters c_1 and c_2 are given by the solution to the equations

$$\frac{\sqrt{8}\alpha\beta}{c_1^2\left(8 - \beta\left[1/c_1 + \{2c_1^2 + km/4\hbar^2\}^{-1/2}\right]\right)^{3/2}} - \frac{\hbar^2}{m} = 0, \tag{54}$$

$$c_2 = \sqrt{2c_1^2 + km/4\hbar^2}. \tag{55}$$

Again, the DFT results are in close agreement with the variational results except near $x = 0$.

V. Summary and Remarks

In this paper we have given a discussion of DFT from the perspective of one-dimensional two-particle systems. An exact DFT solution was found for the system of two coupled harmonic oscillators. We have demonstrated how the exact functional of Eq. (30) may be applied to other two-particle system with the harmonic interaction. The generalization of the basic results of Sec. II to two and three dimensions is straight forward: Replace the differential operators d/dx and d^2/dx^2 everywhere by the vector operators ∇ and ∇^2, respectively. The generalization to more than two particles is greatly complicated by the fact that both $F[\rho]$ and $T_r[\rho]$ are generally unknown. Their determination for the general many-particle problem is the subject of a vast literature[3,4] and current research.[8] We hope that our contribution will help make DFT more accessible at the undergraduate level.

Acknowledgments

The author thanks his colleagues, C. J. Tymczak and Xiao-Qian Wang, for many helpful discussions.

APPENDIX A: Functional Derivatives and the Derivation of Equation (19)

Consider the functional $J[\rho]$ which is of the form

$$J[\rho] = \int f(\rho, \rho', x)\, dx, \tag{A1}$$

where f is a function of ρ, ρ', and x and ρ', denotes derivative of $\rho(x)$ with respect to x. From the calculus of variations[10] we have

$$\delta J = \int \left(\frac{\partial f}{\partial \rho} - \frac{d}{dx}\frac{\partial f}{\partial \rho'}\right)\delta\rho\, dx. \tag{A2}$$

The functional derivative of $J[\rho]$ with respect to $\rho(x)$ is given by

$$\frac{\delta J[\rho]}{\delta \rho(x)} \equiv \frac{\partial f}{\partial \rho} - \frac{d}{dx}\frac{\partial f}{\partial \rho'}. \tag{A3}$$

From this definition we see that we may also write

$$\delta J = \int \frac{\delta J[\rho]}{\delta \rho(x)}\delta\rho\, dx. \tag{A4}$$

From $\rho = 2\phi\phi^*$, we get $\delta\rho = 2\phi\delta\phi^*$. The variation $d(E' - \mu\int\rho\, dx)$ with respect to ϕ^* gives

$$\int\left\{-\frac{\hbar^2}{m}\frac{d^2}{dx^2}\phi + 2v(x)\phi + 2\frac{\delta F_r[\rho]}{\delta\rho(x)}\phi - 2\mu\phi\right\}\delta\phi^* dx = 0, \tag{A5}$$

from which Eq. (19) follows as the terms inside the braces must sum to zero for all values of x.

APPENDIX B: The Parameter ω_0 as a Function of ρ_0

Equation (29) may be manipulated to give

$$\omega_0^4 - \frac{2}{c}\omega_0^3 + \frac{2k}{m}\omega_0^2 - \frac{4k}{mc}\omega_0 + \frac{2k}{mc^2} = 0, \tag{B1}$$

$$c = \frac{8m}{\pi\hbar\rho_0^2}. \tag{B2}$$

The desired solution[9] for ω_0 is

$$\omega_0 = (1/c + R + D)/2,$$
$$R = \sqrt{1/c^2 - 2k/m + y},$$
$$D = \sqrt{3/c^2 - R^2 - 4k/m + (4k/mc + 2/c^3)/R},$$
$$y = \gamma^{1/3} + \left(\frac{2k}{3m}\right)^2 \gamma^{-1/3} + \frac{2k}{3m},$$
$$\gamma = 4\frac{k}{mc^4} + \left(\frac{2k}{3m}\right)^3 + \frac{4}{9}\frac{k}{mc^4}\sqrt{3\{27 + 4c^4(k/m)^2\}}.$$

1 L. Pauling and W. B. Wilson, *Introduction to Quantum Mechanics* (New York, Dover, 1935), p. 57.

2 P. Hohenberg and W. Kohn, "Inhomogeneous Electron Gas," Phys. Rev. **136,** 13864-13871 (1964); W. Kohn and L. Sham, "Self- Consistent Equations Including Exchange and Correlation Effects," Phys. Rev. **140,** A1133-A1138 (1965).

3 R. G. Parr and W. Wang, *Density- Functional of Atoms and Molecules* (New York, Oxford University Press, 1989).

4 R. 0. Jones and 0. Gunnarsson, "The Density Functional Formalism: Its Applications and Perspectives." *Rev. Mod. Phys,* Vol. **61,** 689-746 (1989).

5 As the Hamiltonian is independent of spin, in the case of two spin-1/2 fermions, we do not include the antisymmetric spin part of the ground state wave function in our discussion.

6 D. S. Saxon, *Elementary Quantum Mechanics* (San Francisco, Holden-Day, 1968), pp. 236-238.

7 S. E. Koonin, *Computational Physics* (New York, Addison-Wesley, 1986), chapter 3.

8 A. Samanta and S. K. Ghosh, "Density Functional Approach to the Calculation of Correlation Energies of Two-Electron Atoms and Ions," Phys. Rev. **A43,** 6395-6397 (1991); R. G. Parr and S. K. Ghosh, "Toward Understanding the Exchange-Correlation Energy and Total-Energy Density Functionals," Phys. Rev. **A51,** 3564-3570 (1995).

9 M. Abramowitz and A. 1. Stegun, *Handbook of Mathematical Functions* (Washington, D. C., U. S. Government Printing Office, 1964), p. 17.

10 G. Arfken, *Mathematical Methods for Physicists* (New York, Academic Press, 1985), chapter 17.

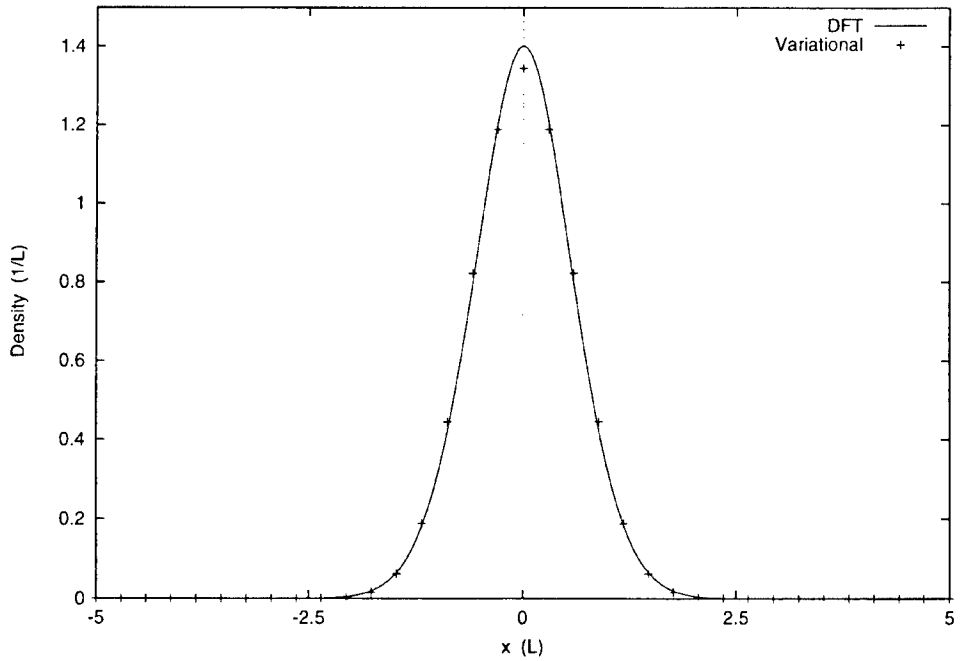

FIGURE 1. Plot of $\rho(x)$ versus x for the external potential given by $v(x) = \alpha|x|$. The DFT calculation (E = 1.96341 J, μ=1.52181 J) is compared to a variational calculation (E = 1.96766 J). The value of α is 1 Joule.

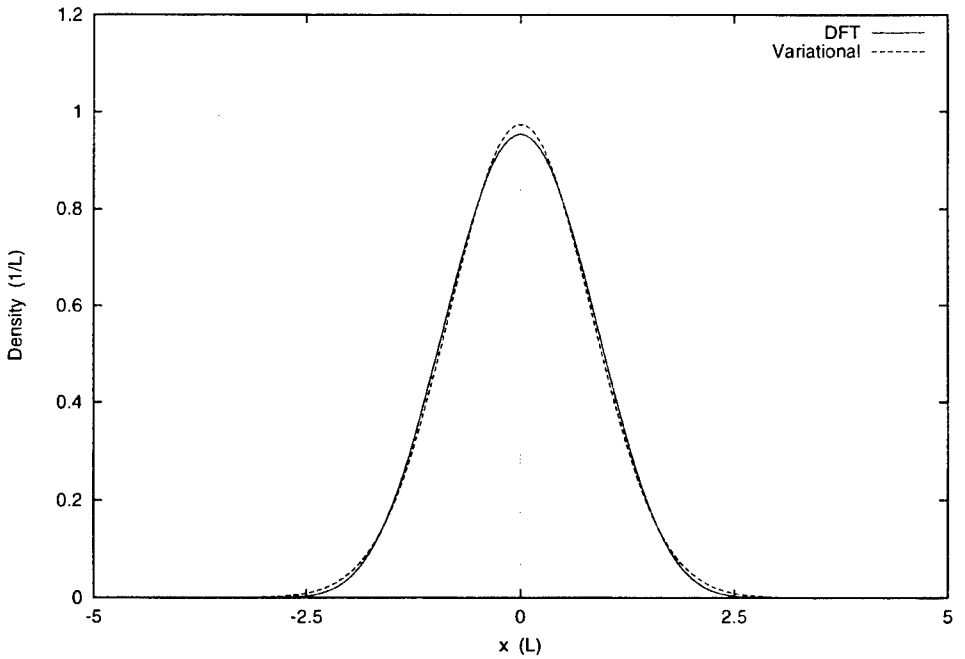

FIGURE 2. Plot of $\rho(x)$ versus x for the external potential given by $v(x) = \alpha \exp(\beta x^2)$ The DFT calculation (E = 2.98021 J, μ=1.64453 J) is compared to a variational calculation (E = 2.98168 J). The values of α and β are 1 Joule and 1 L^{-2}, respectively.

Gravitational Lensing and the Search for Dark Matter

Dara J. Norman

University of Washington

Abstract

Weak gravitational lensing by clusters of galaxies can amplify the light of quasars, which axe some of the most distant objects known. The strength of this amplification depends on the distribution of dark matter in these foreground clusters. Several studies have detected angular correlations between background quasars and foreground galaxies which are consistent with the weak lensing effect. Understanding this correlation is important in interpreting how a magnification bias of quasars might undermine our notions of their cosmological distribution and intrinsic nature. A precise measure of the amplitude and slope of this correlation is also a sensitive test of models of large scale structure formation in the early universe.

Introduction

Most of the universe is made up of dark matter. Likely 95 - 99% of all matter in the universe is non-luminous and therefore cannot be directly observed with telescopes. This is not merely speculation; we see evidence of dark matter on all scales throughout the universe. In our own Milky Way galaxy, we detect dark matter through the motions of stars near the sun. These bright stars trace the gravitational field that is influenced by all the matter present, both light and dark. In our Local Group of galaxies, we see evidence of additional matter through the motions of smaller neighboring galaxies. More distant galaxies have rotation curves that indicate additional matter at larger distances than the light from stars is seen. On still larger scales, we see evidence of dark matter in clusters of galaxies through measurements of velocity dispersions, the pressure balance of galaxies with x-ray emitting gas in the cluster and, finally, through gravitational lensing.

Gravitational Lensing

Although dark matter cannot be seen it does have mass, and thus does have a gravitational influence on luminous matter that can be seen directly with a telescope. In 1916, Einstein published his work on general relativity. One tenet of this work is that light trajectories are bent by massive objects near their path. Because dark matter is massive and clumpy, large concentrations can bend the light of background bright objects. If this lensing phenomenon can be observed and modelled, we can then infer properties about the foreground dark matter acting as the lens. The amount and type of lensing is a function of not only the amount and distribution of mass in the system, but also of the lensing geometry. In some cases, very strong lensing of a background point source can result in multiple images of the source. In other cases, lensing of a background galaxy results in elongated images of the source galaxy or arcs. Other, more subtle effects can also result from gravitational lensing. One of these is known as amplification bias.

Amplification Bias

Amplification bias arises because gravitational lensing conserves surface brightness but changes the solid angle of the source. This change of solid angle means that a patch of sky behind a lens will have its dimensions stretched. An observer looking through a fixed aperture will then see a smaller region of sky than would have been observed in the absence of the lens. This will tend to dilute the number density of sources in the patch.

However, because lensing will also magnify sources, faint sources will be brightened into the observed sample, tending to increase the number density of sources behind the lens. Which of these two effects dominates depends on the slope of the luminosity function (number density per luminosity bin) of the source sample. Source populations with a steep luminosity function may show evidence of amplification bias while populations with a more shallow slope will not. Evidence of this amplification bias would be observed in a statistical overdensity of lenses near the positions of background sources.

In order to search for this amplification bias, we have selected a sample of bright source objects, quasars, that can be seen over large cosmological distances. We expect to see an overdensity of foreground galaxies in the vicinity of these quasars, so long as we have chosen very bright quasars, thus steepening the source luminosity function. The amplitude and shape of this correlation depend strongly on the properties of the lensing cluster of galaxies.

Earlier studies have had mixed results detecting an angular correlation signal between background quasars and foreground galaxies. These inconsistences are possibly the result of differing slopes of the quasar luminosity function for the samples chosen. Most of the previous studies (Bartsch et al., 1997; Benitez & Martinez-Gonzalez 1997; Williams & Irwin, 1998 and references within) of this correlation have used existing photographic surveys (and thus inhomogeneous samples) to characterize the intervening galaxies and quasars. Studies that have used charged coupled devices, CCDs (Tyson, 1986) have looked only on small scales (< 5 arcminutes) and therefore are likely not sampling the galaxy background well.

Our Survey

We have undertaken a survey of galaxies in the vicinity of ~100 quasars that are bright both in the radio ($S_{5GHz} > 1Jy$) and the optical ($V < 20$) to search for this angular correlation signal. Our survey employs large format CCDs and has the advantage of being able to probe to deeper magnitude depths over large areas. With our images, we should be able to look for an overdensity on scales of ~25 arcminutes. We also have data for several control fields not known to be near any bright quasars. These fields will enable us to accurately sample the ambient number density of galaxies.

The figure below shows preliminary results from an initial subsample of 28 quasars. Here we have compared the number density of galaxies in circular annuli close to and far from each quasar. The most distant annulus is used to determine the background number density and extends in radius from 15 - 25.5 arcminutes. At the believed distance of the lens, 15' is $\sim 3h_o^{-1}$ Mpc and is beyond the expected extent of a galaxy cluster at that distance. The inner annuli have radii with outer edges at 4, 8, and 15 arcminutes. The top panel shows the ratio of the galaxy number densities in the inner regions to the background number density. Within our errors, we observe a marginal overdensity of galaxies the closer we look to the quasar. However, the current subsample is still relatively small. To further check our result, we have moved the center position of the annuli 8' from the quasar position in the expectation that this would wash out any correlation signal with the quasars. In bottom panel is plotted the ratio of these off center number densities. It is encouraging that in this case we observe no signal.

Conclusions

Even in this small subsample of quasars presented here, we have observed a marginal overdensity in the number of galaxies near to bright quasars. We are encouraged that our larger sample will enhance the signal and accuracy of these results. An understanding of how foreground structures modify our measurements of the more distance universe is essential in developing a coherent and accurate model of the formation of large scale structures in the early universe.

References

Bartelmann, M. 1995, A&A 298: 661

Bartelmann M. & Schneider, P. 1997 A&A 319 375

Bartelmann M., Schneider, P. & Hasinger, G. 1994 A&A 290 399

Bartsch, A., Schneider, P. & Bartelmann, M. 1997 A&A 319 375

Benitez, N., Martinez-Gonzalez, E., 1995 ApJ 448: L89

Benitez, N., Martinez-Gonzalez, E., 1997 ApJ 477: 27

Boyle, B. J., Fong, R., Shanks, T. 1988 MNRAS 231: 897

Dolag, K. & Bartelmann, M. 1997 MNRAS 291 446

Fugmann, W. 1990 A&A 240: 11

Rodrigues-Williams, L. L. & Hogan, C. J. 1994 AJ 107: 451

Rodrigues-Williams, L. L. & Hawkins, M.R.S. 1995, in AIP Conf. Proc. 336, Dark Matter, ed. S. S. Holt & C. L. Bennett (New Your:AIP),331

Sanz, J. L., Martinez- Gonzalez, E. & Benitez, N. 1997 MNRAS 291 418 ▯

Seitz, S. & Schneider, P. 1995 A&A 302 9

Tyson, J. A. 1986, AJ 92: 691

Williams, L. L. R. & Irwin, M. 1998 MNRAS

Wu, X-P., Han, J. 1995 MNRAS 272: 705

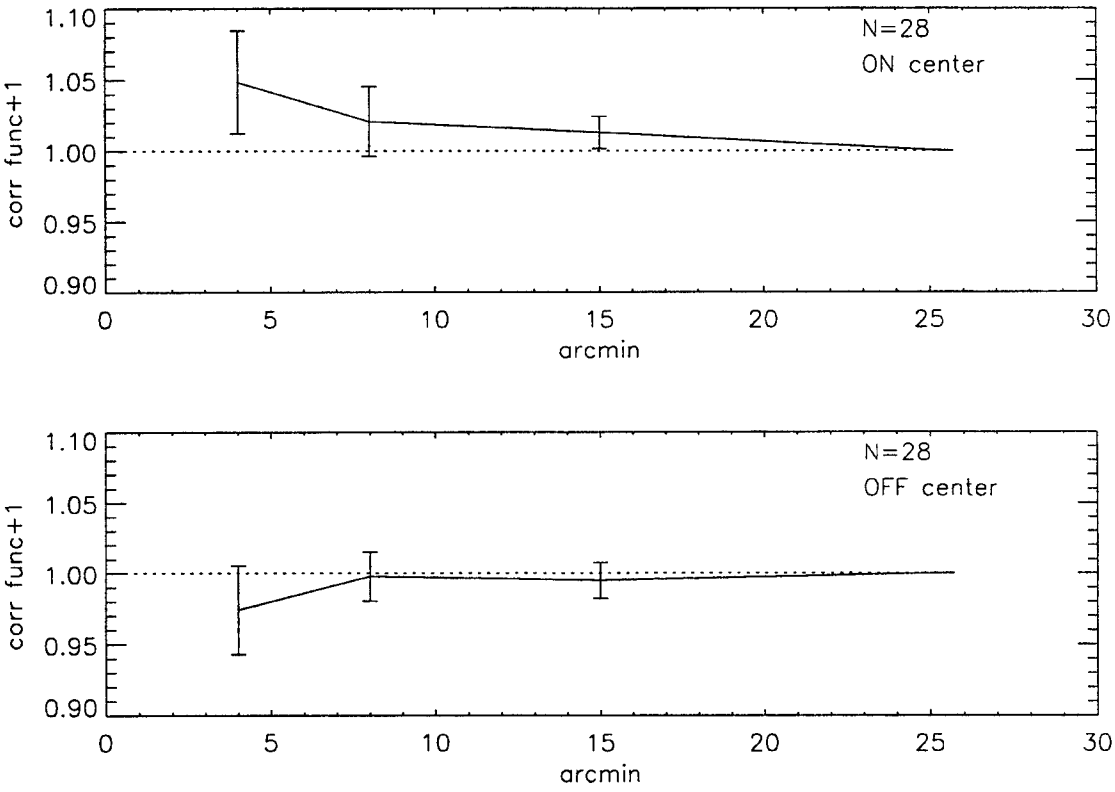

Figure 1. Plot of the correlation function +1 of foreground galaxies in the fields of 28 background quasars. The top panel shows a marginal overdensity close to the quasars. An offset of 8' from the quasar's position eliminates the signal (bottom panel). The error bars are Poisson.

Effect of Zn^{2+} Doping on the Phase Transition Temperature of Cadmium Calcium Acetate Hexahydrate Single Crystals

F. A. Oguama

New Jersey Institute of Technology

H. Shields

D. K. DeOlin

Wake Forest University

Abstract

The effect of Zn^{2+} impurity on the phase transition temperature of Cadmium calcium acetate hexahydrate (CCDAH) crystals has been studied using electron paramagnetic resonance (EPR) technique. The phase transition is detected by monitoring the EPR signal from a negligible amount of Cu^{2+} in the crystal. Above the phase transition, there is no splitting of the Cu^{2+} hyperfine pattern due to inequivalent orientations of the ion. When the temperature is lowered through the phase transition temperature, the hyperfine pattern splits into several components. The observed lowering of the phase transition temperature (136 K - 103 K) with increasing Zn^{2+}, impurity concentration in the crystals is compared with that observed in our earlier studies of Cu^{2+} impurities in CCDAH. The change in transition temperature with Cu^{2+} ion concentrations (143 K - 122 K) is explained well in terms of mean field theory and the soft mode arising out of the harmonic vibration of -Ca-Cd_{1-x} Cu_x-Ca- chain along the c axis of the crystal. Contrary to our expectation, the rate of decrease in the phase transition temperature with increasing Zn^{2+} concentration is significantly higher than that induced by Cu^{2+} of similar concentration. The difference in behavior between the Zn^{2+} and the Cu^{2+} is not due to a difference in ionic size. It may be that the ratio of the mean field constant to the soft mode frequency is not independent of the nature of the impurity ion as expected from the theory of phase transitions.

1. Introduction

Cadmium calcium acetate hexahydrate (CCDAH) forms tetragonal crystal at room temperature, having space group 14/m and containing four magnetically equivalent molecular units per unit cell [1-3]. Chains along the c axis of the crystal consist of alternate Cd^{2+} and Ca^{2+} ions, two to each of the acetate radicals acting as bridging ligands.

The use of electron paramagnetic resonance (EPR) technique for studying phase transitions in single crystals is well established [2-13]. EPR studies of phase transition in Cadmium calcium acetate hexahydrate have been the subjects of a number of investigations [2-6]. A Q-band EPR study by Mabbs and Smail [2] using Cu^{2+} ion as a probe in CCDAH indicated a structural phase transition near 140 K. Eachus *et al.* [3] have investigated the same at X-band EPR and confirmed a structural phase change between room temperature (RT) and Liquid Nitrogen temperature (LNT) in CCDAH, but their interpretations of the EPR spectral data differs from those of Mabbs and Smail [2]. The result of the X-band EPR study by Sikdar and Pal [4] indicated that the phase transition temperature (T_c) of CCDAH ranged

from 140 K in a sample containing 0.5% of copper by weight to 128 K in a sample whose concentration was not specified. The metal ions at $T > T_c$ lie along the c axis, while for $T < T_c$ they are believed to have a zigzag pattern along the c axis, leading to an orthorhombic distortion.

In a recent study, Shields et al. [5] reported that the phase transition temperature of CCDAH is sensitive to Cu^{2+} ion concentrations. They showed that the phase transition temperature of $CaCd_{1-x}Cu_x(CH_3COO)_4.6H_2O$ varied from 143 K to 123 K as the concentration Of CU^{2+} ion varied from 0.07 % (x = 0.005) to 1.3 % (x = 0. 100) of the sample weight (where x is the atomic fraction of the Cu^{2+} impurity). Very recently, Oguama *et al.* [6] have studied the effect of Mn^{2+} ion impurity on the phase transition in CCDAH and observed that the phase transition temperature of $CaCd_{1-x}Mn_x(CH_3C00)_4.6H_20$ varied from 128 K to 118 K as x varied from 0.018 to 0.249. Similar observations have been reported for Zinc fluotitanate hexahydrate (ZNFTH) crystals [7] where it was found that Cu^{2+} and Ni^{2+} impurities modified the phase transition temperature of the material. The change in T_c induced by Cu^{2+} ion in the ZNFTH crystals, was found to be relatively larger than that induced by Ni^{2+} of similar concentration [7].

It may be mentioned that the presence of an impurity in a crystal can change the ionic mass and/or radius. A change in ionic mass changes the soft mode frequency and this provides a large contribution toward the change in T_c [14]. A change in ionic radius causes lattice distortions/strains and this can also bring about slight changes in T_c. If the impurity exhibits Jahn-Teller effect, then the effect can bring an additional change in the soft mode frequency of the host lattice and can lead to an appreciable change in T_c [15-17].

Recently, we have been able to develop a simple theory [6] based on the Landau's mean field theory of phase transition and the simple harmonic vibrational modes of the -Ca-Cd-Ca-Cd- linear chain along the c axis of CCDAH, which accounts very well for the quantitative change in T_c of CCDAH as a function of Cu^{2+} ion concentrations. In the present report, we have extended the study of phase transition in this crystal to investigation of the effect of Zn^{2+} ions (using Cu^{2+} as an EPR probe). Based on the above mentioned theory, we expect that if instead of the Cu^{2+}, Zn^{2+} ion is doped in this crystal, the phase transition temperature should decrease gradually with increasing Zn^{2+} concentration in a similar pattern to that observed in the case of Cu^{2+}, with a slight shift to the high side. The result of the present investigation would help in shedding more light on the roles of impurity metal ions on the modifications of the phase transition in CCDAH.

2. Experimental Details

Single crystals of CCDAH were grown by slow evaporation at room temperature from aqueous solutions containing Calcium acetate, Cadmium acetate and Zinc acetate, such that the molar ratios of Zinc acetate to Cadmium acetate in the solutions were 1/15, 1/20, 1/50, 1/100 and 1/400 respectively. Trace (but fixed) amount of Copper acetate was added to each solution. The Cu^{2+} ion was added to act as a probe for studying the phase transition by EPR while the Zn^{2+} ions were added to affect the phase transition temperature. The crystals grew (in about two weeks) with an elongated habit along the c axis. The percentage weight (w) of Zn^{2+} in each sample was determined accurately by Galbraith Laboratories Inc., Knoxville, TN (USA). The relation between x and percentage weight (w) is shown later. Axes a' and b', perpendicular to the c axis and the well-defined faces described by Eachus *et al* [3] was used to identify the EPR spectra. The EPR spectra of each of the crystal samples were recorded at different temperatures using a Varian E-century line spectrometer, operating at 9.28 GHz. The temperature of the sample in the EPR cavity was varied in the temperature range 300 K to 15 K, using an APD cryogenics HC- 4 close cycle refrigerator. The temperature could be controlled to ± 0.5 K and the accuracy of the reported transition temperatures is ± 1 K. The phase transition temperature for each of the samples was determined from the EPR spectra by noting the temperature at which there is a substantial decrease in the intensity and the onset of splitting of the Cu^{2+} signal (Fig. 1-3).

3. Results and Discussion

Figures 1-3 show the EPR spectra at different temperatures above and below the transition point for samples with x = 0.0205, 0.0034 and 0.0018 respectively. The experimental values of T_c of $CaCd_{1-x}Zn_x(CH_3C00)_4.6H_20$ as a function of x is shown in Figure 4 as well as in Table I. The experimental and calculated values of T_c in $CaCd_{1-x}$ $Cu_x(CH_3COO)_4.6H_20$ as a function of x as derived from our previous study [5,6] are shown in Table 11. As mentioned before, the agreement between the earlier experimental and theoretical values of T_c as a function of x for Cu^{2+} ion is excellent, especially for low concentrations. For high Cu^{2+} impurity concentration, the maximum difference between the computed T_c and experimental T_c is about 2.5 °C. It shows that the assumption that the soft mode frequency which goes to zero at T_c in CCDAH crystal corresponds to the harmonic vibrational mode of the -Ca-$Cd_{1-x}Cu_x$-Ca- chain along the c axis of the crystal holds well, especially for low concentrations. At high Cu^{2+} concentrations, strains may cause additional change in T_c.

Encouraged by the said success of the theory [6], we proceed here to explain the variation of the phase transition temperature of $CaCd_{1-x}Zn_x(CH_3C00)_4.6H_20$ as a function of x as experimentally observed in this present study. It should be noted that the percentage weight from the chemical analysis can be different from that of the solution from which the crystal is grown. The atomic fraction (x) of Zn^{2+} in CCDAH is related to the percentage weight (w) by :

$$x = 4.964w/(65.3+0.471w). \quad (1)$$

According to equation (7) of ref. 6, the transition temperature of the crystal can be calculated from the following expression:

$$(k\Delta T_c)/\omega_{0\delta}^2 = [x(a-b)]/(1+bx), \quad (2)$$

where k is the mean field constant and $\omega_{0\delta}$ is the soft mode frequency of the doped crystal. $\Delta T_c = T_c - T_{co}$, where T_{co} = transition temperature of pure CCDAH, T_c = transition temperature of CCDAH doped with impurity metal ion and

$$a = (M_i-M_{cd})/(M_{ca}+M_{cd}); \; b = (M_i-M_{cd})/ M_{cd}. \quad (3)$$

Here, M represents the atomic mass of the atom or ion concerned and M_i is the atomic mass of the impurity ion, which is Zn^{2+} in this paper. For Zn^{2+} ion, the values of a and b are obtained as: a = -0.3084; b = -0.4184. The computed values of T_c for $CaCd_{1-x}Zn_x(CH_3COO)_4.6H_20$ as a function of x is also shown in Table I along with the experimental values.

The observed lowering of T_c in CCDAH with Zn^{2+} impurity poses an interesting problem on the physics of phase transition in this crystal. If we assume that k of CCDAH remains unaffected by the nature of the metal impurities, then it appears that Zn^{2+} ion should change the T_c in CCDAH in relatively close manner with Cu^{2+} ion. This should be expected, since both the ionic radii and ionic masses of Cu^{2+} and Zn^{2+} do not differ much. Contrary to this, the experimental values of T_c for $CaCd_{1-x}Zn_x(CH_3COO)_4.6H_20$ showed a more pronounced lowering of T_c with increasing Zn^{2+} ion concentrations as compared to that Of Cu^{2+} ion. Our observed T_c with Zn^{2+} impurity ion range from 134 K to 103 K as x varied from 0.0018 to 0.0205, while the reported values of experimental T_c for Cu^{2+} ion (see Table II) ranged from 143 K to 124 K as x varied from 0.0078 to 0.1082 [5,6]. We also note that the computed T_c for $CaCd_{1-x}$ $Zn_x(CH_3COO)_4.6H_20$ using the value of $k/w_{o\delta}^2$ for Cu^2, ($5.547x\ 10^{-4}$) with T_{co} = 136K do not show good agreement with the experimental values (see Table I and Fig. 4). A fairly good agreement is only obtained when the theoretical T_c are computed using the value of $k/\omega^2_{o\delta}$ (6.892 X 10-5) obtained separately for Zn^{2+} ion (Table I & Fig. 4). For this, T_c = 103 K corresponding to x = 0.0205 has been used as a matching point to obtain the value of $k/\omega^2_{o\delta}$. Thus, since the value of $k/\omega^2_{o\delta}$ is expected to be independent of the nature of the impurity ions, the above result is hard to explain at the moment. Further experimental work using other metal impurities may help shed more light on this.

4. Conclusion

We have studied the phase transition temperature of single crystals of $CaCd_{1-x}Zn_x(CH_3COO)_4.6H_20$ as a function of x, using a very small amount of Copper as an

EPR probe. We had earlier studied by EPR, the phase transition temperature of single crystals of $CaCd_{1-x}Cu_x(CH_3COO)_4.6H_20$ and $CaCd_{1-x}Mn_x(CH_3COO)_4.6H_20$ as a function of x. We find that the rate of lowering of T_c with x (i.e. $-dT_c/dx$) by Zn^{2+} exceeds that of Cu^{2+} of similar concentration. We have been able to explain fairly well the lowering of phase transition temperature T_c in $CaCd_{1-x}Cu_x(CH_3COO)_4.6H_20$ as x increases in terms of mean field theory and harmonic vibration of -Ca-$Cd_{1-x}Cu_x$ -Ca- chain along the c axis of the crystal [6]. The same theory is also successful in explaining the absence of a phase transition in $CaCu(CH_3COO)_4.6H_20$. The greater decrease in T_c by Zn^{2+} ion in comparison to that of Cu^{2+} of similar concentration is quite unexpected , since the ionic masses and ionic radii of Cu^{2+} and Zn^{2+} ions are not significantly different. For a given concentration, they are expected contrary to our observation, to modify the phase transition behavior of CCDAH crystals the same way. We also find that the fitting of the phase transition temperature in $CaCd_{1-x}Zn_x(CH_3COO)_4.6H_20$ (assuming Zn^{2+} ion substitutes for Cd^{2+} ion in the crystal) as x increases with the above equation (Eq. 2) is poor if the value of $k/\omega_{o\delta}^2$ for Cu^{2+} is used to compute T_c. A fairly good fitting is however obtained when the value of $k/\omega_{o\delta}^2$ for Zn^{2+} ion is used to compute T_c It may be mentioned that although $\omega_{o\delta}$ should be independent of the nature of the impurity ions, this may not be the case for the mean field constant k. Further investigations are in progress to explore a theoretical explanation of the observed variation of T_c of CCDAH crystals as a function of Zn^{2+} ion concentration. It will be interesting if the phase transition in the Zn^{2+} doped CCDAH can be studied with other techniques such as inelastic neutron scattering, Raman spectroscopy and optical studies to collaborate our EPR results.

References

1. D. A. Langs and C. R. Hare, *Chem. Comm.* 890 (1967).
2. F. E. Mabs and W.R. Smail, *J. Chem. Soc.* (A), 1716 (1970).
3. R. S. Eachus, F.G. Herring & B. Poh, *J. Chem. Soc.* (A), 614 (197 1)
4. R. Skidar and A.K. Pal, *J. Phys. C: Solid State Phys.* **20**, 4903 (1987)
5. H. Shields, T.G. Kleman and D.K. De, *J. Chem. Phys.* **97** 482 (1992).
6. F.A. Oguama, H. Shields and D.K. De, *Phys. Rev. B* **56**, 2611 (1997)
7. D. K. De, *J. Phys. C* **20**, 5911 (1987)
8. E. Lifshitz and A. H. Francis, *Solid state comm.* **45**, 273 (1983).
9. K. H. Kirkklin and G. McPherson, *J. Phys. C* **64**, 4504 (1976).
10. G. C. Upreti, *J. Magn. Reson.* **13**, 1336 (1974).
11. S. D. Panday and G. C. Upreti, *Phys. lett.* **33A**, 5o4 (1990).
12. K. A. Muller and J. C. Fayet, *in structural phase transition II,* edited by K. A. Muller and H. Thomas (Springer-Verlag, Berlin, 1991).
13. F. J. Owen, Charles P. Poole Jr., and Harracio. A. Farach, *Magnetic resonance of Phase transitions* lst edition (Academic press, New York 1979)
14. K. A. Muller, T. Waldkirch: In Local Properties at Phase Transitions, *Proceedings of the Enrico Fermi Intl. School of Physics Course LIX,* Varenna, 1973, ed. by K. A. Muller, A. Rigamonti (North-Holland, Amsterdam 1976)
15. M. C. M. O'Brien and C. C. Chancey, *Am. Journal of Phys.* **61** 688 (1993)
16. K. H. Hock and H. Thomas, *Z Phys.* B **27** 267 (1977)
17. V. S. Vikhnin, *Sov. Phys. Solid State* **23**, 13 84 (198 1)

Table I

Experimental and theoretically computed values of phase transition temperature of $CaCd_{1-x}Zn_x(CH_3COO)_4.6H_20$ as a function of x

Atomic fraction of Zn^{2+} (x)	$T_{c(obs)}$* (K) ± 1 K	$^{+}T_{c(cal)}$ (K) ± 1 K	$^{++}T_{c(cal)}$ (K) ± 1 K
0.0018	134	133	135
0.0034	129	131	135
0.0140	119	114	133
0.0182	107	107	132
0.0205*	103	103	131

*The matching point with theory.

+ obtained using $k\omega_{0\delta}^2 = 6.892 \times 10^{-5}$ for Zn^{2+}

++ obtained using $k\omega_{0\delta}^2 = 5.547 \times 10^{-4}$ for Cu^{2+}

Table II

Experimental and theoretically computed values of phase transition temperature of $CaCd_{1-x}Cu_x(CH_3COO)_4.6H_20$ as a function of x

Percentage Weight of Copper(II) ions	Corresponding x	Exptl. T_c (K) ± 1K	Computed T_c (K)
0.1	0.0078	143.5	143.4
0.2	0.0156	142.0	141.8
0.3	0.0234	140.5	140.1
0.4	0.0312	139.0	138.5
0.5	0.0389	137.6	136.8
0.6	0.0467	136.0	135.2
0.7	0.0544	134.6	133.5
0.8	0.0621	133.1	131.9
0.9	0.0698	131.6	130.2
1	0.0775	130.1	128.5
1.1	0.0852	128.6	126.8
1.2	0.0929	127.1	125.1
1.3	0.1006	125.6	123.3
1.4	0.1082	124.1	121.6

(Table 11 Ref. 6).

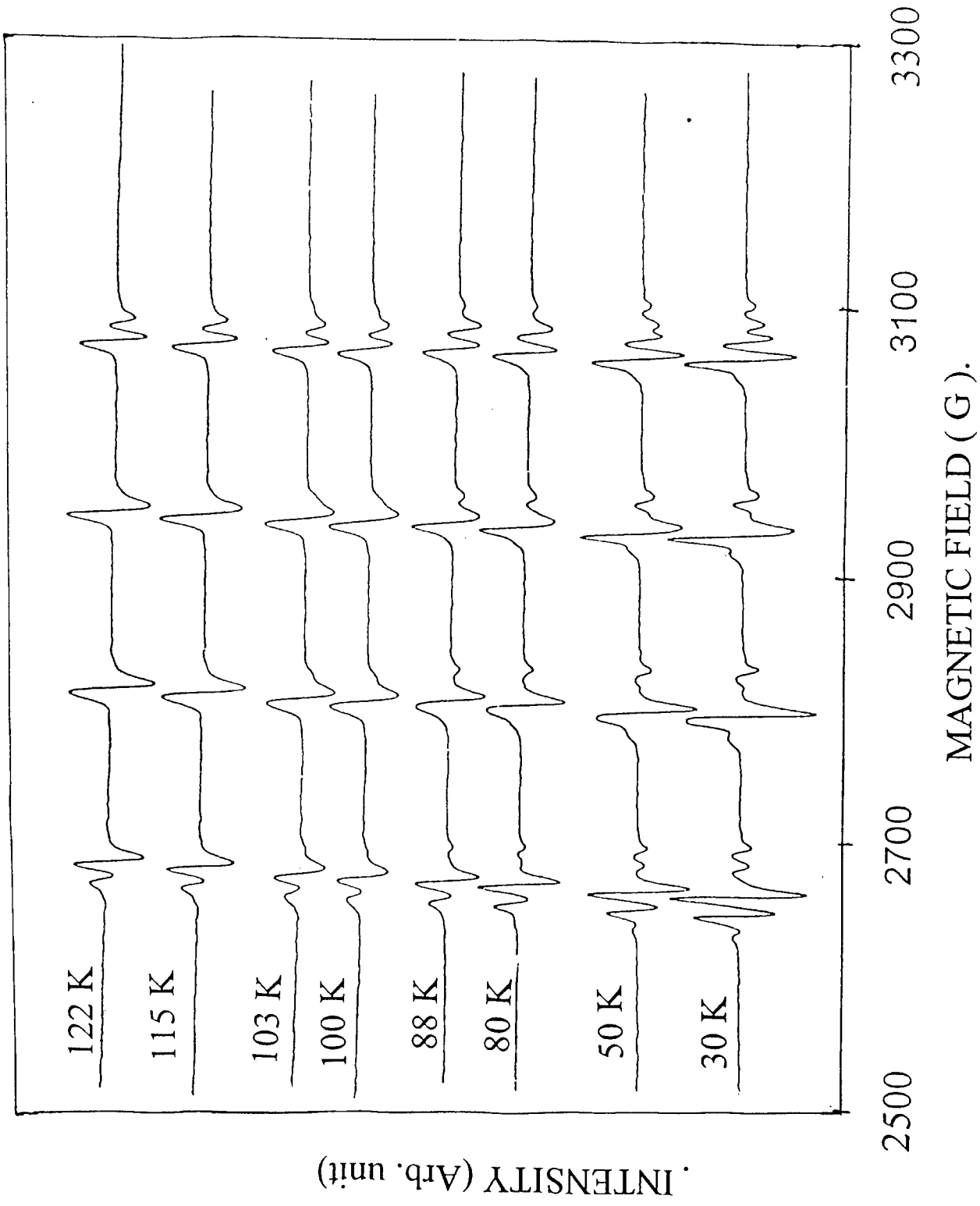

Figure 1. EPR spectra of Cu^{2+} in Zn^{2+} doped CCDAH wth x = 0.0205, at temperatures above and below the phase transition point.

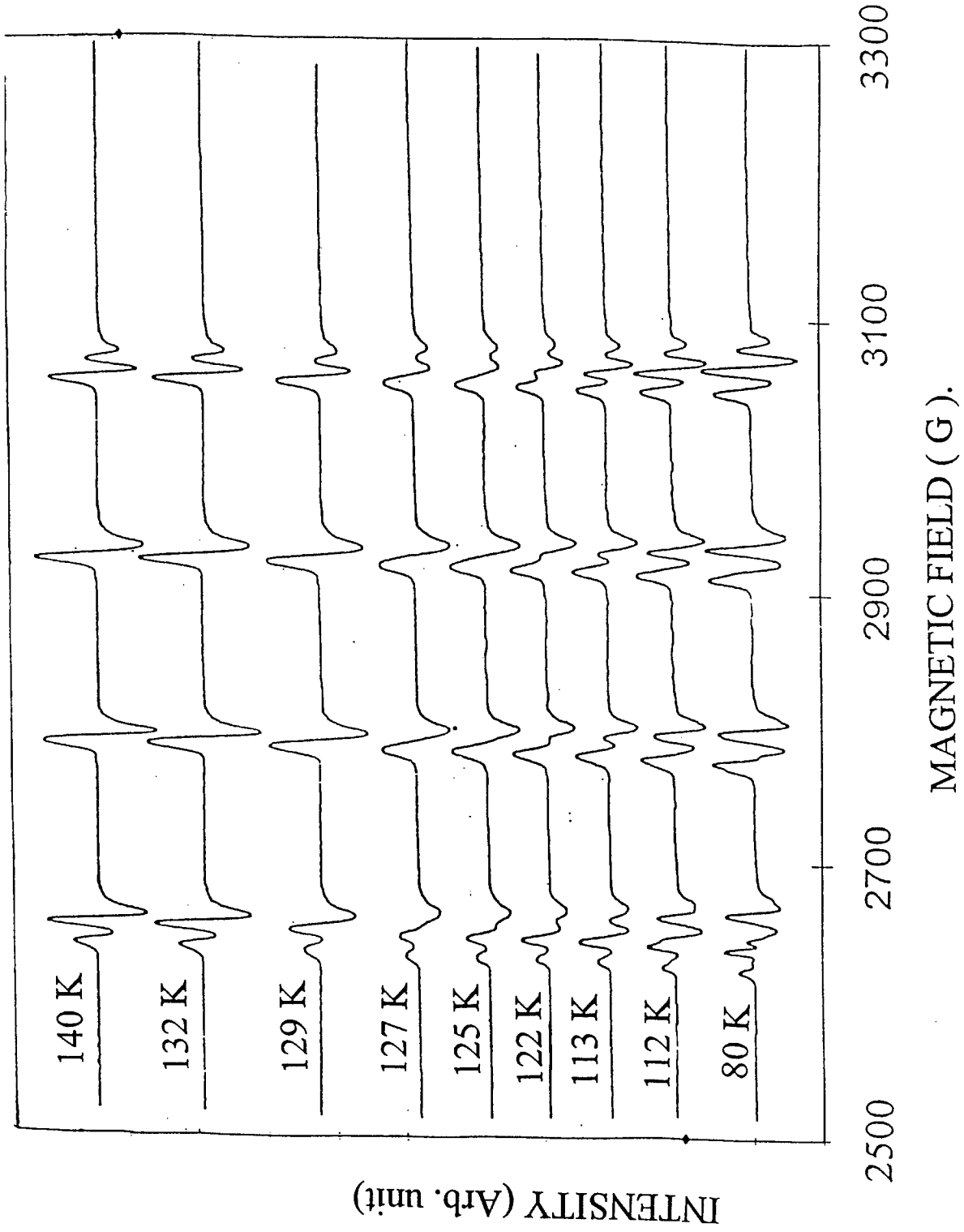

Figure 2. EPR spectra of Cu^{2+} in Zn^{2+} doped CCDAH wth x = 0.0034, at temperatures above and below the phase transition point.

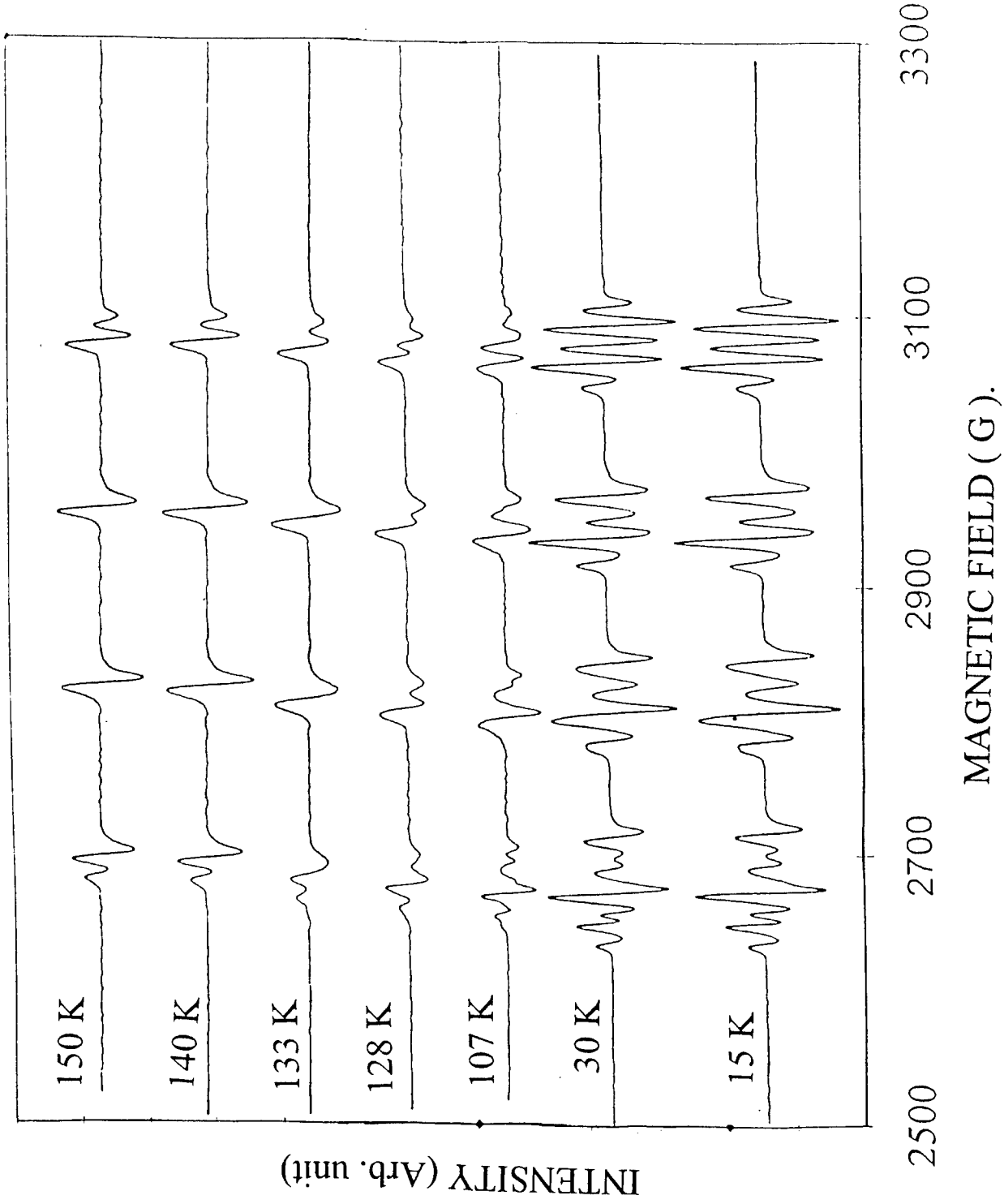

Figure 3. EPR spectra of Cu^{2+} in Zn^{2+} doped CCDAH wth x = 0. 0018, at temperatures above and below the phase transition point.

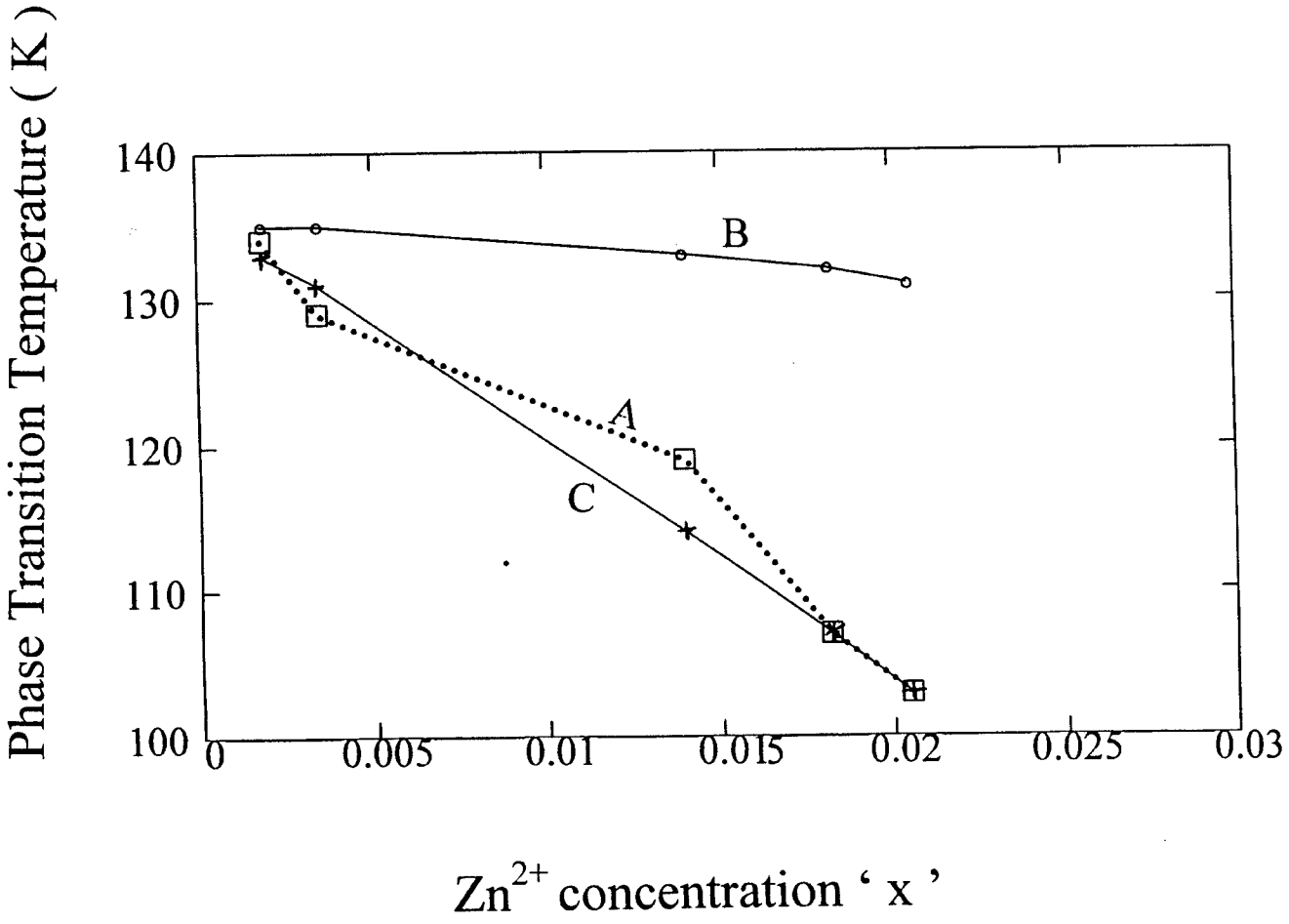

Figure 4. Phase transition temperature in CCDAH as a function of atomic fraction of Zinc ion concentrations. A = experimental values; B = computed values using $k/\omega_{o\delta}^2 = 5.547 \times 10^{-4}$ (for CU^{2+}); C = computed values using $k/\omega_{o\delta}^2 = 6.892 \times 10^{-5}$ (for Zn^{2+}).

Tunable Mid Infrared Downconversion in GaSe and $AgGaS_2$

A. O. Okorogu
S. B. Mirov
W. Lee
D. I. Crouthamell
N. Jenkins
University of Alabama at Birmingham

K. L. Vodopyanov
Imperial College

A. Yu. Dergachev
Swartz Electrooptics

V. V. Badikov
Kuban State University

Abstract

We report on the generation of middle infrared radiation, tunable over 3.5 - 8.5 μm spectral range. This was achieved by difference frequency generation (DFG) in GaSe and $AgGaS_2$ crystals, using the new combination of two solid state lasers, namely the alexandrite (0.73 - 0.75 μm) laser and the alexandrite-pumped tunable $LiF:F_2^{+**}$ (0.8 - 1.2 μm) color center laser.

1. Introduction

Middle-infrared solid state laser sources operating in the range of atmospheric transparency (3-5 and 7.5-9 μm) are of great importance for molecular spectroscopy, eye-safe medical laser sources, eye-safe laser, radar and remote sensing of atmospheric constituents, and for numerous military applications such as target designation, obstacle avoidance and infrared counter-measures, etc.

The alexandrite-color center laser combination has many positive features of a solid state dye-like laser system [1-4]. Advantages include high gain coefficients, broad homogeneous gain profile, low threshold and highly efficient single mode operation with extremely narrow spectral outputs, wide wavelength tunability, compactness, long operational lifetime, rigidity, ease of handling, and insensitivity to the quality of the cavity optical elements, and to the spatial angular and spectral characteristics of the pump source. The system also exhibits virtually no temporal delay between the pump and output pulses, which facilitates nonlinear optical interactions.

The $LiF:F_2^{+**}$ crystals used in the experiments do not exhibit any photodegradation when pumped with radiation at energy densities of up to 5 - 10 J/cm^2 , the limit being set mainly by the optical damage of the LiF crystal [1, 2]. The estimated lifetime of these color center crystals exceed 10 years at room temperature [3]. Mirov et al [4] have shown that $LiF:F_2^{+**}$ yields very high pump radiation conversion efficiencies of up to 60%. The LiF color center lasers have narrow spectral widths, achievable, virtually without loss, while preserving a wide region of continuous tuning (up to 2500cm^{-1}), due to quasi-homogeneous

broadening of their absorption and fluorescence bands [1]. The extension of the LiF:F_2^{+**} laser tuning region into the mid infrared region was made possible using Gase and $AgGaS_2$ crystals. Below, we briefly describe some of the salient properties of these crystals that made them suitable for use in our experiments.

GaSe crystal, first explored as a non-linear optical material in 1972 [5] is now one of the most promising crystals for mid-IR frequency conversion [6]. Amongst its notable properties are its extreme transparency range (0.62-18 μm, Fig. la) and its high second order nonlinearity (d_{NL}= 54 pV/m) [7], which is among the top five measured for birefringent crystals. In addition, due to a very large birefringence of GaSe (Δn~0.35) it can satisfy phase matching conditions for a variety of non-linear optical interactions within the medium.

$AgGaS_2$ crystals on the other hand, are widely used for frequency doubling, frequency mixing, and in parametric oscillators, which can produce continuously tunable radiation from 1.0 to 12 μm with suitable pump laser. $AgGaS_2$ is transparent in the region 0.47-13 μm [7] (see Fig. lb) and has a nonlinear coefficient, d_{NL} = 13 pm/V, and Δn < 10-4. DFG phase-matching conditions are available for this crystal in a wide spectral range of mixed radiations (0.73-0..75 and 0.8-0.95 μm).

Recent advances in crystal growth, have made available, large single GaSe and $AgGaS_2$ crystals with improved transparency. In this paper, we demonstrate a generation of mid-IR light via DFG in these crystals using an efficient combination of room temperature solid state lasers: the alexandrite laser and the alexandrite-pumped tunable LiF:F_2^{+**} (0.8 - 1.2 μm) color center laser.

2. Experiment

GaSe is a layered material, which can be cleaved only along the 001 plane (z-cut orientation). So, we utilized a GaSe crystal, 14 x 14 x 8.3 mm (8.3 mm, along the principal axis) with θ_c=0 (z-cut) and with no antireflection coatings. The linear absorption (Fig. la) was ~0.3 cm^{-1} in the visible (700 -800 nm) and < 0.03cm^{-1} in the IR (1.5 - 12 μm), the measured damage threshold at 750 nm was 20MW/cm^2 for 50 ns pulses.

The 16xl4x38 mm. $AgGaS_2$ crystal was cut at θ_c=65° for type I phase matching. No anti-reflection coatings were applied to this crystal. It is a research grade crystal with a linear absorption in the 0.7-9 μm range of about 0.01 cm^{-1} (Fig.lb) and a measured damage threshold at 750m of about 25MW/cm^2 for 50 ns pulses.

Figure 2 depicts the setup used for the collinear DFG in GaSe and $AgGaS_2$, between the outputs of the alexandrite and the alexandrite-pumped LiF:F_2^{+**} lasers. The LiF:F_2^{+**} laser is pumped with the fundamental output of the alexandrite laser PAL 101 (Light Age Inc.) with an energy of 70- 100 mJ, a pulsewidth of 50 ns and a repetition rate of 20 Hz. The LiF:F_2^{+**} laser output energies of up to 20 mJ (obtained using a Molectron, J3S-10 pyroelectric energy meter) were obtained in the 0.8-1.2 μm spectral region. The rest of the alexandrite laser radiation was directed into the nonlinear crystal (GaSe or $AgGaS_2$), where it is mixed with the tunable near IR LiF:F_2^{+**} laser radiation.

The polarization of the alexandrite laser beam (diameter ~ 3mm) was rotated (from horizontal to vertical) using a polarization rotator (Glan prism combination), and had a power density of about 3MW/cm^2.

The generated middle IR radiation was detected by means of a cryogenically cooled HgCdTe detector or Joulemeter (J3S-10) combined with a digital oscilloscope. A Ge plate was used to filter out near IR input radiations. The IR wavelength verification was performed with the use of LiF, sapphire, MgF_2 and CaF_2 plates as transmission filters.

3. Analysis and discussion

Figure 3a shows the theoretical (solid lines, calculated for type I DFG, e+o=o, using the dispersion relations from [7]), and the experimental angular tuning curves in GaSe, for different wavelengths of the pump radiation (740, 745, and 750 nm - dots, triangles, and squares respectively), versus the spectral output of the alexandrite-pumped LiF:LiF:F_2^{+**} laser. Figure 3b depicts the

wavelengths of the infrared DFG signal, λ_1 versus the wavelengths of tunable LiF:LiF:F_2^{+**} radiation, λ_2. The theoretical and experimental phase matching curves are in a very good agreement over the entire range of the middle IR output. Figure 3b also shows that with the use of GaSe crystal, we experimentally obtained DFG signals over the spectral region 6.5-8.5 μm. Output powers of about 30 μJ and efficiency of 1% were obtained with a very good pulse-to-pulse stability.

Keeping in mind that GaSe can not be cut at an arbitrary angle, DFG phase matching conditions do not exist for the whole range of LiF frequencies. For LiF:F_2^{+**} wavelengths larger than 0.85 μm, the external phase matching angle approaches 90° (Fig. 3a) and IR wavelengths shorter than 5.5 μm (Fig. 3b) will be impossible to obtain. On the other hand, IR wavelengths longer than 9 μm will be difficult to obtain, because they correspond to the short wavelength tail (λ < 820 nm) of the LiF:F_2^{+**} gain profile.

Again, in figure 4, using the dispersion relations as given in [7], we illustrate the theoretically calculated (solid line) and experimental (dots) tuning curves for the pump radiation at a wavelength, λ_3, of 750 nm. Inset shows the dependence of the infrared DFG signal, λ_1 on the wavelength, λ_2 of the tunable LiF:F_2^{+**} laser radiation. Here, as in the case of GaSe, there is a good agreement between the theoretical and experimental phase matching curves. The slight discrepancy between experimental and theoretical curves may be attributed to the necessity to use improved Sellmeier's equations [71 and a possible mistake in the real cut angle of the $AgGaS_2$ crystal.

As mentioned before (similar to GaSe), it is difficult to obtain IR radiation wavelength, λ > 9μm, because they correspond to the short wavelength tail of the LiF:F_2^{+**} gain profile. We obtained DFG signals (Fig. 4b) in $AgGaS_2$ over a spectral region of about 3.6-7 μm, with output powers of about 10 μJ and efficiency up to 0.4%. In principle, by means of mixing the radiations of the alexandrite and LiF:F_2^{+**} lasers, one can cover the spectral range, 3-12 μm.

4. Conclusion

We have demonstrated a tunable middle infrared downconversion in GaSe and $AgGaS_2$ with up to a 10% quantum conversion efficiency, using the convenient combination of two solid state laser sources, the lexandrite laser and the alexandrite-pumped LiF:LiF:F_2^{+**} color center laser. We have shown that both GaSe and $AgGaS_2$, pumped by this laser combination, have potentials for use as mid IR sources in the range 3 - 12 μm for $AgGaS_2$ and 5.5 - 12 3m for GaSe.

Acknowledgements

This work was partially supported by Alabama Space Grant Consortium and DoD Contract # DASG60-97-M-00110.

References

[1] A. Yu. Dergachev, S. B. Mirov, Optics Comm. 145 (1998) 107 - 111.

[2] S. B. Mirov, A. Yu. Dergachev, In Solid State Lasers VI, Proc. SPIE 2986 (1997) 162.

[3] S. B. Mirov, A. Yu. Dergachev, US Patent (pending) (1996).

[4] S. B. Mirov, A. Yu. Dergachev, V. F. Fleurov, V. A. Konyushkin, Technical Digest, CLEO, Anaheim, CA. 9 (June 2 - 7, 1996) 504.

[5] G.B. Abdullaev, L. A. Kulevskii, A. M. Prokhorov, A. D. Savel'ev, E. Yu. Salaev, V. V. Smirnov, JETP Lett. 16 (1972) 90.

[6] N. C. Fernelius, Prog. Cryst. Growth and Charact. 24 (1994) 275.

[7] V. G. Dmitriev, G. G. Gurzadyan, D. N. Nikogosyan, Handbook of Nonlinear

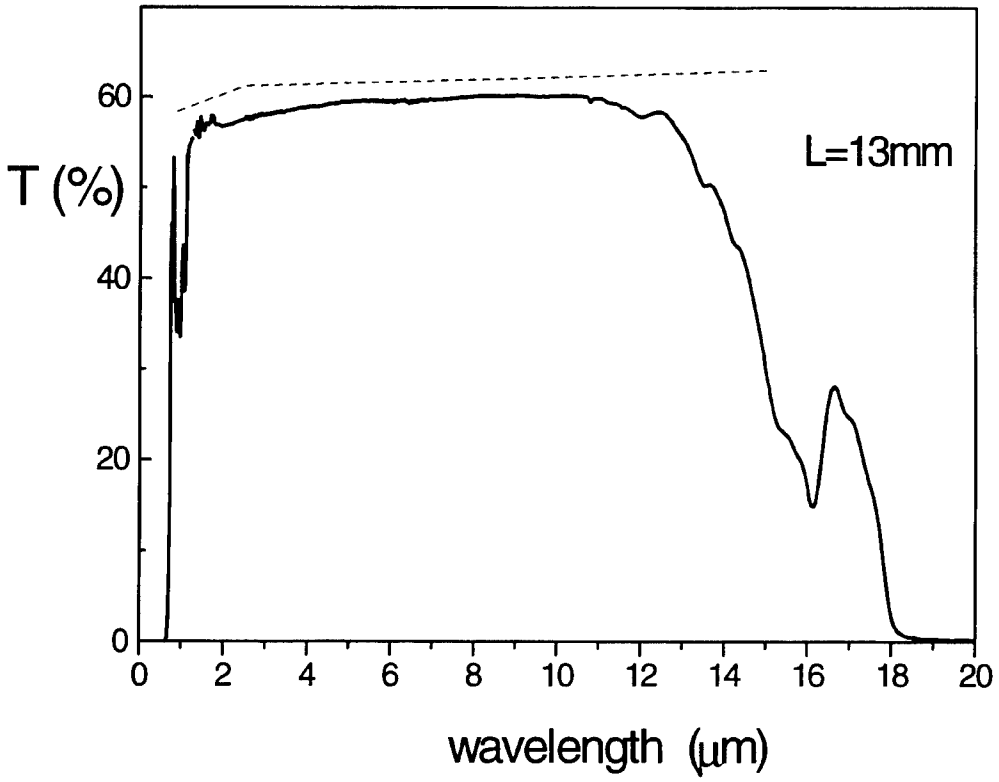

Figure 1a. The transmission curve of GaSe (L = 1.3cm; dotted line represents Fresnel losses only.

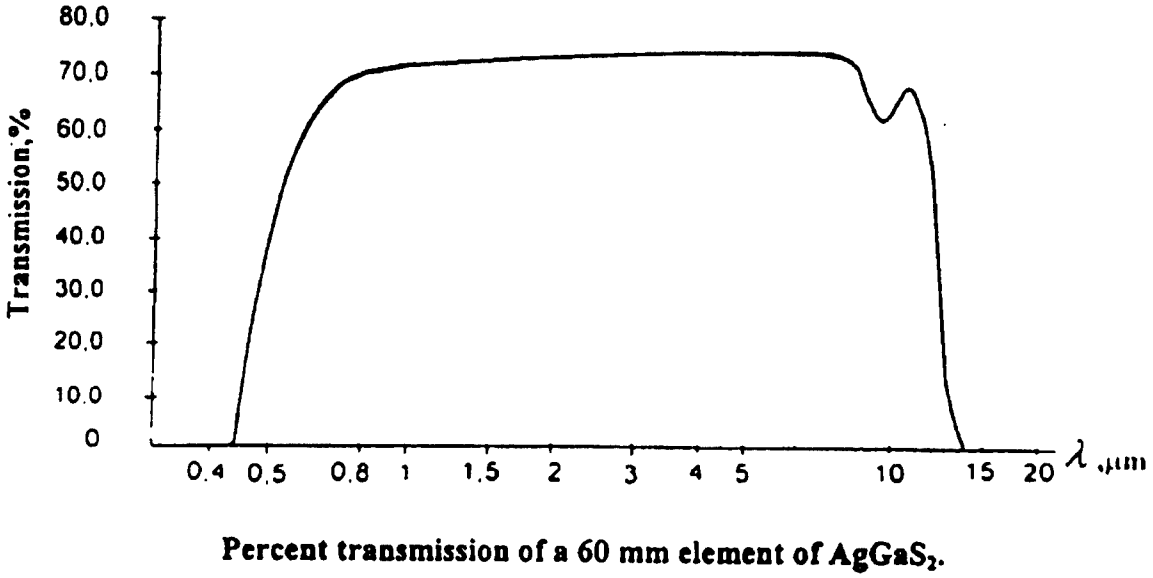

Figure 1b. Transmission curve of $AgGaS_2$.

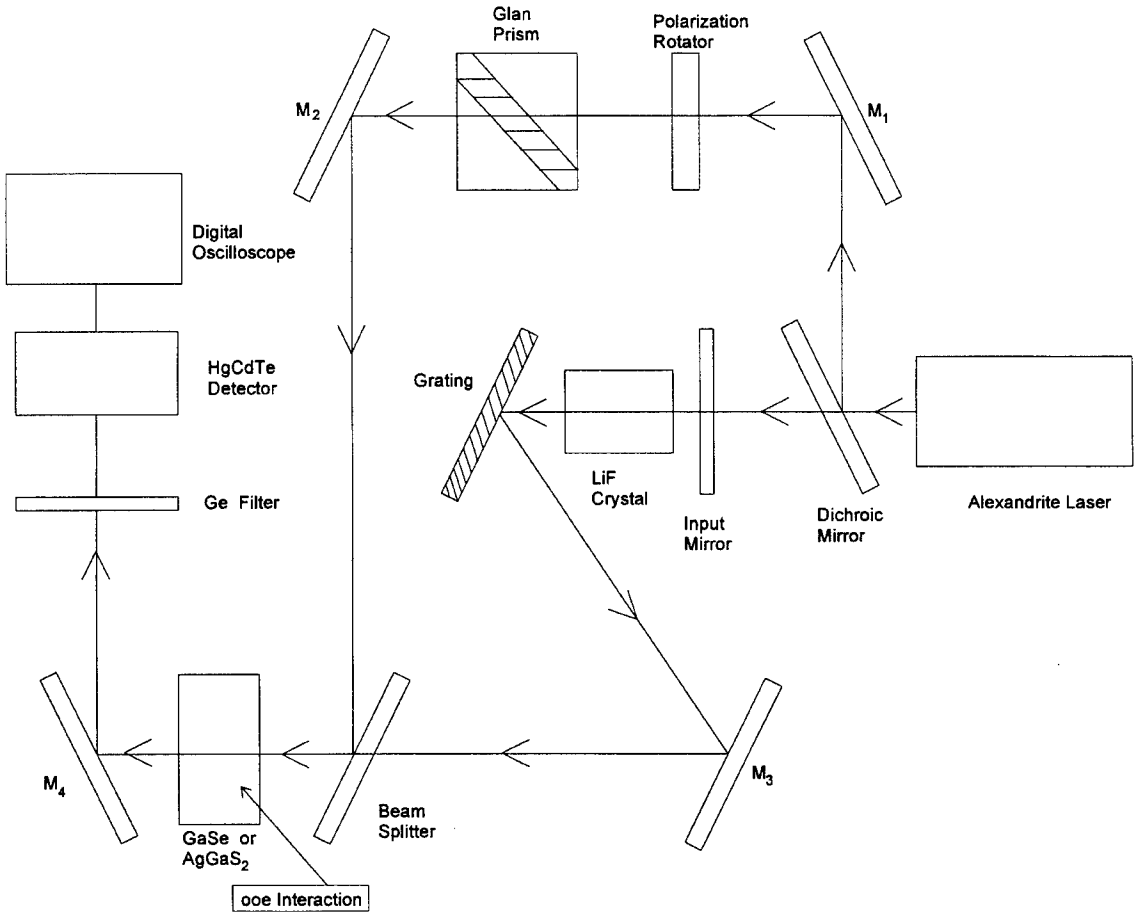

Figure 2. Schematic for the experimental setup of collinear DFM in GaSe or $AgGaS_2$ crystals. For the "ooe" interaction, the first symbol denotes the wave with the lower frequency in the interacting waves. $M_{1..4}$ are mirrors.

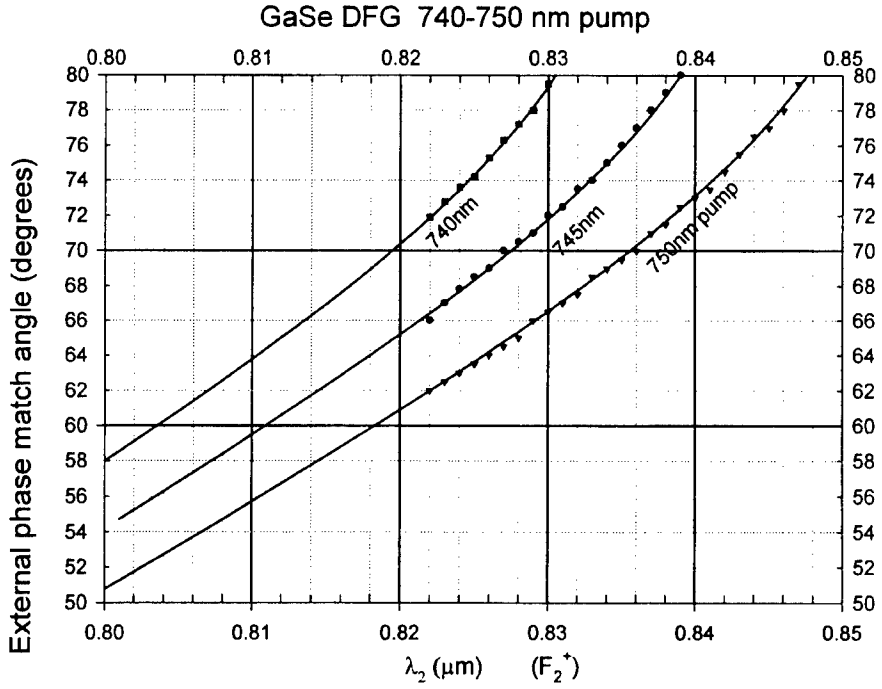

Figure 3a. The external phase matching angle.

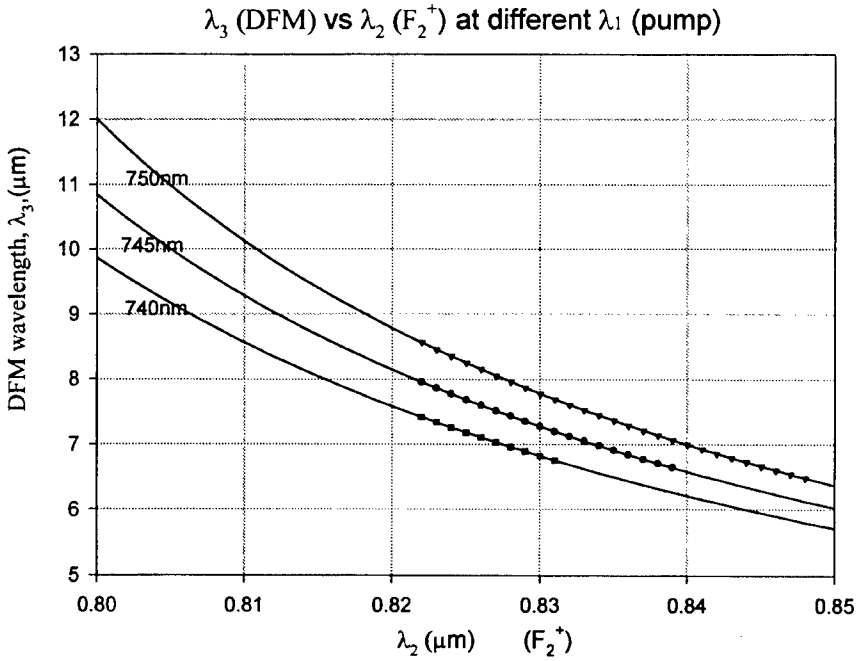

Figure 3b. DFM wavelengths as a function of F_2^{+**} wavelength at different pump wavelengths.

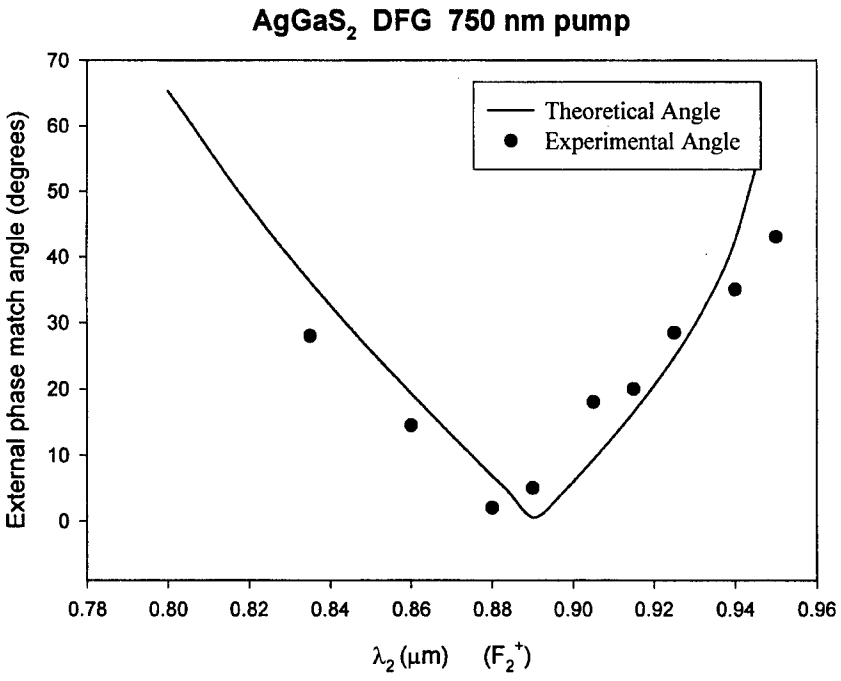

Figure 4a. The external phase matching angle.

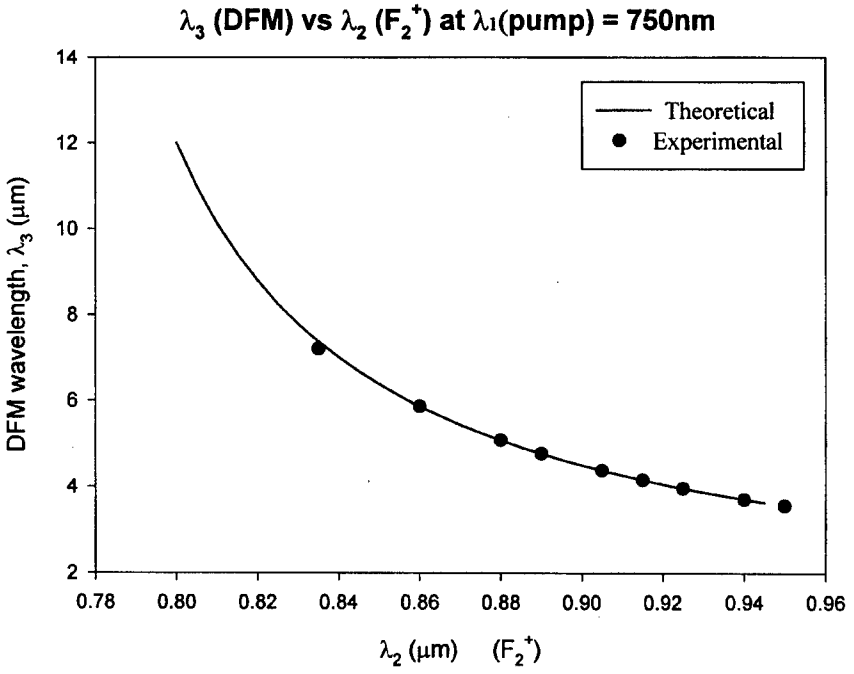

Figure 4b. DFM wavelengths as a function of LiF:F_2^{+**} wavelengths.

Yang-Mills, Gravity, and 2D String Symmetries

V. G. J. Rodgers

University of Iowa

Abstract

General relativity provides us with one of the most successful field theories to describe classical gravity. However the lack of renormalizability and unitarity of general relativity lends suspicion as to whether this is the final word on gravity especially for elementary particles. In this talk we will review some of the salient features of general relativity and propose that the symmetries of string theories suggest a somewhat different view of gravitation. The important concepts here are the field theories on coadjoint orbits and the field theories orthogonal to coadjoint orbits. In particular these symmetries suggests that gravity exists in two dimensions quite unlike Einstein's theory. Furthermore distinct couplings of gravity to electromagnetic fields might provide a framework where one might be able to experimentally yield distinct predictions between this theory and general relativity.

1. Introduction

One of the open questions that still haunts physicists is just how does gravity interact with elemental matter. Since the world at the elementary particle level is quantum, this means that we must find a description of gravity that is consistent with the quantum world. To give you an idea of what to look for consider the hydrogen atom. Here the spectrum displays what is known as the hyperfine structure which is a direct consequence of quantization of the vector and scalar potentials of the electromagnetic fields. Not only do we need to quantize the point particle mechanics of the system, but the field theory that describes the interactions as well.

The same is true for the gravitational system. Unless one has a clever argument as to why only electromagnetism is a quantum system, we must assume the universality of quantum mechanics and include gravitation. In other words, we should be able to answer the question, "what is the hyperfine structure of a gravitational system?", along with a myriad of other interesting questions. Where does quantum gravity manifest itself and can we develop experiments that will access the quantum gravitational world? The hope is that with a consistent mathematical quantum gravitational framework we will be able to guide our experiments into the answers to these questions.

According to Newton, the universal law of gravitation is simply

$$\bar{\mathbf{F}} = -m_1 m_2 G \frac{\bar{r}}{r^3},$$

where the distance, $\bar{r}$, is the relative distance between the two masses. The principle suggests that no matter how far away the masses are from each other that a force will interact with them immediately. In other words there is instantaneous communication between the two masses about their relative positions. This is called "action at a distance". This law admits three conserved quantities that can be used to fix the position and shape of orbits, viz, the energy, angular momentum and the Runge-Lenz vector. The idea works very well for everyday masses and planetary motion, and objects that move slowly with respect to the speed of light, but fails to explain many observations about gravitation including the perihelion shift of the planet Mercury.

Einstein's observation was that for very small objects, (this size restriction is mentioned to avoid tidal effects) one cannot discern the difference between a body that is falling in a gravitational potential from accelerations. This universality puts gravitation on a different footing from other force laws as it does not depend on the particulars of the particle such as mass or charge. The natural mathematical framework for this theory is then the study of what are known as diffeomorphisms and differential geometry. Using just these notions we will show that a theory of the graviton may exists that is somewhat different from Einstein's theory. An important point to keep in mind is that this theory is developed from an arena where Einstein's theory is vacuous, i.e. two dimensions. It is often stated that two dimensions is special or peculiar, however in our frame work two dimensions extrapolates nicely to higher dimensional gravitational theories.

2. Two Dimensional Structures

The study of coadjoint orbits[1-3] for two dimensional theories has been in the literature for some time. The construction geometric actions that enjoy the symmetries of an underlying Lie algebra such as the celebrated WZW[4] model and Polyakov[5] gravity have been shown to be precisely the geometric actions associated with the affine Lie algebra and circle diffeomorphisms respectively[6-8]. In this talk, we turn our attention not to the coadjoint orbits but instead to theories that are "orthogonal" to the orbits. By this we mean to study the field theories associated with the background fields that define the coadjoint orbits, vis the coadjoint vectors. In other words, we promote the fixed coadjoint vectors to dynamical fields and reinterpret the generator of isotropy on the orbits as the Gauss law constraints for a field theory involving the coadjoint vectors. The coadjoint vectors turn out to be vector potentials associated with a gauge theory and another field which we interpret as the gravitational field. In two dimensions these fields are the coadjoint vectors that are coupled to the WZW model and the Polyakov induced gravitational action. Our interpretation of the geometric actions associated with the coadjoint orbits is that these actions are that of bosonized chiral fermions coupled to background gauge and gravitational fields in two dimensions. This is important as Einstein's theory provides no new dynamics for different background gravitational fields whereas in this study distinct orbits correspond to distinct background fields. Since the gauge fields can be identified as Yang-Mills[9] fields we will assume that just as Yang-Mills has meaning in higher dimensions so must its gravitational analogue. For us, recovering the gravitational theory and its interaction with gauge fields is the major thrust of this work. Since the dominant degrees of freedom (the electric fields) of Yang-Mills survived the reduction to two dimensions, we claim that the most relevant degrees of freedom of gravity axe not the metric but instead another rank two tensor that appears as a coadjoint vector in two dimensions. Our claim is that important theoretical clues about the nature of gravity may be recovered from this procedure. We will give the details of this construction and further develop the gravitational theory.

The organization of this talk is designed to give a global picture of our construction and is arranged as follows. In the first section we will review the salient features of the coadjoint orbits associated with the affine Lie algebra and the diffeomorphism algebra. This will allow us to identify both the gauge transformations and the isotropy equations that we later relate to the Gauss law. Next we will give a scant review of Yang-Mills emphasizing the features that are of interest to this talk. Rom there we demonstrate a construction of the Yang-Mills action starting from the isotropy condition of the orbits and the transformation laws of the coadjoint vectors. By demanding features such as local Lorentz invariance we are able to resurrect a theory that has no dimensional restrictions in its classical action. After a brief discussion of general relativity, we use this construction to educe the for the gravitational field. We close with comments about the nature of this new theory.

3. Early Results and 2D Geometric Actions

Since the symmetries of string theory are the pivotal symmetries associated with this

construction, we begin with the semi-direct product of the affine Lie algebra (Kac-Moody)[10,11] and the Virasoro[12] algebra

$$\left[J_N^\alpha, J_M^\beta\right] = i f^{\alpha\beta\gamma} J_{N+M}^\beta + N k \delta_{N+M,0} \delta^{\alpha\beta} \quad (1)$$

$$[L_N, J_M^\alpha] = -M J_{N+M}^\alpha \quad (2)$$

$$[L_N, L_M] = (N-M) L_{N+M} + \frac{c}{12}(N^3 - N)\delta_{N+M,0}. \quad (3)$$

The generators of the affine Lie algebra are J_N^α and the diffeomorphism generators are L_N. A typical bases for the adjoint vectors is,(L_A, J_B^β, ρ) where ρ is the generator of the central extensions. We normalize the generators so that $Tr(\tau^\alpha \tau^\beta) = \delta^{\alpha\beta}$. Then from the commutation relations above one may write the adjoint action on the adjoint vectors as[13]

$$\left(L_A, J_B^\beta, \rho\right) * \left(L_{N'}, J_{M'}^{\alpha'}, \mu\right) = (L_{new}, J_{new}, \lambda) \quad (4)$$

with

$$L_{new} = (A - N') L_{A+N'} \quad (5)$$

$$J_{new} = -M' J_{A+M'}^{\alpha'} + B J_{B+N'}^\beta + i f^{\beta\alpha'\lambda} J_{B+M'}^\lambda \quad (6)$$

and the new central extension is

$$\lambda = \frac{c}{12}(A^3 - A)\delta_{A+N',0} + Bk\delta^{\alpha'\beta}\delta_{B+M',0}. \quad (7)$$

Now the dual space to this Lie algebra, whose elements are spanned by $\left(\tilde{L_N}, \tilde{J_M^\alpha}, \tilde{\mu}\right)$ can be defined by requiring that there exists an inner product such that

$$\left\langle \left(\tilde{L_N}, \tilde{J_M^\alpha}, \tilde{\mu}\right) \middle| \left(L_A, J_B^\beta, \rho\right) \right\rangle = \delta_{N,A} + \delta^{\alpha\beta}\delta_{M,B} + \rho\tilde{\mu}$$

With this the adjoint action on the coadjoint representation[1-3] can be extracted by requiring that

$$\left\langle \left(\tilde{L}_N, \tilde{J}_M^\alpha, \tilde{\mu}\right) \middle| \left(L_A, J_B^\beta, \rho\right) * \left(L_{N'}, J_{M'}^{\alpha'}, \mu\right) \right\rangle \quad (8)$$

$$= -\left\langle \left(L_A, J_B^\beta, \rho\right) * \left(\tilde{L}_N, \tilde{J}_M^\alpha, \tilde{\mu}\right) \middle| \left(L_{N'}, J_{M'}^{\alpha'}, \mu\right) \right\rangle. \quad (9)$$

This means that the action of an adjoint vector on a coadjoint vector yields a new coadjoint vector through,

$$\left(L_A, J_B^\beta, \rho\right) * \left(\tilde{L}_N, \tilde{J}_M^\alpha, \tilde{\mu}\right) = \left(\tilde{L}_{new}, \tilde{J}_{new}, 0\right) \quad (10)$$

with,

$$\tilde{L}_{new} = (2A - N)\tilde{L}_{N-A} - B\delta^{\alpha\beta}\tilde{L}_{M-B} - \frac{\tilde{\mu}c}{12}(A^3 - A)\tilde{L}_{-A} \quad (11)$$

and

$$\tilde{J}_{new} = (M - A)\tilde{J}_{M-A}^\alpha - if^{\beta\nu\alpha}\tilde{J}_{M-B}^\nu - \tilde{\mu} B k \tilde{J}_{-B}^\beta. \quad (12)$$

Instead of using components, let us illuminate the meaning of these expressions by writing $\mathcal{F} = (\xi(\theta), \Lambda(\theta), a)$ as an arbitrary adjoint vector and B = (T (θ) , A (θ) , μ) as an arbitrary coadjoint vector, where ξ, Λ, T, and A are functions constructed from an infinite series in the above mentioned basis vectors. For example we write $A(\theta) = \Sigma_{N,\alpha} a_\alpha^N \tilde{J}(\theta)_N^\alpha$. Here ' denotes ∂_θ. The group action of G on B is generated by the adjoint representation for those elements of the group that are connected to the identity[1]. Those adjoint vectors, $\mathcal{F}$, that leave B invariant will generate the isotropy group for B. By setting this equation to zero one can determine the isotropy algebra for B. With this we find that the infinitesimal action of the adjoint on the coadjoint element spawns a new coadjoint vector through,

$$B_{\mathcal{F}} = (\xi(\theta), \Lambda(\theta), a) * (T(\theta), A(\theta), \mu) = (T(\theta)_{new}, A(\theta)_{new}, 0) \quad (13)$$

where the transported fields are defined by,

$$T(\theta)_{new} = \overbrace{\underbrace{2\xi' T + T'\xi + \frac{c\mu}{24\pi}\xi'''}_{coordinate\ trans} - \underbrace{Tr(A\Lambda')}_{gauge\ trans}}^{new\ diff\ covector} \quad (14)$$

and

$$A(\theta)_{new} = \overbrace{\underbrace{A'\xi + \xi' A}_{coord\ trans} - \underbrace{[\Lambda A - A\Lambda] + k\mu\Lambda'}_{gauge\ trans}}^{new\ gauge\ covector}. \quad (15)$$

Equations 14 and 15 will be of cardinal importance in constructing our theory of gravity.

For completeness, let us remark that geometric actions are constructed as the integral of the symplectic two-form, Ω_B, over a two dimensional submanifold M.

$$S = \int_M \Omega_B,$$

where the symplectic two-form is defined as

$$\Omega_B\left(\widetilde{B_1},\widetilde{B_2}\right) = \left\langle \tilde{B} \mid [a_1, a_2] \right\rangle .$$

and where the coadjoint elements are given by $\widetilde{B}_i = a_i * \tilde{B} = \partial_{a_i}\tilde{B}$. Using methods from[14] one obtains the *two dimensional* action[13],

$$S = \underbrace{\frac{1}{2\pi}\int d^3\theta\, T(\theta)\left(\frac{\partial_\lambda s}{\partial_\theta s}\partial_\theta\left(\frac{\partial_\tau s}{\partial_\theta s}\right) - \frac{\partial_\tau s}{\partial_\theta s}\partial_\theta\left(\frac{\partial_\lambda s}{\partial_\theta s}\right)\right)}_{\text{Diff "Chern-Simons"}}$$
$$+ \underbrace{\frac{1}{2\pi}\int d^3\theta\, \mathrm{Tr}\left(A(\theta)\left(\frac{\partial_\lambda s}{\partial_\theta s}\partial_\theta\left(g^{-1}\partial_\tau g\right) - \frac{\partial_\tau s}{\partial_\theta s}\partial_\theta\left(g^{-1}\partial_\lambda g\right) + \left[g^{-1}\partial_\lambda g, g^{-1}\partial_\tau g\right]\right)\right)}_{\text{Gauge "Chern-Simons"}}$$

$$- \underbrace{\frac{\beta c}{48\pi}\int d\tau d\theta\left(\frac{\partial_\theta^2 s}{(\partial_\theta s)^2}\partial_\tau\partial_\theta s - \frac{(\partial_\theta^2 s)^2}{(\partial_\theta s)^3}\partial_\tau s\right)}_{\text{Polyakov gravity}} \qquad (16)$$
$$- \underbrace{\frac{\beta k}{4\pi}\int d\tau d\theta\, \mathrm{Tr}\left(g^{-1}\partial_\theta g g^{-1}\partial_\tau g\right) + \frac{\beta k}{4\pi}\int d\lambda d\tau d\theta\, \mathrm{Tr}\left(\left[g^{-1}\partial_\theta g, g^{-1}\partial_\lambda g\right] g^{-1}\partial_\tau g\right)}_{\text{Wess-Zumino-Witten}} .$$

This is well known and we emphasis that the geometric action so constructed is restricted to 2D (or 3D and boundary to be more precise). Our role in this work is to build a theory that has no dependence on the dimension. In particular we seek the theory that is "orthogonal" to the orbits. The figure below show the distinction between the symplectic structures on the orbits and those orthogonal to the orbit which define the gravitational and gauge field theories.

Each orbits is characterized by the **isotropy group** of B = (T (θ) , A (θ) , μ) which is a *fixed* coadjoint vector. For the pure affine Lie Algebra case one has for each fixed A(θ), all generators that satisfy

$$[\Lambda A - A\Lambda] + k\mu\Lambda' = 0$$

For the diffeomorphism sector the analogous remark is

$$2\xi' T + T'\xi + \frac{c\mu}{24\pi}\xi''' = 0.$$

The group generated by Λ or ξ characterize the orbit. This group is the **isotropy group** of A(θ), or T respectively.

4. Review of Yang-Mills

Consider Yang-Mills in a temporal gauge, A_0=0. The vector potential $A_i^a(x,t)$ and the electric field $E_i^a(x,t)$ are conjugate variables, with the following commutation relations:

$$\begin{aligned}
&[A_i^a(x,t), A_j^b(y,t)] = 0 \\
&[E_i^a(x,t), E_j^b(y,t)] = 0 \\
&[A_i^a(x,t), E_j^b(y,t)] = i\delta^{ab}\delta(x,y).
\end{aligned} \qquad (17)$$

The gauge transformation laws for vector potential and electric field are given by

$$A_i(x) \to U(x)A_iU^{-1}(x) - \frac{1}{g}\partial_i U(x)U^{-1}(x) \qquad (18)$$

$$E_i(x) \to U(x)E_iU^{-1}(x). \qquad (19)$$

Notice that these transformation laws correspond to coadjoint and adjoint group action, respectively when reduced to one dimension.

From the field equations for A_0 we obtain the Gauss law constraint

$$G^a = \partial_i E_i^a + g[E_i, A_i]^a = 0 \qquad (20)$$

which is the generator of time independent gauge transformations through the Poisson brackets, i.e.,

$$Q_{Gauss} = \int d^3x\; G^a\Lambda^a(x), \qquad (21)$$

where $\Lambda(x)$ is the gauge parameter and,

$$\begin{aligned}
&\{Q_{Gauss}, E\} = [\Lambda, E] \\
&\{Q_{Gauss}, A\} = [\Lambda, A] - \frac{1}{g}\partial\Lambda.
\end{aligned} \qquad (22)$$

The two dimensional action for Yang-Mills can be written as

$$S = \int d^2x\; A_0 \underbrace{\left(g[E_i, A_i] - \partial_i E_i\right)}_{\text{Gauss's law}} + \int d^2x\; \underbrace{\partial_\tau A_i\, E_i}_{\text{Symplectic}} - \frac{1}{2}\int d^2x\; \underbrace{E_i E_i}_{\text{Hamiltonian}} \qquad (23)$$

Since there is no magnetic field in two dimensions, i.e., $B_i = 1/2\epsilon_{ijk}F^{jk} = 0$, upon covariantizing, the above action is the same as

$$S = \int d^2x\; F_{\mu\nu}F^{\mu\nu}. \qquad (24)$$

Now the action $S = \int d^nx F_{\mu\nu}F^{\mu\nu}$ in any dimension has gauge and general covariance, so one can recover the action,

$$S = \int d^4x\; \sqrt{g}\, F^{\mu\nu}F^{\lambda\rho}\, g_{\mu\lambda}g_{\nu\rho} \qquad (25)$$

where as usual $F_{\mu\nu} = \partial_\mu A_\nu - \partial_\nu A_\mu + g\,[A_\mu, A_\nu]$.

It is our intention in this paper to recover a theory, analogous to Yang-Mills, that corresponds to a gravitational action and which has a natural reduction to the T field in 2D. Unlike general relativity, the 2D reduction of this theory is non-trivial. Through the study of symmetries on a circle, we can recover Yang-Mills and its analogue for gravity. Our course of action will be as follows: 1) From circle diffeomorphisms and group transformations extract dual representation and Gauss law from isotropy equations. 2) Use two dimensional anomalies to identify the "carriers" of the interactions. 3) Demand local Lorentz invariance. 4) Demand Gauge invariance. 5) Write down an action for arbitrary dimensions that respects the two dimensional interaction terms.

5. Review of General Relativity

Before proceeding with our work we would like to review some of the essential features of general relativity as gravity. Einstein's[15] theory of gravity is at present the most promising theory of gravity to date. It is based on the fact that gravity can be directly related to a geometric manifold. In this description of gravity, one has a derivative operator, ∇_μ, which can be built from the ordinary derivative operator and the connection, also called Christoffel symbol, $\Gamma^\rho_{\lambda\mu}$. This connection is a pseudo-tensor, which transforms like a tensor with an additional inhomogeneous term,

$$\delta\Gamma^\rho_{\lambda\mu} \rightarrow \underbrace{\delta\Gamma^\rho_{\lambda\mu}}_{tensorial} + \underbrace{\partial_\lambda\partial_\mu\xi^\rho}_{inhomogenous} \tag{26}$$

If the derivative operator ∇_μ is compatible with a metric $g_{\alpha\beta}$ (i.e. $\nabla_\mu g_{\alpha\beta} = 0$), then the Christoffel symbol may be written as

$$\Gamma^\rho_{\lambda\mu} = \frac{1}{2}g^{\rho\alpha}(\partial_\alpha g_{\lambda\mu} - \partial_\lambda g_{\alpha\mu} - \partial_\mu g_{\lambda\alpha}). \tag{27}$$

In general relativity the central tensor that one builds from the derivative operator is the curvature tensor,

$$[\nabla_\mu, \nabla_\nu]\, A_\lambda = R^\rho_{\mu\nu\lambda} A_\rho \tag{28}$$

where A_λ is a generic rank one tensor. One may think of the curvature as the minimal generally covariant tensor that one can construct from $\Gamma^\rho_{\lambda\mu}$ that contains two derivatives of the metric tensor. Thus one may employ it for a field theoretic study of the metric.

By virtue of the Jacobi identity associated with the derivative operators, one recovers the Bianchi identity,

$$\nabla_\alpha R^\rho_{\mu\nu\lambda} + \nabla_\nu R^\rho_{\alpha\mu\lambda} + \nabla_\mu R^\rho_{\nu\alpha\lambda} = 0 \tag{29}$$

Contracting the Bianchi identity leads to

$$\nabla_\mu R^\mu_\nu - \frac{1}{2}\delta^\mu_\nu \nabla_\mu R = 0 \tag{30}$$

where $R_{\mu\nu}$ and R are the Ricci tensor and scalar curvature respectively. The Einstein equations follow immediately since one wants to couple the theory to the divergence free energy-momentum tensor and one writes,

$$R_{\mu\nu} - \frac{1}{2}R\, g_{\mu\nu} = \kappa\Theta_{\mu\nu}. \tag{31}$$

The Einstein-Hilbert action,

$$S = \int d^4x\, \sqrt{g}\, R \tag{32}$$

leads to the free Einstein field equations

$$R_{\mu\nu} - \frac{1}{2}R\, g_{\mu\nu} = 0. \tag{33}$$

The energy-momentum tensor for matter is the symmetric rank two tensor that couples to the metric, $g_{\mu\nu}$. It should be noted that in two dimensions (one space and one time), the combination

$$R_{\mu\nu} - \frac{1}{2}R\, g_{\mu\nu}$$

is identically zero so no gravitational degrees of freedom can arise from Einstein's theory. The T field cannot then be a metric if it distinguishes different orbits.

6. Construction of the Gravitational Theory for the field $T_{\mu\nu}$

As mentioned in Section 2, the geometric actions associated with the coadjoint orbits

have a physical interpretation of fermions coupled to gauge and gravitational fields in two space-time dimensions. We have denoted the background gauge field as A and the background gravitational field as T. In this section we discuss the main points of this work; one may recover field theories in any dimension from the two dimensional symmetries. In particular, one may recover a theory of gravity which is distinct from general relativity.

A. Gauge Transformation Laws

Consider the field A separately from T and set $\xi = 0$, and consider just the gauge variation of a rank 1 tensor A_μ in the temporal gauge, and Equation (15) represents the residual time-independent gauge transformations on A_μ. A is A_θ of $\boldsymbol{A} = (A_\theta, A_\tau)$.

Now lets consider the transport due to ξ and set $\Lambda = 0$. From the fact that tensor fields of rank one transforms as

$$\delta_\xi A_\alpha = \xi^\beta \partial_\beta A_\alpha + A_\beta \partial_\alpha \xi^\beta,$$

under a general coordinate transformation, we see that the ξ transformation in Equation (15) is the residual transformation of time independent spatial translations. It is well known that the Yang-Mills action is the requisite action to describe A_μ as a dynamical field in any dimension. We will utilize this fact in order to understand the gravitational sector.

In a similar way we can deduce the properties of T and extend it to higher dimensions. The analogous constraint equation is

$$2\xi' T + T' \xi + \frac{c\mu}{24\pi} \xi''' = 0$$

Up to inhomogeneous term transforms under diffeomorphisms as $\delta T = 2\xi' T + T'\xi$, corresponding to a rank two tensor, i.e.

$$\xi^a \partial_a T_{lm} + T_{am} \partial_l \xi^a + T_{la} \partial_m \xi^a = \delta_\xi T_{lm}.$$

We conclude that T **is the one remaining field component of a rank two symmetric tensor in 2D after fixing the gauge,** $T_{\mu 0} = 0$. In D dimensions there are D, ξ's that can be used to fix the gauge.

B. Gauss Law Constraints and Field Equations

Equations (14,15) can tell us much more than just the transformation laws in one dimension. Recall that by setting this equation to zero, one defines the isotropy group for a particular coadjoint orbit. From the point of view of two-dimensional geometric actions the isotropy group defines the topology of the orbit through $\Omega(G)/H_{T,A} \otimes \mathrm{Diff}\, S^1$ where G is the gauge group, $\Omega(G)$ is the loop group of G, and $H_{T,A}$ is the isotropy group of the fields T and A. The geometric actions then describe the anomalous two-dimensional fermionic vacuum in the presence of background gauge and gravitational fields. Our purpose here is quite different. We are not at all interested in orbits instead we are interested in making A and T dynamical variables which would certainly move us away from any orbit. In fact if we are to preserve gauge invariance, we must guarantee that we do not incorporate gauge variations into the dynamics. The geometric orbits of WZW and Polyakov represent anomalous contributions to gauge theories and gravity and cannot define gauge invariant theories for T and A. In field theories, this is precisely the role of Gauss Laws. The Gauss Law constraints guarantee that the dynamical field and its associated conjugate momentum will not evolve in any (residual) gauge directions. The Gauss law constraints are the generators of the time independent gauge transformations and spatial translations. Thus the dynamical theory of A and T must be "orthogonal" to the coadjoint orbits. Since the isotropy condition is an equivariant relation between coadjoint vectors and the adjoint representation it is precisely the condition that defines the Gauss Law. One replaces the coadjoint vector with the canonical coordinate and the adjoint element with the conjugate momentum. This follows since the conjugate momentum transforms like the adjoint elements. Therefore we claim that **the isotropy equation is tantamount to the Gauss**

Law constraints of a field theory of the coadjoint vector and its conjugate momentum.

In 2D the field equations of the T_{01} component become constraints; as opposed to dynamical field equations. We need a Gauss law that will deliver the time independent coordinate transformations for the T_{11} component. Let X^{ij} be the conjugate variable to T_{ij}. This is a symmetric object whose transformation law will be determined by the Gauss law. Let

$$(G_{\text{diff}})_a = X^{lm}\partial_a T_{lm} - \partial_l(X^{lm}T_{am}) - \partial_m(T_{la}X^{lm}) - q\partial_a\partial_l\partial_m X^{lm}. \quad (34)$$

This is the generator of time independent coordinate transformations in 1 + 1 dimensions and we have deliberately left in the tensor structure for future use. From the Poisson brackets, one can recover the transformations laws of X^{ab} and T^{ab}. We have

$$Q_{\text{diff}} = \int d^3x\ G_a\xi^a, \quad (35)$$

where the ξ^a are the time independent spatial translations. As a result,

$$\begin{aligned}\{Q_{\text{diff}}, T_{lm}\} &= -\xi^a\partial_a T_{lm} - T_{am}\partial_l\xi^a - T_{la}\partial_m\xi^a - q\,\partial_a\partial_l\partial_m\xi^a = -\delta_\xi T_{lm}\\ \{Q_{\text{diff}}, X^{lm}\} &= \xi^a\partial_a X^{lm} - (\partial_a\xi^l)X^{am} - (\partial_a\xi^m)X^{la} + (\partial_a\xi^a)X^{lm} = \delta_\xi X^{lm}.\end{aligned} \quad (36)$$

The transformation law for X^{lm} defines it as a rank two tensor density of weight one. Thus X^{lm} can carry a factor of $\sqrt{g}$ in its definition. In two dimensions, the transformation law for the "space-space" component of X^{lm} reduces to the transformation law of elements in the adjoint representation of the Virasoro algebra, viz. $X'\xi - \xi'X$.

As can be seen from the above gauge fixed expression, the conjugate momentum X^{ab} comes from a tensor density of the type $X^{\mu\nu}{}_{\rho}$, were ρ has been evaluated in the time direction, i.e $X^{ab} = X^{ab}{}_0$ in analogy with E_i and F_{i0}. This tensor is symmetric in its $\mu\nu$ indices. Furthermore, the appearance of spatial derivatives on T^{a0} in L_0 suggests that $X^{\mu\nu}{}_{\rho}$ comes from a covariant tensor with the structure

$$X_{\alpha\beta\gamma} = \nabla_\gamma T_{\alpha\beta} \quad (37)$$

on arbitrary manifolds.

For the moment let us set $q = 0$, eliminating the 2D inhomogeneous contribution to the transformation law. Then in any dimension the following can be used to recover the homogeneous part of the constraint equation,

$$\mathcal{L}_0 = X^{\lambda\mu\rho}(T^\alpha{}_\rho\nabla_\alpha T_{\lambda\mu} + T_{\lambda\alpha}\nabla_\mu T^\alpha{}_\rho + T_{\alpha\mu}\nabla_\lambda T^\alpha{}_\rho - \nabla_\rho(T^\alpha{}_\lambda T_{\alpha\mu})). \quad (38)$$

By varying the above action with respect to the $T_{0\upsilon}$ components and fixing the temporal gauge on a flat manifold we find

$$X^{lm0}\partial_\nu T^{lm} - \partial_m(X^{ml0}T_{l\nu}) - \partial_l(X^{ml0}T_{m\nu}) = 0. \quad (39)$$

In the above the latin indices refer to-space components and the Greek space-time components. We see that we have recovered the generator of time independent coordinate transformations, eq(34).

In a similar manner the inhomogeneous contributions to the constraints in eq(34) are accessed through the lagrangian

$$\mathcal{L}_\infty = \frac{-q}{4}\nabla_\beta T^\beta{}_\alpha\nabla_\lambda\nabla_\mu X^{\lambda\mu\alpha}, \quad (40)$$

as its field equations for the $T_{0\upsilon}$ components are (on a flat manifold)

$$q\partial_\upsilon\partial_\alpha\partial_\beta X^{\alpha\beta 0}$$

Together the two lagrangians, eqs(38,40), will yield the desired constraints. However they cannot build the full action as they do not contain the Hamiltonian and symplectic structure.

Consider the action,

$$S_I = \int\sqrt{g}\left[(-\nabla_\alpha T_{\beta\gamma})X^{\beta\gamma\alpha} + \frac{1}{2}X^{\beta\gamma\alpha}X_{\beta\gamma\alpha}\right]d^n x. \quad (41)$$

It is obvious that S_I contains that part of the Lagrangian which determines the symplectic structure of the action. A variation of S_I with respect to $\partial_0 T_{\alpha\beta}$ yields $X^{\alpha\beta 0}$ as the conjugate momentum. After gauge fixing only the T_{ij} components have non-trivial conjugate momentum. Furthermore, after gauge fixing, eqs(38,40) *do not* contribute to the conjugate momentum which is required. Notice that there is no contribution to the field equations of T_{10} from S_I.

Putting this all together and writing partial derivatives on $T_{\alpha\beta}$ in terms of X we may write

the fully coordinate invariant action in n dimensions as

$$
\begin{aligned}
S_{\text{grav}} = & \int d^n x \sqrt{g}\, \left(X^{\lambda\mu\rho}\, T^{\alpha}{}_{\rho}\, X_{\mu\lambda\alpha}\right) \\
& +2\int d^n x \sqrt{g}\, \left(X^{\lambda\mu\rho}\, T_{\lambda\alpha}\, X^{\alpha}{}_{\rho\mu}\right) \\
& -2\int d^n x \sqrt{g}\, \left(X^{\lambda\mu\rho} X^{\alpha}{}_{\lambda\rho} T_{\alpha\mu}\right) \\
& -\frac{q}{4}\int d^n x \sqrt{g}\mu^{8-n}\, \left(X^{\alpha\beta}{}_{\beta} \nabla_{\lambda} \nabla_{\mu} X^{\lambda\mu}{}_{\alpha}\right) \\
& -\frac{1}{2}\int d^n x \sqrt{g}\, \left(X^{\beta\gamma\alpha} X_{\beta\gamma\alpha}\right).
\end{aligned}
$$

Variation with respect to T_{v0} and fixing the temporal gauge on a flat manifold we find

$$X^{lm0}\partial_\nu T^{lm} - \partial_m(X^{ml0}T_{l\nu}) - \partial_l(X^{ml0}T_{m\nu}) - q\,\partial_\nu\partial_l\partial_m X^{lm0} = 0.$$

In 1 + 1 this is the isotropy equation,

$\xi T' + 2\xi' T + q\,\xi''' = 0$ where ξ takes the role of X^{11}

7. Conclusions and Questions:

- What is it? More like topological phase of gravity.
- First order $\Box$ operator suggests a Newtonian limit in any dimension.
- Natural quartic term in propagator might soften short distance behavior in a quantum theory.
- Suggests that classical two dimensional gravity is not empty as seen in Einstein's theory
- Naturally close to String theory yet a field theory.
- Easily incorporates supersymmetry through coadjoint orbits.
- Suggest new principle based on diffeomorphism for gravity interacting with matter.
- Still can incorporate metric variations if desired.
- New interaction terms for gravitation and gauge fields might provide a test via pulsars, AGN, etc.
- Method quite general and can be applied to other geometric actions.

8. References

1. A. A. Kirillov, Lect. Notes in Math. 970 (1982) 101, Springer-Verlag (Berlin)
2. A. Pressley and G. Segal, *Loop Groups*, (Oxford Univ. Press, Oxford, 1986)
3. E. Witten, *Comm. Math. Phy.* **114** (1988) 1
4. E. Witten *Comm. Math. Phys.* **92** (1984) 455
5. A. M. Polyakov, *Mod. Phys. Lett.* **A2**, No. 11 (1987) 893
6. B. Rai and V. G. J. Rodgers, *Nucl. Phys.* **B341** (1990) 119
   Gustav W. Delius, Peter van Nieuwenhuizen and V. G. J. Rodgers, *Int. J. Mod. Phys.* **A5** (1990), 3943
7. A. Yu Alekseev and S. L. Shatashvili, *Nucl. Phys.* **B323** (1989) 719
8. P. B. Wiegmann, *Nucl. Phys.* **B323** (1989) 311
9. C. N. Yang and R. L. Mills, *Phys. Rev.* **95** (1954) 631
10. K. Bardakci and M. B. Halpern, *Phys. Rev.* **D3** (1971) 2493
11. V. G. Kac, *J. Funct. Anal. Appl.* **8** (1974) 68
12. M. A. Virasoro, *Phy. Rev. Lett.* **22** (1969) 37
13. R. P. Lano and V. G. J. Rodgers, *Mod. Phys. Lett.* **A7** (1992) 1725

    R. P. Lano, *"Application of Coadjoint Orbits to the Loop Group and the Diffeomorphism Group of the Circle,"* Master's Thesis, The University of Iowa, May 1994
14. A. P. Balachandran, G. Marino, and A. Stern, *Nucl. Phys.* **B162** (1980) 385-7
    A. P. Balachandran, G. Marino, B. S. Skagerstam, and A. Stern, *Nucl. Phys.* **B164** (1980) 427 *Phys. Rep.* **209** (1991) 129
15. A. Einstein, *Annalen der Physik,* 1919 (49)
16. V. G. J. Rodgers, *Phys. Lett.* **B336** (1994) 343
17. Ralph Lano and V. G. J. Rodgers, *Nucl. Phys.* **B347** (1995) 45

Coadjoint Orbits

1) Start with B=(T,A)

2) Act on B=(T,A) with group generated by diffeomorphisms and gauge transformations to produce new coadjoint vectors.

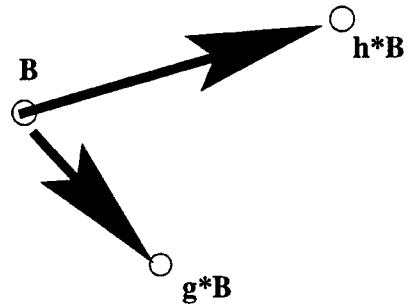

3) Use group elements to span the "orbit" of B.

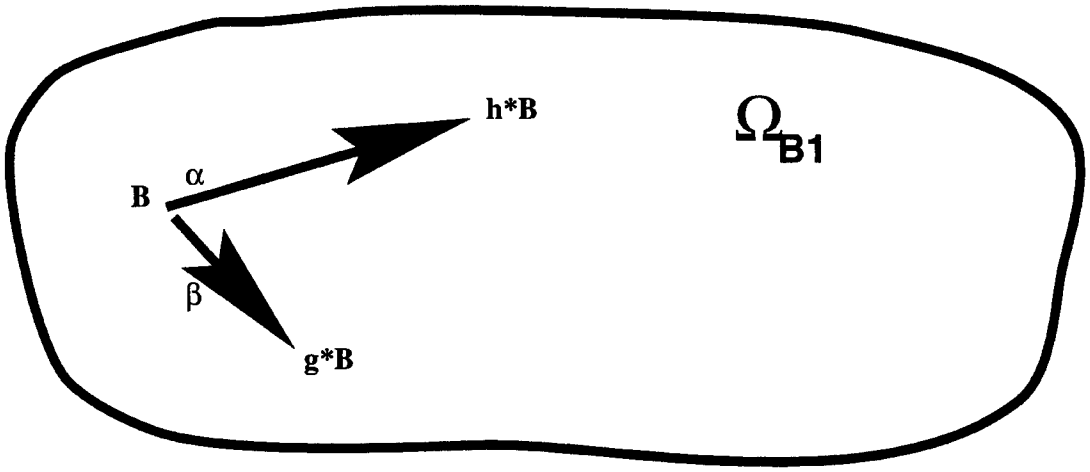

4) Each point on orbit is a coadjoint vector.

5) Define symplectic two form $\Omega_B[\alpha\beta]$
Each Orbit has unique sympletic structure.

The Relationship Between Coadjoint Orbits and the Theories that Define the Dynamics for the Gauge the Gravitional Fields

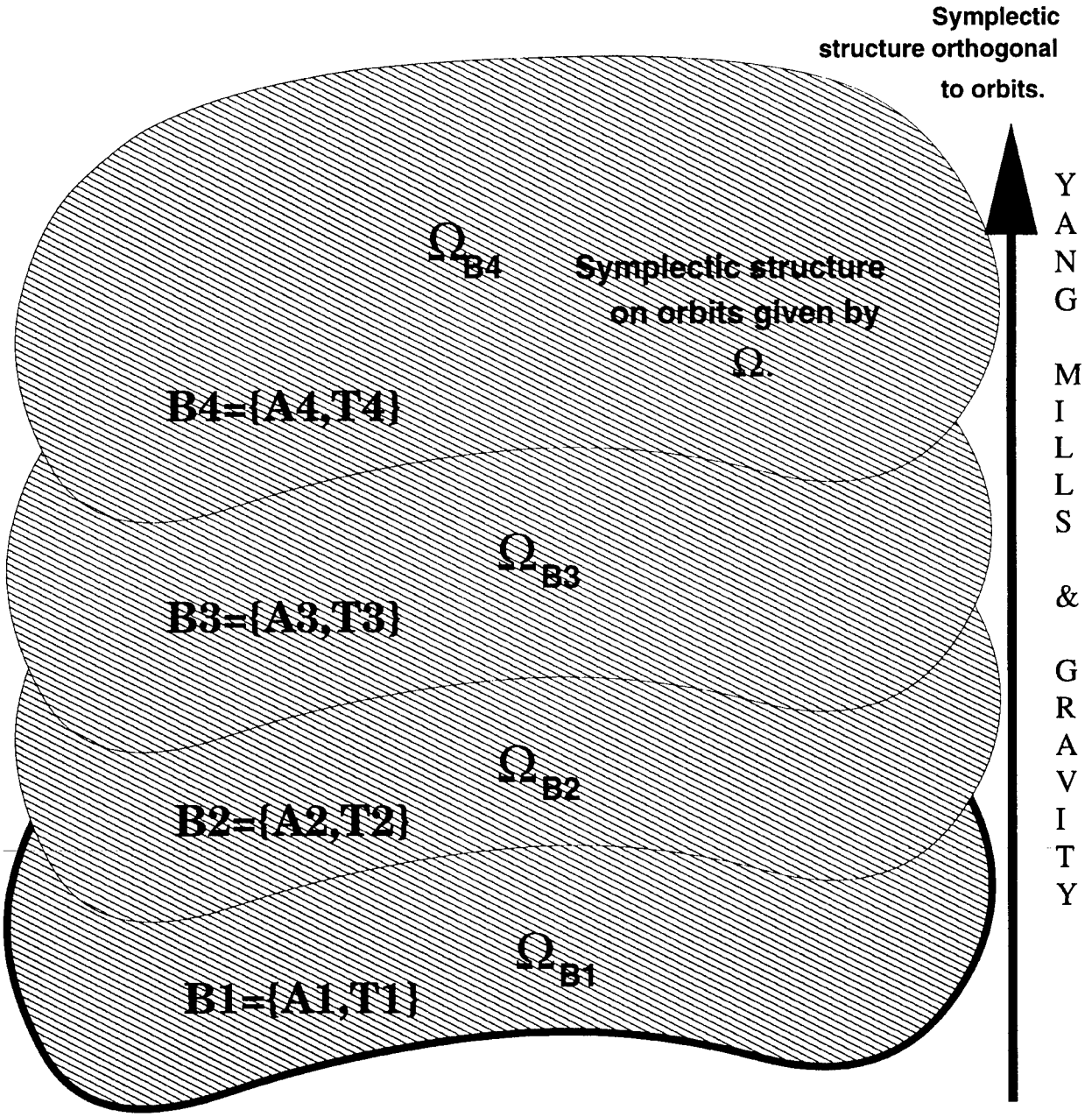

Each surface represents a coadjoint orbit.

Computer Implementation in Various Physics Courses and Laboratories at Kentucky State University

Dr. Rony Shahidain
Dr. Robert Mania

Kentucky State University

Kentucky State University is a small liberal arts university. It does not have a full program in physics. Physics is part of the Applied Mathematics program whose requirement students usually fulfil, in the pursuit of their engineering degree. Students take introductory Physics courses and then courses in Statics, Modem Physics, Engineering Electromagnetics and Thermodynamics. These upper level courses are usually transferred in their respective engineering program. In order to introduce and familiarize the students with the latest software packages and some data acquisition hardwares, we embarked on a project here at KSU. Students are introduced to C++ programming as an application tool, rather than a language. They are supplied with small program in the beginning, which they modify to extract information of interest in physics curriculum. The complexity and expanse of the scope increase with the academic progress. MATLAB is a software widely used by the various engineering disciplines in the processing, modeling, and analysis of data. We have purchased the MATLAB to be used in the Physics curriculum. Also we are requiring students to buy the student version of MATLAB. Another software we have recently procured is called Electronics Workbench. This software is widely used by Physics as well as electrical engineering departments throughout the country. Students not only do their laboratory work implementing various laws of physics and engineering, with this software they also can see the answer to "what if' question by designing various modifications of the main theme. This summer we will install Lab View with the appropriate hardwares and use them in the data acquisition and analysis in the laboratories. This will also give us a way of introducing students to virtual instruments, which students will be able to design once being familiar. Two other softwares that we frequently use and ask students to do their work are EXCEL and MAPLE. Students get quite comfortable in the graphing and presentation of data. These are the various softwares students are exposed to in the Physics part of their program. We are still in the first phase of this implementation. Hopefully, we will see the effects of our endeavor shortly.

Recent Software and Hardware Acquisition

We have added several softwares and we are in the process of implementing hardares in the physics lab. We bought MATLAB, Electronics Workbench to be used in the lab as well as for some courses in the physics curricula. Students are encouraged to buy their own student version of MATLAB. Visual C++ compilers were bought specifically for the Physics students. We bought five DAQ boards from National Instruments, which include Labview 4. 1, multifunction DAQ board and associated hardwares. We will be using them for the data acquisition experiments in the physics lab.

Application of C++ in the Physics Courses

C++ will be introduced as an application tool in various physics courses. Students are introduced to simple programs from which they will write their own programs. They learn the mechanics of compiling, debugging, linking and eventually executing a program. By going through this mechanics of executing programs, students are much comfortable when they deal with programming later on. More appropriate and complex ideas are introduced throughout their program.

Electronics Workbench 5.0 in the Physics Labs

Students in the second Physics course are introduced to EWB. With this software

students get hands on experience to design simple electrical circuit with this software. The circuits could be very simple and gradually get more complicated. They can always try to find answer of "what if' question with this software. Instead of building it with real components, students first design it in the computer. Students may not be able to use it's full potential, but it could also be shown as a demonstration to the students.

MATLAB as a Design Tool

MATLAB is widely used in various Engineering programs in different universities. Simple modeling can be carried out in the upper level courses using MATLAB. We bought MATLAB with several of its toolboxes. Students learn to write their own script files. For data crunching and visual presentation, MATLAB is an excellent tool.

Labview 4.1 Graphical Programming Software

We recently acquired several DAQ boards from National Instruments company. We intend to use them with the data acquisition in the physics lab and incorporate them with experiments. Students will be exposed to virtual instrumentation methods in future labs in physics. By using these DAQ boards many of these experiments will be automated.

Conclusion

Here in Kentucky State University we are trying to introduce to students with some modem state of the art technology. We realize that in order to prepare our students for the 21st century, we have to modernize our labs as well as delivery method for instruction. In this presentation we have included our efforts and trend in order to achieve this goal.

Workbook for Introductory Mechanics Problem-solving

Daniel M. Smith, Jr.
South Carolina State University

I. Motivation

Many introductory physics students regard problem-solving as an exercise in finding an equation containing a single unknown. Such students learn little physics because they remain largely unaware of the important concepts and ideas which give real meaning to equations. Physics instructors are acutely aware of this problem, but almost all of the conceptually-based aids to problem-solving are in formats which are unsuitable for many students: either they require computers, or an instructor's supervision, or they are very much like textbooks, which students tend to read passively. Workbook development is motivated by the need for materials which teach students problem-solving by having them show explicitly (by drawing, writing, and graphing) the relationship between the physical concepts and the equations which represent them.

II. Workbook Philosophy

Physics education research has revealed that misconceptions persist even for many students who are quite successful at problem-solving; they continue to harbor pre-Newtonian conceptions of the world. Development of the workbook is guided by the philosophy that these misconceptions are present even during problem-solving, and that they would be revealed if students are asked specific questions about their thinking. Another guiding philosophy in the workbook development is that the primary focus of problem-solving should be the restatement of the problem in the language of physics. Once a student has learned to restate the problem (first pictorially, or in words, then algebraically), finding the "unknown" should be almost incidental.

III. Workbook Design

Certain design features make the workbook unique. A group of problems (from 4 to 10 in number, depending on the topic) is worked in successive stages, beginning with the simplest conceptual description of a problem at the lowest stage. Work at any stage is completed for all problems of the group before proceeding to the next stage. This ensures that the physics is cleanly separated from the algebra. For a group of problems, the algebraic analyses occur only in the last stages of the solutions. Each stage of the problem solution corresponds to a different representation (drawing, writing, or graphing) of the problem. Multiple representations of a problem in this manner is advocated by Van Heuvelen.[1]

Another unique design feature is the workbook format. Throughout, the format is that of question - student response - answer/discussion so that the student is always active. This format is consistent with the paradigm of elicit, confront, and resolve developed by McDermott at the University of Washington.[2] A page from the chapter "Introduction to Motion" is displayed in the appendix. Note that the problem under consideration appears on every page for easy reference, and the question - response dialogue is organized into numbered frames.

The workbook is self-contained, and is therefore suitable for use with any introductory physics textbook (calculus or algebra-based), or is suitable for self-study. In the fall of 1997, the chapters on vectors, kinematics, and forces were piloted in a classroom setting at South Carolina State University (SCSU). Eventually, all of introductory mechanics is to be covered by the workbook.

IV. Student Acceptance of Workbook

Table I is a summary of student attitudes about the workbook, based on a survey given after a fall 1997 general physics class had completed the chapters on vectors and motion. Although the data overall are positive, there is evidence that steps should be taken to make the workbook more acceptable. For example, the more vocal students complained that there were too many repetitions, a problem easily remedied before the workbook is used again.

More objective data on the workbook's effectiveness for the fall 1997 general physics class are summarized in Table 2. This table shows the pre- and post-test results for the "Force Concept Inventory," a standardized exam in the physics community for assessing the degree to which a student has acquired a Newtonian physical intuition.[3]

Although the sample size is small, these preliminary data are quite promising, showing that, compared to students from previous years, the workbook students have a greater comprehension of Newtonian concepts. (The 11 student sample size is smaller than the 26 student sample in Table I because many students who took the fall 1997 course did not continue in the spring 1998 course, where the post-test was given.)

V. Conclusions

Preliminary indications are that the workbook is useful in helping students to gain a conceptual understanding of physics as they learn to solve problems. This work will continue at SCSU, and the intention is to expand usage of the workbook to other sites.

VI. References

1 A. Van Heuvelen, "Overview Case Study Physics," *American Journal of Physics* **59**, 898-907 (1991).

2 L. C. McDermott, "Guest Comment: How he teach and how students learn - A mismatch?," *American Journal of Physics* **61**, 295-298 (1993).

3 D. Hestenes, M. Wells, and G. Swackhamer, "Force concept inventory," *The Physics Teacher* **30**, 141-158 (1992).

Table 1. Survey of workbook acceptability, fall 1997, 26 Students

Results of Workbook Questionnaire

Did you find that the book helped you to understand vectors and motion?
- helped a lot 30.8%
- helped some 38.5%
- helped a little 19.2%
- no help at all 11.5%

Was the question - answer format agreeable to you?
- very agreeable 23. 1 %
- somewhat agreeable 69.2%
- not agreeable 7.7%

What is your opinion of the level of detail asked in the workbook question?
- questions asked about too many details 46.2%
- questions asked about the right number of details 46.2%
- questions asked about too few details 7.7%

Would this type of book be helpful to you in understanding other physics topics ?
- would help 38.5%
- would help somewhat 50.0%
- would not help 11.5%

Table 2. "Force Concept Inventory" test of Newtonian physical intuition

	PRE-TEST	POST-TEST
Baseline Data, 1995-96 "Control", 80 students	26.1±10%	30.2±11.5
Fall 1997 11 Workbook students	23.6±8.0%	35.4±12.1%

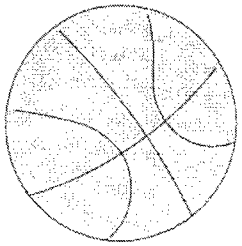

A student places a basketball on an inclined surface, then releases it from rest at the –2.0 m position at the same instant that a clock is started. The ball gains velocity at the uniform rate of 0.5 m/s per second down the plane. (a) What is the ball's velocity when the clock reads 4.0 seconds? (b) What is the ball's position at that time? (c) What distance has the ball traveled when the clock reads 4.0 s, and (d) what is the ball's average velocity over this distance?

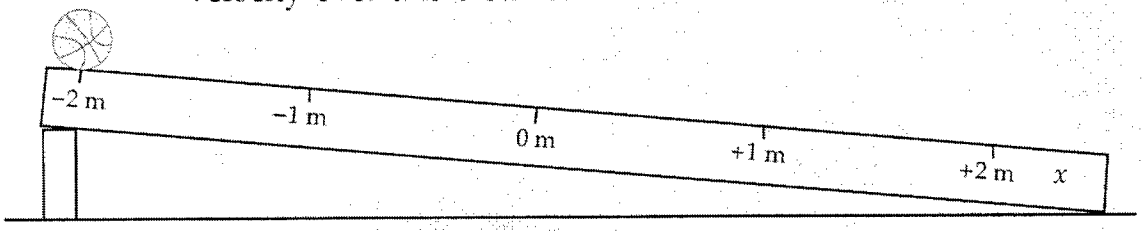

2.35

What is the meaning of the statement "gains velocity at the uniform rate of $0.5\frac{\text{m}}{\text{s}}$ per second"? Write out what you believe to be the meaning whether or not you understand this statement.

2.36

The statement means that the instantaneous velocity of the ball increases by $0.5\frac{\text{m}}{\text{s}}$ during every second. To see if this is clear to you, fill in the following table.

t	v
0	0
1.0 s	
2.0 s	
3.0 s	

Sample page from Workbookfor Introductory Mechanics Problem-Solving

Why Go To Graduate School? / Successful Admission

L. Nan Snow

NPSC, University of California, San Diego

Pursuing a Ph.D. in Physics is absolutely essential if you wish to teach at a leading research university or if you wish to direct your own research project in industry. Those individuals who choose to terminate their education at the masters degree are very likely to find themselves working as a technician.

Graduate school will probably be the most difficult challenge you have ever experienced and the most rewarding.

I would like to share with you, a few tips.

1. Apply to at least 3 - 6 universities, ten is even better.
2. Follow your research. Find out who is doing the cutting edge research in your field of interest and apply there.
3. Take your general GRE exams in the second semester of your junior year. This will allow you the opportunity to retake them if you are dissatisfied with your score. Take your subject matter GRE during your senior year.
4. Take time to write your professional goals/ research experience statement. Remember this is one of the three key items reviewers grade you on along with GPA and recommendation.
5. 5. IF your GPA is less than a 3.0, be sure and state if there are extenuating circumstances such as if you were working full time during your undergraduate program.
6. Your recommendations should come from professors who know you and your work well and from your summer work experience research supervisor. Make sure that you ask your professors if they feel that they can give you a favorable recommendation. If they can't, they will tell you and you can then go to another professor who knows your work better. Also, it is best to get recommendations from those who have a fluent command of the English language. Do not include personal recommendations.
7. Be sure to spell check your applications.

Remember, most reviewers spend fifteen to twenty minutes reviewing an application. It is therefore very important that you put together a tight clear package that shows why the reviewer should pick you for graduate support and/or admission.

Once admitted to a university, and before you register, you should do the following:

1. Visit your school.
2. Speak to your academic advisor.
3. Interview other graduate students in the department.
4. Check out the culture and climate of the campus.

Armed with this information, you will be able to make an informed choice of the university that will be best for you.

Graduate school funding is most frequently from one of three sources:

1. Fellowships
2. Teaching Assistantships (TA)
3. Research Assistantship (RA)

TA's and RA's are available at the universities where you have applied and a limited number of fellowships.

I am here representing one of the organizations that offer fellowship support.

The National Physical Science Consortium, now in it's tenth year, has provided 251 Physical Science Fellowships. As of this reporting 10 NPSC Fellows have been awarded their Ph.D. Degrees. Graduates are employed as research scientists by their sponsoring employers, as university professors, or are

doing prestigious post doctoral work.

NPSC membership now consists of 105 major Ph.D. granting universities, 15 Associate Member universities and 40 private and public employers.

NPSC Fellowship opportunities are open to US citizens who wish to pursue a Ph.D. in one of the physical sciences. Applicants must have a minimum GPA of 3.p. Over the past seven years, the average GPA of the NPSC applicant has been 3.6.

NPSC actively recruits candidates for the fellowship program from all U.S. undergraduate institutions providing a first class physical science curriculum. All applicants are screened by a select committee of science professors from member universities. This committee develops a rank-ordered list of those students they feel will be highly successful in graduate school. NPSC provides employers with this rank-ordered list along with detailed demographics and copies of the student applications.

New NPSC fellowships are awarded annually, during the third week of January. These awards are totally employer-driven and are made only by the employer member at the annual Selection Meeting.

Funding for NPSC fellows is provided by cost-sharing between the university and employer members. Universities provide full tuition and fees; the employer provides the stipend and two summers of employment doing research at the employers site. The stipend is $12,500 for years 1 - 4 and $15,000 for years 5 and 6. The total value of the NPSC fellowship to each student is $180,000 - $200,000.

Many companies and public agencies have adopted vigorous campaigns to seek out, educate and employ underrepresented students. NPSC targets qualified minority and females, encouraging them to pursue Ph.D. degrees in the physical sciences. This approach has given NPSC the opportunity to identify and recruit the most qualified students and the ability to offer the employer members the student diversity necessary to build a balanced work force.

Once selected, mentoring begins with an orientation seminar and continues throughout their program. This mentoring is provided by both the university and the employer. NPSC monitors the students' academic progress and on-the-job performance and is able to provide this information should the sponsoring employer request it.

The NPSC fellowship is the most successful program of it's kind with a retention rate of 92%. This fellowship provides up to 6 years of graduate education. The employer sponsor finds the NPSC program to be very cost-effective. NPSC does all student recruiting and screening, handles student logistics, and provides that interface with the employer and the university so important in creating smooth transitions from undergraduate to graduate studies and employment.

This is our way to assist students to stretch and realize their full potential. Remember, apply to as many financial support opportunities as you can. You can always turn down money offers, but you cant' get an award if you don't apply for it.

Good luck in graduate school.

Magnetic and Structural (EXAFS) Properties of Laser Ablated Magnetic Oxide Films

C. M. Williams

C. O. Clark

Morgan State University

V. G. Harris

Naval Research Laboratory

Abstract

The authors have examined magnetic and structural properties for a series of non stochiometric pulsed laser ablated MnZn-ferrite films, epitaxially grown on (001) MgO substrate at deposition temperatures ranging from 300°C to 800°C in an oxygen pressures of 15, 30, 60 and 90 milliTorr. The results show a number striking features: (1) large variations in the magnetization and magnetic anisotropy with oxygen pressure; (2) scaling of the magnetization with Fe^{2+} ion concentration and (3) a sensitivity of the coercive force and ferrimagnetic resonance linewidth to microstructure. The variation in magnetization is explained in terms of variations in the number of iron ions on the octahedral tetrahedral sites, as observed by EXAFS studies.

Introduction

The emerging shift in high frequency electronic device technology over the past few years has been driven by the desire to have a planar integrated electronic circuit with the non-reciprocal magnetic component integrated as well. While there has been considerable success in the integration of electronic components, such as switches, detectors and amplifiers on a single chip, the integration of magnetic components has been conspicuously absent. Magnetic components add a unique dimension to electronic elements because they exhibit non-reciprocal behavior, i.e., electromagnetic radiation does not propagate reversibly along the direction of magnetization. This non-reciprocal behavior is the basis for many high frequency electronic device applications. The most important being the isolator and circulator which permit a strong microwave signal from an oscillator to pass to the antenna and weak incoming signals from the antenna to pass to the detector without mutual interference.

The isolators and circulators in use today are hybrid, i.e., they are fabricated by epoxying a bulk ferrite hockey puck on the integrated planar electronic circuit. Hybrid isolators and circulators are bulky and impose undesirable cost-size constraints in packaging as well as compromise performance. Since modem technology is shifting towards miniaturization it is highly desirable to explore synthesis techniques that can be used to fabricate novel magnetic ferrite thin films to replace the hockey pucks. Several synthesis processes for ferrite films have been successfully demonstrated. These processes include: plasma spray, sol-gel, rf- and dc-sputtering, ferrite plating [1-6] and pulsed laser deposition [7,8]. With the exception of ferrite plating and pulsed laser deposition, many of these processes require post deposition heat treatments to obtain the desired ferrite structure and for most of these processes the magnetic and/or electrical properties fall short of the expectations required for high frequency microwave applications.

Our immediate interest is the investigation of magnetic and structural properties of non-equilibrium and non-stochiometric pulsed laser deposited single crystal ferrite films. The magnetic and electronic properties which establish the figures of merit for these structures, such as the saturation magnetization $4\bullet M_s$, the remnant magnetization $4\bullet M_r$, the coercive field H_c, the magnetic anisotropy K_1, resonance linewidth ΔH, permeability μ, and the dielectric loss tangent tan δ, depend on the chemical composition, the electronic structure of the magnetic ions, the crystal symmetry and microstructure of magnetic ferrites.

The initial focus of our research has been on the spinel ferrites structures. The spinel ferrite structure is isomorphic with classical spinel $Mg^{++}Al_2O_4$ where the trivalent aluminum is replaced with trivalent iron and magnesium is replaced by divalent metal ions such as Zn^{++}, Mn^{++}, Co^{++}, Mg^{++}, Fe^{++} and Ni^{++}. Spinel ferrites can have either a 'normal' structure, in which the divalent ions are on tetrahedral sites, or an 'inverse' structure in which the divalent ions are on octahedral sites. The distribution of cations over tetrahedral and octahedral sites plays a significant role in determining the magnetic properties of spinel ferrites. The size and the valency of the cations and the crystal field of the anions significantly influence the distribution of cations over tetrahedral and octahedral sites in a spinel.

Magnetic properties such as the magnetization and magnetic anisotropy are controlled by intrinsic interactions such as crystal field and exchange interactions of the metallic ions on the two interacting sublattice. For example, the magnetization of a spinel structure is determined by the net exchange between the oppositely polarized magnetic ion on the octahedral and tetrahedral sites. In general, these interactions are controlled and detemined through equilibrium processes which appear to limit the possibility of synthesizing new materials with improved properties. If new methods of materials synthesis and modification are to be achieved to meet the new demands of modern technology for relevant materials, new directions must be defined which permit the control of the basic intrinsic metallic ion interactions within the crystal structure. The investigation of the intrinsic properties of ferrite films created through non equilibrium synthesis processes will provide new directions for developing improved ferrite materials for high frequency and other device applications.

Earlier results on pulsed laser deposited ferrite films suggest that the cation distribution is a strong function of synthesis temperature and reaction gas pressure. At high temperatures the distribution will tend to be more random. Rapid quenching tends to freeze in these random distributions, thus, leading to a non equilibrium structure. Laser ablation is well suited for the synthesis of thin film spinel ferrites with non equilibrium cation distribution. The extent to which the ions deviate from their equilibrium positions depends on a number of factors which include: 1) the type of reaction gas; 2) the reaction gas pressure; and 3) the substrate temperature during in situ growth.

Results and Discussion

In continuing our investigation of the non equilibrium magnetic properties of spinel ferrite magnetic oxide films, we have examined the magnetic and structural properties for a series of MnZn-ferrite films using vibrating sample magnetometry, to determine the magnetization, $4\bullet M_s$, and coercivity H_c; x-ray fluorescence techniques to determine the cation concentrations; scanning electron microscopy (SEM), to determine the microstructure; X-ray diffraction to determine the structure; extended x-ray absorption fine structure measurements (EXAFS), to determine site occupation of the Fe and Mn ions on the octahedral and tetrahedral sites and ferrimagnetic resonance measurements to determine the resonance linewidth, ΔH.

The study of the magnetic and structural properties of magnetic oxide spinels shows that the magnetic properties of these materials can be significantly enhanced or modified by varying the deposition parameters during pulsed laser ablation. The magnetization $4\bullet M_s$, the coercive force H_c, resonance linewidth ΔH, and the EXAFS data for a series of MnZn-ferrite films pulsed laser deposited in oxygen pressures of 15, 30, 60

and 90 milliTorr at substrate temperatures ranging from 300°C and 900°C are shown in Figures 1 through 8.

Figure 1. shows $4 \bullet M_s$ for MnZn-ferrite can range from 2,000 gauss to 11,000 gauss depending on the oxygen pressure and substrate temperature. The magnetization ranges between 2,000 and 4,000 Gauss for films deposited in 15 and 30 milliTorr oxygen pressure for all deposition temperatures. At 60 milliTorr the magnetization shows a peak with values ranging between 3,900 and 7,000 Gauss for all temperatures except the film deposited at 300°C, which continues to increase to a value of 11,000 Gauss at 90 milliTorr oxygen pressure. This behavior is not characteristic of the bulk equilibrium ferrite structure. The $4 \bullet M_s$ value for single crystalline bulk $Mn_{0.5}Zn_{0.36}Fe_{2.10}O_4$ is about 3,900 gauss.

The magnetization for the spinel structure is determined by the net exchange interaction between the oppositely polarized magnetic ion on the octahedral B-site and A-tetrahedral site, namely the Mn and Fe cations. However, the cation distribution in $Mn_xZn_{1-x}Fe_{2.}O_4$ is not unique. $ZnFe_{2.}O_4$ is a normal ferrite with the divalent ion occupying the A-sites; on the other hand, $MnFe_2O_4$ is mostly normal but about 20% inverted [9, 10] Thus, $Mn_xZn_{1-x}Fe_{2.}O_4$ is a mixed ferrite with the site preference of the Mn ions depending on the Zn Concentration [11]. In order to understand the origin of the magnetization results the cation distribution must be determined.

In order to determine the cation distribution, Fe and Mn EXAFS studies were done on the four films deposited at 300°C in oxygen pressures of 15, 30, 60 and 90 milliTorr. Figures 2 and 3 show the results of Fe and Mn EXAFS studies, respectively. In both studies the EXAFS are compared with a powder MnZn-feffite standard. The peaks of interest are those with radial coordinates between 2.1 and 3.5 Å. The octahedral B-site is relresented by the peak at 2.5 Å and the tetrahedral A-site is represented by the peak 3.1 Å. Fe EXAFS (Figure 2) for the MnZn-ferrite standard powder sample show the Fe cations occupying both the A- and B-sites, with a somewhat smaller occupation of the A-site, indicated by unresolved shoulder at 3.1 Å. Analyses of the thin film Fe EXAFS show Fe has a strong B-site preference for the film deposited in 15 milliTorr oxygen pressure, consistent with that of the standard or equilibrium structure, with a split unresolved asymmetric peak near 3 Å, that results from atomic disorder intrinsic to the structure. With increasing oxygen pressure the Fe site preference changes from the B-site to the A-site, with the 30 milliTorr film showing a relative preference for both sites; and the 60 and 90 milliTorr films showing a strong preference for the A-site. Mn EXAFS for the MnZn-ferrite standard show that Mn has a preference for both the A- and B-sites with a stronger preference for the B-site. Analyses of the thin film Mn EXAFS for the 15 milliTorr film show that Mn has a preference for both the A- and B-sites with a stronger preference for the B-site, similar to that observed for the standard MnZn-ferrite powder sample. However, films deposited at 30, 60, and 90 milliTorr the Mn cations show a preference for the B-site with very little preference for the A-site.

The EXAFS films studies show that 15 milliTorr sample reflects the standard equilibrium $Mn_xZn_{1-x}Fe_{2.}O_4$ structure; however, the preference of the Fe cations for the A-site and the preferential filling of the B-site with Mn cations for films deposited at 30, 60, and 90 rnilliTorr does not reflect that of the standard equilibrium structure.

The increased preference for filling the A-sites by the divalent Fe ions and the preferential filling of the B-sites by the divalent Mn ions represents a significant imbalance in moment between the two sublattices. Although we have not as yet quantified the EXAFS data or examined the EXAFS for the remaining films, we believe the moment imbalance between the Mn and Fe moments between the sublattices can account for the observed magnetization behavior, particularly if the Mn ions on the B-site are coupled or ordered antiferromagnetically [12]. If this is indeed the case then the magnetization should scale with the divalent Fe ion concentration on the A-site. The magnetization, plotted as a function of the divalent Fe ion concentration in Figure 4 shows that the magnetization does indeed scale with Fe^{2+} ion concentration.

The temperature dependence of the coercivity H_c, and ferrimagnetic resonance resonance

ΔH, have been examined. The results shown in Figures 5 and 6 show both H_c and ΔH decrease monotonically with increase in substrate temperature during deposition.

The changes in H_c and ΔH are attributed mostly changes in the microstructure. At low temperatures electron micrographs of the cross section show large number of low angle grain boundaries (Figures 7 and 8). We believe that grain boundaries and associated dislocations act as pinning sites for domain walls. The pinned domain walls, in turn, contribute to the large H_c we observe at low substrate temperatures (300°C). As the temperature is increased, we believe the number of grain boundaries and dislocation are significantly reduced and a lower Hc is observed.

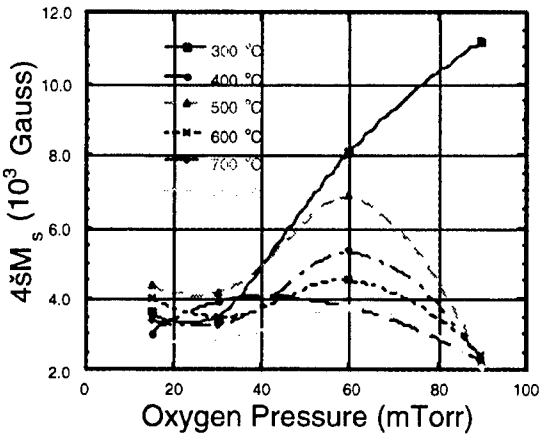

Figure 1. 4•M_s versus O_2 pressures for single crystalline MnZn- ferrite films deposited at substrate temperatures between 300°C and 900°C.

References

1 M. Abe, Y. Tamaura, Y. Gotch, N. Kitamuri, and M. Gomi, J. Appl. Phys. **61**, 3211 (1987).

2 M. Abe, Y. Tamaura, Y. Gotch, N. Kitamuri, and M. Gomi, IEEE Trans. Mag. Mag-**23**, 3736).

3 T. Itoh, M. Abe, and Y. Tamaura, J. Mag. Soc. Jpn. **13**, Suppl. S 1 859 (1989).

4 S.H. Talisa, K.C. Yoo, M. Abe, and Y. Tamaura, J. App. Phys. **64**, 5819 (1988).

5 Q. Zhang, T. Itoh, M. Abe, and Y. Tamaura, J. Appl. Phys. **73**, 6284 (1993).

6 C. M. Williams, M. Abe, T. Itoh, and P. Lubitz, IEEE Trans. Mag. **30**, 4896 (1994).

7 S. B. Ogale, S. M. Kanetkar, S. M. Chaudhari, V. P. Godbole, V. N. Koinkar, Shushama Joshi, Rasmi Nawathey, R. D. Vispute, and A. R. Moghe, Ferroelectrics, **102**, 85 (1990).

8 C. M. Williams, D. B. Chrisey, P. Lubitz, K. S. Grabowski, and C. M. Cottel, J. Appl. Phys. **75**, 1676 (1994).

9 J. M. Hastings and L. M. Corliss, Phys. Rev. **104** 328 (1956).

10 A. H. Morrish and P. E. Clark, Phys. Rev. B, **11**, 278 (1975).

11 M. A. Amer, Phys. Stat. Sol., **A151**, 205 (1995).

12 E. W. Gorter, J. Appl. Phys, **34**, 1253 (1963).

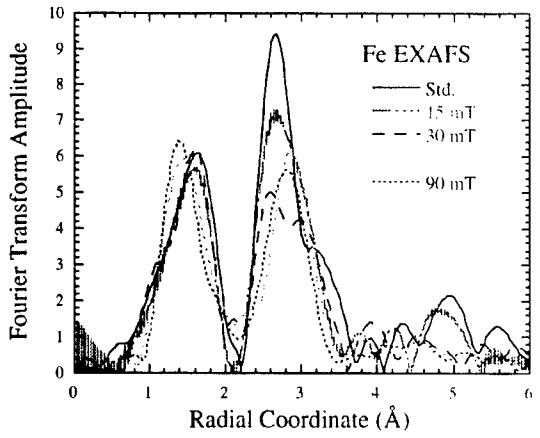

Figure 2. Fourier transform of Fe EXAFS-amplitude for single crystalline MnZn-ferrite films deposied at 300°C for O_2 pressures between 15 and 90 milliTorr.

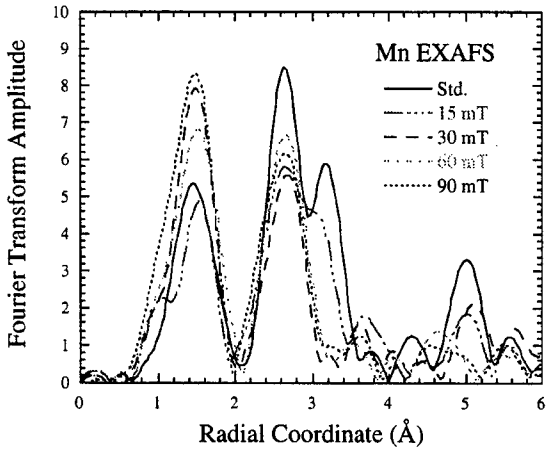

Figure 3. Fourier transform of Mn EXAFS-amplitude for single crystalline MnZn-ferrite fims deposited at 300°C for O_2 pressures between 15 and 90 milliTorr.

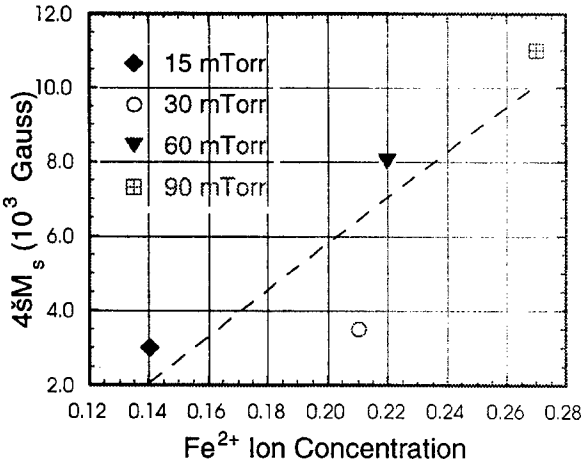

Figure 4. $4 \bullet M_s$ versus Fe^{2+} ion concentrations for single crystalline MnZn- ferrite films deposited at 300°C for O_2 pressures between 15 and 90 milliTorr.

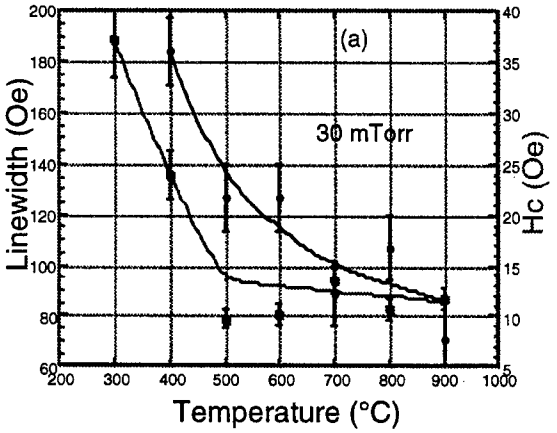

Figure 5. H_c and ferrimagnetic linewidth versus substrate temperature for films deposited in 30 milliTorr oxygen pressure.

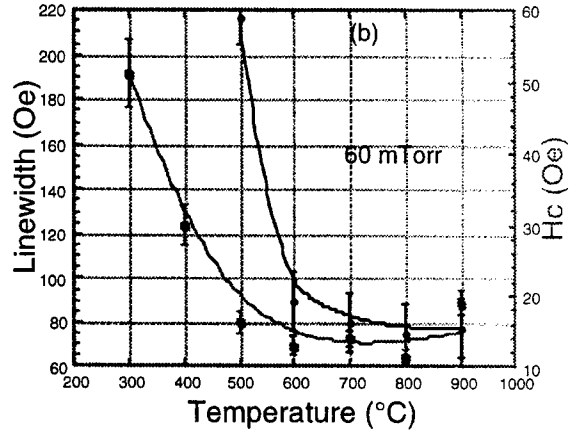

Figure 6. H_c and ferrimagnetic linewidth versus substrate temperature for films deposited in 60 milliTorr oxygen pressure.

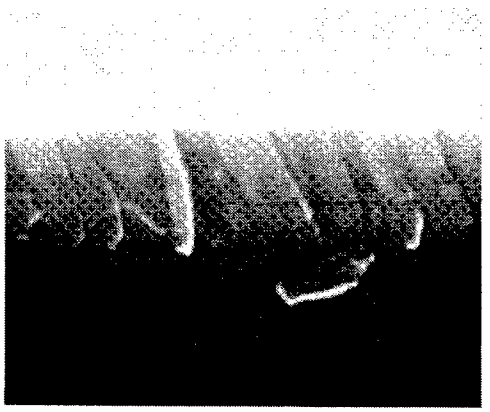

Figure 7. SEM cross section for film deposited at 300°C. Film thickness is 0.5 μm.

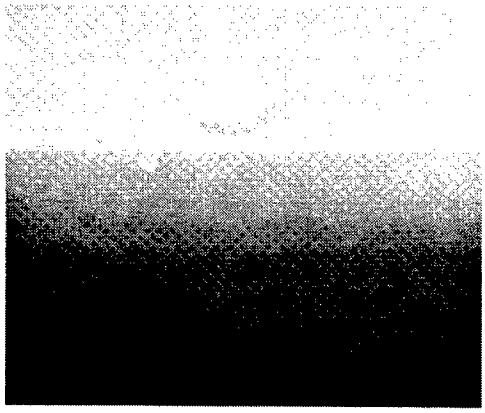

Figure 8. SEM cross section for film deposited at 800°C. Film thickness is 0.5 μm.

Multivariable Optimization Approach for the Construction of Many-Body Potential

Yonas Abraham
Mike Nomura
Xiang- Yang Liu
Xiao-Qian Wang

Clark Atlanta University

Abstract

We have developed an effective multivariable optimization approach for the construction of "pair-functional" many-body interatomic potentials. The "pair-functional" potential is the common choice for large-scale molecular dynamics simulations for closely-packed metal systems. The approach is based on the downhill Simplex method and the constructed potential has shown much improvement for both surface and bulk properties. Herringbone surface reconstruction of Au(111) has been studied using the new potential of gold and the results will be discussed.

Effect of Signal to Clutter Ratio (SCR) on Automatic Target Recognition (ATR)

Edward Asika
Lance Kaplan
Romain Murenzi

Clark Atlanta University

Abstract

The characterization of clutter in images is very useful in the application of a automatic target recognition (ATR) algorithms. Many ATR algorithms can be divided into three processing stages. The three stages consist of a focus of attention (FOA) algorithm (or first level detection) to find hot spots in the image, a second level detection to remove false alarms due to clutter and a final recognition stage to identify and classify the targets that passed the first two stages.

In this work, we focus on the recognition stage by investigating a template matching technique at different signal to clutter ratios (SCR). The images in use are synthetic aperture radar (SAR) images obtained from the MS TAR (public) data. The images are segmented and the segmented images are used with the original image to obtain new target chips at different SCR. Additionally, new templates will be formed at different SCR and the template matching will be investigated.

Currently, we have results of target classification at different SCR values in both the linear and decibel scales of the images and we will be using the Continuous Wavelet Transform (CWT) to minimize clutter.

Resistive Joining Process in a High Temperature Superconducting System

Ian Dean Bachus

University of California, Berkeley

Abstract

Making a 5T insert coil for a 25T NMR magnet requires approximately 10 km of conductor. It impossible to make a single piece of conductor this long, so it is produced in sections. In order to optimize performance, it was decided to make a superconducting insert coil. The sections of this coil would consist of double pancakes: coils of heat treated, insulated, high temperature superconducting (HTS) tape which are impregnated with epoxy. The type of HTS tape used in these pancakes was a silver sheathed, nineteen filament type of HTS tape called OAg-19. A stack of these coils when connected would be the equivalent of a solenoid made of HTS tape. A problem arises, however, in connecting them: how to link these double pancakes without introducing resistance? The pancakes have sections of HTS tape exposed at the rims to allow joining of one pancake to another. Joints would have to be placed across two adjacent pancakes at these points. Ideally, these joints would be superconductive in the 4.2K, high magnetic field environment in which the coils were designed to work, but the best that could be hoped for was to minimize resistance.

To approximate the joints to be placed on the pancakes, strips of heat treated tape were used to fabricate equivalent joints by cutting the strips, overlaying one piece over the other in each, and fusing them together with various alloys of lead and tin. Each joint was then characterized in a liquid helium bath. (temperature: 4.2K) by placing a potential difference across it. It was not possible with the equipment available to introduce a magnetic field to completely mimic the operating environment of the pancakes. The data was used to find the critical current of each joint, the hope being to maximize this current through the choice of an alloy. In this presentation, I will address issues concerning the constraints on fabrication of these joints as well as the respective performances of the alloys available to test.

Strange Physics at Jefferson Lab

Keith Baker

Hampton University

Abstract

Most of the matter in our world is believed to be made up of hadrons containing up and down quarks (and gluons). It is possible to create matter which has strangeness degrees of freedom using modem accelerators. Experiments were completed recently at Jefferson Lab which explored the production of particles composed of strange (constituent) quarks. Some initial results of these experiments will be presented. Plans for future work will be highlighted.

Excitation Energies and Oscillator Strength for *NI*

Christopher Beatty
S. S. Tayal
Clark Atlanta University

Abstract

We have calculated the excitation energies and oscillator strengths for dipole allowed transitions between the terms $^{4,2}D$, $^{4,2}D^0$, $^{4,2}F$, $^{4,2}P$, $^{4,2}P^0$, $^{4,2}S^0$ of neutral nitrogen in the *L-S* coupling scheme. We used flexible radial functions and included a large number of configurations in the configuration expansion calculation. The configuration interaction calculations were performed with the *CIV3* code of Hibbert (1975)[1]. Our calculated energies and oscillator strengths are compared to some of the more reliable experimental and theoretical data.

An Electron Paramagnetic Resonance Analysis of the Wildtype and Mutant Species of the Cobalamin Dependent Methionine Synthase Enzyme

Thomas Butler
Deanne Taylor
Namdoo Moon
Joseph T. Jarrett
Rowena G. Matthews
William R. Dunham

University of Michigan

Abstract

The enzyme Methionine Synthase, which is a cobalamin (Vitamin B) containing methyl transferase that catalyzes the transfer of one-carbon units from methyltetrahydrofolate to homocysteine to generate methionine has been investigated using Electron Paramagnetic Resonance (EPR) Spectroscopy. Per enzyme molecule, Methionine Synthase contains one cobalt ion which is coordinated to four planar nitrogen atoms of a corrin ring with a fifth bond to a histidine nitrogen below and a sixth to a substrate methyl group above the plane EPR data from the Co (11) alamin form of the native enzyme and several mutants were collected at 9 GHZ. These data were analyzed using algorithms developed in the laboratory. These algorithms must take into account the linewidth variation caused by distribution in the parameter g (g-strain) . Efforts to fit the data determined that the algorithms had to additionally allow for contributions to the linewidth due to distribution in the parameter A (a-strain). For EPR spectra with large magnetic hyperfine interactions, it is found that g-strain contributes a linewidth that increases from left-to-right and a-strain contributes a linewidth that increases form the middle to both extremes of a hyperfine pattern. Variation in the a-strain and g-strain parameters throughout the mutant and native species is postulated to arise from concerted displacement of the cobalt ion and the fifth ligand.

Slingshot Effects

Abdoul Dan-Azoumi

Florida A & M University

Abstract

When scientist send spacecrafts (like the Voyager) in orbits through distant domains of the solar system, they use the effect of the gravitational field of a planet on the spacecraft to increase or decrease the velocity of the spacecraft.

This is referred to as "gravity assist". I will present a simple exposition of this effect.

The Physical Response of Meniscal Tissue to Short Pulsed Laser Irradiation

Marta L. Dark
L. T. Perelman
I. Itzkan
J. L. Schaffer
M. S. Feld

Massachusetts Institute of Technology

Abstract

Over the past two decades, the laser has become a useful tool in many medical specialties, excluding orthopedics. Attempts at using lasers, such as the CO_2 laser, in orthopedic surgery were not successful[1]. It appears that the laser has no advantage over current orthopedic tools used for tissue cutting. However, laser light may prove useful in diagnosing mechanical properties of orthopedic tissues.

Following irradiation by a 10 ns laser pulse (Nd:YAG, λ = 355 nm), tissue undergoes thermoelastic expansion in response to the stress distribution created by the laser light[2]. If the laser-induced stresses exceed the material's strength, then ablation occurs—the material ruptures. Below the ablation threshold, the material will remain in an expanded state until thermal relaxation occurs (τ_{th} ~ 100 ms). I am using numerical methods to solve the thermoelastic wave equation in three dimensions of a two component substance, water and collagen. In addition to the linear thermoelastic expansion of meniscus, the excess expansion due to the formation of cavitation bubbles within the meniscal fluid will be considered. Cavitation occurs when tensile stresses rupture a fluid[3] and may be an indication of weak regions in the meniscus.

The laser-induced response of a gelatin phantom will be measured with a Michelson interferometer and compared to the numerical calculations. Once the behavior of gelatin is well understood, I will use human knee meniscus as an experimental sample. The numerical model depends on physical properties such as speed of sound, Poisson's ratio (σ), thermal expansion coefficient (β), and tensile strength. The model will be compared with experimental results, giving values for the physical properties of the tissue. This research should lead to greater understanding of the interaction of short pulsed laser irradiation with soft musculoskeletal tissues.

(1) T. L. Whipple, J. J. Marotta, T. C. May, R. B. Caspari, and J. F. Meyers. 1987 *Lasers Surg. Med.* **7** 184-188

(2) I. Itzkan, D. Albagli, M. L. Dark, L. T. Perelman, C. von Rosenberg, and M. S. Feld. 1995 *PNAS* **92** 1960-1964

(3) G. Paltauf, E. Reichel, and H. Schmidt-Kloiber 1992 *SPIE Laser-Tissue Interaction III* **1646** 343-352

Preliminary Results of the Electron Paramagnetic Resonance of Fe^{3+} and Mn^{4+} in $LiNbO_3$ Single Crystal

A. M. Darwish
J. Morris
A. Williams

Alabama A & M University

Abstract

We have recorded the x-band electron paramagnetic Resonance (EPR) of the $LiNbO_3$: Mn^{4+}:Fe^{3+} crystals. Two samples were irradiated with γ-rays. In addition to the EPR lines of Fe^{3+} and Mn^{4+} a new EPR line was observed. This was due to a free radical which resulted from γ-rays irradiation. This new EPR signal disappeared after exposure to Ar^{+} laser. A preliminary analysis of the Electron Paramagnetic Resonance Spectrum for Mn^{4+} and Fe^{3+} will be presented.

Numerical Cosmology and the Study of Quasar Absorption Lines

Romeel Dave'

University of California, Santa Cruz

Abstract

I introduce the subject of numerical cosmology, and present its application to the recently-blossoming field of quasar absorption lines. Combining high-resolution simulations done on parallel supercomputers with the latest observations from Keck and Hubble Space Telescopes provides a remarkable new picture for the evolution of the intergalactic medium over ~90\% of the age of the Universe. This has significant implications for primeval galaxy formation, the evolution of large-scale structure, and the underlying cosmology of our Universe.

An Investigation of the Relationship between Structure and Electron Transport in $La_{1-x}(Ca_{1-y}, Sr_y)_xMnO_3$

LaShondria B. Dixon

Southern University and A & M College

Abstract

Pure $LaMnO_3$ is an antiferromagnetic insulator with a familiar perovskite structure. When a divalent alkaline dopant A such as Ca, Sr, or Ba is introduced, the resulting alloy $La_{1-x}A_xMnO_3$ exists in a ferromagnetic metallic state at low temperatures and a paramagnetic semiconducting state at higher temperatures for a doping range centered at x = 0.33. This investigation is a study of $La_{1-x}(Ca_{1-y}, Sr_y)_xMnO_3$, where A = Ca and Sr, $x < 1$, and $y < 1$. X-ray diffraction, electron transport, and magnetic measurement techniques will be used to collect the data. The primary objective is to understand the colossal magnetoresistance (CMR) properties of this material by studying the effects of structure and composition on the magnetic behaviors and electron transport properties. The research involves structural characterization using x-ray diffraction techniques, magnetic characterization using a commercial Superconducting Quantum Interference Device (SQUID) magnetometer, and resistance calculations using four-probe current-voltage (I-V) measurements.

Apparent Clustering of Droplet Microemulsions in the Presence of Electrical Fields

M. E. Edwards
Spelman College[1]

X.-L. Wu
University of Pittsburgh [2]

J. S. Wu
Fayetteville State University

J. S. Huang
Exxon Research and Engineering Co.

H. Kelly
Universite Bordeaux

Abstract

In a recent paper[3], we presented new results of the Kerr effect in a model three-component microemulsion using an improved experimental setup. Our new measurements indicate that the Kerr coefficient, K, scales as ϕ^2 throughout the entire range of concentrations, $0\% < \phi < 30\%$. This scaling behavior suggests that the Kerr effect in the microemulsion is intrinsically a many-body problem rather that a singlebody problem as previously suggested. It remains as intriguing possibility that the microemulsion forms clusters comprising many droplets even in dilute concentration. Further results of this research, considering the precise cross-over points for microemulsions of varying concentrations and aliphatic oils, will be discussed in this presentation.

1 Work partially supported by NIH under grant No. GM08206 and

2 Work partially supported by ACS under Grant No. PRF 30083-AC9, and NASA under Grant No. NAS3-2789.

3 Edwards, M. E., et. al., Physical Review E, **57**, No. 1, 797 (1998).

External Feedback Effects on Powder Laser Threshold

S. U. Egarievwe
Alabama A&M University

M. A. Nogonov
N. E. Noginova
Norfolk State University

A. Anderson
J. C. Wang
Alabama A&M University

H. J. Caulfield
Fisk University

Paitz
Institut für Kristallzüchtung

Abstract

The laser action of optically pumped powders of laser crystals was first observed and reported in 1986 by Markushev *et al*[1]. after the light generation in scattering media was theoretically predicted in 1968 by Letokhov[2]. These *random lasers* differ from conventional lasers mainly because they comprise an optical inhomogeneous active medium, and the radiation is generated in the intersteller medium with feedback (non-resonant) realized by scattering particles. The effects of external feedback in this group of lasers has been of great interest recently. [3,4]

In this paper, we report the external feedback effects on the laser pumping threshold in micro-particle powder laser made from $Nd_{0.5}La_{0.5}Al_3(BO_3)_4$ ceramic synthesized by a solid-state reaction of mixed and pressed starting components. External reflections were obtained by mirror and gold cavity. Exciting samples with 532-nm Q-switched (about 15-ns) Nd:YAG laser, and using a laser power meter, a 0.3 μm monochromator, and a streak camera, we measured the input-output characteristics of the samples. We found that external feedback provided by reflections from mirror and gold walls significantly reduces the pumping threshold of the powder laser.

1. V. M. Markushev, V. F. Zolin, Ch. M. Briskina, 1986 *Sov. J. Quantum Electron.* **16** 281
2. V. S. Letokhov, 1968 *Sov. Phys. JETP* **26** 835
3. R. M. Balachandran and N. M. Lawandy, 1995 *Optics Letters* **20** 1271
4. P. C. de Oliverira, J. A. McGreevy, and N. M. Lawandy, 1997 *Optics Letters* **22** 897

Singular Behavior in Electron-Atom Scattering at Small Momentum Transfer*

Z. Felfli
D. Bessis+
A Z. Msezane

Clark Atlanta University

Abstract

At fixed electron impact energy, E, contrary to common belief that the electron-atom Differential Cross Section (DCS) is an analytic function of the momentum transfer squared k^2 around $k^2 = 0$, we demonstrate the presence of **non-analytical** terms of the form $\sqrt{k^2}$ coming from the second-order terms. This result, combined with the Regge pole representation[1], without the imaginary part, yields a new generalized Lassettre expansion for extracting the optical oscillator strengths through extrapolation to $k^2 = 0$ and the normalization of measured relative DCSs.

We demonstrate the dramatic improvement over existing methods introduced by the new analysis by using the electron excitation H 1s-2p for which the OOS is known exactly and reliable theoretical calculations[2] exist. With only three energy parameters, our formula yields the OOS within 2.2% of the exact value even at the low energy of 35eV. When all the 75 data (15 angles, 0-90° at five energies) are used simultaneously, our global analysis extracts the OOS within 1%, again with only three parameters (including the unknown OOS). The exceptional results confirm the physical content of the Regge pole[1] approach which should become the new formalism for medium to high energy electron-atom scattering.

When used with the forward scattering function[3], in an appropriate representation, the approach can be utilized to obtain absolute DCSs from the relative measurements[4].

+ Also at: Service de Physique Theorique CEN-Saclay, France

* Supported by NSF, DoE Division of Chemical Sciences, Office of Basic Energy Sciences, Office of Energy Research and AFOSR.

[1] A. Haffad *et. al.*, Phys. Rev. Lett. **76**, 2456 (1996)

[2] I. Bray *et. al.*, Phys. Rev. A **44**, 5586 (1991)

[3] N. Avdonina, Z. Felfli and A. Z. Msezane, J. Phys. B**30**, 2591 (1997)

[4] Z. Felfli and A. Z. Msezane, J. Phys. B**31**, Lxxx (1998)

Searching for Period Changes in the Eclipsing Contact Binary System 44i Boo

J. Brodney Fitzgerald
Paul W Donnelly
Ryan C. Culler
Anthony Williams

Western Kentucky University

Abstract

We observe 44i Boo around times of preliminary minimum for 5 nights, collecting data on 2 of those nights during July and August 1997. Performing differential photometry using comparison stars within the field of the CCD, we constructed partial light curves for 44i Boo and measured the times of primary minima. With the acquired data, we calculated an updated ephemeris. We determined any period change by comparing our observed times of primary minima with those of published literature. We then saw how this change in period relates to the various theories that have been proposed to explain the internal physical structure of contact binary systems. The funding for this project is made possible by NASA grant NCCS-228.

Searching for Extra-Solar Planets by Examining Eclipsing Binaries

Philip E. George
Charles McGruder, III

Western Kentucky University

Abstract

Our research is pertaining to searching for Extra Solar Planets by the use of lunar occultation. We are currently waiting on some preliminary calculations concerning the feasibility of the project. If the calculations prove correct, then we will begin to construct a photometer head, so that we may then do occultations with the on-site telescope. We gratefully acknowledge the support of NASA grant NCC5-228.

Distribution Theory and its Application to Solving Linear Differential Equations

Lynford Goddard

Stanford University

Abstract

In this paper, we will analyze the spaces of distributions and test functions and show that they are sequentially complete. We will discuss the Dirac Delta distribution and give criteria for regular distributions to converge to it. Further, we will prove that every distribution can be approximated by a regular distribution and that locally every distribution is generated by a finite order derivative of a continuous function. We will introduce the Green's function and Duhamel's principle and use them to solve inhomogeneous differential equations. Finally, we will present the Fourier and Laplace transformations, prove their inversion theorems and discuss their application to solving ordinary and partial differential equations.

Moment-Wavelet Quantization: A First Principles Analysis of Quantum Mechanics through Continuous Wavelet Transform Theory

Carlos R. Handy
Romain Murenzi

Clark Atlanta University

Abstract

The space of polynomials is invariant under affine maps. This suggests that a moment based analysis can facilitate a first principles incorporation of continuous wavelet transform (CWT) theory into quantum mechanics. We show that this is indeed the case for a large class of Hamiltonians and mother wavelet functions. We establish the equivalency between moment quantization (MQ) and CWT. By so doing, we clearly demonstrate the inherent multiscale structure of MQ analysis with regards to determining physical energies and corresponding wavefunctions.

Atoms and Molecules in Intense Laser Fields: What Can We Learn?

Wendell T. Hill, III

University of Maryland

Abstract

The study of atoms and molecules in intense laser fields is now about twenty years old yet it continues to command the attention of atomic theorists and experimentalists. The reasons can be traced to new and peculiar physics as well as new technologies associated with "dressing" the quantum states of the system by the radiation field. Unlike exposing atoms and molecules to weak or moderately intense laser fields, at high intensities the effective electric field strength can exceed that experienced by an electron in the first Bohr orbit in a hydrogen atom, more than 5 GV/cm. At this level, the laser field is no longer a small perturbation compared with the internal fields holding the atom together - perturbations theory is no longer valid. Our experimental tool for understanding the new physics associated with this nonperturbative regime has been ionization processes. More specifically, focus has been on multiphoton ionization often involving several different stages of ionization. For atoms, nearly all the energy imparted to the system by the laser field goes into the ejected electrons. The energy and angular distributions of these electrons are vastly different from their lower intensity counter parts and nonintuitive, at first glance. For molecules, ionization is also important but the energy is now shared between the nuclear and electronic motion. Entanglement of ionization with dissociation (i.e., the breakdown of the Born-Oppenheimer approximation) plays a major role in the decay dynamics of molecules and has inhibited a complete understanding of ionization with more than one positive charge center. In this talk we will review some of the most salient features of intense field effects, look at some new technologies that could result and discuss future prospects for the field. A precise measure of the amplitude and slope of this correlation is a sensitive test of models of large scale structure formation in the early universe.

Implementing a New Parameterization for Turbulent Vertical Mixing in the Ocean

Armando Howard
Vittorio Canuto
Ye Cheng
Mikhail Dubovikov

Goddard Institute for Space Studies
National Aeronautics and Space Administration

Abstract

The modeling of the Earth's climate has become a task of increasing scientific and practical interest. Because the oceans play a critical role in regulating the Earth's climate, the accurate modeling of the latter requires an adequate representation of the physical processes occurring in the former. Contemporary ocean models employ equations which describe the largescale flows of water, heat and salt, evolving physical variables in terms of their values on the relatively large scales which it is feasible to resolve and terms introduced to describe small-scale processes such as turbulent mixing which are beneath the resolution of numerical simulations' grids. Although these models reproduce many features of the actual Ocean, they also have deficiencies. For example they seriously underestimate the Ocean's transport of heat from the equator to the poles if a value for the vertical heat diffusivity indicated by experiment is used. Currently most Ocean General Circulation Models (OGCM) use highly simplified representations of turbulence. Large, et. al., have recently proposed (JGR 32, 1994) and implemented in an OGCM (JPO 27, 1997) a partly phenomenological model which has made significant improvements. The goal of our research on ocean turbulence at NASA-GISS is to implement better theoretical models of the fundamental physical processes of turbulence in the ocean and thus improve the subgridscale modeling there so as to provide a more reliable base for the modeling of the oceans and hence the climate under both actual and hypothetical conditions.

We have a hierarchy of turbulence models to represent heat and tracer transports in the ocean more realistically. We tested first the simplest of these, a fully algebraic (Level 2) model, in a 1D case, a model of the Ocean's Mixed-Layer at a given spot on the globe. Martin (JGR 90, 1985) had tested previous turbulence parameterizations in the Mixed-Layer and found that a state of the art turbulence model, the Mellor-Yamada closure (Levels 2 and 2 1/2), underpredicted the Mixed-Layer Depth because it makes turbulence cease at

too weak a stratification, a Richardson number of 0.2. Our model permits turbulence up to higher Ri and it also uses a lengthscale in much better agreement with LES data than Mellor-Yamada's. This enabled it to produce Mixed-Layer Depths greater than those of Mellor-Yamada. We then proceeded to a more sophisticated model which included a differential equation to evolve the turbulent kinetic energy (Level 2 1/2) and performed a 1D simulation of the November and Papa Ocean Weather Stations using it. We reproduced observed results for the Sea Surface Temperature and Mixed-Layer Depth throughout an annual cycle. After improving the physics of our model to include a better formulation of the third-order turbulence moments and a representation of the effects of surface waves, we re-ran the 1D simulations to obtain temperature profiles for the same Papa case reported by Large, et. al., (1994) and we did comparably as well with our turbulence closure model as they had with their more phenomenological one. We also managed to match the data of Wang, et. al., Large Eddy Simulation (JGR 1996) and ocean turbulence measurements by Moum (JPO 22, 1992). In addition to our above work with a model in the spirit of Mellor-Yamada, Dubovikov and Canuto have recently developed a Stochastic Model, derived from the turbulence spectrum, in which the model constants are no longer free parameters but can be calculated a priori. We have implemented this model also in a 1D simulation and tested it successfully against the Papa. LES and ocean turbulence measurement results. We are currently implementing both models in an OGCM.

Essence of M-Theory

Clifford V. Johnson
University of Kentucky

Abstract

Recently, understanding of the nature of the leading candidates for a complete theory of Nature, the "Superstring Theories", has undergone dramatic advances. There have been discoveries of many new remarkable properties which illustrate the fact that string theory is not a theory of strings at all, but part of something called 'M-Theory'. This is what is referred to as the "Second Superstring Revolution". The discoveries have led to a complete reorganization of the expectations for a "Theory of Everything". Research continues into understanding the nature of M-theory. There are tantalizing hints that the end of the story, of which we so far know little, will tell us about many fundamental issues, such as how and why Nature combines both Spacetime and Quantum Mechanics to give rise to the world around us.

Design Strategies for Two Simultaneously Modelocked Laser Oscillators

Darryl K. Jones
Richard L. Fork

University of Alabama

Abstract

Modelocking of each of two lasers, combined with synchronization of the pulse envelopes and phaselocking of the optical carrier fields of the two lasers yields, in effect, a simple modelocked two laser array. We report simulation work directed toward realizing this, and larger, arrays of simultaneously modelocked laser oscillators with a device capable of delaying short optical pulses, with low distortion and low loss.

The Dynamics of Controlled Optical Delay Lines

Darryl K. Jones
Richard L. Fork
University of Alabama

Abstract

Capability for large controllable group velocity delays for short optical pulses, with low distortion and low loss for the pulse, is essential to many optical processing strategies. We examine recent experimental work and calculations for a one dimensional photonic bandgap device, and propose strategy to control the relative optical carrier fields and envelopes between pulses generated from two physically distinct modelocked laser oscillators, as a mechanism to construct reconfigurable, beam steerable, time resolved, coherent wavefronts (i.e., optical phased arrays).

Nonlinear Optical Properties of Silicon Nanoclusters Made By Laser Ablation

Elaine N. Lalanne
Hernando Garcia
A. M. Johnson
S. Vijayalakshmi
H. Grebel

New Jersey Institute of Technology

Abstract

Silicon nanoclusters have been shown to photoluminesce in the visible. It is not well understood why this occurs. Using a sensitive single beam technique, Z-scan, we are able to measure both the nonlinear refractive index and nonlinear absorption coefficients. In these experiments 50 ps pulses at a wavelength of 532 nm from a frequency doubled Nd:YAG laser are used to, induce nonlinear changes in the material.

Plasma Processing of Metallic and Semiconductor Thin Films in the Fisk Plasma Source

Gregory Lampkin
Edward Thomas, Jr.
Michael Watson
Kent Wallace
Henry Chen
Arnold Burger

Fisk University

Abstract

The use of plasma to process materials has become widespread throughout the semiconductor industry. Plasmas are used to modify the morphology and chemistry of surfaces. We report on initial plasma processing experiments using the Fisk Plasma Source. Metallic and semiconductor thin films deposited on a silicon substrate have been exposed to argon plasmas. Results of microscopy and chemical processed materials are presented.

A Gravitational Temperature Generated by Spacetime Curvature

Manasse Mbonyo

University of Michigan

Abstract

In this talk it is suggested that in generating curvature, gravity induces a temperature-like quantity on space-time. We derive this temperature for the simple but important case of a Schwarzchild spacetime. It is demonstrated that in the event the matter fields generating curvature are enveloped in an event horizon the above surface temperature smoothly goes to the Hawking Temperature. We suggest the origins of this phenomenon and point out its astrophysical/cosmological importance.

Local Lyman-Alpha Absorption Systems: A Study of the Distribution of Matter in the Universe

Kevin M McLin

University of Colorado

Abstract

QSO absorption systems provide a way to study material, even at great distances, which is too diffuse and faint to be seen in its own emitted radiation. Futhermore, absorption studies can detect matter in amounts much smaller than is associated with typical bright matter such as stars and galaxies. Absorption thus might well give us a less biased view of the distribution of baryons in the universe than do studies of luminous matter. Understanding the local Lyman-alpha absorption systems will be key to our understanding of QSO absorption systems in general. Though many Lyman-alpha clouds are seen at high redshift ($z>1$), galaxies at these distances are too faint to be seen. Only by studying the local clouds will we be able learn the relationship between absorption systems and galaxies, assuming one exists, and only then can we begin to understand how the clouds are related to filaments and voids.

Preliminary Results of the Electron Paramagnetic Resonance of Fe^{3-} and Mn^{4-} in $LiNbO_3$ Single Crystal

J. Morris
A. Darwish
A. Williams

Alabama A&M University

Abstract

$LiNbO_3$ is a ferroelectric crystal with a variety of applications. Dopants play an important role in developing favorable properties for optical purposes. Transition metals (e.g. Fe, Mn) increase the photorefractive sensitivity.

We report the EPR investigations of LiNbO3: Fe^{3-}:Mn^{4-} single crystal for photorefractive and nonlinear optical applications. By using x-band Electron Paramagnetic Resonance spectrometer, the EPR spectra of the $LiNbO_3$:Mn^{4+}:Fe^{3-} crystals were recorded. Analysis of defects and the possible sites for both Mn^{4-} and Fe^{3-} on the single crystal will be presented.

Although there have been many studies of impurity states in $LiNbO_3$ by EPR, the analysis of Fe impurity is especially of importance because this impurity appears to be responsible for optical refractive index damage and phase holographic storage in $LiNbO_3$. The crystals were doped with Fe while manganese was apparently present in the ion doped.

Identification of the specific impurities and other defects, which participate in the photorefractive effect, is an important goal since this information will allow a material to be optimized for any particular set of applications.

1 A. Darwish, D. McMillen, T. Hudson. and P. Banerjee, "Investigations of the charge transfer and the photosensitivity in single and double doped $LiNbO_3$ single crystals; an optical-electron paramagnetic resonance study (Part 1)", J. Opt. Eng., Tech Digest , Vol. 2362, 29-31, (1997).

2 A. A. Mirzakhanyan, "The splitting in zero. field ofground state levels of the Ni^{2+} ion in LiNbO3" *Sov. Phys. Solid State* **23**, 8, (1981).

3 F. Jermann and J. Otten, "Light induced charge transport in $LiNbO_3$:Fe at high light intensities," *J. Opt. Soc. Am. B,* Vol. **10**, 11, 2085-2092, (1993).

4 H. Towner and H. Story, "EPR studles of crystal field parameters in Fe^{3+}:$LiNbO_3$," *The J. of Chem. Phys.,* Vol. 56, 7, (1972).

5 L. E. Halliburton and C. Chen, "ESR and optical point defects in Lithium Niobate," *Nuc. Inst. and Meth. in Phys. Res.,* B1, 344-347, (1984).

Continuous Wavelet Transform and its Application to Automatic Target Detection and Recognition

Romain Murenzi
Dennis Semwogerere
Davida Johnson
Lance Kaplan
Kamesh Namuduri

Clark Atlanta University

Abstract

Automatic target detection and recognition (ATR) requires the ability to optimally extract the essential features of an object from (usually) cluttered environments. In this regard, efficient data representation domains are required in which the important target features are both compactly and clearly represented, enhancing ATR. Since, both detection and identification are important, multidimensional data representations and analysis techniques, such as continuous wavelet transform (CWT), are highly desirable.

We first introduce the 2D CWT and we review some of its relevant properties (such as the energy conservation, the reconstruction formula), and apply it to the analysis and selection of features in images. A special attention will be given to orientational features. We then discuss the use of these features for detection and classification of targets in infrared images (IR).

Problems and Solutions in Molecular Physics

Lawrence S. Norris

Northwestern University

Abstract

Advances in computer technology is being matched by powerful algorithms in quantum chemistry which allow for the theoretical study of large molecules and extended systems with an unprecedented level of accuracy. This has opened new vistas for theory in molecular engineering and rational materials design. Material behavior can be "tested" using theoretical analysis and the methods of molecular biology and epitaxial growth can be employed to tailor make matter with nearly unlimited specification.

In this talk I will talk about some of the newest advances in computational quantum chemistry and two examples of application from biochemistry.

Minority Physicist Archive

George Ofori-Boadu
Cynthia Keppel

Hampton University.

Abstract

With support from the American Physical Society, the Hampton University chapter of the Society of Physics Students has embarked on a project to create a Minority Physicist Archive centered around a world wide web home page. The goal of this page is to be a resource for anyone interested in the lives and works of minority physicists. It is hoped that the archive will serve as a valuable educational tool for students and educators, both as a resource and as an inspiration. This home page may be visited currently at http://phy.hamptonu.edu/sps/sps.htm. The archive features Edward Bouchet Award winners, Fellows of the American Physical Society, and historical figures. We are currently gathering information regarding historical figures for the archive. If you are interested in nominating yourself or a person with great achievements to be included in this page, please send a brief biography of the person to Dr. Cynthia Keppel, Dept. Of Physics, Hampton University, Hampton, VA 23668.

Application of Moment-Wavelet Transform to Quantum Mechanics

Asmerom Ogbazghi
Carlos R. Handy
Romain Murenzi

Clark Atlanta University

Abstract

For a given a one dimensional Schrodinger equation, can be transformed into an equivalent Continuous Wavelet Transformed (CWT) representation (involving scaled and translated moments), $\mu_{1/a,b} = x^p e^{-Q(\frac{x}{a})}\Phi(x + b)$. This depend on a mother wavelet of the form $W(x) = N\delta_x^i e^{-Q(x)}$ and this has been confirmed by Handy and Murenzi (HM[1,2]). The descrete bound state configuration wavelet transform can be determined through a multiscale process involving the integration of finite number of coupled linear first order differential equation for the moments $m_{1/a,b(}p)$. We examine for the anharmonic oscillator potential $V(x) = mx^2 + gX^{2q}$, $(q=2,3,4,...)$.

1 Carlos R. Handy and Romain Murenzi 1996 Physical Review A 54,5

2 Carlos R. Handy and Romain Murenzi 1997 J. Phys. A: Math. Gen. 30 4709-4729

Tunable Mid Infrared Downconversion in GaSe and $AgGaS_2$

A. O. Okorogu
S.B. Mirov
D. I. Crouthamel
N. Jenkins
University of Alabama

K. L. Vodopyanov
Imperial College

A. Yu. Dergachev
Swatrz Electrooptics

V. V. Badikov
Kuban State University

Abstract

We report a generation of tunable middle infrared radiation and a conversion of high power LiF:F_2^{+**} color center crystal's radiation to the spectral region of 3.5 - 8.5 μm. Here, we identified a method of generating difference frequency mixing in GaSe and AgC+GaS_2, based on our newly designed solid state laser combination, consisting of the alexandrite and alexandrite-pumped tunable LiF:F_2^{-**} (0.8 - 1.2 μm) color center lasers.

Precision-Resolution Bragg Filter Fiber Optic Strain Sensor Application

L. Phillips
A. Sharma
T. George

Alabama A & M University

Abstract

In 1978, it was discovered[1] that gratings could be written in a photosensitive germanosilicate fiber by passing either 488.0 nm or 514.5 nm argon Ion laser light through it. The formation of a standing wave of blue-green laser light and the consequent two-photon absorption of the light by a defect band of GeO result in the permanent periodic perturbation in the core refractive index[2]. Many advances have been made in both fiber- manufacture and applications since that time. Currently the most widely-used process for grating formation involves the interference in the fiber core of two coherent ultraviolet (UV) beams from the side of the fiber with the centered near 244 nm.

Most applications of fiber gratings are in the areas of communications and fiber optic sensors. It was proposed early in the development of Bragg gratings that they be used as sensor elements to measure temperature, pressure, strain, and in smart structures. Primarily, the advantage derives from the absolute nature of measurand-encoding in wavelength which makes the sensors essentially insensitive to intensity fluctuations of the sources, connector losses, etc.

The research presented here is the result of a continuing effort to advance the development of interferometric fiber optic gyroscopes (IFOG's) and fiber optic pay dispensers, in addition to associated diagnostic test instrumentation and analytical computer simulations. In a novel application. Bragg gratings are used to measure the localized axial strain in various layers of fiber-optic coils similar to those typically used as IFOG sensing coils and in fiber optic data link payout dispensers. The results of numerical analysis using a cable packs mechanics model (CPPM) and the subsequent technique for fabricating these precision winding coils are also discussed.

Fiber coils incorporating fiber-optic Bragg sensors were tested using a tunable laser light source from an Optical Parametric Oscillator (OPO). The OPO, which is pumped by the third harmonic (344 nm) of a pulsed ND:YAG laser, is tunable from 400 nm to 1600 nm with a linewidth of 0.2 cm^{-1}. The strain sensing method used involves measurement of shift of Bragg wavelength due to axial strain.

Shift in the Bragg wavelength is linearly related to change in the spacing between Bragg planes of the grating and is, therefore, also linearly related to the axial strain in an optical fiber containing a Bragg filter. The tunable laser's narrow linewidth gives the capability to measure axial strain to a sensitivity of 1 microstrain, however, for reasons to be explained during the presentation, sensitivity was limited to $2x10^{-5}$ microstrain.

1 K. O. Hill, Y. Fuji, D. C. Jackson, and B. S. Kawasaki, 1978 *Appl. Phys. Lett.* **32**, 674

2 J. Bures, J. Lapierre, and D. Pascale, 1980, *Appl. Phys. Lett.* **37**, 860

Magnetic Monopoles: believe it or not!! An Introduction and Review of Montonen and Olive's 1977 Paper

Aaron F. Roane

The Johns Hopkins University

Abstract

Although magnetic monopoles have never been experimentally observed, an interest in them has generated an enormous amount of research over the past several decades. The recent excitement in magnetic monopoles is in the context of duality. In 1977 C Montonen and D. Olive wrote a paper entitled "Magnetic Monopoles As Gauge Particles?" in which they studied the possible existence of monopoles and an electric/magnetic duality in the Georgi-Glashow model.

This talk is an introduction and review of this classic paper and is intended for the nonspecialist (although all are welcome).

Crossed Phase Gratings Using Diffractive Optical Elements

Dr. Willie S. Rockward

Air Force Research Laboratory
Eglin AFB

Abstract

By orienting two identical or complementary diffractive gratings with a small angle between the grating grooves, a new crossed grating device can be constructed, This device has an effective profile that varies locally. To understand the effects of this variation and the diffraction efficiency of the gratings, a determination of the location and description of the local profiles were correlated to the moire period of the crossed grating system using various techniques in conjunction with the grating models. Asymmetric intensity behavior in the first order of the crossed gratings was seen. Effectively, the diffraction efficiency of the crossed gratings yielded a response equivalent to that of a grating with variable blaze which could be useful in optical computing as a passive optical switching device, One of several models is described that creates greater asymmetric behavior.

Gravity and String Symmetries

V. G. J. Rodgers

The University of Iowa

Abstract

We are able to use symmetries of string theory, namely the dual space of the semi-direct product of the Virasoro algebra and the affine Lie algebra, to write a theory of gravitation which is a natural analogue of Yang-Mills theory. The theory provides a covariant local Lagrangian for two dimensional gravity. By interpreting the isotropy equations of coadjoint orbits as Gauss law constraints for a field theory in two dimensions, we are able to extend to higher dimensions. The theory has a Newtonian limit in any space-time dimension. Our approach introduces a novel relationship between string theories and 2D field theories that might be useful in defining dual theories.

Sensitivity of the Sun's Oscillation Frequency Spectrum to the Structure of its Core

I. Preliminary results relative to the low degree p-modes of oscillation

Carl A. Rouse

Rouse Research Incorporated

Abstract

At the 19th Annual Meeting of the National Society of Black Physicists, a report on "Stellar structure as a resolution of the solar neutrino problem" was given[1]. A review was given of the Rouse approach to calculating models of the present sun with the theoretical solar neutrino counting rates for three models. The three models described in[2] are a standard model, the reference high-Z core (HZC) model and a variation on the core of the reference HZC model. Only the counting rates from the reference HZC model are consistent with two of the three experimental observed counting rates. In the present report, frequencies of oscillation from the same three models are compared In these three models the chemical abundances outside the core and the temperature gradients in the outer convective region are the same. The basic one-dimensional structure of the cores is represented by their mean molecular weight profiles since this is the only aspect of the chemical composition that enters the oscillation equations. For the oscillation equations with and without the gravitation perturbation, the input gamma-1 function, Γ_1, is calculated in two ways, viz., with the equivalent input of the standard gamma-1 function and with only Rouse effective gamma, γ_e, where γ_e is defined by $\gamma_e - 1 = P/E$, with P and E the total pressure and internal energy at the given density and temperature, respectively. This quantity was defined and used since 1962. Used in the oscillation equations for degree $l = 1$, p-mode oscillations, the results for five-minute band (5MB) frequencies for the three models are shown to be separated by 20 uHz or more, demonstrating a very significant effect of the cores of the three models on the degree $l = I$ 5MB p-mode frequencies. The mean molecular weight variations of the cores will also be shown and discussed. Future research will be outlined.

1 C. A. Rouse, in Proceedings of the 23rd Annual Day of Scientific Lectures and 19th Annual Meeting of the National Society of Black Physicists. Eds. C. H. McGruder, III and W. E. Collins, March 27 - 3-, 1996, Fisk University and Western Kentucky University.

2 C. A. Rouse, Astronomy and Astrophysics 304, 431 (1995).

Mechanical Alloying

D. Seifu

Morgan State University

Abstract

Mechanical alloying is a non-equilibrium process that allows one to prepare amorphous and nano crystalline materials, including a variety of application related magnetic materials. Many important questions remain unanswered concerning the alloying process. Mössbauer spectroscopy provides important information about phase transformation and magnetic properties of these materials. In this work mechanical alloying of Sm, Zr, and Fe with the composition $SmFe_3$[1] and $Sm_{0.25}Zr_{0.75}Fe_3$[2] were studied as a function of milling time up to 20 hours using Mössbauer spectroscopy. The initial sextet in the Mössbauer spectrum changed to a broad singlet, indicating a nonmagnetic material. Low temperature Mössbauer and magnetic measurements showed that the material has transformed from a ferromagnetic to a superparamagnetic phase. Comparison of the rate of mechanical synthesis in $SmFe_3$ and $Sm_{0.25}Zr_{0.75}Fe_3$ shows the addition of Zr has accelerated the synthesis.

1 D. Seifu, F. W. Oliver, E. Hoffman, A. Aning, V. S. Babu, M. S. Seehra, and R. M. Catchings, J. Appl. Phys. **81**, 8 (1997).

2 D. Seifu, F. W. Oliver, E. Hoffinan, A. Aning, V. S. Babu, M. S. Seehra, (submitted for publication), Appl. Phys. Lett. (1998).

Contributions of High-N Satellites to the Kβ Resonance Line of Heliumlike Argon

A. J. Smith
Morehouse College

P. Beiersdorfer
V. Decaux
K. Widmann
K. J. Reed
M. H. Chen
Lawrence Livermore National Laboratory

Abstract

We present measurements of the contributions from high-n dielectronic satellite transitions to the resonance line ($1s^2\ ^1S_0$- $1s3p\ ^1Pi$) of heliumlike Ar^{16+}. We have used a high resolution Bragg crystal spectrometer to analyze the x-rays emitted by ions trapped and excited in an electron beam ion trap (EBIT). Satellite transitions of the type $1s3lnl'$ - $1s^2n1'$, for n = 3, 4, 5, and $n \geq 6$ have been studied. The resonance strength of the n = 3 satellites was measured to be $(4.65\pm0.65) \times 10^{-21}$ cm^2 eV, that of the n = 4 satellites was determined to be larger than this value, while that of the n = 5 satellites was found to be nearly equal to the resonance strength of the n = 3 satellites. The n^{-3} dependence of resonance strengths expected from the n-scaling of the Auger rates is thus shown to not be valid for the satellites studied in our measurements. We gratefully acknowledge the LLNL Research Collaborations Program for HBCUs. This work was performed under a Department of Energy contract No W-7405-ENG-48 at LLNL.

Shape Memory and Gels

Kimani A. Stancil
Guoqiang Wang
Toyoichi Tanaka

Massachusetts Institute of Technology

Abstract

Gels have been useful in biochemical techniques like gel chromatography and electrophoresis. The lens and vitreous humor of the eye are gels whose viscoelastic properties influence how we see.

Over the past twenty years, Prof. Toyoichi Tanaka-M.I.T. has studied and quantified the properties of certain synthetic gels. Gels undergo phase transitions depending on their environment. These transitions can be temperature or ion induced. In gels, a phase transition is defined by the discontinuous change of a gel from a dense or collapsed phase to a more dilute or swollen phase or the reverse. Experimentally, these transitions are determined by changes in relative volume or density.

In this poster, we discuss the method of preparing planar slab shaped bigel structures consisting of temperature sensitive gels and pH(ion) sensitive gels. Hu et al., has investigated shapes using an interpenetrating network where one gel is allowed to polymerize within the pores of another. This results in an interlocking connection (without chemical bonding)between the two materials. Our method emphasizes the use of disulfide bonds as surface connectors between the two gels which form a bigel. The bigel's ability to respond reversibly to its environment establishes its memory.

1 T. Tanaka, L. Hocker, and G. Benedek 1973 J. Chemical Physics **59** 5151

2 S. Hirotsu, Y. Hirokawa, and T. Tanaka 1987 J. Chemical Physics **87** 1392

3 Z. Hu, X. Zhang, and Y. Li 1995 Science **269** 525

^{1}H Signal Enhancement Using Hyperpolarized ^{129}Xe

A. L. Stith
T. Maier
R. G. Bryant
J. R. Brookeman

University of Virginia

Abstract

Circularly polarized light centered at 795 nm can be used to optically pump either the $S_{+1/2}$ or $S_{-1/2}$ spin energy level of the valence electron of Rubidium (Rb). Through spin-exchange it is possible to transfer energy from the valence electrons of Rb to the unpaired proton of the ^{129}Xe nucleus, The excess of protons in the spin up orientation results in an increased Nuclear Magnetic Resonance (NMR) signal intensity as large as 10^5 times the signal from Boltzman polarization levels. This 'hyperpolarized' ^{129}Xe has introduced a new means for understanding atomic and molecular interactions in physics and biophysics and provided new opportunities in Magnetic Resonance Spectroscopy (MRS) and Imaging (MRI).

Solution phase Magnetic Resonance studies using ^{129}Xe at thermal equilibrium (with extremely small signal intensities) have been limited due to the extensive signal averaging required, making data acquisition lengthy. With polarized ^{129}Xe, data acquisition now can be achieved in minutes instead of hours or days. The 10^5 increase of nonrenewable ^{129}Xe signal is transferable to other nuclei. This phenomenon is described by the Nuclear Overhauser Effect (NOE). By observing the ^{129}Xe directly and measuring the spin-lattice relaxation (T_1) of ^{129}Xe in solutions of α-cyclodextrin (α-CD), we have estimated crossrelaxation values that agree with published values[1]. The cross relaxation rate for polarization from the hyperpolarized ^{129}Xe to the remaining hydrogen nuclei (^{1}H) on a partially deuterated α-CD molecule is $\sigma_{IS}=3.7*10^{-4}s^{-1}$. The resulting polarization enhancement between ^{129}Xe and ^{1}H is small and is limited by the low solubility of ^{129}Xe in aqueous solutions, its short correlation times with molecular solutes and the relatively short T_1 of ^{1}H in solution.

1 Y. Q. Song, B. M. Goodson, R. E. Taylor, D. D. Laws, G. Navon, A. Pines 1997 *Angew, Chem. Int, Ed. Engl.* **36** 2368

Novel Fiber Lasers

Donnell T. Walton

Howard University

Abstract

Fiber lasers, due to their long interaction lengths and confinement of high intensities, are of great interest in the fields of nonlinear optics and ultrafast phenomena. With the advent of compact, high-brightness diode pumps, fiber lasers are becoming ubiquitous outside of the laboratory. For example, fiber lasers have demonstrated potential in the areas of telecommunications, medicine, and materials processing.

In this talk, several recent experiments in this field will be discussed. Included are the spectroscopy and investigation of laser potential of two trivalent rare-earth doped glass systems: ytterbium-doped silicate and concentrated thulium-doped fluorozirconate. The talk will conclude with an overview of work with the Howard University, University of Michigan, and Bell Laboratories Collaborative Access Team at the Advanced Photon Source (MHATT-CAT) on high spatio-temporal resolution x-ray techniques.

Magnetic and Structural (EXAFS) Properties of Laser Ablated Magnetic Oxide Films

C. M. Williams
Morgan State University

V. Q. Harris
Naval Research Laboratory

Abstract

Magnetic oxide crystals were the focus of intense study during the 1950's and '60's when the use of ferrites as microwave devices in radar systems first became a reality. More recently interest in oxides had been waning, but in the last few years the field has undergone a renaissance. The current spurt of activity in the field is caused by two developments: 1) the increasing importance of magnetic oxides in magnetic recording technology and in a new generation of integrated thin film microwave devices and 2) the development of advanced new techniques to synthesize and analyze thin film oxide materials. Several synthesis processes for depositing magnetic oxide films have been demonstrated with varying degrees of success. However, pulsed laser ablation has enjoyed the most success. The authors have examined magnetic and structural properties for a series of non stochiometric pulsed laser ablated MnZn-ferrite films, epitaxially grown on (001) MgO substrate at deposition temperatures ranging from 300°C to 800°C in an oxygen pressures of 15, 30, 60 and 90 milliTorr. The results show a number striking features: 1) large variations in the magnetization and magnetic anisotropy with oxygen pressure; 2) scaling of the magnetization with Fe^{2+} ion concentration and 3) a sensitivity of the coercive force and ferrimagnetic resonance linewidth to microstructure. The variation in magnetization is explained in terms of variations in the number of iron ions on the octahedral tetrahedral sites, as observed by EXAFS studies.

A New Method for Searching for Extra-Solar Planets

William Wright
Charles McGruder, III

Western Kentucky University

Abstract

Our research is pertaining to searching for extra-solar planets and/or brown dwarfs by the use of lunar occultation. We have concluded some preliminary calculations concerning the feasibility of the lunar project. The main objective of the calculations is to determine whether or not the solar planets and/or brown dwarfs can be seen if they are close to their parent stars. We gratefully acknowledge the support of NASA grant NCC5-228.

NSBP/NCBPS CONFERENCE
March 4-7, 1998

AGENDA
National Society of Black Physicists

NSBP'98: "The Next Generation"

Hosted by the University of Kentucky and Kentucky State University

Wednesday, March 4, 1998

2:00 pm - 1:00 am	Hospitality Suite ..... Contemporary Suite #1426
6:00 pm – 8:00 pm	Registration for NSBP ..... Hyatt Lobby
6:00 pm – 8:00 pm	Welcoming Reception ..... Regency West Ballroom

Thursday, March 5, 1998 (NSBP-Day of Scientific Lectures)
Kentucky State University, Frankfort, KY

7:15 am	NSBP Buses leave hotel for KSU, Frankfort
7:15 am – 8:00 am	Travel time to Frankfort
8:00 am – 8:45 am	Continental Breakfast
8:45 am – 9:00 am	Kentucky State University Welcome ..... Bradford Hall Theater (Host Paul Bibbins, President Mary Smith)
9:00 am – 10:40 am	Session I Moderator: Alfred Z. Msezane, Clark Atlanta University
9:00 am - 9:20 am	Rony Shahidain, Kentucky State University "Implementational Software Development for Physics Courses"
9:20 am - 9:40 am	G. Y Ndefru, University of Kentucky "The Use of Non-Traditional Tutorials in General Physics"
9:40 am - 10:10 am	H.L. Neal, Clark Atlanta University "Teaching Density Functional Theory to Undergraduates"
10:10 am - 10:25 am	Coffee Break

10:25 am - 12:10 am	Session II Moderator: Stephen C. McGuire, Cornell University
10:25 am - 10:55 am	Robert H. (Pete) Bragg, University of California, Berkeley "The Kinetics of Graphitization Revisited: A First Principles Derivation"
10: 55 am - 11:20 am	Kenneth Brown, Jet Propulsion Laboratory "VIGILANTE: An overview of a GPS-based ATR System"
11:20 am - 11:45 am	Armando Howard, NASA-GISS "Implementing a New Parametrization for Turbulent Mixing in the Ocean"
11:45 am - 12:05 pm	Darryl K. Jones, University of Alabama, Huntsville "The Dynamics of Controlled Optical Delay Lines"
12:10 pm - 1:50 pm	Lunch: ..... Hill Student Center Ballroom Speaker: Keith Jackson, Lawrence Berkeley National Laboratory
2:10 pm - 3:20 pm	Session III Moderator: Benjamin Zeidman, Argonne National Laboratory
2:10 pm - 2:40 pm	Donnell Walton, Howard University "Novel Fiber Lasers"
2:40 pm - 3:00 pm	Lawrence Norris, Northwestern University "Problems and Solutions in Molecular Physics"
3:00 pm - 3:20 pm	A. O. Okorogu, University of Alabama, Birmingham "Tunable Mid-Infrared Downconversion in GaSe and $AgGaS_2$"
3:20 pm - 3:35 pm	Break
3:35 pm - 5:15 pm	Session IV Moderator: Donnell Walton, Howard University
3:35 pm - 4:05 pm	Conrad Williams, Morgan State University "Magnetic and Structural (EXAFS) Properties of Laser Ablated Magnetic Oxide Films"
4:05 pm - 4:25 pm	Willie Rockward, US Air Force Research Laboratory, Eglin AFB "Crossed Phase Gratings using Diffractive Optical Elements"

4:25 pm - 4:45 pm	Thomas Butler, University of Michigan "An Electron Paramagnetic Resonance Analysis of the Wildtype and Mutant Species of the Cobalamin Dependent Methionine Synthase Enzyme"
4:50 pm	Buses leave KSU campus for Hyatt Regency, Lexington
2:00 pm - 1:00 am	Hospitality Suite ..... #1426
5:00 pm – 8:00 pm	Registration for NCBPS/NSBP ..... Hyatt Lobby
7:30 pm – 9:30 pm	Reception for NSBP/NCBPS ..... Patterson Ballroom
8:30 pm - 8:45 pm:	University of Kentucky Welcome Keith MacAdam, Chair: Dept. of Physics & Astronomy Allan Richards, Associate Dean, The Graduate School

Friday, March 6, 1998 :
University of Kentucky, Lexington, KY

6:45 am – 7:45 am	Buses leave every 10 min. between Hyatt Hotel .... Front of Hyatt Hotel and UK's Student Center (Latecomers will need to walk about 1/2 mile to campus)
7:30 am	Registration/Information Desk will be available during conference..... Outside Worsham Theater
7:00 am – 7:55 am	Continental Breakfast(NCBPS/NSBP) ..... Outside Worsham Theater
8:00 am – 8:15 am	UK Welcome ..... Worsham Theater
8:15 am – 10:40 am	Joint Session (NSBP/NCBPS/High School Students): Moderator, Cynthia McIntyre, George Mason University
8:15 am - 8:50 am	NSBP Speaker: S. James Gates, University of Maryland "Frontiers in Physics"
8:50 am - 9:10 am	NCBPS/NSBP Speaker: Jarita Holbrook, University of California, Los Angeles "African Astronomy"
9:10 am - 9:30 am	NCBPS Speaker: Aaron Roane, Johns Hopkins University "Magnetic Monopoles: Believe it or not!! An Introduction and Review of Montonen and Olive's 1977 Paper
9:30 am - 9:50 am	NSBP Speaker Wendell T. Hill, III, University of Maryland "Atoms and Molecules in Intense Laser Fields: What Can We Learn?"
9:50 am - 10:10 am	NSBP Speaker: Peter Delfyett, Central Florida University "Ultrafast Semiconductor Lasers: Fundamental Physics & Applications for Ultra-Highspeed Communications & Signal Processing"
10:10 am -10:30 am	NCBPS Speaker: Beth Brown, University of Michigan "A New View of the X-Ray Emission from Elliptical Galaxies"
10:30 am - 10:40 am	Break, NCBPS Leaves for Recruiting Session
10:40 am - 11:40 am	NSBP Session V: ..... Center Theater

Moderator: Floyd James, North Carolina A & T University

10:40 am - 11:00 am

Daniel M. Smith, Jr, South Carolina State University
"Workbook for Introductory Mechanics Problem-Solving"

11:00 am - 11:20 am

Augustine J. Smith, Morehouse College
"Contributions of High-n Satellite Lines to
the Resonance Line of He-like Argon"

11:20 am - 11:40 am	Edward Thomas, Jr., Fisk University "Studies of Dusty Plasmas and Ionization Instabilities in the Fisk Plasma Source"
11:45 pm – 1:45 pm	Lunch (NSBP/NCBPS/High School Students) ..... Grand Ballroom Hosted by NASA/Kentucky Space Grant Consortium: Moderators: Richard and Karen Hackney, KSGC/Western Kentucky University
12:15-12:45	George Cooper "Meteorites" NASA Ames Research
12:45-12:50	Richard Hackney: Introductions
12:50-1:10	Carl Holden, NASA Marshall Space Flight Center
1:10-1:20	Arthur Cammers-Goodwin, UK Chemistry Department
1:20-1:35	Charles McGruder, Western Kentucky University
1:35-1:45	Suketu Bhavsar, UK Physics and Astronomy
1:50 pm - 3:35 pm	SessionVI: ..... Center Theater Moderator: Charles McGruder, Western Kentucky University
1:50 pm - 2:10 pm	Romeel Dave, University of California, Santa Cruz "Numerical Cosmology and the Study of Quasar Absorption Lines
2:10 pm - 2:30 pm	Jason Best, Shepherd College "The Pointwise Dimension Applied to Astronomical Clustering Studies"
2:30 pm - 2:50 pm	Dara J. Norman, University of Washington "Gravitational Lensing and the Search for Dark Matter"
2:50 pm - 3:10 pm	Kevin McLin, University of Colorado "The Local Lyman-Alpha Absorption Systems: A Study of the Distribution of Matter in the Universe"
3:15 pm - 3:35 pm	Carl Rouse, Rouse Research Inc. "Sensitivity of the Sun's Oscillation Frequency Spectrum to the Structure of its Core: 1. Preliminary Results Relative to the Low Degree p-modes of Oscillation"
3:35 pm - 3:55 pm	Break
4:00 pm – 4:50 pm	Joint UK Physics & Astronomy /NSBP Colloquium: .... Center Theater Keith Baker, Hampton University "Strange Physics at Jefferson Lab"

4:55 pm - 5:15 pm	NSBP President's Report to Members: Lonzy J. Lewis, Clark Atlanta University
5:15 pm - 6:15 pm	NSBP Business Meeting
5:30 pm – 6:30 pm	Buses leave every 10 min. ..... Student Center Parking Lot between Student Center and Hyatt Hotel
7:30 pm – 9:30 pm	Awards Banquet (NSBP/NCBPS) .....Patterson Ballroom Keynote Speaker, James Stith, American Institute of Physics, Physics Programs Director Awards: NSBP Outstanding Ph.D. Dissertation, 1997: Dr. Edward Thomas, Auburn University NCBPS Lifetime Achievement Award: Robert H. (Pete) Bragg, University of California, Berkeley
2:00 pm - 1:00 am	Hospitality Suite .....#1426

Saturday, March 7, 1998
University of Kentucky, Lexington, KY

7:10 am – 7:40 am	Buses leave every 10 min. between Hyatt Hotel .... Front of Hyatt Hotel and UK's Student Center
7:20 am – 7:55 am	Continental Breakfast ..... Location of Group Picture Site
8:00 am - 8:20 am	Group Photograph with NCBPS
8:20 am - 9:40 am	Joint Recruiter and NCBPS/NSBP Poster Session ..... 257, 259, Small Ballroom FOR ABSTRACT SPEAKERS AND TITLES SEE END OF AGENDA
9:30 am - 11:10 am	NSBP Session VIII ..... Center Theater Moderator: Lonzy J. Lewis, Clark Atlanta University
9: 30 am - 9:48 am	Dereje Seifu, Morgan State University "Mechanical Alloying"
9:48 am -10:06 am	Carlos R. Handy, Clark Atlanta University "Moment-Wavelet Quantization: A First Principles Analysis of Quantum Mechanics through Continuous Wavelet Transform Theory"
10:06 am - 10:24 am	Romain Murenzi, Clark Atlanta University "Continuous Wavelet Transform and its Application to Automatic Target Detection and Recognition"
10:24 am - 10:42 am	A. Z. Msezane, Clark Atlanta University "Singular Behavior in Electron-Atom Scattering at Small Momentum Transfer"
10:42 am - 11:00 am	M. E. Edwards, Spelman College "Apparent Clustering of Droplet Microemulsions in the Presence of Electric Fields"
11:00 am - 11:10 am	Break
11:10 am - 12:45 pm	NSBP Session IX ..... Center Theater Moderator: Milton D. Slaughter, University of New Orleans
11:10 am - 11:35 am	Clifford V. Johnson, University of Kentucky "Essence of M - Theory"

11:35 am - 12:00 pm	Vincent G. J. Rodgers, University of Iowa "Gravity and String Symmetries"
12:00 pm - 12:25 pm	Manasse Mbonye, University of Michigan "A Gravitational Temperature Generated by Spacetime Curvature"
12:45 pm – 2:00 pm	Lunch (NSBP/NCBPS) ..... Grand Ballroom Speaker: Poetry readings by Nikky Finney Professor of Creative Writing, English Department University of Kentucky

NSBP Conference Concludes ..... Buses return to Hyatt Regency

Afternoon Session of NCBPS (NSBP Invited)

2:15 pm - 4:30 pm	**Panel on Opportunities for**
	Physics and Astronomy Graduates ..... Center Theater
2:15 pm - 2:35 pm	Moderator: Joseph Johnson, Florida A & M University
2:35 pm - 2:55 pm	Colleges and Universities: Anthony Johnson, New Jersity Institute of Technology
2:55 pm - 3:15 pm	Government Laboratories: John D. Galambos, Oak Ridge National Laboratory
3:15 pm - 3:35 pm	Industry: Eric Lee, SEMATECH Fellow on leave from Motorola Corp.
3:35 pm - 3:45 pm	Break
3:45 pm - 4:30 pm	Panelist Q & A Session with Audience
4:35 pm - 5:15 pm	Buses return to Hyatt Regency
7:00 pm – 9:00 pm	NCBPS Buffet Dinner ..... Hyatt Ballroom (NSBP invited) Speaker: Ronald Mickens, Clark Atlanta University "History of the Electron"
9:15 pm – 1:00 am	Dance (NCBPS) ..... Hyatt Ballroom
2:00 pm – 1:00 am	Hospitality Suite (NCBPS/NSBP/Recruiters) ..... Hyatt Suite

Sunday, March 8, 1998

6:00 am – 3:00 pm	Van Shuttles to and from Hyatt Regency and Bluegrass Airport

POSTER PRESENTATIONS:

8:20 am - 9:40 am ..... 257, 259, Small Ballroom

Edward Asika, Clark Atlanta University
"Effect of Signal to Clutter Ratio(SCR)
on Automatic Target Recognition (ATR)"

H. L. Neal, Clark Atlanta University
"Teaching Density Functional Theory to Undergraduates"

L. Phillips, Alabama A & M University
"Precision-Resolution Bragg Filter
Fiber Optic Strain Sensor Application

J. Morris, Alabama A & M University
"Preliminary Results of the Electron Paramagnetic
Resonance of Fe^{3-} and Mn^{4+} in $LiNbO_3$ Single Crystal"

A.M. Darwish, Alabama A & M University
"Preliminary Results of the Electron Paramagnetic
Resonance of Fe^{3-} and Mn^{4+} in $LiNbO_3$ Single Crystal"

Yonas Abraham, Clark Atlanta University
"Multivariable Optimazation Approach for the Construction of
Many-Body Potential"

Asmerom Ogbazghi, Clark Atlanta University
"Application of Moment -Wavelet Transform to Quantum Mechanics"

S.U. Egarievwe, Alabama A & M University
"External Feedback Effects on Powder Laser Threshold"

William Wright, Western Kentucky University
"A New Method for Searching for Extra-Solar Planets"

Philip E. George, Western Kentucky University
"Searching for Extra-Solar Planets by Examining Eclipsing Binaries"

J. Brodney Fitzgerald, Western Kentucky University
"Searching for Period Changes in the
Eclipsing Contact Binary System 44i Boo"

LaShondria B. Dixon, Southern University and A & M College
"An Investigation of the Relationship between Structure and Electron
Transport in $La_{1-x}(Ca_{1-y,}\ Sr_y)_x\ Mn)_3$"

George Ofori-Boadu, Hampton University
"Minority Physicist Archive"

Kimani A. Stancil, Massachusetts Institute of Technology
"Shape Memory and Gels"

Marta L. Dark, Massachusetts Institute of Technology
"The Physical Response of Meniscal Tissue
to Short Pulsed Laser Irradiation"

C.M. Williams, Morgan State University
"Magnetic and Structural (EXAFS) Properties of Laser
Ablated Magnetic Oxide Films"

Christopher Beatty, Clark Atlanta University
"Excitation Energies and Oscillator Strength for NI"

F.A. Aguama, New Jersey Institute of Technology
"Effect of Zn^{2+} Doping on the Phase Transition Temperature of
Cadmium Calcium Acetate Hexahydrate Single Crystals"

A.L Stith, University of Virginia
"^{1}H Signal Enhancement Using Hyperpolarized ^{129}Xe"

Elaine N. Lalanne, New Jersey Institute of Technology
"Nonlinear Optical Properties of Silicon Nanoclusters Made
by Laser Ablation"

Ian Dean Bacchus, University of California, Berkeley
"Resistive Joining Process in a High Temperature
Superconducting System"

NSBP/NCBPS CONFERENCE
March 4-8, 1998
AGENDA
National Conference of Black Physics Students
NCBPS '98: Physics: "Life in Motion"

Hosted by the University of Kentucky

Thursday, March 5, 1998

Students arrive at Airport: Vans will be arranged for tranportation to hotel

2:00 pm - 5:00 pm — Hospitality Suite ..... *Contemporary Suite #1426, Hyatt*

5:00 pm - 8:00 pm — Registration for NCBPS/NSBP ..... *Hyatt Lobby*

7:30 pm - 9:30 pm — Reception for NSBP/NCBPS ..... *Patterson Ballroom*

8:30 pm - 8:45 pm — University of Kentucky Welcome
Keith MacAdam, Chair, Department of Physics and Astronomy
Allan Richards, Associate Dean, The Graduate School

8:30 pm - 1:00 am — 3 Study Rooms ..... *Washington, Atlanta, Chicago Rooms*
Break Out Sessions (NCBPS)

Hospitality Suite ..... *Contemporary Suite #1426, Hyatt*

Friday, March 6, 1998

6:45 am - 7:45 am — Buses leave ..... *front of Hyatt Hotel*
2 buses leave every 10 minutes between Hyatt Hotel and UK's Student Center
(Latecomers will need to walk about 1/2 mile to campus)

7:30 am — Registration/Information Desk ..... *outside Worsham Theater*
available during conference.

7:00 am - 7:55 am — Continental Breakfast (NCBPS/NSBP) ..... *outside Worsham Theater*

8:00 am - 8:15 am — UK Welcome ..... Worsham Theater
Lauretta Byars, Vice Chancellor for Minority Affairs

8:15 am - 10:40 am — Joint Session NSBP/NCBPS/High School Students:
Moderator, Cynthia McIntyre, George Mason University

8:15 am - 8:50 am — NSBP Speaker: S. James Gates, University of Maryland
"Frontiers in Physics"

8:50 am - 9:10 am — NCBPS/NSBP Speaker:Jarita. Holbrook, University of California, Los Angeles
"African Astronomy"

9:10 am - 9:30 am — NCBPS Speaker: Aaron Roane, Johns Hopkins University
"Magnetic Monopoles: Believe it or not!!"
An Introduction and Review of Montonen and Olive's 1977 Paper

9:30 am - 9:50 am — NSBP Speaker: Wendell T. Hill, III, University of Maryland
"Atoms and Molecules in Intense Laser Fields: What Can We Learn?"

9:50 am - 10:10 am — NSBP Speaker: Peter Delfyett, Central Florida University

"Ultrafast Semiconductor Lasers: Fundamental Physics and Applications for Ultra-Highspeed Communications and Signal Processing"

10:10 am -10:30 am — NCBPS Speaker: Beth Brown, University of Michigan
"A New View of the X-Ray Emission from Elliptical Galaxies"

10:40 am - 11:40 am — Recruiter Session ..... *Rms. 257, 259, Small Ballroom*

11:45 pm - 1:45 pm — Lunch (NSBP/NCBPS/High School Students) ..... *Grand Ballroom*

Hosted by NASA

12:15-12:45 — George Cooper "Meteorites" NASA Ames Research

12:45-12:50 — Richard Hackney Introductions:

12:50-1:10 — Suketu Bhavsar, UK Physics and Astronomy

1:10-1:30 — Carl Holden, NASA Marshall Space Flight Center

1:30-1:40 — Arthur Cammers-Goodwin, UK Chemistry Department

1:40-1:50 — Charles McGruder, Western Kentucky University

2:00 pm - 2:50 pm. — "Physics Spectacular": ..... *Worsham Theater*
Joseph Straley, Tom Troland, Crystal Brogan, UK Physics and Astronomy (NCBPS/High School Students)

3:00 pm - 4:00 pm — Recruiters give Short Talks to NCBPS Students ..... *Worsham Theater*

4:15 pm - 5:30 pm — Departmental Lab Visits (NCBPS) ..... *Chem/Physics, ASTECC Bldgs*

5:40 pm - 6:20 pm — Buses leave ..... *Student Center Parking Lot*
every 10 minutes between Student Center and Hyatt Hotel

7:30 pm - 9:30 pm — Awards Banquet (NSBP/NCBPS) ..... *Patterson Ballroom*
Keynote Speaker, James Stith,
American Institute of Physics, Physics Programs Director

Awards: NSBP Outstanding Ph.D. Dissertation, 1997:
Dr. Edward Thomas, Auburn University
NCBPS Lifetime Achievement Award: Robert H. (Pete) Bragg,
University of California, Berkeley

9:30 pm - 1:00 am. — 3 Study Room Break Out Sessions ..... *Atlanta, Washington, Chicago*

2:00 pm - 7:00 pm — Hospitality Suite ..... *#1426*

Saturday, March 7,1998

7:10 am - 7:40 am — Buses leave ..... *Front of Hyatt Hotel*
every 10 min. between Hyatt Hotel and UK's Student Center

7:20 am - 8:55 am — Continental Breakfast ..... *Location of Group Picture Site*

8:00 am - 8:20 am — Group Photograph with NSBP

8:20 am - 9:40 am — Joint Recruiter and NCBPS/NSBP Poster Session ..... *257, 259, Small Ballroom*
ABSTRACT SPEAKERS AND TITLES SEE END OF AGENDA

9:40 am - 11:10 am — NCBPS Session ..... *Worsham Theater*
Moderator, Alphonse Loper, University of Kentucky

9:40 am - 10:10 am — L. Nan Snow, NPSC, University of California, San Diego

"How to Achieve Success in Graduate School"

10:10 am - 10:30 am — Fred Hall, University of Alaska, Fairbanks
"The Role of Magnetic Reconnection in the Terrestrial Magnetosphere"

10:30 am - 10:50 am — Abdoul Dan-Azoumi, Florida A & M University
"Slingshot Effects"

10:50 am - 11:10 am — Lynford Goddard, Stanford University
"Distribution Theory and Its Application to Solving Linear Differential Equations"

10:55 am - 11:15 am — Break

11: 15 am - 12:40 am. — Surviving Graduate School ..... *230 Student Center*
Facilitator: Eugine Collins, Fisk University

or
Getting into Graduate School ..... *Worsham Theater*
Facilitator: Ronald Mallett, University of Connecticut

12:45 pm - 2:00 pm. — Lunch (NSBP/NCBPS) ..... *Grand Ballroom*
Speaker: Poetry readings by Nikky Finney
Professor of Creative Writing, English Department
University of Kentucky

2:15 pm - 4:30 pm — Panel on Opportunities for Physics and Astronomy Graduates *Center Theater*

- 2:15 pm. - 2:35 pm — Moderator: Joseph Johnson, Florida A & M University
- 2:35 pm - 2:55 pm. — Colleges and Universities: Anthony Johnson, New Jersey Institute of Technology
- 2:55 pm - 3:15 pm — Government Laboratories: John D. Galambos, Oak Ridge National Laboratory
- 3:15 pm - 3:35 pm — Industry: Eric Lee, SEMATECH Fellow on leave from Motorola Corp.
- 3:35 pm - 3:45 pm — Break
- 3:45 pm - 4:30 pm — Panelist Q & A Session with Audience

4:35 pm - 5:15 pm — Buses return to Hyatt Regency

7:00 pm - 9:00 pm — NCBPS Buffet Dinner ..... *Patterson Ballroom*
(NSBP invited)
Speaker: Ronald Mickens, Clark Atlanta University
"History of the Electron"

9:15 pm - 1:00 am — Dance (NCBPS) ..... *Patterson Ballroom*

2:00 pm - 1:00 am — Hospitality Suite (NCBPS/NSBP/Recruiters) ..... *#1426*

Sunday, March 8, 1998

6:00 am - 3:00 pm — Van Shuttles to and from Hyatt Regency and Bluegrass Airport

Poster Presentations

8:20 am - 9:40 am ..... *257, 259, Small Ballroom*

Edward Asika, Clark Atlanta University
"Effect of Signal to Clutter Ratio(SCR)
on Automatic Target Recognition (ATR)"

H. L. Neal, Clark Atlanta University
"Teaching Density Functional Theory to Undergraduates"

L. Phillips, Alabama A & M University
"Precision-Resolution Bragg Filter
Fiber Optic Strain Sensor Application
J. Morris, Alabama A & M University
"Preliminary Results of the Electron Paramagnetic
Resonance of Fe 3- and Mn 4+ in LiNb03 Single Crystal"

A.M. Darwish, Alabama A & M University
"Preliminary Results of the Electron Paramagnetic
Resonance of Fe 3- and Mn 4+ in LiNb03 Single Crystal"

Yonas Abraham, Clark Atlanta University
"Multivariable Optimazation Approach for the Construction of
Many-Body Potential"

Asmerom Ogbazghi, Clark Atlanta University
"Application of Moment -Wavelet Transform to Quantum Mechanics"

S.U. Egarievwe, Alabama A & M University
"External Feedback Effects on Powder Laser Threshold"

William Wright, Western Kentucky University
"A New Method for Searching for Extra-Solar Planets"

Philip E. George, Western Kentucky University
"Searching for Extra-Solar Planets by Examining Eclipsing Binaries"

J. Brodney Fitzgerald, Western Kentucky University
"Searching for Period Changes in the
Eclipsing Contact Binary System 44i Boo"

LaShondria B. Dixon, Southern University and A & M College
"An Investigation of the Relationship between Structure and Electron
Transport in $La_{1-x}(Ca_{1-y}, Sr_y)_xMnO_3$"

George Ofori-Boadu, Hampton University
"Minority Physicist Archive"

Kimani A. Stancil, Massachusetts Institute of Technology
"Shape Memory and Gels"

Marta L. Dark, Massachusetts Institute of Technology
"The Physical Response of Meniscal. Tissue
to Short Pulsed Laser Irradiation"

C.M. Williams, Morgan State University
"Magnetic and Structural (EXAFS) Properties of Laser
Ablated Magnetic Oxide Films"

Christopher Beatty, Clark Atlanta University
"Excitation Energies and Oscillator Strength for NI"

F.A. Oguama, New Jersey Institute of Technology
"Effect of Zn 2+ Doping on the Phase Transition Temperature of Cadmium Calcium Acetate Hexahydrate Single Crystals"

A.L Stith, University of Virginia
641 H Signal Enhancement Using Hyperpolarized 129 Xe

Elaine N. Lalanne, New Jersey Institute of Technology
"Nonlinear Optical Properties of Silicon Nanoclusters Made by Laser Ablation"

Ian Dean Bacchus, University of California, Berkeley
"Resistive Joining Process in a High Temperature Superconducting System"

Participant List
Annual Conference of the
National Society of Black Physicists

Al Ashley	SLAC, Stanford University
Edward Asika	Clark Atlanta University
John Baker	University of Michigan
Keith Baker	CEBAF, Hampton University
Christopher Beatty	Clark Atlanta University
Jason Best	Shepherd College
Suketu Bhavsar	University of Kentucky
Paul E. Bibbons Jr.	Kentucky State University
Robert H. (Peter) Bragg	University of California, Berkeley
Rachel Branson	Lincoln University
Beth Brown	University of Michigan
Kenneth A. Brown	Jet Propulsion Laboratory
Thomas Butler	University of Michigan
Arthur Cammers-Goodwin	Chemistry Department, University of Kentucky
W. Eugene Collins	Fisk University
George Cooper	NASA Ames Research
Peter Custis	Lincoln University
Abdoul Dan-Azouni	Florida A & M University
Romeel Dave'	University of California, Santa Cruz
Peter Delfyeft	CREOL, University of Central Florida
Lamine Dieng	Wesleyan University
Julius Dollison	American Institute of Physics
Matthew E. Edwards	Spelman College
Tehani Finch	Massachusetts Institute of Technology
Nikky Finney	English Department, University of Kentucky
Virginia Fluitt	North Carolina A & T University
Kerwin C. Foster	Penn State University
John D. Galambos	Oak Ridge National Laboratory
Farrah Gaskins	Lincoln University
S. James Gates	University of Maryland
Philip E. George	Western Kentucky University
Jason-Patrick Gilchrist	North Carolina A & T University
Seke Godo	Lincoln University
J. Brodney Fitzgerald	Western Kentucky University
Karen Hackney	KSGC, Western Kentucky University
Richard Hackney	KSBC, Western Kentucky University
Philip (Bo) Hammer	SPS/American Institute of Physics
Carlos Handy	Clark Atlanta University
Dionna K. Harris	University of California, Berkeley
Richard Harris	North Carolina A & T University
Wendell T. Hill III	University of Maryland
Jarita C. Holbrook	University of California, Los Angeles
Armando Howard	NASA, Goddard Institute Space Studies
Gia Hunter	North Carolina A & T University
Keith H. Jackson	Lawrence Berkeley Laboratory
Floyd J. James	North Carolina A & T University
Clifford V. Johnson	University of Kentucky
Ralph E. Johnson	Tennessee Valley Authority
Tracey Johnson	University of California, Davis
Anthony M. Johnson	New Jersey Institute of Technology
Darryl K. Jones	University of Alabama, Huntsville
Kelvin Kibler	North Carolina A & T University

Eric Lee	Motorola/SEMATECH
Lonzy J. Lewis	Clark Atlanta University
Alan MacKellar	University of Kentucky
Ronald Mallett	University of Connecticut
Robert C. Mania Jr.	Kentucky State University
Nafataril Manigault	Lincoln University
Manasse Mbonye	University of Michigan
Benjamin McCarter	North Carolina A & T University
Charles McGruder	Western Kentucky University
Stephen C. McGuire	Cornell University
Cynthia McIntyre	George Mason University
Kevin McLin	University of Colorado
Windsor Morgan	Dickinson College
Alfred Z. Msezane	Clark Atlanta University
Romain Murenzi	Clark Atlanta University
G. Y. Ndefru	University of Kentucky
Henry Neal	Clark Atlanta University
Dara Norman	University of Washington
Lawrence Norris	Northwestern University
Albert 0. Okorogu	University of Alabama, Birmingham
Peter Ozimba	Georgia State University, Clark Atlanta University
Kendall Peace	Lincoln University
Alfred Phillips Jr.	Cornell University
Jorge Pullin	Penn State University
Allan Richards	University of Kentucky
Aaron Roane	John Hopkins University
Lynn E. Roberts	Lincoln University
Willie S. Rockward	AFRUMNG Advanced Guidance Division, Eglin AFB
Vincent Rodgers	University of Iowa
Carl Rouse	Rouse Research Inc.
Dereje Seifu	Morgan State University
Misganaw Setaneh	Lincoln University
Johnny Seymore III	Daytona Beach, FL
Rony Shahidain	Kentucky State University
Anouk Shambrook	University of California, Santa Cruz
Catrice Simmons	Lincoln University
Michael L. Simpson	North Carolina A & T University
Kennon Slade	Lincoln University
Milton D. Slaughter	University of New Orleans
Daniel Smith Jr.	South Carolina State University
Augustine J. Smith	Morehouse College
Tehma Smith	Lincoln University
Timothy Southern	North Carolina A & T University
Ayana Stephens	Lincoln University
James H. Stith	American Institute of Physics
Edward 0. Taylor	Lincoln University
Edward Thomas Jr.	Fisk University
Brian Tuttle	North Carolina A & T University
Demetrius Venable	Howard University
Traci Walker	Lincoln University
Donnell Walton	Howard University
Conrad Williams	Morgan State University
Elvira Williams	North Carolina A & T University
Krystaufaux Williams	Lincoln University
William Lee Wright	Western Kentucky University
Ben Zeidman	Argonne National Laboratory

Participant List
NCBPS

Yonas Abraham	Clark Atlanta University
Kodjo Adovor	Hampton University
Clement Adu	University of Kentucky
Cynthia Aku-Leh	Chicago State University
Ian Bacchus	University of California - Berkeley
Colley Baldwin	Pennsylvania State University
Christopher Bates	Johns Hopkins University
Gaycia Bowen	Fisk University
Louis J. Beathley	Southern University Baton Rouge
Bereket Berhane	Georgia Institute of Technology
Christopher Beatty	Clark Atlanta University
Jenese M. Bowles	Tougaloo College
Kent Bradford	Tougaloo College (Faculty)
Juronica Bradley	Fisk University
Beth Brown	University of Michigan
Denise Brown	University of Alabama - Birmingham
Sandra Brown	Massachusetts Institute of Technology
Elana Bryant	Fisk University
Jay F. Bulkley	University of California, Los Angeles
Shenetra Burse	Tougaloo College
Andre Burton	North Carolina A&T State University
Kevin Calhoun	Alabama A&M College
Frances Carter	Spelman College
Lovie L. Cason	California State University, San Bernardino
Charley Cheney	Tougaloo College
Manford Chinkhota	Southern University & A&M College
Branch Coleman III	North Carolina A&T State University
James Conner	Fisk University
Sarenee Cooper	Southern University & A&M College
Ronald Craig	University of Mississippi
Horace Crogman	University of Arkansas
Peter Custis	Lincoln University
Abdoul Latif Dan-Azoumi	Florida A&M
Marta L. Dark	Massachusetts Institute of Technology
Romeel Dave'	University of California - Santa Cruz
Christopher Davis	South Carolina State University
Dennis Denmark	Fisk University
Darnell E. Diggs	Alabama A&M College
Tommy Dodson	Southern University & A&M College
Mavis Donkor	Bethune Cookman
George Dritsas	Chicago State University
Angelique Dunn	Grambling State University
Lisa Dyson	Imperial College, University of London
Mika Edmonson	Hampton University
Jerral C. Edwards	University of Maryland - Baltimore County
Stephen U. Egarievwe	Alabama A&M College
Gordon Elmore	Eastern Kentucky University
Natnael Embaye	Clark Atlanta University
Lanette D. Ferguson	Alabama A&M University
Aisha B. Fields	Alabama A&M University
Tehani K. Finch	Massachusetts Institute of Technology
Virginia Fluitt	North Carolina A&T State University
Yashika N. Forrester	Alabama A&M University
Kerwin C Foster	Pennsylvania State University
Khristen Foster	Fisk University

Lakindra Francis	Southern University
Cemal Furman	Hampton University
David Garrison	Pennsylvania State University
Jeremiah Gates, Jr.	Tougaloo College
Kassatihun Gebre-Amlak	Florida A&M University
Jason Gilchrist	North Carolina A&T State University
William S. Giles	San Jose State University
Lynford L. Goddard	Stanford University
Edray Herber Goins	Stanford University
Bernard Griggs	University of Maryland, Baltimore County
Lamont Grissom	University of North Carolina, Charlotte
Horace T. Grogman	University of Arkansas
Kenji Haley	Tougaloo College
Fred Hall, IV	University of Alaska - Fairbanks
Akilan J. Harmon	Alabama A&M University
Dionna Harris	University of California - Berkeley
Ahmasi D. Harris	Morehouse College
Richard Harris	North Carolina A&T State University
Miguel Hayes	Fisk University
Malcolm Heard	Southern University & A&M College
Jamie Henderson	South Carolina State University
Paul Hillard	Southern University & A&M College
Carl Holden Jr.	Alabama A&M University
Michael E. Holmes	Florida A&M University
Holli Horton	Norfolk State University
Melvin Hunt, III	Fisk University
Gia Hunter	North Carolina A&T State University
Jeremy Jackson	Southern University & A&M College
Kim Jackson	Hampton University
Hosea R. James	Tougaloo College
Chandler Johnson	Tougaloo College
Philip Jones	Southern University & A&M College
Christopher Jones	Morehouse College
Ruth D. Jones	Alabama A&M University
Clarence Jones Jr.	Hampton University
Kelvin Kibler	North Carolina A&T State University
Stefen L. King	Tougaloo College
Bern'Nadette Knight	Tougaloo College
Jamal R. Knight	Indiana University of PA
Kurtrease Lafate	Fisk University
Elainė N. LaLanne	New Jersey Institute of Technology
Gregory Lampkin	Fisk University
Pierre Leaks	Tougaloo College
Benita Lee	Southern University & A&M College
Ely Leon	Chicago State University
Alphonse Loper	University of Kentucky
Jamie Macbeth	Stanford University
Shawntelle Madison	Iowa State University
Talib-Ud-Din Mahmoud	Alabama A&M University
Shala Mance	Spelman College
Patrick A. Manigault	Georgia Institute of Technology
Nayda Mason	Stanford University
Manyalibo Matthews	Massachusetts Institute of Technology
Kevin Maxey	Chicago State University
Christopher Maxie	Michigan State University
Erick May	University of North Carolina, Chapel Hill
Benjamin McCarter	North Carolina A&T State University
Darrick McNeill	Hampton University

Michelle Millican	Southern University & A&M College
Kenneth Mims	Hampton University
Tedla Mochena	University of Kentucky
Edris Mohammed	Georgia Institute of Technology
David Moore	University of California, Berkeley
Jesse Morris	Alabama A&M University
Kristen Morrow	Spelman College
Ariano Munden	Hampton University
Ghesu Ndefru	University of Kentucky
George Ofori-Boadu	Hampton University
Asmerom Ogbazghi	Clark Atlanta University
Ferdinand Oguama	New Jersey Institute of Technology
Anthony Ololo	Alabama A&M University
Hakeem Oluseyi	Stanford University
Dafney Parker	Alabama A&M University
Nathaniel C. Payne	Southern University, Baton Rouge
Leon Phillips	Alabama A&M University
Christopher Pickens	Johns Hopkins University
Gena Poe	Georgia Institute of Technology
Carramah Quiett	Hampton University
Rosiland S. Ramsey	Tougaloo College
Aaron Roane	Johns Hopkins University
Lenward Seals	Georgia Institute of Technology
Edwin Segbefia	Hampton University
Selemani Seif	Alabama A&M University
Vanessa Self	Southern University
Denis Semwogerere	Georgia Institute of Technology
Anouk Shambrook	University of California -Santa Cruz
NeShana Shaw	Southern University & A&M College
Jeremiah Smith	University of Maryland, Baltimore County
Timothy Southern	North Carolina A&T State University
Kimani Stancil	Massachusetts Institute of Technology
Ayanna Stephen	Lincoln University
Jason-Dennis Stewart	Miami University
Andrea Stith	University of Virginia
Kwesi R. Stone	Morehouse College
Ryan D. Swain	Alabama A&M University
Michael Swilley	Southern University & A&M College
Jamil Taylor	Hampton University
J. David Teal	Tougaloo College
Grum Teklemariam	Massachusetts Institute of Technology
Sheryl J. Tolbert	Virginia Tech
Marcia R. Trahan	University of Massachusetts, Boston
Kevin Tubbs	Southern University
Courtney L. Turner	Alabama A&M University
George E. Turner	Alabama A&M University
Bryan Tuttle	North Carolina A&T State University
Jamie Valentine	Brown University
Bryan Wallace	Fisk University
Tamara Williams	Tennessee State University
Troy Williams	Southern University & A&M College
Keisha Williams	Southern University
Mandell Williams	Florida A&M University
Candace Williamson	Tougaloo College
Lyndie Williamson	Massachusetts Institute of Technology
Sterling T. Windsor	Southeast Missouri State University
Adrienne B. Woodard	Tougaloo College
H. Omar Wooten	Morehouse College
Monika R. Wright	Southern University & A&M College
Richard E. Yarbrough	Antioch College

NCBPS and NSBP '98
Joint Conference
March 4-8, 1998
University of Kentucky\Kentucky State University

Findings from the Survey of Participants of the 12th Annual National Conference of Black Students

Report prepared by:
Julius Dollison and Michael Neuschatz

Education and Employment Statistics Division American Institute of Physics College Park, Maryland June 1998

Introduction

It has been a very fruitful conference, and apartfrom meeting other Black physicists, I also had the opportunity to hear about new discoveries in thefield of physics.

A student from Virginia

I enjoyed meeting with the NSBP because we were able to see the achievements of black physicists from several generations. The conference with NSBP served as motivation for most aspiring physicists.

A student from Georgia

The twelfth annual National Conference of Black Physics Students (NCBPS) was held concurrently with the annual meeting of the National Society of Black Physicists (NSBP). The joint meeting, held March 5 through 8th, 1998, was hosted by the University of Kentucky, Lexington. Meeting with the professional society afforded the undergraduate and graduate students attending the NCBPS a unique opportunity to establish contact with experienced black scientists, receive greater exposure to scientific research, and enjoy an opportunity to learn of contributions to physics made by blacks. As in previous years, the organizers of the conference contacted the Education and Employment Statistics Division of the American Institute of Physics and asked the Division to survey the students and conduct an evaluative study of the conference.

As before, the objectives of the study were to describe the background and demographic characteristics of the students, to explore their goals in attending the conference, and to assess whether the conference succeeded in meeting those goals. The participants were queried on physics research experience and their career goal choices. They were also asked to provide background data as well as their ratings of various aspects of the conference. In addition, this year, students were asked for their evaluation of their physics courses and the professors that they had encountered during their academic career.

The survey instrument was designed by the Employment and Statistics Division in consultation with organizers of the conference, and structured to allow comparison with participant reactions from earlier years. The questionnaire was distributed when the students signed in at the conference. Of the 164 students registered, 157 attended and were given the four-page questionnaire to complete. Responses were collected on the last day of the conference, with 139 (89%) returning completed questionnaires. This was similar to last year's response rate.

Background and Demographic Characteristics

This conference, as always, inspires me to go just a little bit further. It's one of the reasons why I'm in the doctoral program in physics today.

A student from Georgia

This year's conference attendees were evenly divided between undergraduates and graduate students, as was also the case last year. Regardless of their current level of study, essentially all of the participants indicated a desire to earn a graduate degree, with around 83% aspiring to a PhD.

The questionnaire instrument asked conference participants to provide background information on age (Figure I). The median age for undergraduates was 21 years, and for graduate students 27 years.

Among undergraduates, there was no age difference between men and women. However, we did find a difference between male and female graduate students. While among females the median age was 24, for graduate men the median age was 27 years. This difference closely mirrors the national pattern — according to AEP's broader surveys of physics graduate students, the median age for African-American females was 26 and for males 30. Interestingly, there is no corresponding difference between the ages of graduate males and females from other ethnic groups.

The fact that graduate student conference participants of both sexes tended to be younger than Black graduate physics students nationally is appropriate in light of the focus on networking rather than job placement. Another way of expressing this difference was that nationally, 40% of Black physics graduate students were 30 years or older, whereas among conference participants only 19% of the graduate students were this old.

Turning to gender distribution, we found that the proportion of females among NCBPS undergraduate students was 38%, slightly higher than last year. (Nationally, by comparison, only around one in five physics bachelors recipients are female. Among black physics bachelors recipients, that number is around one in three). Among NCBPS graduate students, the proportion of females was 26%, similar to last year's data. Nationally, around 17% of the graduate students are women, and among Black graduate students that number is 20%.

Respondents were asked to provide information on the minority composition at their high school and undergraduate institution, as shown in Figure II. As in years past, students from minority majority schools were most heavily represented, with 62% reporting that they came from schools where more than 90% of the students were members of a minority group.

Similar to last year, we found that around 67% of the undergraduate students, and 42% of the graduate students at the conference, reported that they currently attended an Historically Black College or University (HBCU). This suggests that participants drawn to the conference represent relatively accurately the population of all African-American physics students in the US, since nationally 61% of Black physics bachelors recipients, 35% of Masters, and 36% of PhDs went to HBCU's according to AIP's most recent Enrollments and Degrees study.

Student attendees were also asked about their course work, career aspirations, and the professors they had encountered during their school career (Figure III). The majority (74%) indicated that they would major in physics again if they had to do it over, and 83% felt that their physics course work would provide a solid background for heir future careers. Seventy percent of the students felt that in general the professors that they had encountered were supportive and helpful. There was no notable difference between graduate and undergraduate students. However, one point of interest was that fewer students who attend HBCU's felt that their physics course work would provide a solid background for their future careers than did those respondents who did not attend an HBCU (73% vs. 90%). This could be attributed to the fact that the physics programs at HBCU's tend to be smaller and not offer the variety of courses that the physics programs at non-HBCU's do. However, the trade-off to this, as will be discussed later, is that fewer students at HBCU's reported that their professors were unsupportive and inaccessible.

Around 60% of this year's conference participants reported that they had attended previous NCBPS meetings, and of'these, 83% reported attending last year's conference at MIT. Conference organizers went to great lengths this year in their recruiting efforts, and in some ways it paid off. Even though there was a high repeat attendance at this year's conference, many new schools were represented for the first time. One student even flew in from England to attend the conference.

Respondents were also asked about their experience with physics research and, as we found in previous years, the overwhelming majority (93% of the graduates and 77% of the undergraduates) have had one type of research experience or another. As shown in

Figure IV, slightly less than half of the undergraduate and 60% of the graduate students reported that they had been a research assistant for a professor. Even more surprising, around half of the graduate and slightly less than half (41 %) of the undergraduate attendees indicated that they had an off-campus position while attending school.

A finding worth mentioning is while only 29% of the undergraduates at non-HBCU's indicated that they had been a research assistant for a professor, around half of the undergraduates at HBCU's had. This finding is similar to last year's data and may suggest that professors at HBCU's are more accessible to, and willing to foster relationships with, Black physics students than are their counterparts at non-HBCU's.

Academic and Career Goals

Overall the conference was very informative and helped give additional direction to my fiiture career choice.

A student from Mississippi

Conference attendees were again queried about their current scholastic situati6n and their future academic and career goals. As was true last year, the overwhelming majority of the conference participants (88%) reported that their major department was physics with another 6% majoring in math. As mentioned earlier, virtually all of the conference attendees indicated plans to pursue, or were already pursuing, a graduate degree, with 83% of them aspiring to a PhD. Nationally, by comparison, around 40% of the 1997 Black physics Bachelors degree recipients indicated plans to on to graduate study at the point of actual graduation — less than half in physics or astronomy and the rest in other fields (AIP 1997 Bachelors Degree Recipients Survey unpublished data). Unfortunately, data on degree recipients indicate that far less actually reach this goal, suggesting that strategies to retain those students is vitally important.

Students were also asked about their future career goals. (see Table 1). Around sixty percent of the conference attendees reported a preference for physics research or teaching, with an additional 15% indicating an interest in physics research but unsure of the employment sector they preferred. Graduate students were more likely than undergraduates to favor physics research and teaching (48% vs. 19%), while the undergraduate attendees tended to favor careers outside of physics altogether (18% vs. 5%). Interestingly, women were more likely to favor a career outside of physics altogether than men (22% vs. 13%).

The participants were also asked to indicate the most important factors that led to their career goals. We found that 56% of them were primarily looking for challenging work. We also found that 24% wanted to give something back to the community, while 16% were more interested in the money or prestige. Upon closer inspection. we found that female students were more likely than their male counterpart to mention the intrinsic challenge of the work (65% vs. 51 %), while the men put more stress on money and prestige (18% vs. 8%). Students at HBCU's were more concerned with giving something back to the community than were students at non-HBCU's (28% vs. 19%).

Assessment of the Conference

These conferences have provided so many opportunities for myself and others. My graduate school placement was a direct result of the 1997 conference in Boston. That is where I met my present advisor. Thank you for the chance to continue my endeavors. Please do not stop!

A student from Tennessee

I would like to see more job recruiters at upcoming conferences.

A student from Virginia

Students were asked to assess the conference in terms of their objectives for attending the meeting (see Table 2). We found networking with other Black physics students to be the number one reason participants chose as their objective for attending the conference. Networking with black physics professionals was also popular, chosen by a fourth of all the conference attendees. This was a slight increase from last year, perhaps due to the NSBP holding their meeting at the same time,

giving the students more of chance to network with Black professionals. Less than a quarter of the participants (versus 35% last year) indicated that leaming about further physics study was their primary reason for attending the conference. Students at HBCU's were more likely that students at non-HBCU's to choose meeting with school or job recruiters as the primary reason for attending the meeting (19% vs. 8%), while a higher proportion of students at non-HBCU's stressed networking with black physics professionals (32% vs. 19% at HBCU's) as their main reason for attending, probably a reflection of their greater isolation.

Another indication of the importaAce of networking comes from the 60% of the participants who reported that they had attended earlier meetings. Like last year, the vast majority of this year's repeat attendees (84%) reported that they had kept in touch with students they had met at previous meetings — either socially or professionally. Even more surprising, almost as many (77%) reported that they had kept in touch with faculty members or recruiters first encountered at prior NCBPS conferences.

Other major objectives of the conference were to offer students tools and contacts to assist them in their academic endeavors and to give them an opportunity to hear about recent research and general topics of interest in physics. However, very few students (14%) reported meeting recruiters as their primary objective for attending the meeting. By the same token, only 2% mentioned hearing research talks as their main impetus for attending. However, attendance at research talks seemed to have increased from last year. This year only 15% of the siudents reported attending fewer than 4 research talks, while last year 40% indicated that they had attended fewer than 4 sessions.

As in years past, the conference received outstanding marks from its student participants for assisting in the development and maintenance of an ongoing network of Black physics students. This was one of the conference's key objectives, and as noted above, also the students' top priority. In this respect, the conference received its highest ratings (Table 3). The overwhelming majority (96%) rated the conference as excellent or good in providing opportunities for networking with other Black physics students. We also see that networking with Black professionals and learning about further study in physics (numbers 2 and 3 on the participants' priority lists, respectively) were rated excellent or good by a large majority of the attendees. Although not a priority of attendees, hearing research talks was also given high marks (90%). However, meeting with job recruiters did not score as well this year as it did last year, with 26% of the students rating it fair or poor. A number of students also mentioned in the comment section that they thought that there weren't enough job recruiters present at this year's meeting. Further evidence of the enthusiasm of the participants emerges from the overall assessment of the conference (see Table 4). Around three-quarters of the attendees (down from last year's 87%) rated all or most of the research talks as exceptional. While the quality of the speakers was rated somewhat lower this year than last year (76% vs. 90%), the sessions on pursuing graduate school and career options retained last year's high marks.

Attendees were also asked to rate the practical arrangements of this year's conference, and for an overall impression of certain key aspects of the meeting (Table 5). As we can see, travel arrangements were rated excellent or good by virtually all the students (97%). 'Me ratings for the housing facilities and overall length of the conference improved from last year's high level. Student evaluation of the length of the sessions showed improvement this year compared to last year.

Conclusion

The conference, as always, was informative and insightful. The administrators, recruiters, and students are sincerely pleasant to talk to. They are equally willing to share whatever information that may be helpful to your present studies as well as yourfuture goals. Keep up the good work.

A student from Louisiana

Based on the findings and the comments from the attendees, we can conclude that the conference seems to have fulfilled the goals and met the expectations of those attending. The ratings for the content of the sessions and

the speakers, although not as high as in previous years, were still good. The ratings for the practical arrangements of the conference, once again, received glowing marks. Perhaps the only two stated shortcoming this year, repeatedly mentioned in the comment section, were: 1) that there weren't enough job recruiters present; and 2) the menu (a perennial sore point) left something to be desired.

Figure I. Age by degree of the NCBPS attendees, 1998.

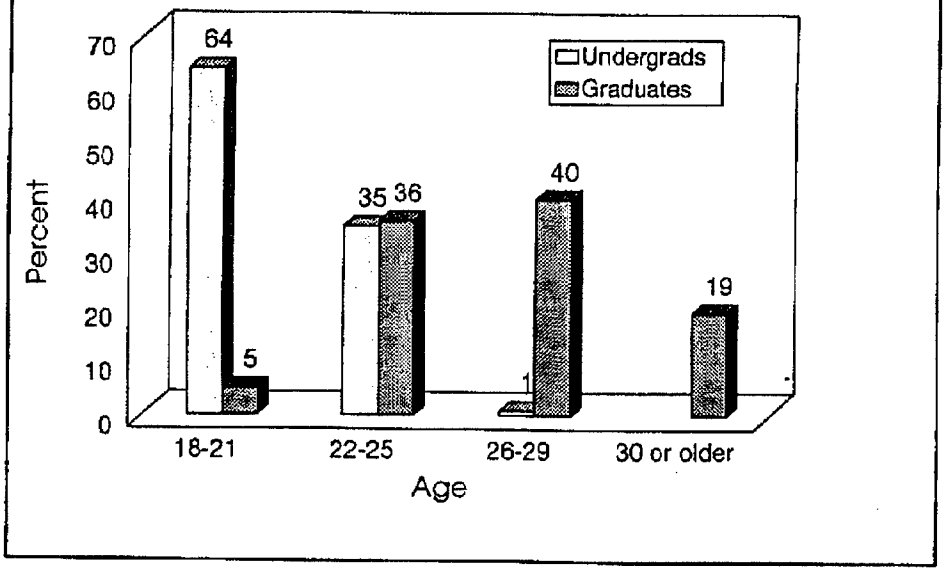

Figure II. Minority composition at respondents' undergraduate college / university, 1998.

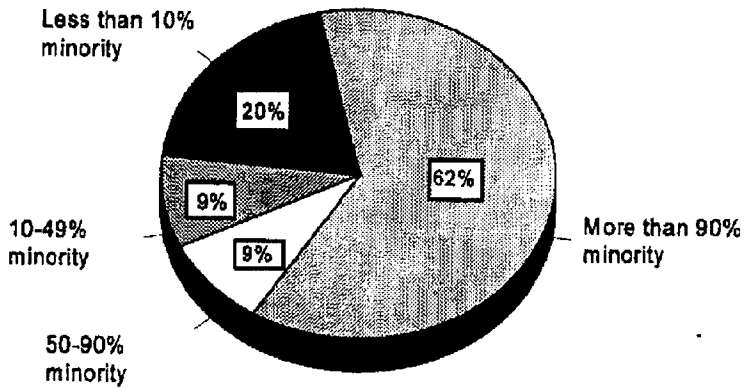

Figure III. Extent to which NCBPS participants agree with the following statements, 1998.

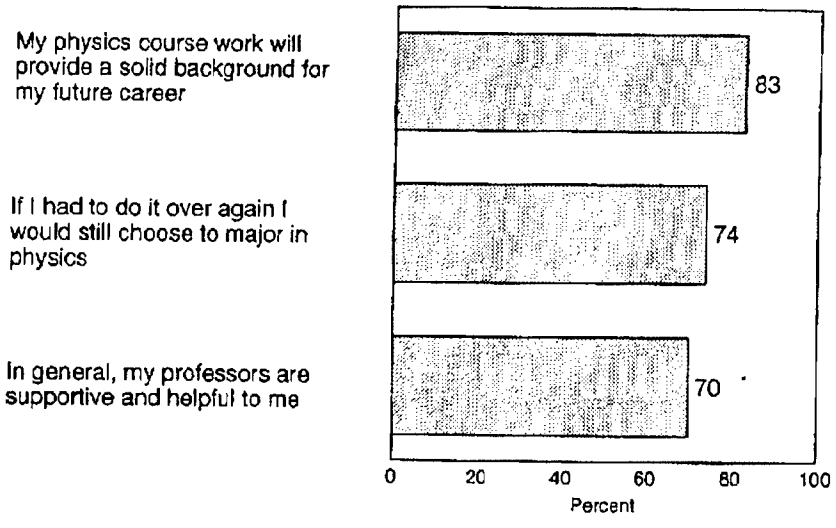

Figure IV. Proportion of undergraduate and graduate attendees reporting different types of physics research, 1998.

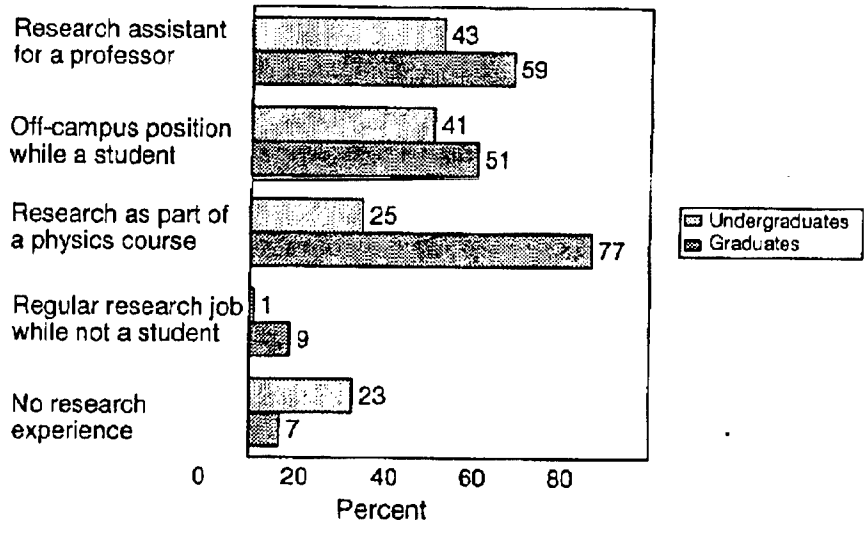

Table 1. NCBPS participants' anticipated career goals, 1998	
	Percent
Academic teaching or research in physics	33
Non-academic physics research:	
in industry	18
in government/national labs	8
unspecified employment sector	15
Other types of positions in physics	10
Careers in other sciences	11
Careers outside of physics altogether	5

Table 2. Goals in attending NCBPS conference, 1998		
	Top Goal %	Among Top 3 %
Networking with other Black students	35	85
Networking with Black professionals	25	82
Learning about further physics study	23	60
Meeting with recruiters	14	45
Hearing research talks	2	25

Table 3. Performance of conference in meeting goals, 1998				
	Excellent %	Good %	Fair %	Poor %
Networking with other Black students	72	24	4	-
Networking with Black professionals	59	33	8	-
Learning about further physics study	51	42	6	1
Meeting with recruiters	38	36	18	8
Hearing research talks	49	41	8	2

Table 4. Overall assessment of key aspects of the conference, 1998

	Proportion rated exceptional			
	All %	Most %	Half %	Few/None %
Content of research talks	20	54	25	1
Quality of speakers	18	58	20	4
Sessions on pursuing graduate school and career options	44	42	14	-

Table 5. Ratings of the pratical arrangements at the conference, 1998

	Excellent %	Good %	Fair %	Poor %
Travel arrangements	84	13	3	-
Housing facilities	92	7	1	-
Length of sessions	43	41	15	1
Length of conference	63	31	6	-